frontiers | Research Topics

Nutrition and chemistry of cereal macromolecules in cereal-based products

Edited by
Kunlun Liu, Hongshun Yang, Sen Ma and Hua-Min Liu

Published in
Frontiers in Nutrition

ISSN 1664-8714
ISBN 978-2-83251-054-4
DOI 10.3389/978-2-83251-054-4

About Frontiers

Frontiers is more than just an open access publisher of scholarly articles: it is a pioneering approach to the world of academia, radically improving the way scholarly research is managed. The grand vision of Frontiers is a world where all people have an equal opportunity to seek, share and generate knowledge. Frontiers provides immediate and permanent online open access to all its publications, but this alone is not enough to realize our grand goals.

Frontiers journal series

The Frontiers journal series is a multi-tier and interdisciplinary set of open-access, online journals, promising a paradigm shift from the current review, selection and dissemination processes in academic publishing. All Frontiers journals are driven by researchers for researchers; therefore, they constitute a service to the scholarly community. At the same time, the *Frontiers journal series* operates on a revolutionary invention, the tiered publishing system, initially addressing specific communities of scholars, and gradually climbing up to broader public understanding, thus serving the interests of the lay society, too.

Dedication to quality

Each Frontiers article is a landmark of the highest quality, thanks to genuinely collaborative interactions between authors and review editors, who include some of the world's best academicians. Research must be certified by peers before entering a stream of knowledge that may eventually reach the public - and shape society; therefore, Frontiers only applies the most rigorous and unbiased reviews. Frontiers revolutionizes research publishing by freely delivering the most outstanding research, evaluated with no bias from both the academic and social point of view. By applying the most advanced information technologies, Frontiers is catapulting scholarly publishing into a new generation.

What are Frontiers Research Topics?

Frontiers Research Topics are very popular trademarks of the *Frontiers journals series*: they are collections of at least ten articles, all centered on a particular subject. With their unique mix of varied contributions from Original Research to Review Articles, Frontiers Research Topics unify the most influential researchers, the latest key findings and historical advances in a hot research area.

Find out more on how to host your own Frontiers Research Topic or contribute to one as an author by contacting the Frontiers editorial office: frontiersin.org/about/contact

Nutrition and chemistry of cereal macromolecules in cereal-based products

Topic editors

Kunlun Liu — Henan University of Technology, China
Hongshun Yang — National University of Singapore, Singapore
Sen Ma — Henan University of Technology, China
Hua-Min Liu — Henan University of Technology, China

Citation

Liu, K., Yang, H., Ma, S., Liu, H.-M., eds. (2022). *Nutrition and chemistry of cereal macromolecules in cereal-based products*. Lausanne: Frontiers Media SA.
doi: 10.3389/978-2-83251-054-4

Table of contents

frontiers | Frontiers in Nutrition

TYPE Editorial
PUBLISHED 30 November 2022
DOI 10.3389/fnut.2022.1097060

OPEN ACCESS

EDITED AND REVIEWED BY
Michael Rychlik,
Technical University of Munich, Germany

*CORRESPONDENCE
Kunlun Liu
knlnliu@126.com

SPECIALTY SECTION
This article was submitted to Food Chemistry, a section of the journal Frontiers in Nutrition

RECEIVED 13 November 2022
ACCEPTED 21 November 2022
PUBLISHED 30 November 2022

CITATION
Liu H-M, Ma S, Yang H-S and Liu K (2022) Editorial: Nutrition and chemistry of cereal macromolecules in cereal-based products. *Front. Nutr.* 9:1097060. doi: 10.3389/fnut.2022.1097060

Editorial: Nutrition and chemistry of cereal macromolecules in cereal-based products

Hua-Min Liu[1], Sen Ma[1], Hong-Shun Yang[2] and Kunlun Liu[1,3]*

[1]College of Food Science and Engineering, Henan University of Technology, Zhengzhou, China, [2]Department of Food Science and Technology, National University of Singapore, Singapore, Singapore, [3]School of Food and Strategic Reserves, Henan University of Technology, Zhengzhou, China

KEYWORDS

cereal, macromolecules, chemistry, nutrition, cereal-based products

Editorial on the Research Topic
Nutrition and chemistry of cereal macromolecules in cereal-based products

Cereals belong to the family of Gramineae, which produce dry, one-seeded fruits called grains that consist of seed and pericarp. The seed itself consists of the seed coat, the nucellar epidermis, the endosperm, and the embryo. Recently, cereals and their ingredients are accepted as nutraceuticals and functional food due to providing dietary fiber, energy, proteins, vitamins, minerals, and phytochemicals required for human health. Nutrition and chemistry of cereals and cereal-based food are the pillars of wellbeing and health in society because humans rely on cereals not only to supply energy but also for essential nutrients that maintain the body and keep the immune system in a good state of recovery. Adequate nutrition, therefore, correlates with lower mortality and morbidity from both non-infectious and infectious diseases and is particularly important in pregnant women and children where the lack of essential nutrients can result in irreversible mental and physical damage during development.

Nowadays, the nutrition and chemistry of cereals and its processed products are a major priority to human health. The main compositions in cereal and cereal-based products are carbohydrate (starch and structural compositions), lipid, and protein, which belong to macromolecules and provide basic nutrition for humans and animals. Therefore, given the significance of the project, the journal has been seeking original research papers and review articles to organize a Research Topic focused on *Nutrition and chemistry of cereal macromolecules in cereal-based products*. After 6 months of preparation, we believe that this Research Topic is ready to be shared with researchers around the world. We have received many research papers and review articles since the opening of the submission system. The interesting ideas, unique insights and positive feedback from all researchers were very impressive in preparation for the Research Topic. Excitingly, finally, there are nine papers covering almost all features of *Nutrition*

and chemistry of cereal macromolecules in cereal-based products and they provide an in-depth understanding of the techniques and methodologies used in the journal.

Firstly, scientists investigated the functional and nutritional changes of macromolecules in cereal-based foods after fermentation and enzyme treatment. For example, the paper from Liu X. et al. investigated the effects of fermented and germinated foxtail millet whole grain (FG-FM) on kidney lesions in a diabetic mouse model (Db/Db mice). The paper found that the FG-FM consumption significantly alleviated the kidney tissue damage in the diabetic mouse model. They also concluded that the over activation of signaling pathways related to inflammation and immunity in the diabetic mouse model was significantly inhibited with the FG-FM intake. This investigation confirmed foxtail millet as a potential source of functional food for the non-pharmacological intervention of DKD. The second paper (Fan et al.) evaluated the effect of fermented wheat bran dietary fiber (FWBDF) on the rheological properties of the dough and the quality of noodles and to compare it with the effect of the unfermented WBDF (UWBDF). It revealed that fermentation could reduce the destructive effects of WBDF on the quality of noodles, providing a new perspective on balancing dietary fiber-rich and high-quality foods. The third paper (Qin et al.) investigated the transglutaminase treatments on the structure of pea protein isolate under conditions relevant to high-moisture extrusion processing by using a closed cavity rheometer. The findings can help to better understand the relationships of material-structure during the extrusion process, and also provide guidance for further optimization of the quality of meat substitutes. Wang et al. discussed the structural properties and aggregation behavior of gluten containing wheat bran dietary fiber under the conditions of synergistic fermentation of *Lactobacillus plantarum* and *Saccharomyces cerevisiae*, which provides new data for the improved production of sourdough whole grain and/or high fiber flour products. Liang et al. investigated the physicochemical and functional properties of soybean protein concentrate by using Alcalase protease and high-pressure homogenization for the combined modification. The results indicated the modification technology could improve the functionality and application range of soybean protein concentrate, which could also provide a theoretical basis for its high-value utilization in food industry.

Secondly, four articles present the functional and structural properties of starch or starch-based foods during processing. Guo et al. determined the effect of three kinds of natural antioxidants on the structural and physicochemical properties of sweet potato starch in noodles. They found that the broken rates, iodine blue values, hardness, and chewiness of the noodles were increased with the addition of the tested natural antioxidants. Additionally, the adding natural antioxidants could improve the sensory quality and antioxidant function of starch noodles. Liu G. et al. analyzed the oral processing properties and the starch fine structure of japonica rice. Additionally, the relationship between starch fine structure and oral processing of cooked japonica rice was further investigated. Ji et al. studied the pasting, retrogradation, and structural properties of three different crystalline starches compounded with natural inulin. The potential mechanism of interaction between inulin and starch was also investigated. The results could develop the theoretical system of inulin with starch compound system and could provide a solid theoretical basis of further applications. Yan et al. modified wheat flour by annealing using plasma-activated water. This method has a potential for further application in wheat flour modification as a green technology.

In conclusion, the collections in this Research Topic covers the effects of cereal macromolecules including starch, polysaccharide, and protein on the functional and nutritional properties of cereal-based foods during processing. We hope that this Research Topic will further promote the interests in *Nutrition and chemistry of cereal macromolecules in cereal-based products*.

Author contributions

H-ML and KL prepared, checked, and revised the manuscript and approved the submitted version. All authors contributed to manuscript revision, read, and approved the submitted version.

Conflict of interest

The authors declare that the research was conducted in the absence of any commercial or financial relationships that could be construed as a potential conflict of interest.

Publisher's note

frontiers | Frontiers in Nutrition

ORIGINAL RESEARCH
published: 16 June 2022
doi: 10.3389/fnut.2022.940404

The Preventive Effects of Fermented and Germinated Foxtail Millet Whole Grain on Kidney Damage in a Diabetic Mouse Model

Xia Liu[1,2], Bin Qiu[2], Wei Liu[2,3], Yuhan Zhang[3], Xianshu Wang[2], Xingang Li[3,4], Lingfei Li[5] and Di Zhang[1,3,4]**

[1] Medical Integration and Practice Center, Cheeloo College of Medicine, Shandong University, Jinan, China, [2] Shandong Academy of Agricultural Sciences, Jinan, China, [3] Jinan Microecological Biomedicine Shandong Laboratory, Jinan, China, [4] Department of Neurosurgery, Qilu Hospital, Shandong University, Jinan, China, [5] College of Food Science and Technology, Yunnan Agricultural University, Kunming, China

OPEN ACCESS

Edited by:
Sen Ma,
Henan University of Technology, China

Reviewed by:
Yanhui Han,
University of Massachusetts Amherst, United States
Min Gu,
Louisiana State University, United States

***Correspondence:**
Lingfei Li
lilf@ynau.edu.cn
Di Zhang
dizhang@sdu.edu.cn

Specialty section:
This article was submitted to Food Chemistry, a section of the journal Frontiers in Nutrition

Received: 10 May 2022
Accepted: 26 May 2022
Published: 16 June 2022

Citation:
Liu X, Qiu B, Liu W, Zhang Y, Wang X, Li X, Li L and Zhang D (2022) The Preventive Effects of Fermented and Germinated Foxtail Millet Whole Grain on Kidney Damage in a Diabetic Mouse Model. Front. Nutr. 9:940404. doi: 10.3389/fnut.2022.940404

Diabetic kidney disease (DKD) is an important complication of diabetes. The prevention of DKD can effectively reduce the mortality rate of diabetic patients and improve their quality of life. The present study examined the effects of fermented and germinated foxtail millet whole grain (FG-FM) on kidney lesions in a diabetic mouse model (Db/Db mice). The results proved that the FG-FM consumption significantly alleviated the kidney tissue damage in the diabetic mouse model. The transcriptome analysis of kidney tissues demonstrated that the overactivation of signaling pathways related to inflammation and immunity in the diabetic mouse model was significantly inhibited with the FG-FM intake. Moreover, the consumption of the FG-FM diet effectively elevated the bacterial diversity, increased the relative abundance of probiotics and decreased the relative abundance of previously reported DKD-related bacteria in the gut microbiota of diabetic mice. Our study confirmed foxtail millet as a potential source of functional food for the non-pharmacological intervention of DKD.

Keywords: foxtail millet, fermentation, germination, diabetic kidney disease, gut microbiota

INTRODUCTION

Diabetes mellitus (DM) is a chronic metabolic disease with a dramatically increased incidence globally in the past decades. Over one million deaths are directly attributed to DM each year (1), and the main factors responsible for DM-related mortality are diabetes complications (2). Diabetic kidney disease (DKD) is one of the major complications of diabetes and the leading cause of chronic kidney disease and 20%-40% of diabetic patients have combined diabetic kidney disease (3, 4). The population survey showed that kidney disease is an important risk factor accounting for the increased mortality in patients with type 2 diabetes (5). Although the progress in pathology research has facilitated the study of target drug discovery, there is still no ideal drug for DKD because the success rate of these compounds in clinical trials has been disappointingly low (6). Therefore, the development of non-pharmacological DKD intervention is of great significance for improving both length and quality of life in the diabetic population.

The growing evidence support that gut microbiota plays a pivotal role in the pathogenesis of DKD. As a complex ecosystem with 100 trillion microbes, the gut microbiota executes a wide range of important biological functions, including nutrient absorption and metabolism, vitamin production, regulation of development, resistance to pathogens, and maintenance of immune homeostasis (7–11). Significant changes in the gut microbiota have been confirmed in a variety of diseases, including obesity, DM, DKD, inflammatory bowel disease, cardiovascular disease, and cancer (12–14). The composition of gut microbiota in the DKD patients was significantly different from that of non-DKD diabetes patients (15). A marked expansion of bacterial communities at different classification levels, including *Proteobacteria*, *Selenomonadales*, *Neosynechococcus*, *Shigella*, *Escherichia coli*, etc., were found in DKD patients when compared to diabetic patients without kidney disease (15). Consequently, the gut microbiota dysbiosis induces intestinal barrier damage, prompts the translocation of endotoxin and other toxins, aggravates the system inflammatory levels, and finally contributes to kidney injury (16–18). Moreover, Cai *et al*. also reported that the proportion of short chain fatty acids (SCFAs)-producing bacteria in gut microbiota was decreased in DKD patients, and the oral supplement of SCFAs could improve kidney injury in the diabetic mouse model (19). These studies suggested that targeting the gut microbiota could be a novel strategy for the prevention of DKD.

Diet is a direct and effective factor affecting the gut microbiota (20). The foxtail millet (*Setaria italica*) is one of the major food crops in northern China, which is rich in dietary fiber, minerals, vitamins, and proteins (21–23). Previously studies have proved that foxtail millet has anti-inflammatory property and may prevent chronic diseases such as atherosclerosis and diabetes (24, 25). Moreover, animal studies proved that the intake of cereal bran effectively promotes beneficial bacteria and increases the production of SCFAs in gut microbiota (26). Thus, foxtail millet can serve as an important source of prebiotics. In our previous study, the effects of different pretreated foxtail millet cereal flour on an acute colitis mouse model with severe gut microbial dysbiosis were studied (20). The results showed that the fermented and germinated foxtail millet whole grain (FG-FM) cereal flour had the strongest prebiotic function and could almost completely restore the gut microbiota disorder in the colitis mouse model (20). Our findings coincide with studies that have shown that germination or fermentation can improve the prebiotic performance of whole grain (27–29).

Based on the fact that the gut microbiota plays an important role in the pathogenesis of DKD, as well as the powerful prebiotic properties of the FG-FM, we hypothesize that FG-FM has an impact on the prevention or treatment of DKD. In the current study, we tested the effects of fermented and germinated foxtail millet whole grain (FG-FM) intake on diabetes-related kidney injuries in genetically diabetic C57BL/KsJ-db/db (Db/Db) mice and explored its impact on gut microbiota. Our study provides a cost-effective non-pharmacological strategy for the prevention or treatment of DKD.

MATERIALS AND METHODS

Preparation of Cereal Flour From Fermented and Germinated Foxtail Millet Whole Grain (FG-FM)

The foxtail millet seeds were provided by the Crop Institute of Shandong Academy of Agricultural Sciences. The FG-FM cereal flour used for the animal study was produced from foxtail millet seeds as described previously (20). In brief, foxtail millet seeds were soaked in tap water for 12 h at room temperature. After the water was drained, the seeds were left to sprout at room temperature for 24 h. The germinated seeds were dried, ground, and then passed through an 80-mesh sieve to produce germinated whole-grain foxtail millet flour. The germinated whole grain foxtail millet flour was mixed with water (1:2), cooked for 10 min in a 75 ± 5°C water bath, and then fermented with *Lactobacillus Plantarum* NBRC 15,891 (obtained from NITE Biological Resource Center) at 37°C. The resulting slurry was dried, ground, and then passed through an 80-mesh sieve to produce germinated and fermented foxtail millet whole grain (FG-FM) cereal flour used in this study. The prepared FG-FM cereal flour contained 58.54% starch, 10.87% protein, 2.85% fat, 19.41% dietary fiber,5.47% moisture, and 2.87% ash.

Animal Diets

The FG-FM cereal flour diet was designed based on the AIN-93M standard rodent formula. The cereal flour diet contained 50% FG-FM cereal flour, and the remaining 50% was supplemented with standard nutrients according to the AIN-93M formula. The control diet in the study was a standard AIN-93M rodent diet. The animal diets were prepared by Nantong Troffe feed Technology Co., Ltd (Jiangsu, China), and the detailed compositions of experimental diets were listed in the **Supplementary Table S1**.

Animal Experiment Design

The 8–10 weeks old male genetically diabetic C57BL/KSJ-db/db (Db/Db) mice and their non-diabetic littermates C57BL/KSJ-m+/+db (Db/m) were obtained from GemPharmatech Co. Ltd. (Nanjing, China). The mice were housed in a specific pathogen-free facility (12 h daylight cycle) with *ad libitum* access to food and water, and the body weights were recorded every week. After 2 weeks of acclimation, mice were assigned into three groups (10 mice/group) with two different genotypes and two dietary treatments: 1) Db/m mice fed a standard AIN-93M rodent diet (CTRL group); 2) Db/Db mice fed a standard AIN-93M rodent diet (Db-93M group); 3) Db/Db mice fed an FG-FM cereal flour-based diet (Db-FM). The animal protocol was approved by the Institutional Animal Care and Use Committees of the Qilu Hospital of Shandong University.

Tissue Collection and Histopathological Analysis

After 8 weeks on a diet, the mice were anesthetized with isoflurane inhalation and then terminated by cervical dislocation. By opening the abdomen cavity, the large intestine was removed and placed on an ice plate. Then cecal content was collected,

snap-frozen in liquid nitrogen, and stored at −80°C until further analysis. The kidneys were removed and weighed, one of the kidneys was snap-frozen in liquid nitrogen and stored at −80°C for further total RNA extraction and transcriptome analysis, the other was processed for paraffin embedding, cut into 5 μm sections, and finally stained with hematoxylin and eosin (H&E) for histopathological analysis. The pathological features of liver tissue were also analyzed by H&E staining. Other tissues were removed and weighed, including the spleen and epididymal fat.

Analysis of Cecal Microbiota Composition by 16s Ribosomal RNA (16s rRNA) Gene Sequencing

Total bacterial DNA was extracted from frozen cecal contents using a QIAamp DNA Stool Mini Kit (Qiagen, Valencia, CA). The region V3–V4 of the 16S rRNA gene was amplified, purified, and quantified sequentially. Then the DNA libraries were constructed following the manufacturer's instructions. After quality inspection, the constructed DNA library was sequenced with Illumina HiSeq 2,500 platform (Illumina, Inc, San Diego, California). The resulting pair-end reads were joined by fastq-join (Version 1.3.1, https://code.google.com/p/ea-utils/) and pear (30), and then cut and quality filtered by Cutadapt (version 1.18) (31) to obtain clean tags. After that, the resulting clean tags were assigned to OTUs using USEARCH (Version 11.0.667, http://www.drive5.com/usearch/) with a 97% threshold of pairwise identity. The OTUs were then aligned against the Silva database (Release132, http://www.arb-silva.de) (32). QIIME (33) software was used to generate an information table of the relative abundance of bacterial communities at different classification levels, and then the R software was used to plot the community structure at each taxonomic level of the sample. The linear discriminant analysis (LDA) effect size (LEfSE, https://huttenhower.sph.harvard.edu/galaxy/) was applied to identify bacterial communities responsible for the differences in cecal microbiota compositions between different groups, using an LDA score threshold of >4.0. The raw Illumina read data were uploaded into SRA at NCBI under the BioProject ID PRJNA835687.

RNA Sequencing of Kidney Tissue and Analysis of Transcriptome Profiling Data

Total RNA was extracted from frozen kidney tissue, and the concentration and quality of extracted total RNA were determined by Nanodrop 2000, agarose gel electrophoresis, and Agilent 2100 bioanalyzer (Agilent, Santa Clara, CA, USA) in order. After the mRNA was purified from total RNA using Oligo (dT) beads (NEB, San Diego, CA, USA). The Illumina TruseqTM RNA sample prep Kit was used for sequencing library preparation based on purified mRNA samples. The resulting library fragments were quantified using an Agilent High Sensitivity DNA assay on a Bioanalyzer 2100 system (Agilent, Santa Clara, CA, USA) for concentration and size distribution, and the molar concentration of DNA libraries was analyzed by q-PCR using KAPA SYBR FAST Universal 2X qPCR Master Mix and DNA Quantification Standards and Primer Premix Kit (KAPA Biosystems, Woburn, MA, USA). The prepared libraries were mixed proportionally, then sequenced using an Illumina Novaseq 6000 platform (read length 2 × 150 bp).

After adaptor removal, quality and size trimming, low complexity filtering, and ribosomal RNA (rRNA) removal of raw data, the resulting clean reads were mapped to the Mus musculus reference genome using the program HISAT2 (https://ccb.jhu.edu/software/hisat2/index.shtml) (34). After assessment of mapping results, the transcripts were assembled and annotated using Cufflinks (https://cole-trapnelllab.github.io/cufflinks/) (35) or StringTie (https://ccb.jhu.edu/software/stringtie/) (36). Then, read counts of annotated transcripts (genes) were calculated using RSEM (37), and then transformed into FPMK (fragments per kilobases per million fragments) values for further analysis. Differentially expressed genes (DEGs) were analyzed using DESeq2 or edgeR software (38, 39). GO (Gene Ontology) and KEGG (Kyoto Encyclopedia of Genes and Genomes) enrichment analysis of DEGs was performed with Goatools (https://github.com/tanghaibao/GOatools) (40) and R software.

Statistical Analysis

One-way analysis of variance (ANOVA) followed by Fisher's LSD test (GraphPad Software, Inc., La Jolla, California) was used for multiple comparisons. The results were considered statistically significant when $p < 0.05$. Data were expressed as means ± SEM.

RESULTS

Physiological Parameters of Mice

As demonstrated in **Figure 1A**, the body weights of Db/Db mice (Db-93M group and Db-FM group) were significantly higher than that of Db/m mice (CTRL group) due to the genotypic difference. In the first 4 weeks on diets, the body weights of both groups of Db/Db mice (Db-93M and Db-FM) increased with no significant difference observed between groups. However, from the 5th week, the body weights of the mice in the Db-93M group began to decline, resulting in significantly lower body weights of the mice in the Db-93M group than those of mice in the Db-FM group. Consistent with body-weight loss, the epididymal fat weights of mice from the Db-93M group were significantly lower than that of the Db-FM group (**Figure 1B**, $p = 0.0127$). On the contrary, the kidney weights of mice from the Db-93M group were significantly higher than those from the Db-FM group ($p < 0.0001$, **Figure 1C**). Liver and kidney weights did not differ significantly between Db-93M and Db-FM groups.

Histopathological Analysis

The experimental mice were executed after 8 weeks on diets. It was found that the kidneys in the CTRL group (**Figure 2A**) were normal in appearance and morphology while in both groups of Db mice, the kidney was surrounded by a large amount of fat. Six of the total nine mice in the Db-93M group had severe lesions in at least one of the kidneys (**Figure 2B**, right; **Figure 2C**), while the kidney of mice in the Db-FM group showed no morphological abnormalities (**Figure 2B**, left). The result of H&E staining (**Figure 2D**) clearly showed that the normal micro-structure of the kidney tissues was almost destroyed in the

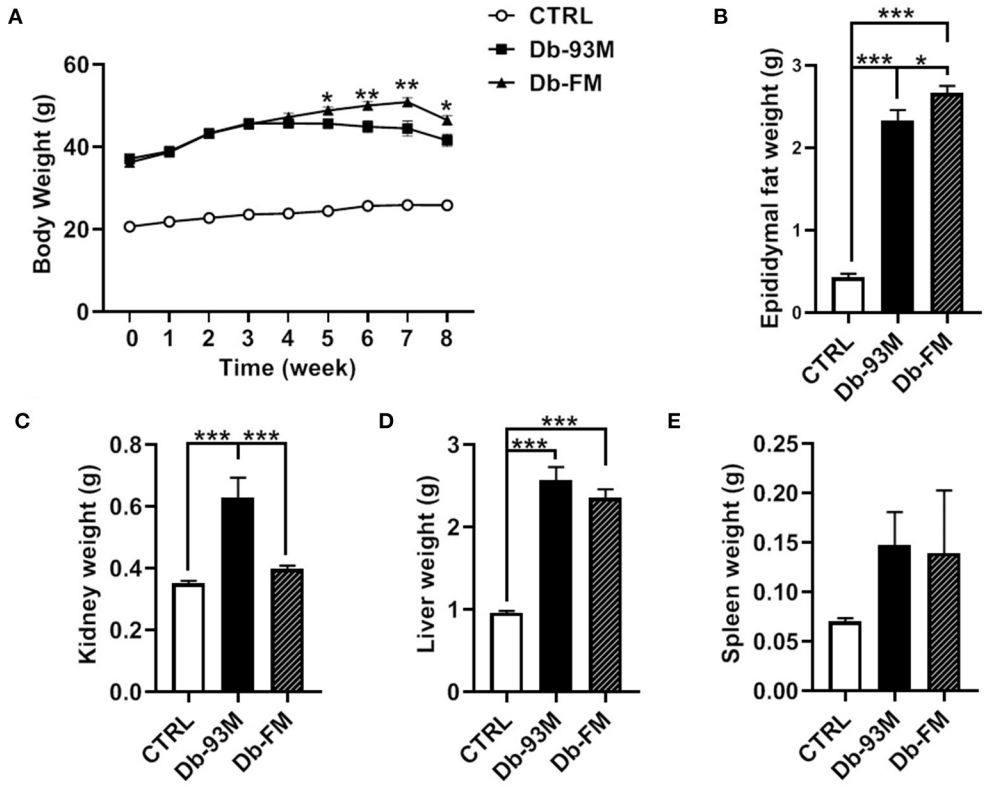

FIGURE 1 | Physiological parameters. **(A)** Body weight changes during 8 weeks on diets, asterisks indicate significant differences between the Db-93M group and the Db-FM group (*$p < 0.05$, **$p < 0.01$). **(B)** Epididymal fat weights comparison. **(C)** Kidney weights comparison. **(D)** Liver weights comparison. **(E)** Spleen weights comparison. Data are expressed as the mean ± SEM.

Db-93M group. In contrast, in the CTRL and Db-FM groups, the micro-structure of kidney tissues remained intact. These results together suggested that the FG-FM diet significantly alleviated kidney injury in the diabetic mouse model.

The kidney lesions of the mice in the Db-93M group were also associated with weight loss in the later period of feeding (from the 5th week onwards), due to the weight loss is an important feature of a mouse model with kidney disease. The Db/Db mice (Db-93M and Db-FM) had obvious fat droplets formation in the liver tissue compared to the CTRL group (**Figure 2E**).

Comparative Transcriptome Analysis of Kidney Tissues

An average of 50.38 ± 0.31, 52.23 ± 0.40, and 50.72 ± 0.34 million clean reads were obtained for the kidney tissues in mice from CTRL, Db-93M, and Db-FM groups, respectively. The clean reads were mapped to the mouse reference genome (http://asia.ensembl.org/Mus_musculus/Info/Index) with high proportions: CTRL group, 96.41%; Db-93M group, 96.94%; and Db-FM group, 96.93%.

The significantly differentially expressed genes (DEGs) were identified based on the quantification and comparison of gene expression levels of kidney tissues in mice from CTRL, Db-93M, and Db-FM groups. As shown in **Figure 3**, when comparing the groups with different genotypes fed with the same AIN-93M diet (CTRL *vs.* Db-93M), 4,112 DEGs, including 3,187 upregulated and 925 downregulated genes, were identified. When comparing the Db/Db groups fed with different diets (Db-93M *vs.* Db-FM), 2,800 DEGs, including 226 upregulated and 2,574 downregulated genes, were identified. Surprisingly, two groups of mice with different genotypes and different feeding (CTRL *vs.* Db-FM) showed minimal differences. Only 984 DEGs were identified, including 486 upregulated and 498 downregulated genes.

The KEGG enrichment analyses were performed to identify biological pathways significantly affected by different treatments. As shown in **Figure 4A**, when comparing the CTRL group and the Db-93M group, several signaling pathways related to inflammation, infection, and immunity were affected, including cytokine-cytokine receptor interaction pathway, natural killer mediated cytotoxicity pathway, B cell receptor signaling pathway, NF-κB signaling pathway, *etc*. The comparison between the Db-93M group and the Db-FM group also showed similar characteristics (**Figure 4C**). However, the affected signaling pathways in the comparison between the CTRL group and the Db-FM group did not show obvious associations with inflammation and immunity biological process (**Figure 4B**). Furthermore, among the top 20 most significant pathways resulting from KEGG enrichment analysis, 15 signaling pathways contained more than 100 DEGs in the comparison between CTRL and Db-93M, and also 15 in the comparison between

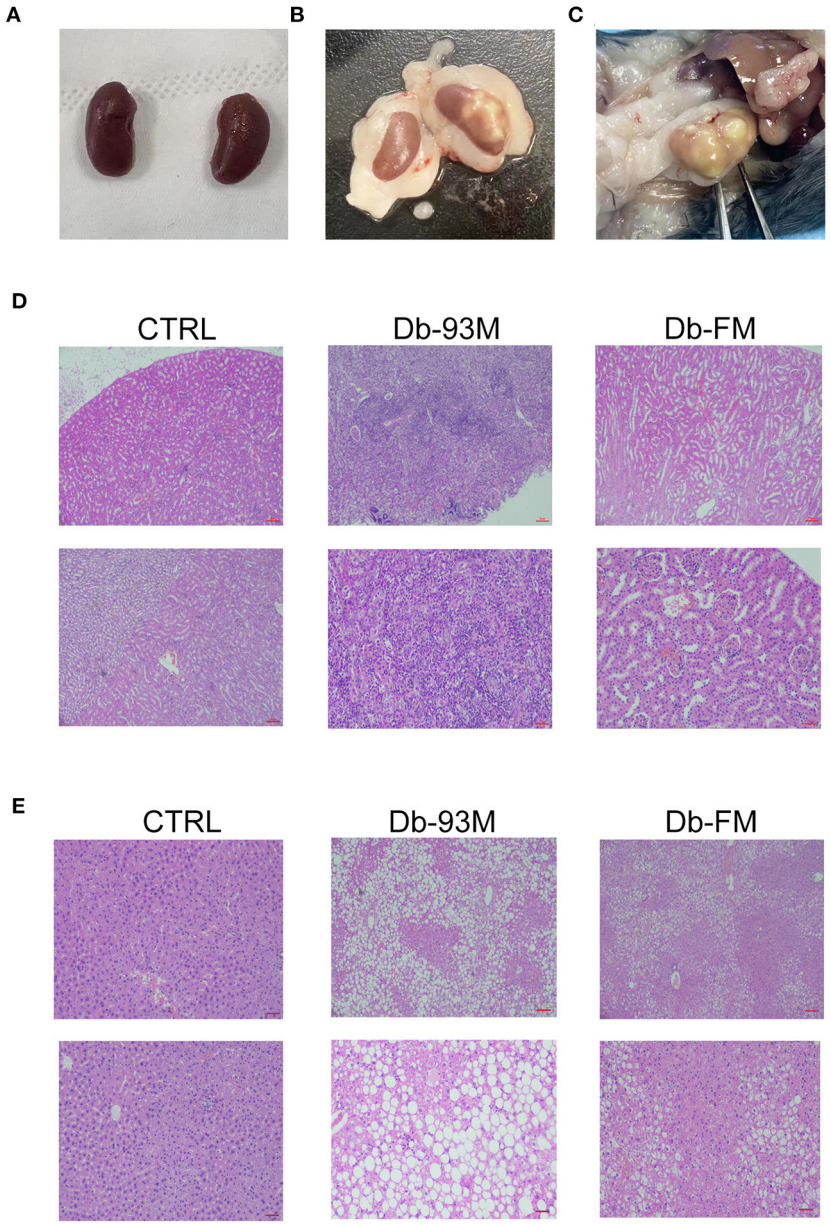

FIGURE 2 | Histopathological analysis. **(A)** The appearance and morphology of the kidneys from CTRL group; **(B)** the appearance and morphology of the kidneys, the left one is the kidney from the Db-FM group, the right one is the kidney from the Db-93M group; **(C)** the kidney of mice from the Db-93M group; **(D)** histopathological examination of kidney tissues (top: 40×; bottom: 200×); **(E)** histopathological examination of liver tissues (top: 40×; bottom: 200×).

Db-93M and Db-FM. Notably, none of the signaling pathways had more than 100 DEGs in the comparison between CTRL and Db-FM, and even the most affected signaling pathway contained only 36 DEGs. This also proved that, from the perspective of the transcriptome, the difference between the CTRL group and the Db-FM group was relatively inconspicuous, while the Db-93M group was significantly different from the other two groups.

When further analyzing the details of DEGs, a clear trend was observed. The changes that occurred in the Db-93M group (compared to the CTRL group) could be corrected in the Db-FM group. Take the cytokine-cytokine receptor interaction pathway as an example (**Supplementary Figure S1**), the abundance of chemokines and their receptors, including CCLs and CXCLs, as well as inflammatory cytokines and corresponding receptors, were significantly elevated in the Db-93M group when compared to CTRL group (**Supplementary Figure S1A**). Simultaneously, most of these upregulated genes were found to be significantly downregulated in the Db-FM group, when compared to the Db-93M group (**Supplementary Figure S1B**). Subsequently, the overactivation of the downstream signaling

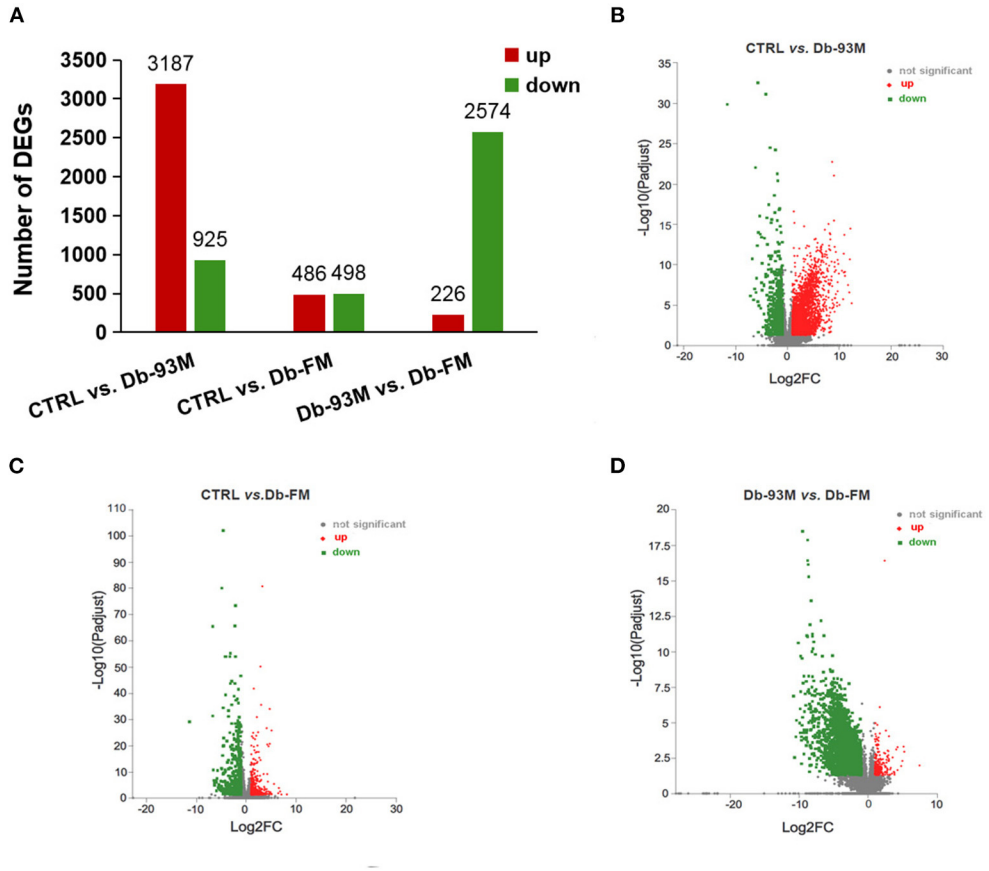

FIGURE 3 | The gene expression analysis performed by RNA-sequencing (RNA-Seq, $n = 6$). **(A)** Numbers of differential expressed genes (DEGs) in kidney tissue of different groups; the volcanic maps for DEGs in **(B)** CTRL *vs.* Db-93M group; the red dots were up-regulated, and the green dots were down-regulated in Db-93M group when compared to CTRL group. **(C)** CTRL *vs.* Db-FM groups; the red dots were up-regulated, and the green dots were down-regulated in the Db-FM group when compared to the CTRL group. **(D)** Db-93M *vs.* Db-FM group; the red dots were up-regulated, and the green dots were down-regulated in the Db-FM group when compared to the Db-93M group.

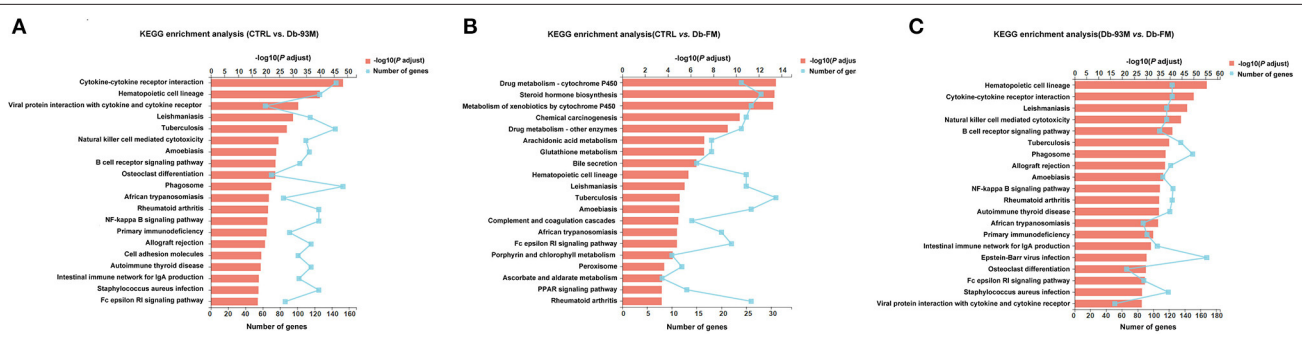

FIGURE 4 | The KEGG enrichment results (kidney tissues) based on the identified DEGs from. **(A)** Comparison of CTRL group and Db-93M group. **(B)** Comparison of CTRL group and Db-FM group. **(C)** Comparison of Db-93M group and Db-FM group.

pathway, such as the NF-κB signaling pathway caused by the overexpression of chemokines and inflammatory cytokines in the Db-93M group was also normalized in the Db-FM group (**Supplementary Figure S2**). In addition, other signaling pathways related to inflammation and immunity also showed a similar trend, which was overactivated in Db-93M, and this overactivation was re-inhibited in the Db-FM group (**Supplementary Figures S3**, **S4**, and **S5**). Taken together, these results showed that intake of FG-FM could significantly alleviate kidney damage in diabetic mice by inhibiting the overactivation

of signaling pathways in inflammation, infection, or immunity in the kidney.

The Gut Microbiota Composition Analysis

The microbial species richness (Chao, **Supplementary Figure 5A**) and diversity (Shannon, **Supplementary Figure 5B**) index were calculated to analyze the effect of FG-FM on the gut microbiota of Db/Db mice. There was no significant difference in the Chao index among the three groups, indicating that neither the genotypic difference nor FG-FM had a significant effect on the bacterial species richness of the gut microbiota. Moreover, no significant variations in the species diversity between the CTRL group and Db/Db groups were evidenced by the Shannon diversity index ($p = 0.17$). However, the Shannon index of Db-FM mice was significantly higher than that of Db-93M mice ($p = 0.0061$), indicating that FG-FM significantly enhanced the bacterial species diversity of gut microbiota in Db/Db mice.

The shared and specific OTUs analysis was demonstrated by the Venn diagram in **Figure 5C**. The gut microbiota of mice from the CTRL group had the largest number of unique OTUs (174), followed by that of the Db-FM group (144). Moreover, except for the OTUs shared by three groups (1093), the CTRL group and Db-FM had 432 shared OTUs, while the Db-93M group only shared 68 OTUs with the CTRL group and 55 OTUs with the Db-FM group. From these results, the intake of FG-FM could effectively change the gut microbiota of Db/Db mice, making them have more common microbiota characteristics with the CTRL group.

As illustrated in **Figures 5D,E**, gut microbiota composition varied in different groups. At the phylum level, the most abundant bacterial taxa was *Firmicutes* (CTRL, 43.90%; Db-93M, 41.93%; Db-FM, 43.60%) in all the three groups. The second dominant phylum was *Bacteroidetes* in gut microbiota (CTRL, 23.61%; Db-93M, 23.78%; Db-FM, 27.66%). Whereas in the Db-93M group, the relative abundance of phylum *Proteobacteria* (21.52%) increased dramatically, far more than the proportion of *Proteobacteria* in the gut microbiota from the other two groups (CTRL, 16.83%; Db-FM, 10.70%). At the genus level, the most abundant bacterial taxa in the CTRL group was *Akkermansia* (CTRL, 10.59%), followed by the *Lachnospiraceae* NK4A136 group (5.42%); in the Db-93M group, the most abundant bacterial taxa was *Lachnospiraceae* NK4A136 group (7.78%), followed by genus *Blautia* (6.58%); in Db-FM group, the most abundant bacterial taxa was *Mucispirillum* (11.32%), followed by genus *Lachnospiraceae* NK4A136 group (9.90%).

Taken together, these results showed that the consumption of FG-FM could effectively increase the bacterial diversity and reduce the proportion of phylum *Proteobacteria* in the gut microbiota of Db/Db mice. These prebiotic properties may contribute to preventing kidney disease in the diabetic mouse model.

LEfSe Analysis of Gut Microbiota

The effects of FG-FM on the gut microbiota of Db/Db mice were further analyzed by LFfSe (LDA Effect Size), and the results (LEfSe Cladogram and histogram of LDA scores) were demonstrated in **Figures 6A,B**. By comparing the gut microbiota of the Db-93M and Db-FM groups, a total of 57 different bacterial taxa were found, including 22 dominant bacterial taxa in the gut microbiota of the Db-FM group and 35 dominant bacterial taxa in the Db-93M group. The relative abundances of several commensal bacteria that have been reported contributing to inflammation control and disease prevention were significantly higher in the Db-FM group than in the Db-93M group. For example, *Ruminococcaceae* (41), *Odoribacter* (42), *Ileibacterium* (43), *Lachnospiraceae* NK4A136 (44), *Rikenellaceae* RC9 gut group (45), and *Mucispirillum schaedleri* (46). The details of representative taxa are shown in **Figure 6C**. Furthermore, the important "signature" bacteria of dysbiosis in gut microbiota, including *Proteobacteria* and *Escherichia-Shigella* (47–49) were found to be significantly enriched in the Db-93M group. The results of the LEfSe analysis further validated the prebiotic characteristics of FG-FM cereal flour, including promoting the proliferation of probiotics and limiting the expansion of previously reported DKD-related bacteria in the gut microbiota of diabetic mouse model (15).

DISCUSSION

A substantial proportion of diabetic patients will develop DKD, which is the leading cause of chronic kidney disease and even end-stage kidney disease globally (50). Dietary and nutritional factors play key roles in the progression of DKD (51, 52). Foxtail millet is a typical underutilized crop which has received less attention than main crops. In the current study, we have identified a novel function of FG-FM in preventing kidney damage associated with diabetes mellitus. The FG-FM diet significantly alleviated the morphological lesions of the kidney as well as the overactivation of inflammatory and cytokine signaling pathways in the kidney of diabetic mice. Moreover, the gut microbiota analysis revealed the FG-FM diet as an excellent prebiotic in the prevention of kidney disease. Our study provided a novel non-pharmacological intervention strategy for Diabetic kidney disease (DKD)

Transcriptomics analysis revealed that a large number of genes involved in inflammatory and immune signaling pathways were overactivated in the kidney tissues of Db-93M mice, indicating a high level of inflammation in the kidney of diabetic mice. In addition, we also observed severe kidney lesions in these mice when no special diet intervention was applied. These results clearly demonstrated the development of DKD in diabetic mice. However, the FG-FM intervention protected the kidney from developing both the high levels of inflammation and the morphological damage in the diabetic mice. Inflammation is a well-established feature of DKD, manifested as the increased level of inflammatory cytokines in the serum of DKD patients, as well as anti-inflammatory treatments are effective in the prevention of DKD (53, 54). Notably, we found that the transcription of chemokines and their receptors, including CCLs and CXCLs, as well as several inflammatory cytokines, such as IL1β and TNFα, were significantly upregulated in the kidney of diabetic mice, while such elevation was not observed in mice fed with the

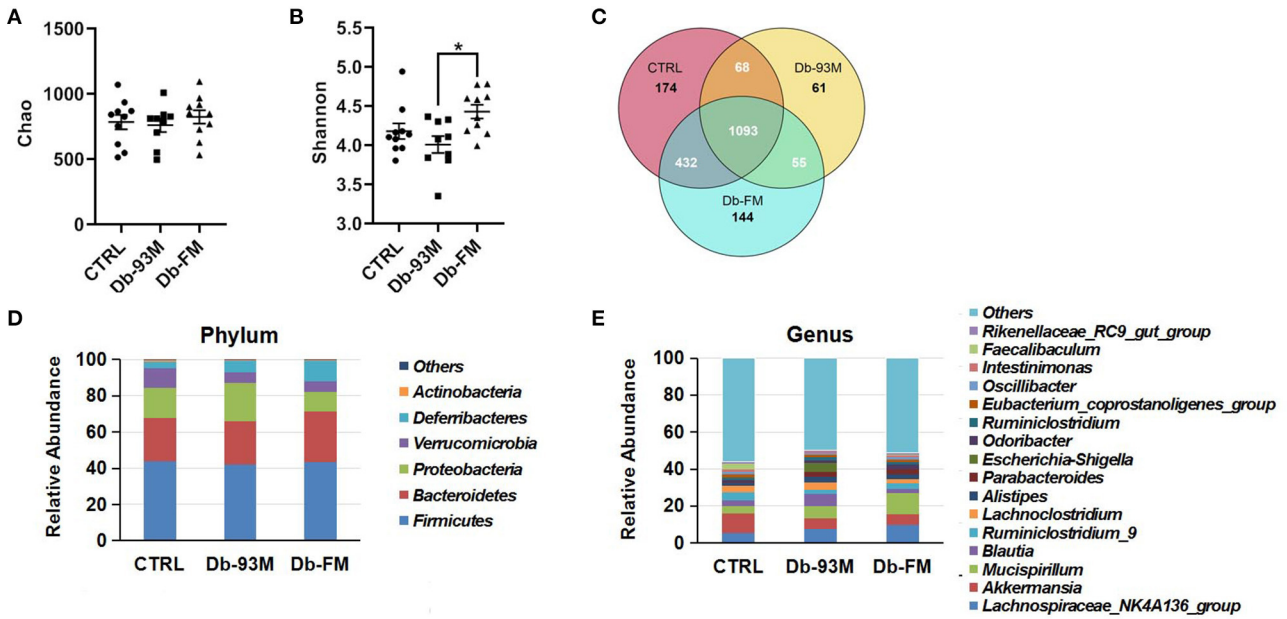

FIGURE 5 | The gut microbiota composition analysis. **(A)** The microbial richness index of Chao. **(B)** The microbial diversity index of Shannon. **(C)** Venn diagrams that illustrated observed overlap of OTUs from different groups. **(D)** The composition of gut microbiota in mice at phylum level. **(E)** The composition of gut microbiota in mice at the genus level. "Others" represent the sum of all the phyla/genera, which abundances were under 1%. Data are expressed as the mean ± SEM.

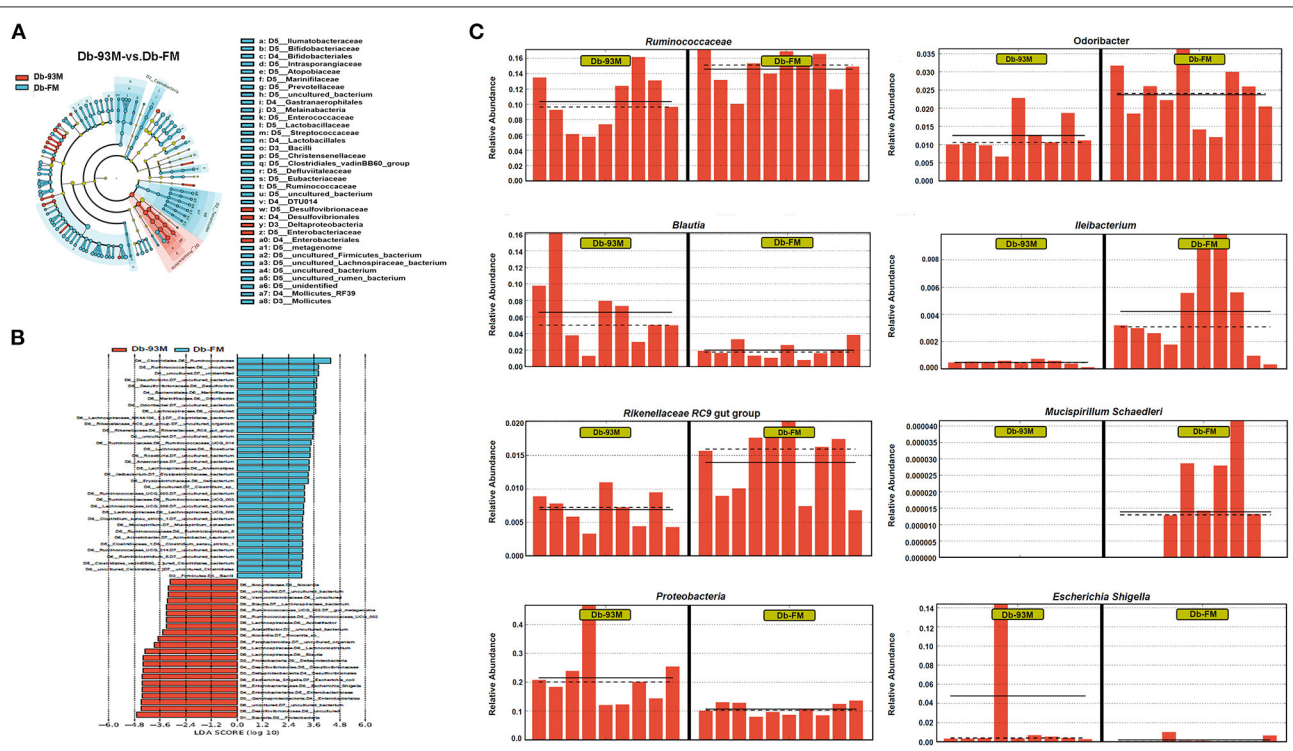

FIGURE 6 | LEfSe analysis of gut microbiota. **(A)** Effect size of significantly enriched taxa in each group when performing a comparison between Db-93M group and Db-FM group. **(B)** Taxonomic cladogram obtained using LEfSe analysis result from the comparison between Db-93Mgroup and Db-FM group. **(C)** Relative abundance of representative bacterial taxa in the gut microbiota of Db-93M group and Db-FM group identified by LEfSe analysis.

FG-FM diet. In support of our results, the overexpression of CCLs, CXCLs, and inflammatory cytokines has been proved to be associated with DKD or other kidney diseases (55–57) and has been widely used to induce kidney injury in animal models (58–60). Besides chemokines, the over expression of several inflammatory cytokines, such as IL1β and TNFα, have been identified as biomarkers in diabetic kidney disease (61). Their overexpression is not only an indicator of kidney inflammation but also a trigger for further deterioration of renal lesions (62). Therefore, the suppression of these hyperactivated inflammatory or immune-related cytokines and signaling pathways in the Db-FM group could strongly explain the rescue effects of FG-FM on kidney lesions in diabetic mice. Our findings not only confirmed the function of the FG-FM diet at the transcriptional level, but also partially explained its molecular mechanism for relieving renal lesions.

Consistent with the alleviated DKD symptoms in Db-FM groups, improvement in the gut microbiota was also identified. In line with what we found, the reduction of bacterial diversity has been reported previously exist in patients (63, 64) and animal models (65) with kidney disease. We, therefore, speculate that the promotion of microbial diversity index may be attributed to the prebiotic properties of FG-FM and beneficial for the alleviation of nephropathy symptoms in diabetic mice (66). The proliferation of probiotics in the gut microbiota of the Db-FM group is also important evidence of the prebiotic function of FG-FM. For example, the relative abundance of several SCFAs producing bacteria, such as *Odoribacter*, *Lachnospiraceae NK4A136*, and *Rikenellaceae RC9 gut group* (67–69), was obviously increased by FG-FM ingestion. SCFAs have the ability to ameliorate diabetic nephropathy via inhibition of the NF-κB signaling pathway (70). Coincidentally, the transcriptome analysis displayed that the overactivation of the NF-κB signaling pathway in the Db-93M group was normalized in the Db-FM group. Furthermore, the unusual expansion of *Proteobacteria* and *Escherichia-Shigella* has been considered as common features of the imbalanced gut microbiota in different inflammatory-related diseases (49, 71, 72), and the decrease in the proportion of *Proteobacteria* and *Escherichia-Shigella* in the gut microbiota of mice in the Db-FM group could be regarded as a sign of the improved gut microbiota. Taken together, our study proved that FG-FM could inhibit the overactivation of inflammatory signaling pathways via restoring the pro-inflammatory characteristics of gut microbiota, thereby preventing the occurrence of renal lesions in diabetic mice.

In conclusion, our study demonstrated that diet intervention with fermented and germinated foxtail millet whole grain (FG-FM) could effectively prevent and protect DKD in the diabetic mouse model. At the same time, we revealed the excellent prebiotic function of FG-FM in preventing kidney disease. The promising results from our animal study provide a non-pharmacological strategy for preventing DKD through functional foods developed based on foxtail millet whole grain.

DATA AVAILABILITY STATEMENT

The datasets presented in this study can be found in online repositories. The names of the repository/repositories and accession number(s) can be found below: NCBI SRA; PRJNA835687.

ETHICS STATEMENT

The animal study was reviewed and approved by Institutional Animal Care and Use Committees of the Qilu Hospital of Shandong University.

AUTHOR CONTRIBUTIONS

Conceptualization, data curation, and validation: DZ and LL. Methodology: XLiu, WL, and BQ. Investigation: XLiu, WL, BQ, YZ, and XW. Writing-original draft preparation: XLiu and WL. Writing-review and editing: DZ and XLi. Project administration: DZ. Funding acquisition: DZ and BQ. All authors have read and agreed to the published version of the manuscript.

FUNDING

This research was funded by National Science Foundation of China grants (82071512), Shandong Provincial Natural Science Foundation grant (ZR2019ZD33), Shandong Provincial Key Research and Development program (2019GHZ031), and Research Project of Jinan Microecological Biomedicine Shandong Laboratory (JNL-2022003A to XLi).

SUPPLEMENTARY MATERIAL

The Supplementary Material for this article can be found online at: https://www.frontiersin.org/articles/10.3389/fnut.2022.940404/full#supplementary-material

REFERENCES

1. Organization. WH. Diabetes (10 November 2021). Available online at: https://www.who.int/health-topics/diabetes#tab=tab_1
2. Papatheodorou K, Banach M, Bekiari E, Rizzo M, Edmonds M. Complications of Diabetes 2017. *J Diabetes Res.* (2018) 2018:3086167. doi: 10.1155/2018/3086167
3. Afkarian M, Zelnick LR, Hall YN, Heagerty PJ, Tuttle K, Weiss NS, et al. Clinical manifestations of kidney disease among us adults with diabetes, 1988–2014. *JAMA.* (2016) 316:602–10. doi: 10.1001/jama.2016.10924
4. Srivastava SP, Zhou H, Setia O, Liu B, Kanasaki K, Koya D, et al. Loss of endothelial glucocorticoid receptor accelerates diabetic nephropathy. *Nat Commun.* (2021) 12:2368. doi: 10.1038/s41467-021-22617-y
5. Afkarian M, Sachs MC, Kestenbaum B, Hirsch IB, Tuttle KR, Himmelfarb J, et al. Kidney disease and increased mortality risk in type 2 diabetes. *J Am Soc Nephrol.* (2013) 24:302–8. doi: 10.1681/ASN.2012070718
6. Koya D, Araki S, Haneda M. Therapeutic management of diabetic kidney disease. *J Diabetes Investig.* (2011) 2:248–54. doi: 10.1111/j.2040-1124.2011.00112.x

7. Backhed F, Ley RE, Sonnenburg JL, Peterson DA, Gordon JI. Host-bacterial mutualism in the human intestine. *Science.* (2005) 307:1915–20. doi: 10.1126/science.1104816
8. Upadhyaya S, Banerjee G. Type 2 Diabetes and gut microbiome: at the intersection of known and unknown. *Gut Microbes.* (2015) 6:85–92. doi: 10.1080/19490976.2015.1024918
9. Saxena R, Sharma VK. Chapter 9 - a Metagenomic Insight into the Human Microbiome: Its Implications in Health and Disease. In: Kumar D, Antonarakis S, editors. *Medical and Health Genomics*. Oxford: Academic Press (2016). p. 107-19.
10. Yu LC. Microbiota Dysbiosis and barrier dysfunction in inflammatory bowel disease and colorectal cancers: exploring a common ground hypothesis. *J Biomed Sci.* (2018) 25:79. doi: 10.1186/s12929-018-0483-8
11. Wu HJ, Wu E. The role of gut microbiota in immune homeostasis and autoimmunity. *Gut Microbes.* (2012) 3:4–14. doi: 10.4161/gmic.19320
12. Ni J, Wu GD, Albenberg L, Tomov VT. Gut microbiota and ibd: causation or correlation? *Nat Rev Gastroenterol Hepatol.* (2017) 14:573–84. doi: 10.1038/nrgastro.2017.88
13. Tremaroli V, Backhed F. Functional interactions between the gut microbiota and host metabolism. *Nature.* (2012) 489:242–9. doi: 10.1038/nature11552
14. Cheng WY, Wu CY Yu J. The role of gut microbiota in cancer treatment: friend or foe? *Gut*. (2020) 69:1867–76. doi: 10.1136/gutjnl-2020-321153
15. He X, Sun J, Liu C, Yu X, Li H, Zhang W, et al. Compositional alterations of gut microbiota in patients with diabetic kidney disease and type 2 diabetes mellitus. *Diabetes Metab Syndr Obes.* (2022) 15:755–65. doi: 10.2147/DMSO.S347805
16. Ramezani A, Raj DS. the gut microbiome, kidney disease, and targeted interventions. *J Am Soc Nephrol.* (2014) 25:657–70. doi: 10.1681/ASN.2013080905
17. Koppe L, Fouque D, Soulage CO. Metabolic abnormalities in diabetes and kidney disease: role of uremic toxins. *Curr Diab Rep*. (2018) 18:97. doi: 10.1007/s11892-018-1064-7
18. Salguero MV, Al-Obaide MAI, Singh R, Siepmann T, Vasylyeva TL. Dysbiosis of gram-negative gut microbiota and the associated serum lipopolysaccharide exacerbates inflammation in type 2 diabetic patients with chronic kidney disease. *Exp Ther Med.* (2019) 18:3461–9. doi: 10.3892/etm.2019.7943
19. Cai K, Ma Y, Cai F, Huang X, Xiao L, Zhong C, et al. Changes of gut microbiota in diabetic nephropathy and its effect on the progression of kidney injury. *Endocrine.* (2022) 76:294–303. doi: 10.1007/s12020-022-03002-1
20. Kolodziejczyk AA, Zheng D, Elinav E. Diet-microbiota interactions and personalized nutrition. *Nat Rev Microbiol.* (2019) 17:742–53. doi: 10.1038/s41579-019-0256-8
21. Devi PB, Vijayabharathi R, Sathyabama S, Malleshi NG. Priyadarisini VB. Health benefits of finger millet (*Eleusine Coracana L*) polyphenols and dietary fiber: a review. *J Food Sci Technol.* (2014) 51:1021–40. doi: 10.1007/s13197-011-0584-9
22. Verma S, Srivastava S, Tiwari N. Comparative study on nutritional and sensory quality of barnyard and foxtail millet food products with traditional rice products. *J Food Sci Technol.* (2015) 52:5147–55. doi: 10.1007/s13197-014-1617-y
23. Dong JL, Wang L, Lu J, Zhu YY, Shen RL. Structural, Antioxidant and adsorption properties of dietary fiber from foxtail millet (*Setaria Italica*) bran. *J Sci Food Agric.* (2019) 99:3886–94. doi: 10.1002/jsfa.9611
24. Kam J, Puranik S, Yadav R, Manwaring HR, Pierre S, Srivastava RK, et al. Dietary interventions for type 2 diabetes: how millet comes to help. *Front Plant Sci.* (2016) 7:1454. doi: 10.3389/fpls.2016.01454
25. Liu F, Shan S, Li H, Li Z. Treatment of peroxidase derived from foxtail millet bran attenuates atherosclerosis by inhibition of Cd36 and Stat3 *in vitro* and *in vivo*. *J Agric Food Chem.* (2020) 68:1276–85. doi: 10.1021/acs.jafc.9b06963
26. Kumar A, Henderson A, Forster GM, Goodyear AW, Weir TL, Leach JE, et al. Dietary rice bran promotes resistance to salmonella enterica serovar typhimurium colonization in mice. *BMC Microbiol.* (2012) 12:71. doi: 10.1186/1471-2180-12-71
27. Chu J, Zhao H, Lu Z, Lu F, Bie X, Zhang C. Improved physicochemical and functional properties of dietary fiber from millet bran fermented by bacillus natto. *Food Chem.* (2019) 294:79–86. doi: 10.1016/j.foodchem.2019.05.035
28. Sharma S, Saxena DC, Riar CS. Changes in the gaba and polyphenols contents of foxtail millet on germination and their relationship with in vitro antioxidant activity. *Food Chem.* (2018) 245:863–70. doi: 10.1016/j.foodchem.2017.11.093
29. Sharma N, Alam T, Goyal SK, Fatma S, Pathania S, Niranajan K. Effect of different storage conditions on analytical and sensory quality of thermally processed, milk-based germinated foxtail millet porridge. *J Food Sci.* (2018) 83:3076–84. doi: 10.1111/1750-3841.14371
30. Zhang J, Kobert K, Flouri T, Stamatakis A. Pear: a fast and accurate illumina paired-end read merger. *Bioinformatics.* (2014) 30:614–20. doi: 10.1093/bioinformatics/btt593
31. Kechin A, Boyarskikh U, Kel A, Filipenko M. Cutprimers: a new tool for accurate cutting of primers from reads of targeted next generation sequencing. *J Comput Biol.* (2017) 24:1138–43. doi: 10.1089/cmb.2017.0096
32. Quast C, Pruesse E, Yilmaz P, Gerken J, Schweer T, Yarza P, et al. The silva ribosomal rna gene database project: improved data processing and web-based tools. *Nucleic Acids Res.* (2013) 41:D590–6. doi: 10.1093/nar/gks1219
33. Caporaso JG, Kuczynski J, Stombaugh J, Bittinger K, Bushman FD, Costello EK, et al. Qiime allows analysis of high-throughput community sequencing data. *Nat Methods.* (2010) 7:335–6. doi: 10.1038/nmeth.f.303
34. Kim D, Langmead B, Salzberg SL. Hisat: a fast spliced aligner with low memory requirements. *Nat Methods.* (2015) 12:357–60. doi: 10.1038/nmeth.3317
35. Trapnell C, Williams BA, Pertea G, Mortazavi A, Kwan G, van Baren MJ, et al. Transcript assembly and quantification by rna-seq reveals unannotated transcripts and isoform switching during cell differentiation. *Nat Biotechnol.* (2010) 28:511–5. doi: 10.1038/nbt.1621
36. Pertea M, Pertea GM, Antonescu CM, Chang TC, Mendell JT, Salzberg SL. Stringtie enables improved reconstruction of a transcriptome from Rna-Seq reads. *Nat Biotechnol.* (2015) 33:290–5. doi: 10.1038/nbt.3122
37. Li B, Dewey CN. Rsem: Accurate transcript quantification from Rna-Seq data with or without a reference genome. *BMC Bioinformatics.* (2011) 12:323. doi: 10.1186/1471-2105-12-323
38. Love MI, Huber W, Anders S. Moderated estimation of fold change and dispersion for Rna-Seq data with Deseq2. *Genome Biol.* (2014) 15:550. doi: 10.1186/s13059-014-0550-8
39. Robinson MD, McCarthy DJ, Smyth GK. Edger: a bioconductor package for differential expression analysis of digital gene expression data. *Bioinformatics.* (2010) 26:139–40. doi: 10.1093/bioinformatics/btp616
40. Klopfenstein DV, Zhang L, Pedersen BS, Ramirez F, Warwick Vesztrocy A, Naldi A, et al. Goatools: a python library for gene ontology analyses. *Sci Rep.* (2018) 8:10872. doi: 10.1038/s41598-018-28948-z
41. Schirmer M, Garner A, Vlamakis H, Xavier RJ. Microbial genes and pathways in inflammatory bowel disease. *Nat Rev Microbiol.* (2019) 17:497–511. doi: 10.1038/s41579-019-0213-6
42. Hiippala K, Barreto G, Burrello C, Diaz-Basabe A, Suutarinen M, Kainulainen V, et al. Novel odoribacter splanchnicus strain and its outer membrane vesicles exert immunoregulatory effects *in vitro*. *Front Microbiol.* (2020) 11:575455. doi: 10.3389/fmicb.2020.575455
43. Wang Y, Ablimit N, Zhang Y, Li J, Wang X, Liu J, et al. Novel Beta-Mannanase/Glp-1 fusion peptide high effectively ameliorates obesity in a mouse model by modifying balance of gut microbiota. *Int J Biol Macromol.* (2021) 191:753–63. doi: 10.1016/j.ijbiomac.2021.09.150
44. Li L, Bao J, Chang Y, Wang M, Chen B, Yan F. Gut microbiota may mediate the influence of periodontitis on prediabetes. *J Dent Res.* (2021) 100:1387–96. doi: 10.1177/00220345211009449
45. Hu C, Ding L, Jiang C, Ma C, Liu B, Li D, et al. Effects of management, dietary intake, and genotype on rumen morphology, fermentation, and microbiota, and on meat quality in yaks and cattle. *Front Nutr.* (2021) 8:755255. doi: 10.3389/fnut.2021.755255
46. Herp S, Brugiroux S, Garzetti D, Ring D, Jochum LM, Beutler M, et al. Mucispirillum schaedleri antagonizes salmonella virulence to protect mice against colitis. *Cell Host Microbe*. (2019) 25:681–94. doi: 10.1016/j.chom.2019.03.004
47. Thingholm LB, Ruhlemann MC, Koch M, Fuqua B, Laucke G, Boehm R, et al. Obese individuals with and without type 2 diabetes show different gut microbial functional capacity and composition. *Cell Host Microbe.* (2019) 26:252–64. doi: 10.1016/j.chom.2019.07.004
48. Baothman OA, Zamzami MA, Taher I, Abubaker J, Abu-Farha M. The role of gut microbiota in the development of obesity and diabetes. *Lipids Health Dis.* (2016) 15:108. doi: 10.1186/s12944-016-0278-4

49. Shin NR, Whon TW, Bae JW. Proteobacteria: microbial signature of dysbiosis in gut microbiota. *Trends Biotechnol.* (2015) 33:496–503. doi: 10.1016/j.tibtech.2015.06.011
50. Alicic RZ, Rooney MT, Tuttle KR. Diabetic kidney disease: challenges, progress, and possibilities. *Clin J Am Soc Nephrol.* (2017) 12:2032–45. doi: 10.2215/CJN.11491116
51. Li Q, Wen F, Wang Y, Li S, Lin S, Qi C, et al. Diabetic kidney disease benefits from intensive low-protein diet: updated systematic review and meta-analysis. *Diabetes Ther.* (2021) 12:21–36. doi: 10.1007/s13300-020-00952-5
52. Pereira RA, Ramos CI, Teixeira RR, Muniz GAS, Claudino G, Cuppari L. Diet in Chronic Kidney Disease: An Integrated Approach to Nutritional Therapy. *Rev Assoc Med Bras.* (1992) (2020):s59–s67. doi: 10.1590/1806-9282.66.S1.59
53. Garcia-Garcia PM, Getino-Melian MA, Dominguez-Pimentel V, Navarro-Gonzalez JF. Inflammation in diabetic kidney disease. *World J Diabetes.* (2014) 5:431–43. doi: 10.4239/wjd.v5.i4.431
54. Perez-Morales RE, Del Pino MD, Valdivielso JM, Ortiz A, Mora-Fernandez C, Navarro-Gonzalez JF. Inflammation in diabetic kidney disease. *Nephron.* (2019) 143:12–6. doi: 10.1159/000493278
55. Pawlak K, Kowalewska A, Mysliwiec M, Pawlak D. 3-Hydroxyanthranilic acid is independently associated with monocyte chemoattractant protein-1 (Ccl2) and macrophage inflammatory protein-1beta (Ccl4) in patients with chronic kidney disease. *Clin Biochem.* (2010) 43:1101–6. doi: 10.1016/j.clinbiochem.2010.06.008
56. Guo L, Lv J, Zhang J, Deng H, Feng S, Liu S, et al. Elevated serum Il-21 levels are associated with stable immune status in kidney transplant recipients and a mouse model of kidney transplantation. *Aging.* (2020) 12:18396–414. doi: 10.18632/aging.103713
57. Mehaffey E, Majid DSA. Tumor necrosis factor-alpha, kidney function, and hypertension. *Am J Physiol Renal Physiol.* (2017) 313:F1005–F8. doi: 10.1152/ajprenal.00535.2016
58. Unsal V, Cicek M, Sabancilar I. Toxicity of carbon tetrachloride, free radicals and role of antioxidants. *Rev Environ Health.* (2021) 36:279–95. doi: 10.1515/reveh-2020-0048
59. Sahreen S, Khan MR, Khan RA, Alkreathy HM. Protective effects of carissa opaca fruits against ccl4-induced oxidative kidney lipid peroxidation and trauma in rat. *Food Nutr Res.* (2015) 59:28438. doi: 10.3402/fnr.v59.28438
60. Pedigo CE, Ducasa GM, Leclercq F, Sloan A, Mitrofanova A, Hashmi T, et al. Local Tnf causes Nfatc1-dependent cholesterol-mediated podocyte injury. *J Clin Invest.* (2016) 126:3336–50. doi: 10.1172/JCI85939
61. Araujo LS, Torquato BGS, da Silva CA, Dos Reis Monteiro MLG, Dos Santos Martins ALM, da Silva MV, et al. Renal expression of cytokines and chemokines in diabetic nephropathy. *BMC Nephrol.* (2020) 21:308. doi: 10.1186/s12882-020-01960-0
62. Wen Y, Lu X, Ren J, Privratsky JR, Yang B, Rudemiller NP, et al. Klf4 in macrophages attenuates tnfalpha-mediated kidney injury and fibrosis. *J Am Soc Nephrol.* (2019) 30:1925–38. doi: 10.1681/ASN.2019020111
63. Wu PH, Liu PY, Chiu YW, Hung WC, Lin YT, Lin TY, et al. Comparative gut microbiome differences between ferric citrate and calcium carbonate phosphate binders in patients with end-stage kidney disease. *Microorganisms.* (2020) 8:2040. doi: 10.3390/microorganisms8122040
64. Jiang S, Xie S, Lv D, Wang P, He H, Zhang T, et al. Alteration of the gut microbiota in chinese population with chronic kidney disease. *Sci Rep.* (2017) 7:2870. doi: 10.1038/s41598-017-02989-2
65. Singh H, Miyamoto S, Darshi M, Torralba MG, Kwon K, Sharma K, et al. Gut microbial changes in diabetic db/db mice and recovery of microbial diversity upon pirfenidone treatment. *Microorganisms.* (2020) 8:1347. doi: 10.3390/microorganisms8091347
66. Chen C, You LJ, Huang Q, Fu X, Zhang B, Liu RH, et al. Modulation of gut microbiota by mulberry fruit polysaccharide treatment of obese diabetic Db/Db mice. *Food Funct.* (2018) 9:3732–42. doi: 10.1039/c7fo01346a
67. Brandsma E, Kloosterhuis NJ, Koster M, Dekker DC, Gijbels MJJ, van der Velden S, et al. A proinflammatory gut microbiota increases systemic inflammation and accelerates atherosclerosis. *Circ Res.* (2019) 124:94–100. doi: 10.1161/CIRCRESAHA.118.313234
68. Zhang J, Song L, Wang Y, Liu C, Zhang L, Zhu S, et al. Beneficial effect of butyrate-producing lachnospiraceae on stress-induced visceral hypersensitivity in rats. *J Gastroenterol Hepatol.* (2019) 34:1368–76. doi: 10.1111/jgh.14536
69. Jiang W, Wu N, Wang X, Chi Y, Zhang Y, Qiu X, et al. Dysbiosis gut microbiota associated with inflammation and impaired mucosal immune function in intestine of humans with non-alcoholic fatty liver disease. *Sci Rep.* (2015) 5:8096. doi: 10.1038/srep08096
70. Huang W, Man Y, Gao C, Zhou L, Gu J, Xu H, et al. Short-chain fatty acids ameliorate diabetic nephropathy Via Gpr43-mediated inhibition of oxidative stress and Nf-Kappab signaling. *Oxid Med Cell Longev.* (2020) 2020:4074832. doi: 10.1155/2020/4074832
71. Rizzatti G, Lopetuso LR, Gibiino G, Binda C, Gasbarrini A. Proteobacteria: a common factor in human diseases. *Biomed Res Int.* (2017) 2017:9351507. doi: 10.1155/2017/9351507
72. Bradley PH, Pollard KS. Proteobacteria explain significant functional variability in the human gut microbiome. *Microbiome.* (2017) 5:36. doi: 10.1186/s40168-017-0244-z

Conflict of Interest: The authors declare that the research was conducted in the absence of any commercial or financial relationships that could be construed as a potential conflict of interest.

frontiers | Frontiers in Nutrition

ORIGINAL RESEARCH
published: 07 July 2022
doi: 10.3389/fnut.2022.952525

Impact of Fermented Wheat Bran Dietary Fiber Addition on Dough Rheological Properties and Noodle Quality

Ling Fan[1], *Li Li*[2,3], *Anmin Xu*[2], *Jihong Huang*[1,2,3]* *and Sen Ma*[1,2,3]*

[1] Food and Pharmacy College, Xuchang University, Xuchang, China, [2] College of Food Science and Engineering, Henan University of Technology, Zhengzhou, China, [3] State Key Laboratory of Crop Stress Adaptation and Improvement, College of Agriculture, Henan University, Kaifeng, China

This study aimed to evaluate the effect of fermented wheat bran dietary fiber (FWBDF) on the rheological properties of the dough and the quality of noodles and to compare it with the effect of the unfermented WBDF (UWBDF). WBDF was fermented with *Auricularia polytricha*. The results showed that adding UWBDF/FWBDF increased the storage modulus *G'* and loss modulus *G"* of the dough, converted α-helices and β-turns into β-sheets and random coils, respectively, inhibited water flow, increased cooking loss, and decreased the maximum resistance in the noodles. The formed gluten network had a more random and rigid structure, resulting in the deterioration of the quality of noodles. Furthermore, the number of α-helices and the peak proportions of weakly bound water A_{22} increased but the number of β-sheets and cooking loss decreased in the FWBDF group compared with the UWBDF group. FWBDF (≤4%) improved the hardness of noodles, while UWBDF decreased it. These changes indicated that fermentation could reduce the destructive effects of WBDF on the quality of noodles, providing a new perspective on balancing dietary fiber-rich and high-quality foods.

Keywords: wheat bran, dietary fiber, fermentation, protein network, noodle quality

OPEN ACCESS

Edited by:
Jinsong Bao,
Zhejiang University, China

Reviewed by:
Di Zhao,
Nanjing Agricultural University, China
Bin Du,
Hebei Normal University of Science and Technology, China

***Correspondence:**
Jihong Huang
huangjih1216@126.com
Sen Ma
masen@haut.edu.cn

Specialty section:
This article was submitted to Food Chemistry, a section of the journal Frontiers in Nutrition

Received: *25 May 2022*
Accepted: *09 June 2022*
Published: *07 July 2022*

Citation:
Fan L, Li L, Xu A, Huang J and Ma S (2022) Impact of Fermented Wheat Bran Dietary Fiber Addition on Dough Rheological Properties and Noodle Quality. Front. Nutr. 9:952525. doi: 10.3389/fnut.2022.952525

INTRODUCTION

Developing food products with high dietary fiber content has become an effective way to change the dietary pattern of consumers for meeting the growing demand for healthy food. An increase in the consumption of dietary fiber is recommended in most European countries, as adequate intake of dietary fiber can improve human health and the management of health diseases (1, 2). Dietary fiber is an important natural carbohydrate polymer that is major component of plant cell walls and is not digested or absorbed by the small intestine. Due to its porous physical structure and the abundant hydroxyl groups in the side chain, dietary fiber has good water retention and hydrogen bond forming capabilities (3). Moreover, in the plant cell walls, phenolic compounds are always combined with the backbone of dietary fiber, which gives dietary fiber good antioxidant capacity (2, 4). In addition, dietary fiber can selectively stimulate the activity or growth of probiotic bacteria in the colon, thereby improving the microbial balance in the gut, which in turn has a beneficial effect on the health of the host (2, 5). Also, dietary fiber effectively prevents colonic diseases, loses weight, lowers cholesterol, and regulates gut microbe metabolism and intestinal microbial metabolism (6, 7).

Recently, the trend is to enhance the dietary fiber content of traditional flour-based products, such as noodles. However, dietary fiber is associated with the low quality of wheat flour products based on the interaction between dietary fiber and the gluten matrix. Many researchers focused on modifying the properties of dietary fiber to reduce its destructive effects on end-use products while anticipating the desirable effects on its physiological and functional properties (8–10). Several studies have emphasized that fermentation is an effective way to improve the properties of wheat bran, thus increasing the content and bioavailability of the functional compounds such as soluble fiber and phenolic substances, degrading antinutritive factors such as phytic acid, and significantly improving the antioxidant capacity (11–13). Meanwhile, fermentation can effectively reduce the side effects of bran on bread volume, positively affecting the overall characteristics of the final bread (14, 15). The fermentation of *Fomitopsis pinicola* can not only increase the contents of total phenol and alkylresorcinols of wheat bran but also improve the textural properties of the dough and bread (16).

Auricularia polytricha (*A. polytricha*), an edible fungus classified as a Basidiomycota, has been shown to efficiently degrade lignocellulose *via* its oxidative ligninolytic systems. At present, edible fungi are recognized as safe strains producing various enzymes such as cellulase and amylase during the fermentation process (17). Also, these enzymes can improve the chemical composition and biological activity of the substrates. *A. polytricha* is reported to have many functions such as anti-oxidation, tumor suppression, and anti-nociceptive activity; it has been widely used as a healthy food in Oriental countries, especially in China and Korea (18). Lignin creates the recalcitrant and complex structure in WBDF by filling the spaces around the cellulose and hemicellulose structures and binding them together, thus serving as a barrier to the formation of the gluten network structure (19). Furthermore, wheat bran dietary fiber (WBDF) can cause deterioration in the quality of products due to its specific structure. *A. polytricha* may be a good solution to the aforementioned issue. However, no reports have emphasized the effect of *A. polytricha*–fermented WBDF (FWBDF) on the rheological properties of dough and the quality of noodles.

In the present study, WBDF was fermented using the *A. polytricha* strain. The effects of FWBDF on the dynamic rheological properties of dough, structural properties of gluten, water distribution, cooking, texture, and extension properties of noodles were evaluated and compared with those of unfermented WBDF (UWBDF). This study provided new prospects for balancing dietary fiber-rich and quality foods with fermented dietary fiber, and facilitated the basic theory for the comprehensive utilization of fermented dietary fiber in the food industry.

MATERIALS AND METHODS

Materials

Wheat flour was purchased from Zhengzhou Jinyuan Noodles Industry Co. (Henan, China). Wheat bran was purchased from Henan Zhonghe Agricultural Development Group Co., Ltd. (Henan, China). *A. polytricha* 5.584 (CGMCC 5.584), an edible jelly fungus, was supplied by China General Microbiological Culture Collection Center (CGMCC, Beijing, China). The activity of laccase production by *Auricularia polytricha* 5.584 was 188.54 U/mL, and the degradation rate of lignin from wheat bran reached 68.72% (20).

Preparation of UWBDF and FWBDF

UWBDF and FWBDF were prepared by the method proposed by Jiang et al. (21) with some modifications. The powdered wheat bran was suspended in ultrapure water (1:10, *w*/*v*) for 30 min with gentle stirring at 95°C. The pH of the mixture was adjusted to 5.6 with HCl and then 1.5% (*w*/*w*) of thermostable α-amylase (40,000 U/g) was added to react for 30 min at 95°C. After the temperature was dropped to 50°C, the pH of the mixture was adjusted to 9.0 with NaOH and 3% (*w*/*w*) alkaline protease was added (≥2,00,000 U/g) to react for 2 h. The mixture was centrifuged at 4,390 g for 20 min. The supernatant was removed and filtered with ultrapure water until the filtrate was clarified. The resultant precipitate was immediately dried in an oven for 24 h at 60°C and then ground through a 150-μm mesh screen to obtain UWBDF. Ten milliliters of the *A. polytricha* 5.584 culture solution (188.54 U/mL) was inoculated into 100 mL of UWBDF-containing fermentation medium (41.5 g/L) and incubated at 26°C in a shaker for 15 days. The FWBDF was dried in an oven at 60°C and then ground through a 150-μm mesh screen.

Preparation of Dough, Gluten, and Noodles

The noodles were made from 100 g of total flour and 38 g of distilled water (30°C). Zero percent (control), 2, 4, 6, 8, and 10% UWBDF and FWBDF were added based on the total weight of the flour. The flour was stirred using a JHMZ200 pin mixer (East Fude Technology Development Center, Beijing, China) for 7 min at 104 rpm. The dough was put into a plastic bag and allowed to rest for 30 min at 30°C. It was divided into three groups: the first was sheeted with a JMTD168/140 sheeting machine (Beijing Dongfu Jiuheng Instrument Technology Co., Ltd., Beijing, China) for the rheological measurement of dough; the second was washed with distilled water to obtain the gluten, freeze-dried, and ground through a 150-μm mesh sieve; and the third was sheeted and then cut into strips to obtain the noodles (thickness 1.25 mm, width 2.0 mm).

Dynamic Rheological Properties

The dynamic rheological properties of dough were determined using a RheoStress 6,000 rotational rheometer (Thermo Fisher Haake, Hamburg, Germany) with a 20-mm diameter steel plate (2-mm gap) by the method proposed by Guadarrama et al. (22) with some modifications. A frequency sweep test was performed from 0.1 to 10 Hz at 25°C. A creep and recovery test was performed under the following conditions: fixed stress 100 Pa, the creep phase lasting 180 s, and the recovery phase lasting 300 s.

Fourier-Transform Infrared Spectroscopy

The gluten structure was measured using a Fourier-transform infrared spectrometer (Nicolet iS50, Thermo Fisher Scientific, Waltham, MA, USA) as described by Zhan et al. (23). The freeze-dried gluten sample (2 mg) and predried potassium bromide

(200 mg) were fully ground and pressed into thin slices. The spectra in the range of 4,000–400 cm^{-1} were recorded with 32 scans per spectrum at a resolution of 4 cm^{-1}. The structure information of gluten was analyzed using PeakFit V4.12 software (SPSS Inc., Chicago, IL, USA).

The most sensitive spectral region for gluten was the amide I band (1,600–1,700 cm^{-1}), where C–O was the stretching vibration of the peptide linkages. The β-sheets (1,610–1,640 cm^{-1}), random coils (1,640–1,650 cm^{-1}), α-helices (1,650–1,660 cm^{-1}), and β-turns (1,660–1,670 cm^{-1}) were the protein secondary structures with the corresponding ranges of the amide I (23, 24).

Low-Field Nuclear Magnetic Resonance

The noodle sample (3 g) was cut and placed in a test tube. The water distribution of noodles was measured using a low-field nuclear magnetic resonance system (VTMR20-010V-T, Shanghai Niumai Electronic Technology Co., Ltd., Shanghai, China) by the experimental method proposed by Yu et al. (25) with some modifications. The number of sampling points (TD) was 66,666, the sampling frequency (SW) was 333.33 kHz, the sampling interval time (TW) was 3,000 ms, the number of echoes was 2,000, the echo time was 0.1 ms, and the number of repeated scans was 16.

Cooking Property

The fresh noodles were boiled in 400 mL of boiling water until the optimum cooking time was reached, quickly removed, and rinsed with cold water for 30 s as described by Sandhu et al. (26) with some modifications. Then, the cooking water was collected in a volumetric flask and mixed with 500 mL of water. The aliquots of 100 mL were dried to constant weight at 105°C. The residue was weighed and reported as a cooking loss.

Texture and Extension Properties

An A-XT2i texture analyzer with an HDP/PFS probe (Stable Micro Systems, London, England) was used to analyze the texture of cooked noodles by the method described by Gao et al. (27). The pretest, test, and post-test speeds were 2.0, 0.8, and 0.8 mm/s, respectively. The interval time of compressions was 1 s, the strain rate was 75%, and the trigger force was 10 g. The extensional test was carried out using an A/SPR probe, and the distance and trigger force were 100 mm and 0.5 g, respectively. The analyses were repeated six times for each sample.

Statistical Analysis

The data were expressed as the mean ± standard deviation of triplicate replications. SPSS 16.0 was used to perform the analysis of variance and significant difference test (Duncan, $P < 0.05$), and Origin 8.5 was used for plotting.

RESULTS AND DISCUSSION

Dynamic Rheological Properties of Dough

Frequency Sweep

Dough viscoelasticity is related to the network formed by the hydrated gluten, which has an important influence on the processing quality of the dough. As shown in **Figure 1**, concomitant increases in the UWBDF/FWBDF content led to an overall upward trend in *G*' and *G*" compared with that in the control. However, the same trend of $G' > G''$ was observed in the presence of different concentrations of UWBDF/FWBDF, indicating that the addition of UWBDF/FWBDF did not change the inherent rheological property of the dough. *G*' reflects the storage modulus and *G*" the loss modulus. This result showed that WBDF could be responsible for the lack of water in the gluten or it acted as a filler in the viscoelastic matrix, thereby increasing the elasticity of the dough (28). Furthermore, the tan δ (G''/G') showed a pronounced decrease following the inclusion of UWBDF/FWBDF, suggesting an increasing trend in relation to the elasticity. WBDF made the dough a more solid-like material, which might be because of the excessive competition of moisture by WBDF with the existence of a gluten network (29). Similarly, Sui et al. (9) reported that the addition of bran could increase the solid-like behavior of the dough.

However, the *G*', *G*", and tan δ values of the samples did not change significantly with the same UWBDF/FWBDF. Fermentation promoted the release of some small molecules in WBDF, such as ferulic acid, which were reported to facilitate the formation of larger network structures through oxidative cross-linking with gluten proteins, thereby enhancing the elasticity and stability of gluten networks (9). In this study, the effect of fermentation on the viscoelasticity of dough was not significant, which was probably due to the limited release or the complex interaction of various small-molecule substances with the dough.

Creep Sweep

The creep recovery was related to the microstructure changes and the reorientation of chemical bonds, which were usually used to characterize the viscoelastic properties of gluten and dough (30). As shown in **Figure 2**, the deformation of the sample increased with the extension of time in the creep stage, while the deformation slowly recovered and became stable in the recovery phase after the external force was removed. Increasing UWBDF/FWBDF resulted in a decrease in the creep value, suggesting that dough with WBDF had a firmer texture, and the firmness of the dough positively correlated with the WBDF content. A previous study showed that creep was related to the moisture content of the dough (31). It was inferred that the redistribution of moisture in the dough was responsible for the reduction of the creep value. Furthermore, the recovery rate gradually increased with the addition of WBDF after the external force was removed, indicating that WBDF-containing dough had a more strain-hardening response and stretching stiffness. These results showed that adding WBDF resulted in the dough with higher resistance to deformation and impaired viscoelasticity, thus adversely affecting the quality of the end-use product. No significant change was observed between FWBDF and UWBDF at the same addition level, except for a slight decrease following the addition of 4% FWBDF. Also, the creep of WBDF-containing dough was not significantly affected by fermentation.

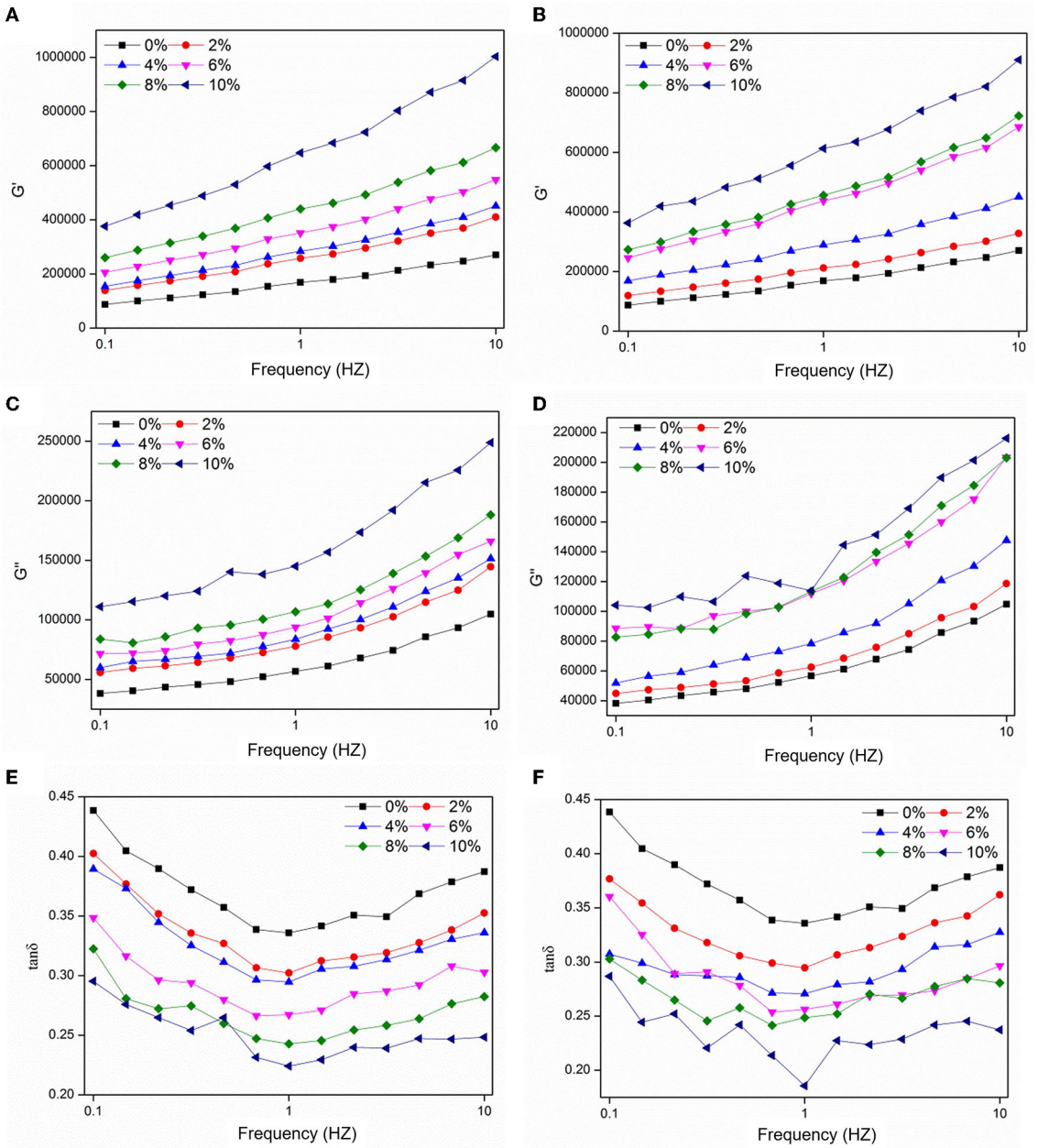

FIGURE 1 | Effect of UWBDF and FWBDF addition on frequency scan curve of dough: **(A,C,E)** dough with UWBDF and **(B,D,F)** dough with FWBDF.

Analysis of Gluten Secondary Structure

The secondary structure of gluten proteins is closely related to gluten network development and the resulting gluten strength. As displayed in **Table 1**, an overall decrease in the number of α-helices and β-turns and an increase in the number of β-sheets and random coils were observed with the increasing UWBDF/FWBDF ratio. No obvious change was observed in the secondary structure of the gluten following the addition of 2% UWBDF or 2–6% FWBDF. The increased α-helix conformation resulted in a more ordered structure (23, 32). However, a decrease in the α-helix content was accompanied by an increase in the number of random coils; α-helices could be converted into random coils. The dietary fiber competed with the water molecules of the gluten protein, resulting in the redistribution of water in the dough, which caused the breakage of some α-helix hydrogen bonds and the disintegration of the helical structure (23). That is to say, these changes led to the formation of disordered structures. The increased β-sheet and decreased β-turn conformation indicated the formation of a more complex and stronger gluten network. The β-sheet was referred to as the

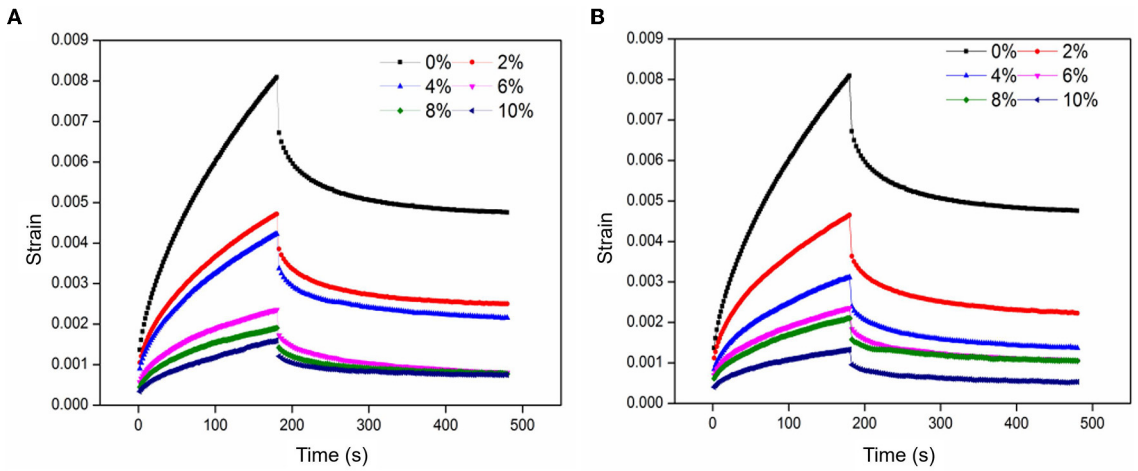

FIGURE 2 | Effect of UWBDF and FWBDF addition on the creep-recovery curve of dough: **(A)** dough with UWBDF and **(B)** dough with FWBDF.

TABLE 1 | Effect of UWBDF/FUWBD addition on the secondary structure of gluten proteins.

Types	Content (%)	α-helix (%)	β-sheet (%)	β-turn (%)	Random coil (%)
UWBDF	0	20.14 ± 1.33^{a}	32.34 ± 1.76^{de}	36.93 ± 0.93^{a}	10.56 ± 1.36^{ef}
	2	20.07 ± 1.50^{a}	32.68 ± 1.27^{de}	36.33 ± 1.42^{a}	10.93 ± 0.35^{ef}
	4	17.71 ± 1.21^{b}	34.27 ± 1.11^{cd}	35.81 ± 0.94^{a}	12.21 ± 1.26^{cde}
	6	16.54 ± 1.21^{bc}	36.61 ± 1.21^{bc}	32.98 ± 1.86^{bc}	13.87 ± 0.55^{bc}
	8	14.31 ± 1.33^{d}	38.24 ± 1.03^{b}	32.22 ± 1.29^{cd}	15.23 ± 1.07^{ab}
	10	13.14 ± 0.43^{d}	40.81 ± 1.08^{a}	28.59 ± 1.25^{e}	17.46 ± 1.77^{a}
FWBDF	0	20.14 ± 1.33^{a}	32.34 ± 1.76^{de}	36.93 ± 0.93^{a}	10.56 ± 1.36^{ef}
	2	21.34 ± 1.26^{a}	31.27 ± 1.87^{e}	37.78 ± 1.23^{a}	9.61 ± 1.01^{f}
	4	21.11 ± 1.23^{a}	31.34 ± 1.07^{e}	37.81 ± 1.48^{a}	9.74 ± 1.57^{f}
	6	20.15 ± 0.57^{a}	33.17 ± 1.24^{de}	35.47 ± 1.41^{ab}	11.21 ± 1.81^{def}
	8	17.65 ± 1.78^{b}	35.73 ± 1.41^{c}	33.16 ± 1.85^{bc}	13.46 ± 1.29^{bcd}
	10	14.64 ± 1.26^{cd}	38.91 ± 1.69^{ab}	30.27 ± 1.43^{de}	16.18 ± 1.33^{a}

Means in the same column with different small letters indicate a significant difference at $P < 0.05$.

most stable protein conformation (23, 32). This phenomenon could be attributed to the fact that dietary fiber might cause changes in the structure of the gluten proteins (possibility of protein aggregation or abnormal folding), which was more conducive to the formation of a β-sheet structure (33). The result was consistent with the report published by Bock et al. (34), who showed that the addition of wheat bran caused the formation of an intermolecular β-sheet from a β-turn due to moisture redistribution in the dough. However, Zhou et al. (1) demonstrated that the addition of dietary fiber induced the formation of the intermolecular β-sheet from the α-helix than from the β-turn. Also, the changes in structure were related to the interaction among side-chain amino acids or between side-chain amino acid and polysaccharide molecule. The formation of the β-sheet structure in gluten was at least partially derived from the β-turn due to WBDF addition. Within a certain deformation range, the decreased β-turn structure was more unfavorable for the ductility of the peptide chain, resulting in poor gluten extensibility (35). This contributed to the collapse-prone fragile structural properties of the gluten network. Previous studies showed that one of the reasons for the adverse effects of WBDF on the gluten network was the collapse of the β-spiral structure, which was a helical structure composed of repetitive β-turns, into an intermolecular β-sheet (36). This was in good agreement with the findings of this study on dynamic rheological properties.

Furthermore, with 4–8% addition, the number of α-helices in the FWBDF group was higher than, while the number of β-sheets in the FWBDF group was lower, than that in the UWBDF group. No obvious change was observed in the number of β-turns and random coils between UWBDF and FWBDF, despite a slight drop in the number of random coils following the addition of 4% FWBDF ($P > 0.05$). The effectiveness of fermentation might be associated with the degradation of WBDF. The macromolecular components of WBDF were partially decomposed into small-molecule compounds, thereby changing the structure of WBDF and affecting its physicochemical properties (21). Besides,

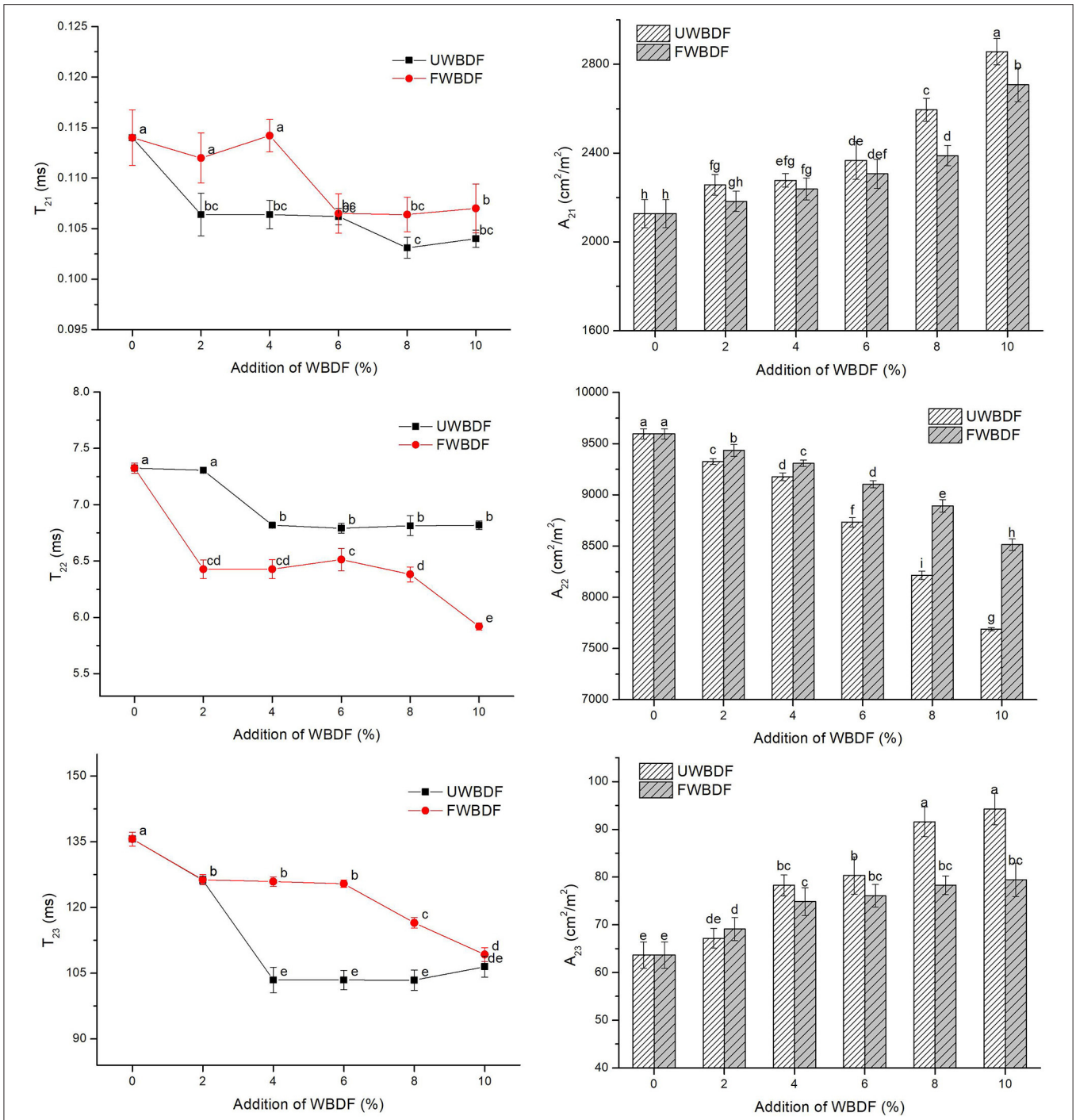

FIGURE 3 | Effect of UWBDF and FWBDF addition on the water distribution of noodles.

fermentation softened and hydrolyzed the lignin encapsulated on the cellulose, breaking the multilayered porous network of the plant. FWBDF was found to be easier to grind compared with UWBDF, which might be due to the degradation of the porous structure of WBDF caused by fermentation. Also, all of these changes inevitably affected the secondary structure of gluten and were beneficial in alleviating the destructive effect of dietary fiber on the gluten.

Water Distribution

Figure 3 shows the influence of UWBDF/FWBDF on the water distributions in noodles. The T_{21}, T_{22}, and T_{23} represented

TABLE 2 | Effect of UWBDF/FUWBD addition on cooking and texture properties of noodles.

Types	Content (%)	Cooking property	Texture properties				Extension properties	
		Cooking loss (g/100g)	Hardness (g)	Cohesiveness	Springiness	Chewiness	Rmax (g)	Lmax (mm)
UWBDF	0	7.72 ± 0.07^{f}	4723 ± 74^{c}	0.64 ± 0.01^{a}	89.19 ± 1.87^{a}	2821 ± 26^{a}	17.49 ± 0.81^{a}	65.52 ± 3.12^{a}
	2	8.34 ± 0.30^{e}	4280 ± 81^{d}	0.58 ± 0.00^{bc}	86.68 ± 2.46^{ab}	2147 ± 45^{d}	16.27 ± 0.53^{ab}	56.52 ± 4.24^{b}
	4	9.31 ± 0.25^{d}	3993 ± 44^{e}	0.56 ± 0.01^{c}	85.91 ± 0.62^{bc}	1956 ± 52^{e}	14.19 ± 1.00^{c}	47.41 ± 4.53^{c}
	6	10.28 ± 0.55^{c}	3487 ± 64^{f}	0.50 ± 0.01^{d}	80.94 ± 1.06^{def}	1481 ± 92^{f}	11.3 ± 0.64^{d}	39.61 ± 5.08^{de}
	8	10.87 ± 0.09^{ab}	3268 ± 81^{h}	0.46 ± 0.01^{e}	78.36 ± 1.15^{f}	1264 ± 11^{h}	9.88 ± 0.78^{e}	36.61 ± 2.78^{e}
	10	11.28 ± 0.28^{a}	3157 ± 9^{h}	0.44 ± 0.02^{e}	79.49 ± 1.15^{ef}	1298 ± 68^{h}	7.33 ± 0.96^{f}	25.83 ± 3.60^{f}
FWBDF	0	7.72 ± 0.07^{f}	4723 ± 74^{c}	0.64 ± 0.01^{a}	89.19 ± 1.87^{a}	2822 ± 26^{a}	17.49 ± 0.81^{a}	65.52 ± 3.12^{a}
	2	7.34 ± 0.23^{f}	5572 ± 23^{a}	0.60 ± 0.00^{b}	89.07 ± 0.30^{a}	2925 ± 69^{a}	16.86 ± 0.53^{a}	59.00 ± 3.64^{ab}
	4	9.05 ± 0.39^{d}	5069 ± 10^{b}	0.60 ± 0.02^{b}	88.47 ± 1.39^{ab}	2676 ± 26^{b}	15.08 ± 0.56^{bc}	51.87 ± 5.42^{bc}
	6	9.51 ± 0.20^{d}	4638 ± 171^{c}	0.58 ± 0.02^{bc}	87.50 ± 3.37^{ab}	2366 ± 133^{c}	12.09 ± 0.72^{d}	44.61 ± 4.19^{cd}
	8	10.13 ± 0.07^{c}	4659 ± 15^{c}	0.52 ± 0.01^{d}	83.48 ± 1.24^{cd}	2018 ± 31^{e}	10.92 ± 0.86^{de}	39.29 ± 4.69^{de}
	10	10.61 ± 0.30^{bc}	4639 ± 18^{c}	0.52 ± 0.01^{d}	82.15 ± 0.84^{de}	2022 ± 61^{e}	8.53 ± 0.48^{f}	28.65 ± 3.26^{f}

Means in the same column with different small letters indicate a significant difference at $P < 0.05$.

strongly bound water, weakly bound water, and free water, and their proportions were written as A_{21}, A_{22}, and A_{23}, respectively (37). An overall decrease in T_{21}, T_{22}, and T_{23} following UWBDF/FWBDF addition indicated that water and macromolecules such as proteins were closely bound. WBDF, containing hydroxyl groups, could bind with water than with protein or starch, thus inhibiting the water flow. The gradual decrease in A_{22} and increase in A_{21} and A_{23} followed the UWBDF/FWBDF addition. The increased A_{21} probably contained the water absorbed by WBDF plus intra-granular water in starch; meanwhile, the higher exposure of binding sites in WBDF was also responsible for the increased A_{23} in noodles (32). The reduction in A_{22} implied that WBDF limited water availability for the interaction between the dietary fiber and the gluten matrix, hindering the formation of the gluten network. Thus, the reduction in A_{22} also confirmed the reduced gluten strength in the noodles induced by the addition of WBDF.

The FWBDF group showed an increased A_{22} compared with the UWBDF group. As mentioned previously, fermentation was associated with the release of small molecules. It could expose these groups or binding sites so that WBDF contained functional groups such as phenolics, carboxylic acids, and ether linkages, resulting in changes in the water solubility and water-holding capacity of WBDF (38). Meanwhile, the degradation of lignin in WBDF resulted in converting some insoluble dietary fibers into low-soluble soluble dietary fiber and other substances with low polymerization degree and water-binding capacity, further changing the water distribution of the dough. In this way, the ability of dietary fiber to compete with gluten for water was weakened, resulting in a decrease in A_{22}.

Cooking, Texture, and Extension Properties of Cooked Noodles

Cooking loss, texture, and extension were important parameters to evaluate the quality of cooked noodles. As shown in **Table 2**, the addition of UWBDF/FWBDF increased the cooking loss of noodles. The result was in agreement with the findings of Shiau et al. (39). This might be due to the leaching of starch and the dissolution of some proteins due to the loosening of the gluten network. No significant difference was observed in cooking loss at a 2% FWBDF addition level compared with the blank group. Moreover, under the same addition, the cooking loss in the FWBDF group was significantly lower than that in the UWBDF group. Liquor koji and yeast fermentation treatment had positive effects on the cooking and texture properties of noodles, reducing cooking loss and increasing the hardness of whole wheat noodles (40). Cooking loss was the total amount of solid substances left in the cooking process, and the reduction in cooking loss, to some extent, prevented the loss of nutrients. Fermentation improved the cooking quality of WBDF-containing noodles.

The texture is one of the key parameters for evaluating the sensitivity of consumers. As shown in **Table 2**, the increase in the levels of FWBDF added ($\leq$4% addition) improved the hardness of the cooked noodles ($P < 0.05$), while UWBDF addition led to a decrease in hardness. An increase in hardness levels correlated with an increase in dough firmness, most likely due to the formation of the firm protein network analyzed earlier. A previous study showed that fermentation and enzymatic synergy inhibited the damage caused by wheat bran to dough and gluten polymerization (41). The UWBDF addition decreased water availability due to the physicochemical nature of UWBDF to hydrate quickly. Thus, the UWBDF combination with gluten protein resulted in a change in their spatial configuration, preventing them from further cross-linking and resulting in a decrease in the hardness of the noodles. Furthermore, increasing the addition levels of UWBDF/FWBDF resulted in a significant decrease in cohesiveness, springiness, and chewiness, but no significant change was observed in springiness and chewiness with the addition of 2% FWBDF. Rough WBDF was believed to yield an open and disaggregated gluten structure and reduced the cohesiveness, springiness, and chewiness of noodles. These results were similar to the previous findings on noodles by Chen

et al. (42). This implied that the redistribution of water and the physical damage due to water-absorbing capacity and hard texture of WBDF might be the main influencing factors (42, 43). These might be the reasons for the changes in the texture of cooked noodles after WBDF addition.

Regarding the extensional properties of cooked noodles, the maximum tensile resistance R_{max} and maximum tensile length L_{max} decreased remarkably ($P < 0.05$) following the addition of UWBDF/FWBDF. No significant change in the levels was observed after the addition of 2% of FWBDF. No obvious change was observed in the R_{max} and L_{max} between UWBDF and FWBDF at the same addition level. The decrease in R_{max} and L_{max} indicated a decrease in the gluten strength and extensibility of noodles, which was basically in agreement with the properties of the dough, implying that noodle quality was related to the gluten conformation. Besides, WBDF with a rougher surface and a higher mechanical strength was responsible for the weakening and disruption of the gluten network by increasing the friction with gluten branches. WBDF created a steric hindrance around the gluten protein, which negatively affected the connection expansion of the gluten network.

In this study, the addition of UWBDF/FWBDF increased the *G'* and *G"* of the dough. Following the analysis of the secondary structure of proteins, the relative abundance of β-sheets and random coils increased. In contrast, the abundance of α-helices and β-turns decreased with the increasing UWBDF/FWBDF ratio. These suggested that the protein conformation changed, resulting in the poor extensibility of gluten and the fragile structural characteristics of the gluten network. Combined with the analysis of noodle texture and extension properties, it was concluded that the change in gluten structure by WBDF was one of the main factors affecting noodle quality. Next, the analysis of water distribution in noodles using low-field nuclear magnetic resonance confirmed that the addition of WBDF inhibited the flow of water in noodles, and the rearrangement of water also affected the quality of noodles. Our analysis showed that FWBDF reduced the destructive effects of dietary fiber on noodle quality by changing the protein conformation and rearrangement of water. Furthermore, the properties of the dough played crucial roles in predicting the quality of noodles.

CONCLUSIONS

This study revealed the effects of FWBDF and UWBDF on the rheological properties of the dough and the quality of noodles. The *G'* and *G"* of the dough increased after adding FWBDF/UWBDF. When the added level of UWBDF reached 6% or that of FWBDF reached 8%, the protein conformation was transformed from α-helix and β-turn to β-sheet and random coil, respectively. Besides, when the addition was in the range of 4–8%, the number of α-helices of FWBDF was higher than that of UWBDF, while the number of β-sheets of FWBDF was lower than that of UWBDF, indicating that adding FWBDF to gluten prevented some of the damage to the gluten network structure compared with UWBDF. The addition of FWBDF/UWBDF facilitated the inhibition of water flow in the noodles; the FWBDF group showed an increased A_{22} compared with the UWBDF group. Additionally, an increase in the levels of FWBDF added ($\leq$4% addition) improved the hardness of the cooked noodles, while the addition of UWBDF decreased the hardness of the noodles. Meanwhile, the addition of FWBDF/UWBDF decreased the cooking loss, R_{max}, and L_{max} in the noodles, except for no significant change with the addition of 2% FWBDF. The cooking loss in the FWBDF group was significantly lower than in the UWBDF group. These changes showed that fermentation had positive effects on the cooking and texture properties of WBDF-containing noodles. This study provided new prospects for balancing dietary fiber-rich and quality foods with fermented dietary fiber, thus facilitating a comprehensive understanding of the relationship between WBDF and flour processing. Besides, WBDF could be fermented by various bacterial groups, which was expected to further improve the quality of the end-use products.

DATA AVAILABILITY STATEMENT

The original contributions presented in the study are included in the article/supplementary material, further inquiries can be directed to the corresponding author/s.

AUTHOR CONTRIBUTIONS

LF and AX: conceptualization and writing—original draft. LL: review and editing. JH: conceptualization and supervision. SM: review, editing, and supervision. All authors contributed to the article and approved the submitted version.

FUNDING

This work was supported by the Open competition Research Projects of Xuchang University (No. 20220504), Major Science and Technology Projects for Public Welfare of Henan Province (201300110300), Zhongyuan Scholars in Henan (No. 214400510015), and School-land Cooperation Project from Xuchang University (No. 980262).

REFERENCES

1. Zhou Y, Zhao D, Foster TJ, Liu Y, Wang Y, Nirasawa S, et al. Konjac glucomannan-induced changes in thiol/disulphide exchange and gluten conformation upon dough mixing. *Food Chem.* (2014) 143:163–9. doi: 10.1016/j.foodchem.2013.07.088
2. He C, Sampers I, Raes K. Dietary fiber concentrates recovered from agro-industrial by-products: functional properties and application as physical carriers for probiotics. *Food Hydrocoll.* (2021) 111:106175. doi: 10.1016/j.foodhyd.2020.106175
3. Wang Z, Yan J, Ma S, Tian X, Sun B, Huang J, et al. Effect of wheat bran dietary fiber on structural properties of wheat starch after synergistic fermentation of

Lactobacillus plantarum and Saccharomyces cerevisiae. *Int J Biol Macromol.* (2021) 190:86–92. doi: 10.1016/j.ijbiomac.2021.08.179
4. Wang Z, Yan L, Ning T, Wang X, Li R, Zhang H. Increasing soluble dietary fiber content and antioxidant activity of wheat bran through twin-screw extrusion pretreatment. *Prep Biochem Biotechnol.* (2020) 50:954–60. doi: 10.1080/10826068.2020.1777424
5. Luo Y, He J, Li H, Lan C, Cai J, Chen H, et al. Wheat bran fermented by mixed fungal strains improves the digestibility of crude fiber and may benefit the gut health without impacting the growth performance in weaned pigs. *Food Func.* (2021) 12:2962–71. doi: 10.1039/D1FO00273B
6. Bai Y. Zhao JB, Tao SY, Zhou XJ, Pi Y, Gerrits WJ, et al. Effect of dietary fiber fermentation on short-chain fatty acid production and microbial composition *in vitro*. *J Sci Food Agri.* (2020) 100:4282–91. doi: 10.1002/jsfa.10470
7. Joye IJ. Dietary fibre from whole grains and their benefits on metabolic health. *Nutrients.* (2020) 12:3045. doi: 10.3390/nu12103045
8. Zhang MY, Liao AM, Thakur K, Huang JH, Zhang JG, Wei ZJ. Modification of wheat bran insoluble dietary fiber with carboxymethylation, complex enzymatic hydrolysis and ultrafine comminution. *Food Chem.* (2019) 297:124983. doi: 10.1016/j.foodchem.2019.124983
9. Sui W, Xie X, Liu R, Wu T, Zhang M. Effect of wheat bran modification by steam explosion on structural characteristics and rheological properties of wheat flour dough. *Food Hydrocoll.* (2018) 84:571–80. doi: 10.1016/j.foodhyd.2018.06.027
10. Spaggiari M, Ricci A, Calani L, Bresciani L, Neviani E. Dall'Asta C, et al. Solid state lactic acid fermentation: a strategy to improve wheat bran functionality. *LWT.* (2020) 118:108668. doi: 10.1016/j.lwt.2019.108668
11. Zhao HM, Guo XN, Zhu KX. Impact of solid state fermentation on nutritional, physical and flavor properties of wheat bran. *Food Chem.* (2017) 217:28–36. doi: 10.1016/j.foodchem.2016.08.062
12. Jiang X, Liu X, Xu H, Sun Y, Zhang Y, Wang Y. Improvement of the nutritional, antioxidant and bioavailability properties of corn gluten-wheat bran mixture fermented with lactic acid bacteria and acid protease. *LWT.* (2021) 144:111161. doi: 10.1016/j.lwt.2021.111161
13. Verni M, Rizzello CG, Coda R. Fermentation biotechnology applied to cereal industry by-products: Nutritional and functional insights. *Front Nutri.* (2019) 6:42. doi: 10.3389/fnut.2019.00042
14. Hartikainen K, Poutanen K, Katina K. Influence of bioprocessed wheat bran on the physical and chemical properties of dough and on wheat bread texture. *Cereal Chem.* (2014) 91:115–23. doi: 10.1094/CCHEM-04-13-0074-R
15. Messia MC, Reale A, Maiuro L, Candigliota T, Sorrentino E, Marconi E. Effects of pre-fermented wheat bran on dough and bread characteristics. *J Cereal Sci.* (2016) 69:138–44. doi: 10.1016/j.jcs.2016.03.004
16. Tu J, Zhao J, Liu G, Tang C, Han Y, Cao X, et al. Solid state fermentation by Fomitopsis pinicola improves physicochemical and functional properties of wheat bran and the bran-containing products. *Food Chem.* (2020) 328:127046. doi: 10.1016/j.foodchem.2020.127046
17. Wanzenböck E, Apprich S, Tirpanalan Ö, Zitz U, Kracher D, Schedle K, et al. Wheat bran biodegradation by edible Pleurotus fungi–A sustainable perspective for food and feed. *LWT.* (2017) 86:123–31. doi: 10.1016/j.lwt.2017.07.051
18. Chen Y, Xue Y. Purification, chemical characterization and antioxidant activities of a novel polysaccharide from Auricularia polytricha. *Int J Biol Macromol.* (2018) 120:1087–92. doi: 10.1016/j.ijbiomac.2018.08.160
19. Lin Y, Chen K, Tu D, Yu X, Dai Z, Shen Q. Characterization of dietary fiber from wheat bran (*Triticum aestivum L*) and its effect on the digestion of surimi protein. *LWT.* (2019) 102:106–12. doi: 10.1016/j.lwt.2018.12.024
20. Xu A, Li L, Ma S, Wang X. Study on the optimization of laccase fermentation conditions and the degradation of wheat bran by *Auricularia polytricha* 5. 584. *J Henan Univ Technol (Nat Sci Ed).* (2020) 41:65–71. doi: 10.16433/j.1673-2383.2020.03.011
21. Jiang S, Li L, Li L, Zheng X, Li Z, Song X. The products from fermentation of wheat bran fiber by Auricularia polytricha strain and the effects of the products on rheological properties of dough sheet. *Food Sci Nutri.* (2020) 8:1345–54. doi: 10.1002/fsn3.1366
22. Guadarrama-Lezama AY, Carrillo-Navas H, Vernon-Carter E, Alvarez-Ramirez J. Rheological and thermal properties of dough and textural and microstructural features of bread obtained from nixtamalized corn/wheat flour blends. *J Cereal Sci.* (2016) 69:158–65. doi: 10.1016/j.jcs.2016.03.011
23. Zhan J, Ma S, Wang XX, Li L, Zheng Xl. Effect of baked wheat germ on gluten protein network in steamed bread dough. *Int J Food Sci Technol.* (2019) 54:2839–46. doi: 10.1111/ijfs.14200
24. Yu XY, Zou Y, Zheng QW, Lu FX, Li DH, Guo LQ, et al. Physicochemical, functional and structural properties of the major protein fractions extracted from Cordyceps militaris fruit body. *Food Res Int.* (2021) 142:110211. doi: 10.1016/j.foodres.2021.110211
25. Yu X, Wang Z, Zhang Y, Wadood SA, Wei Y. Study on the water state and distribution of Chinese dried noodles during the drying process. *J Food Eng.* (2018) 233:81–7. doi: 10.1016/j.jfoodeng.2018.03.021
26. Sandhu KS, Kaur M. Studies on noodle quality of potato and rice starches and their blends in relation to their physicochemical, pasting and gel textural properties. *LWT-Food Sci Technol.* (2010) 43:1289–93. doi: 10.1016/j.lwt.2010.03.003
27. Guo XN, Wei XM, Zhu KX. The impact of protein cross-linking induced by alkali on the quality of buckwheat noodles. *Food Chem.* (2017) 221:1178–85. doi: 10.1016/j.foodchem.2016.11.041
28. Lin S, Jin X, Gao J, Qiu Z, Ying J, Wang Y, et al. Impact of wheat bran micronization on dough properties and bread quality: Part I–Bran functionality and dough properties. *Food Chem.* (2021) 353:129407. doi: 10.1016/j.foodchem.2021.129407
29. Liu D, Song S, Tao L, Yu L, Wang J. Effects of common buckwheat bran on wheat dough properties and noodle quality compared with common buckwheat hull. *LWT.* (2022) 155:112971. doi: 10.1016/j.lwt.2021.112971
30. Lei M, Huang J, Tian X, Zhou P, Zhu Q, Li L, et al. Effects of insoluble dietary fiber from wheat bran on noodle quality. *Grain Oil Sci Technol.* (2021) 4:1–9. doi: 10.1016/j.gaost.2020.11.002
31. Ma S, Han W, Li L, Wang X. Small and large strain rheology of gluten and gluten–starch doughs containing wheat bran dietary fiber. *J Sci Food Agric.* (2020) 100:177–83. doi: 10.1002/jsfa.10012
32. Xiong L, Zhang B, Niu M, Zhao S. Protein polymerization and water mobility in whole-wheat dough influenced by bran particle size distribution. *LWT-Food Sci Technol.* (2017) 82:396–403. doi: 10.1016/j.lwt.2017.04.064
33. Nawrocka A, Szymanska-Chargot M, Mis A, Wilczewska AZ, Markiewicz KH. Dietary fiber-induced changes in the structure and thermal properties of gluten proteins studied by Fourier transform-Raman spectroscopy and thermogravimetry. *J Agric Food Chem.* (2016) 64:2094–104. doi: 10.1021/acs.jafc.5b05712
34. Bock JE, Damodaran S. Bran-induced changes in water structure and gluten conformation in model gluten dough studied by Fourier transform infrared spectroscopy. *Food Hydrocoll.* (2013) 31:146–55. doi: 10.1016/j.foodhyd.2012.10.014
35. Zhang LL, Guan EQ, Yang YL, Liu YX, Zhang TJ, Bian K. Impact of wheat globulin addition on dough rheological properties and quality of cooked noodles. *Food Chem.* (2021) 362:130170. doi: 10.1016/j.foodchem.2021.130170
36. Han W, Ma S, Li L, Zheng X, Wang X. Gluten aggregation behavior in gluten and gluten-starch doughs after wheat bran dietary fiber addition. *LWT.* (2019) 106:1–6. doi: 10.1016/j.lwt.2019.02.051
37. Hong T, Ma Y, Yuan Y, Guo L, Xu D, Wu F, et al. Understanding the influence of pullulan on the quality changes, water mobility, structural properties and thermal properties of frozen cooked noodles. *Food Chem.* (2021) 365:130512. doi: 10.1016/j.foodchem.2021.130512
38. Zheng Y, Li Y. Physicochemical and functional properties of coconut (*Cocos nucifera L*) cake dietary fibres: Effects of cellulase hydrolysis, acid treatment and particle size distribution. *Food Chem.* (2018) 257:135–42. doi: 10.1016/j.foodchem.2018.03.012

39. Shiau SY, Wu TT, Liu YL. Effect of the amount and particle size of wheat fiber on textural and rheological properties of raw, dried and cooked noodles. *J Food Qual.* (2012) 35:207–16. doi: 10.1111/j.1745-4557.2012.00436.x
40. Xu CY, Guo XN, Zhu KX. Effect of pre-treated wheat bran on semi-dried whole wheat noodles for extending shelf-life and improving quality characteristics. *LWT*. (2021) 146:111503. doi: 10.1016/j.lwt.2021.111503
41. Zhang H, Zhang X, Cao XR, Iftikhar M, Wang J. Semi-solid state fermentation and enzymatic hydrolysis impeded the destroy of wheat bran on gluten polymerization. *LWT*. (2018) 98:306–13. doi: 10.1016/j.lwt.2018.08.047
42. Chen J, Fei M, Shi C, Tian J, Sun C, Zhang H, et al. Effect of particle size and addition level of wheat bran on quality of dry white Chinese noodles. *J Cereal Sci.* (2011) 53:217–24. doi: 10.1016/j.jcs.2010.12.005
43. Han W, Ma S, Li L, Zheng X, Wang X. Influence of wheat starch on the structural changes and size distribution of gluten induced by adding wheat bran dietary fiber. *Starch-Stärke.* (2018) 70:1700302. doi: 10.1002/star.201700302

Conflict of Interest: The authors declare that the research was conducted in the absence of any commercial or financial relationships that could be construed as a potential conflict of interest.

frontiers | Frontiers in Nutrition

TYPE Original Research
PUBLISHED 11 August 2022
DOI 10.3389/fnut.2022.951588

OPEN ACCESS

EDITED BY
Hua-Min Liu,
Henan University of Technology, China

REVIEWED BY
Bao Zhang,
Hefei University of Technology, China
Qunyu Gao,
South China University of Technology, China
Binjia Zhang,
Huazhong Agricultural University, China

*CORRESPONDENCE
Yizhe Yan
yanyizhe@zzuli.edu.cn
Yuan He
heyuan818@163.com

SPECIALTY SECTION
This article was submitted to Food Chemistry, a section of the journal Frontiers in Nutrition

RECEIVED 24 May 2022
ACCEPTED 18 July 2022
PUBLISHED 11 August 2022

CITATION
Yan Y, Xue X, Jin X, Niu B, Chen Z, Ji X, Shi M and He Y (2022) Effect of annealing using plasma-activated water on the structure and properties of wheat flour.
Front. Nutr. 9:951588.
doi: 10.3389/fnut.2022.951588

Effect of annealing using plasma-activated water on the structure and properties of wheat flour

Yizhe Yan[1]*, Xinhuan Xue[1], Xueyuan Jin[2], Bin Niu[3], Zhenzhen Chen[1], Xiaolong Ji[1], Miaomiao Shi[1] and Yuan He[1]*

[1]College of Food and Bioengineering, Henan Key Laboratory of Cold Chain Food Quality and Safety Control, Zhengzhou University of Light Industry, Zhengzhou, China, [2]School of Clinical Medicine, Hainan Vocational University of Science and Technology, Haikou, China, [3]College of Food Science and Technology, Henan Agricultural University, Zhengzhou, China

In this study, wheat flour (WF) was modified by annealing (ANN) using plasma-activated water (PAW) for the first time. Compared with WF and DW-WF, the results of scanning electron microscopy (SEM) and particle-size analysis showed that the granule structure of wheat starch in PAW-WF was slightly damaged, and the particle size of PAW-WF was significantly reduced. The results of X-ray diffraction and Fourier transforming infrared spectroscopy indicated that PAW-ANN could reduce the long-range and short-range order degrees of wheat starch and change the secondary structure of the protein in WF, in which the content of random coils and α-helices was significantly increased. In addition, the analysis of solubility, viscosity, and dynamic rheological properties showed that PAW-ANN improved the solubility and gel properties of WF and decreased its viscosity properties and short-term regeneration. PAW-ANN, as a green modification technology, has the potential for further application in WF modification, as well as in the production of flour products.

KEYWORDS

plasma-activated water, annealing, wheat flour, structure, properties

Introduction

Wheat is a cereal crop that is widely grown all over the world. After being ground into wheat flour (WF), it is widely used in food and can be used to make bread, steamed bread, biscuits, noodles, and other foods (1). The quality of flour products is often related to the functional properties of WF, such as gelatinization and gelling properties. However, due to the limitations of milling process and equipment, it is difficult for WF to meet the requirements of a specific food. Therefore, the modification of WF is required to expand its application. In addition to modification by chemical and enzymatic methods, physical methods have also become increasingly important due to good safety. The most used methods of physical modification include hydrothermal,

extrusion, microwave, irradiation, and micronization. Bhat et al. irradiated WF and found that the water absorption, oil absorption, and swelling power (SP) of WF decreased, while its water solubility index, stability, and foaming ability increased (2). Lazaridou et al. showed that the reduction in the particle size of WF by micronization techniques largely affected their functional properties, such as water absorption and the amount of damaged starch, as well as the extractability of their components, such as arabinoxylan and molecular properties, which are important factors in determining starch gelatinization and dough rheological properties in WF (3).

Annealing (ANN) is a physical modification method that is usually carried out under excessive water (>40%) and low temperature above the glass transition temperature but below the gelatinization temperature for a period (usually more than 16 h). ANN conditions are relatively mild, involving only water and heat, so it has attracted wide attention (4). The structural and functional properties of starch and starch-based products are changed after ANN, making them easier to process and use in some unique environments.

The water obtained by the plasma discharge treatment of distilled water is called plasma-activated water (PAW). Plasma equipment can make the water environment acidic, increase redox potential, and enhance electrical conductivity by the generation of reactive oxygen species (ROS) and reactive nitrogen species (RON). PAW is gentler than direct plasma treatment. It uses water as the medium to avoid direct plasma damage to the surface caused by specific substances such as charged particles, ultraviolet rays, and electrons. Meanwhile, it exists in the form of liquid, which is more convenient and flexible. It can directly use air as a working gas and distilled water as an activation liquid, with low cost and no secondary pollution. Distinctive physicochemical properties make it widely employed in the food industry (5). Recently, PAW has been used to modify the structure and improve the properties of the starch by our group (6, 7). The multi-scale structure of various starches was modified, and their physicochemical and digestive properties were also improved by PAW combined with heat-moisture treatment or ANN. Wheat starch, as the main component of WF, is related to the properties of WF. Therefore, PAW modification could provide a possible way to change the structure and properties of WF.

In this study, PAW and ANN were used to synergistically modify WF, changing the multi-scale structure of starch and protein in WF, and improving the physicochemical properties of WF. The dual physical modification method is simple, convenient, green, and safe, avoiding the use of chemical substances or biological enzymes, and has the potential for modification of flour in the future.

Materials and methods

Materials

WF was obtained from COFCO Grain and Oil Co., Ltd. (Zhengzhou, China). All chemicals used were of analytical grade.

Preparation and characterization of plasma-activated water

In this study, PAW was prepared by an atmospheric pressure plasma jet device (Easton Geake Automation Equipment Co., Ltd., Shenzhen, China). Approximately 100 ml of distilled water (DW) was placed in a cylindrical plastic bottle with the plasma nozzle 2 cm from the water surface. PAW was obtained after plasma jet treatment for 2 min under high frequency and high pressure (40 kHz, 5 kV). The pH value, oxidation-reduction potential (ORP), and conductivity of PAW were determined by the pH/ORP meter and conductivity meter (Yidian Scientific Instrument Co., Ltd., Shanghai, China). Notably, PAW was suggested to be further used within 12 h.

Annealing treatment of wheat flour with distilled water or plasma-activated water

WF (25 g, dry basis) was placed in a Petri dish and dried at 50°C until about 5% moisture content. DW and PAW were used to adjust moisture content to 70%, respectively. After stirring and mixing, WF was put into hydrothermal reactors and then placed into an oven at 50°C for 12 h. After cooling to room temperature, WF was poured into a Petri dish, lyophilized, ground, and sieved to obtain the modified WF. These modified WF samples were denoted as DW-WF and PAW-WF. All samples are prepared in triplicates for further analysis.

Scanning electron microscopy

The samples were evenly attached to the sample stage with conductive adhesive, sprayed with gold for 120 s in the ion sputtering device, and then observed under a high-resolution field emission scanning electron microscope (Regulus 8100, Hitachi, Tokyo, Japan). Under the accelerating voltage of 3 kV, the surface microstructure of the samples was observed at 1,000 times magnification.

Particle size analysis

The samples to be tested were prepared into a flour emulsion (1%, w/w). The samples were tested for particle size distribution using a laser particle size analyzer (LS13320/ULM2, Beckman Coulter Ltd., United Kingdom). The corresponding data were recorded and analyzed.

X-ray diffraction

Before the test, the samples were placed in saturated NaCl solution for 1 week at room temperature to equilibrate the moisture (8). An appropriate amount of WF sample powder was placed on the circular test board and compacted with a smooth glass sheet. The samples were analyzed using an X-ray diffractometer (D8 Advance, Bruker, Karlsruhe, Germany). The test conditions are as follows: 40 kV pipe pressure, 30 mA pipe flow, 4°/min scan speed, 5°–35° scanning area, 0.02° step, continuous scanning, and repeated once. The relative crystallinity (RC) of flour samples was calculated according to our previous method (6).

Fourier transform infrared spectroscopy

Before the test, the potassium bromide required for the test was dried at 105°C for 5 h. WF sample and potassium bromide, according to the mass ratio of 1:100, were mixed, ground, and pressed into the tablet. A Fourier transform infrared (FTIR) spectrometer (Vertex 70, Bruker, Karlsruhe, Germany) was used to measure the FTIR spectra of WF samples. The test conditions are as follows: 4,000–400 cm^{-1} scanning wave number range, 4 cm^{-1} resolution, and 64 s scanning time. All measurements were performed in triplicates. The OMNIC 8.2 software (Thermo Nicolet Inc., United States) was used to analyze all the measured data. FTIR spectra data in the range of 1,200–800 cm^{-1} were deconvolved and normalized. The short-range ordered structure of starch in WF was detected by calculating the absorbance ratio at 1,047/1,022 cm^{-1} ($R_{1047/1022}$) (7, 9). The FTIR spectra were fitted and analyzed by the Peakfit software 4.12 (SPSS Inc., Chicago, IL, United States), and then the ratio of the secondary structure of the protein in WF was calculated based on the peak area. Amide I bands (1,600–1,700 cm^{-1}) were assigned as follows: 1,612–1,618 cm^{-1}, 1,625–1,635 cm^{-1}, and 1,685–1,695 cm^{-1} were β-sheets; 1,640–1,655 cm^{-1} was random coils; 1,658–1,665 cm^{-1} was α-helixes; and 1,670–1,680 cm^{-1} was β-turns (10, 11).

TABLE 1 Physicochemical properties of DW and PAW.

Water	pH	Conductivity (μ S/cm)	ORP (mV)
DW	6.44 ± 0.33^{a}	3.57 ± 0.27^{b}	284.67 ± 1.62^{b}
PAW	2.68 ± 0.01^{b}	832.58 ± 4.76^{a}	581.50 ± 2.13^{a}

Values are expressed as means ± standard deviation of three measurements. Means with different lowercase letters in the same column indicate significant differences ($p < 0.05$).

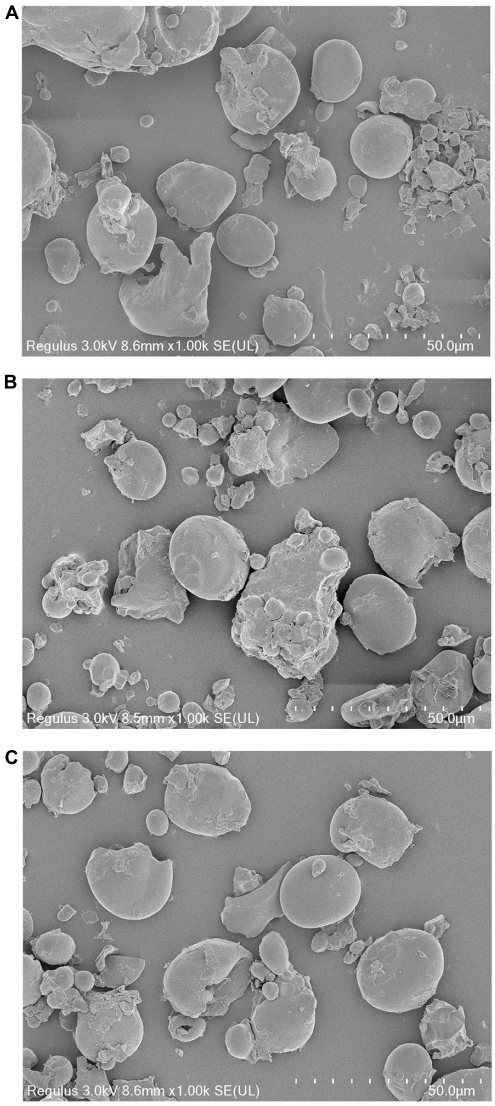

FIGURE 1
SEM images of WF and modified WF. **(A)** WF; **(B)** DW-WF; and **(C)** PAW-WF.

Determination of free sulfhydryl content

The determination of free sulfhydryl content of protein referred to the method of Suo et al. (12) with minor

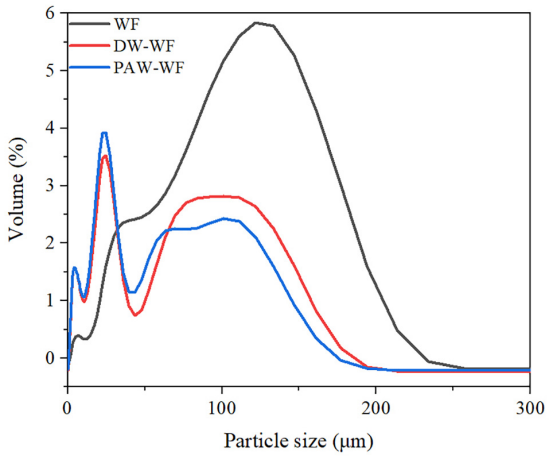

FIGURE 2
Particle size distribution of WF and modified WF.

modifications. The samples were dissolved in 6 ml of Tris-Gly buffer (8 M Urea, 0.086 M Tris, 0.092 M Gly, 0.004 M EDTA, pH 8.0) and extracted with shaking for 60 min. After centrifugation for 20 min, the supernatant (4 ml) was taken out, and Ellman's reagent (80 μl, 4 mg/ml DTNB in buffer) was added. The mixture of the two was reacted for 5 min, and then the absorbance was measured at 412 nm. The following formula was used to calculate the free sulfhydryl content of protein in WF:

$$C_{SH} = \frac{73.53 \times A_{412}}{C}$$

C represents the concentration (mg/ml) of protein in the samples.

Color analysis

Color measurements were conducted at room temperature with a Ci6x color difference analyzer (Aiselicai Technology Co., ltd., Shanghai, China). Before the testing, background calibration was performed using white and black. The measured brightness value (L*, 100 = white, 0 = black), red-green value (a*, positive value = red), and yellow-blue value (b*, positive value = yellow) were recorded (13). The following formula was used to calculate the whiteness index (WI) of WF.

$$WI = 100 - \sqrt{(100 - \mathrm{L}^*)^2 + a^{*2} + b^{*2}}$$

The total color difference (ΔE) was calculated according to the following equation as a measure of the total color change between modified WF and WF (represented by an index 0).

$$\triangle E = \sqrt{(L^* - L_0^*)^2 + (a^* - a_0^*)^2 + (b^* - b_0^*)^2}$$

Solubility and swelling power

Samples were analyzed for solubility (S) and SP using the Chaple's method (14). The sample (0.5 g, dry basis) and distilled water (25 ml) were added into a centrifuged tube and mixed well. The mixture was heated at 90°C for 30 min, taken out to cool, and centrifuged (3,000 r/min). After the separation of the supernatant and sediment, the supernatant was dried at 105°C to constant weight (W_1). The weight of sediment in the centrifuge tube was recorded as W_2. The weight of the sample was recorded as W. The S and SP were calculated by the following formula.

$$S\,(\%) = W_1/W \times 100$$

$$SP(\mathrm{g/g}) = W_2/(W - W_1)$$

Rapid viscosity analysis

The viscosity of WF was analyzed by a Rapid Viscosity Analyzer (RVA4500, Perten Instruments, Hägersten, Germany). The samples (2.5 g, dry basis) were added into an aluminum can, and then distilled water was added to make the total weight of 28 g. After mixing evenly, the mixture was put into the measuring tank of RVA for analysis. The test conditions were as follows: equilibrated at 50°C for 1 min, heated to 95°C at 12°C/min, kept warm for 2.5 min, cooled down to 50°C at the same rate and held for 2 min. The speed in the first 10 s was 960 r/min, and the rest was 160 r/min. Finally, the viscosity curve was obtained.

Dynamic rheological analysis

The rheological properties of WF were tested by a rheometer (Discovery HR-1, TA instrument Inc., Newcastle, DE, United States). The samples were prepared according to the method of Solaesa et al. (15) and modified appropriately in specific operations. The linear viscoelastic region was determined using a shear strain at 25°C at a scanning frequency of 1 Hz. The dynamic frequency was 0.1–10 Hz, and the shear strain was 1%. The diameter of the test probe is 40 mm, and the gap is 1 mm. The prepared WF pastes were put on the flat mold, and the edge was smeared with methyl silicone oil to prevent the sample from volatilizing. The storage modulus (G', Pa), loss modulus (G", Pa), and loss tangent (tan δ) of WF were obtained.

Statistical analysis

All experiments were repeated at least three times, and the data were obtained from the average and standard deviation

TABLE 2 Particle size, RC, short-range ordered structure of starch in WF, and modified WF.

Samples	D (4.3) (μ m)	D10 (μ m)	D50 (μ m)	D90 (μ m)	RC (%)	$R_{1047/1022}$
WF	83.96 ± 0.12^{a}	10.21 ± 0.39^{a}	79.53 ± 0.64^{a}	163.25 ± 1.39^{a}	28.17 ± 0.15^{a}	0.913 ± 0.019^{a}
DW-WF	44.47 ± 1.17^{b}	3.20 ± 0.00^{b}	24.36 ± 0.23^{b}	120.66 ± 4.74^{b}	26.33 ± 0.15^{b}	0.886 ± 0.030^{a}
PAW-WF	38.45 ± 0.56^{c}	3.15 ± 0.01^{b}	23.43 ± 0.15^{b}	105.02 ± 1.04^{c}	25.30 ± 0.20^{c}	0.878 ± 0.027^{a}

Values are expressed as means ± SD of three measurements. Means with different lowercase letters in the same column indicate significant differences ($p < 0.05$). D (4.3) is the volume average diameter. D10, D50, and D90 are the particle sizes at 10, 50, and 90% of the volume of all particles, respectively.

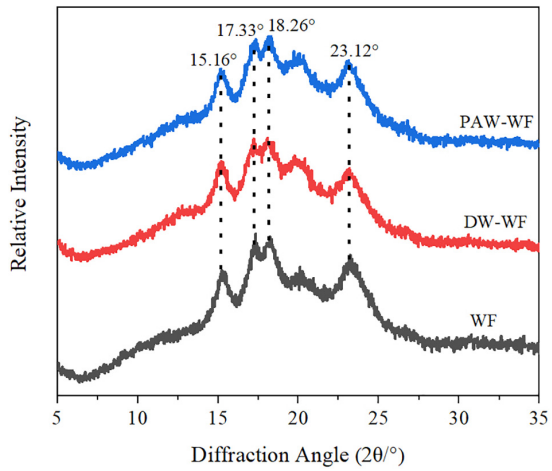

FIGURE 3
XRD patterns of WF and modified WF.

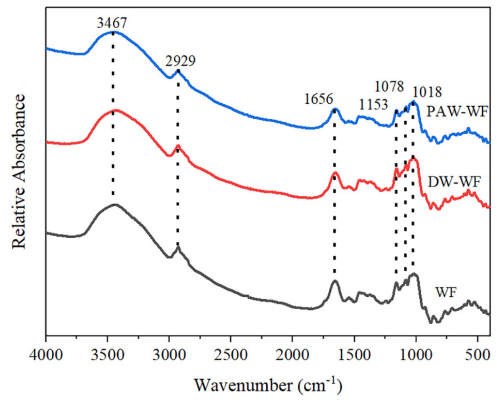

FIGURE 4
FTIR spectra of WF and modified WF.

(SD) of all repeated measured data. ANOVA and Duncan's multiple comparison tests ($p < 0.05$) were performed using SPSS statistics 26.0 software (IBM, Chicago, IL, United States) to determine significant differences between means. Graphs were made using Origin 2018 (Origin-Lab Inc., Northampton, MA, United States).

Results and discussion

Physicochemical properties of plasma-activated water

The pH value, conductivity, and ORP of DW and PAW are shown in Table 1. The pH value represents the hydrogen ion concentration in an aqueous solution. Compared with DW (6.44), the pH value of PAW decreased significantly to 2.68 ($p < 0.05$) after plasma treatment for 2 min. This indicated that the plasma treatment of DW would lead to the acidification of water. This may be due to the decomposition of N_2 and O_2 by the plasma discharge to generate nitrogen oxides, which were decomposed into H^+, NO_2^-, and NO_3^- after the reaction with water, resulting in a decrease in pH value in PAW (16).

Conductivity can be used to measure the ability of a solution to conduct electricity. Plasma treatment significantly increased the conductivity from 3.57 (DW) to 832.58 μS/cm (PAW) ($p < 0.05$). This may be related to the pH of PAW and the formation of NO_3^- and NO_2^- after plasma treatment, resulting in an increase of conductivity (17).

ORP can represent the redox properties of the solution. After plasma treatment, ORP significantly increased from 284.67 (DW) to 581.50 mV (PAW) ($p < 0.05$). The increase of ORP indicated that various ROS and RON, such as H_2O_2, O_3, OH, and $ONOO^-$, were produced by the plasma treatment (18).

Granular morphology

The scanning electron microscopy (SEM) observation results of WF and modified WF are shown in Figure 1. WF was mainly composed of starch particles, which were irregular, spherical, and rough on the surface. The rough part of the surface of starch particles and the debris around the particles are non-starch components, such as protein. After ANN treatment, a part of the starch particles was destroyed. This may be due to excessive water and heat during ANN, causing the gelatinization of part of the starch and, thereby, breaking the starch granules. In addition, the granular morphology of PAW-WF did not change significantly compared with DW-WF.

TABLE 3 Secondary structure and free sulfhydryl content of protein in WF and modified WF.

Samples	β-sheets (%)	Random coils (%)	α-helices (%)	β-turns (%)	Free sulfhydryl (μ mol/g)
WF	36.72 ± 2.75^{a}	25.20 ± 1.14^{c}	12.67 ± 1.53^{b}	25.41 ± 1.73^{a}	10.68 ± 0.02^{a}
DW-WF	36.18 ± 2.81^{a}	28.86 ± 1.69^{b}	13.39 ± 1.80^{b}	21.57 ± 2.91^{b}	5.72 ± 0.04^{b}
PAW-WF	30.67 ± 1.36^{b}	34.96 ± 1.49^{a}	16.04 ± 1.42^{a}	18.32 ± 1.44^{c}	5.54 ± 0.02^{c}

Values are expressed as means ± SD of three measurements. Means with different lowercase letters in the same column indicate significant differences ($p < 0.05$).

TABLE 4 Color, solubility, and swelling power of WF and modified WF.

Samples	L*	a*	b*	WI	ΔE	S (%)	SP (g/g)
WF	92.03 ± 0.02^{a}	0.80 ± 0.01^{b}	10.76 ± 0.04^{a}	86.59 ± 0.04^{b}	0	14.25 ± 0.12^{b}	11.15 ± 0.14^{a}
DW-WF	91.24 ± 0.01^{b}	0.70 ± 0.02^{c}	9.12 ± 0.07^{c}	87.34 ± 0.04^{a}	1.82 ± 0.09^{b}	15.25 ± 0.27^{b}	10.41 ± 0.49^{a}
PAW-WF	90.51 ± 0.02^{c}	0.85 ± 0.00^{a}	9.27 ± 0.01^{b}	86.71 ± 0.02^{b}	2.13 ± 0.01^{a}	18.75 ± 0.66^{a}	10.52 ± 0.66^{a}

Values are expressed as means ± standard deviation of three measurements. Means with different lowercase letters in the same column indicate significant differences ($p < 0.05$).
*Means to distinguish it from HunterLab.

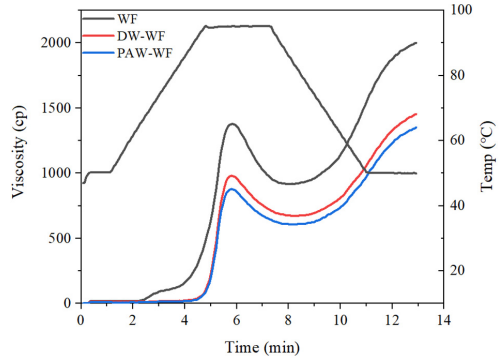

FIGURE 5
Pasting properties of WF and modified WF.

Particle size distribution

The particle size distribution of WF and modified WF, and the size changes of the WF particles are shown in Figure 2 and Table 2. After ANN treatment, the large-sized particles in the WF were significantly reduced, while the smaller particles were relatively increased. This result may be explained by the fact that some starch granules were gelatinized and ruptured during ANN, which was in accordance with the observation results of SEM. Compared with WF, D (4.3), D10, D50, and D90 of DW-WF and PAW-WF were significantly lower ($p < 0.05$), which also indicated that ANN would lead to the destruction of starch granules instead of aggregation. This may be attributed to the cleavage of intermolecular hydrogen bonds in starch granules during ANN. Compared with DW-WF, the D (4.3), D10, D50, and D90 of PAW-WF were slightly lower. This trend may be due to the fact that during ANN, the acid component in PAW broke the molecular chain in starch, resulting in smaller and looser particles (6).

Crystalline structure

X-ray diffraction patterns and RC of WF and modified WF are shown in Figure 3 and Table 2. Both WF and modified WF showed obvious diffraction peaks at $2\theta = 15.16°$, 17.33°, 18.26°, and 23.12°, which indicated that the crystal structure of starch in WF, DW-WF, and PAW-WF showed a typical A-type crystal structure (19). After ANN treatment, the position and peak shape of the diffraction peaks of WF did not change much, and no new characteristic peaks were generated. It can be concluded that ANN had no effect on the crystalline morphology of WF. However, ANN resulted in a significant decrease in the RC of the WF from 28.17 to 26.33% or 25.30% ($p < 0.05$). This is because the amylopectin structure in starch was destroyed,

TABLE 5 Pasting properties of WF and modified WF.

Samples	Peak viscosity (cP)	Final viscosity (cP)	Breakdown viscosity (cP)	Setback viscosity (cP)
WF	1374.00 ± 7.07^{a}	1997.50 ± 4.95^{a}	463.00 ± 0.00^{a}	1086.50 ± 2.12^{a}
DW-WF	985.50 ± 4.95^{b}	1462.50 ± 9.19^{b}	310.50 ± 0.71^{b}	787.50 ± 4.95^{b}
PAW-WF	879.00 ± 1.41^{c}	1355.50 ± 4.95^{c}	274.00 ± 0.00^{c}	750.50 ± 6.36^{c}

Values are expressed as means ± SD of three measurements. Means with different lowercase letters in the same column indicate significant differences ($p < 0.05$).

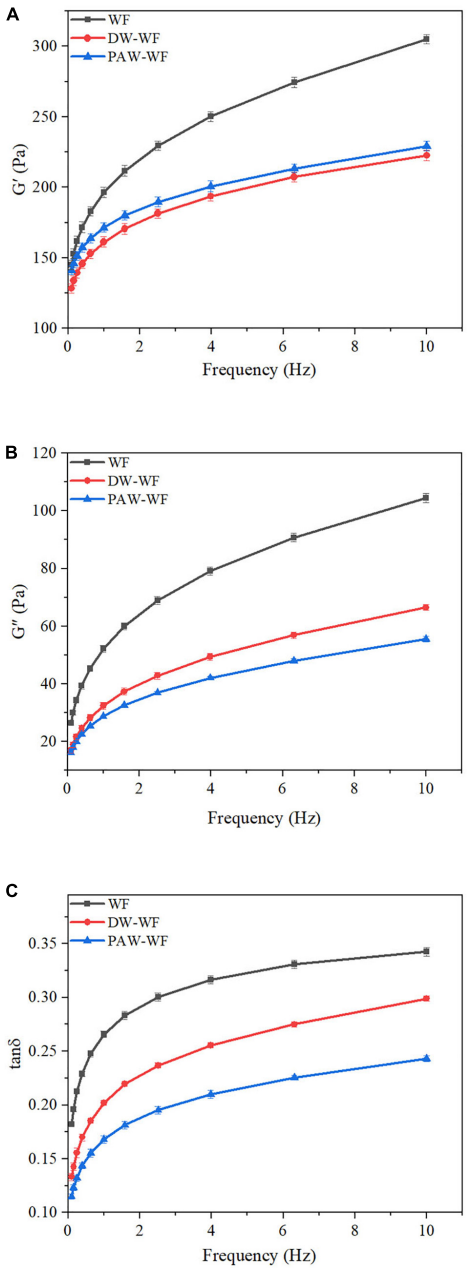

FIGURE 6
Dynamic rheological curves of WF and modified WF. **(A)** Storage modulus (G') of WF, DW-WF and PAW-WF; **(B)** Loss modulus (G") of WF, DW-WF and PAW-WF; and **(C)** Loss tangent (tanδ) of WF, DW-WF, and PAW-WF.

and the crystalline region was reduced during ANN. Moreover, partial starch granule gelatinization and double helical motion during processing may destroy starch crystallites or change crystallite orientation, which may also be the reason for the decreased RC (20). Additionally, PAW-WF had the lowest RC (25.30%) because the active species in PAW reacted with WF during PAW-ANN, resulting in the depolymerization of starch molecular chains (21). This was consistent with the findings of Zhu et al. (13), who studied the impact of plasma on the crystallinity of WF.

Short-range ordered structure of starch in wheat flour

As shown in **Figure 4**, the characteristic peaks of the FTIR spectra of WF and modified WF hardly changed. This indicated that the functional group of the modified WF was not affected. FTIR spectra in the range of 1,200–800 cm^{-1} are sensitive to short-range molecular order changes of starch. The absorption peaks of WF at 1,047 cm^{-1} and 1,022 cm^{-1} represent the ordered and disordered structures of starch molecules, respectively (22, 23). Therefore, $R_{1047/1022}$ is used to identify the degree of the ordered structure of starch molecules. The larger $R_{1047/1022}$, the higher the degree of short-range molecular order. According to **Table 2**, $R_{1047/1022}$ did not significantly change ($p < 0.05$), indicating that the short-range ordered structure of starch in the modified MF was not changed.

Secondary structure and free sulfhydryl content of protein in wheat flour

FTIR spectroscopy is commonly used to characterize the secondary structure of the protein. There are several characteristic absorption bands in the FTIR spectroscopy of protein, among which the amide I band (1,600–1,700 cm^{-1}) is often used to study their secondary structure. After PAW-ANN and DW-ANN, the secondary structure of the protein in WF was changed significantly (**Table 3**). Compared with WF and DW-WF, the content of β-sheets and β-turns were significantly reduced to 30.67 and 18.32% ($p < 0.05$), respectively, while the content of random coils and α-helices were significantly increased to 34.96 and 16.04% ($p < 0.05$), respectively, which indicated that the stability of the protein decreased, the hydrophobic groups inside the protein were exposed, and the partially ordered structure was transformed into a random coil structure after PAW-ANN. The increased irregular structures inhibited starch crystal arrangement, resulting in the decrease of RC, which was in consistent with XRD results.

The free sulfhydryl content of WF and modified WF is shown in **Table 3**. After ANN treatment, the free sulfhydryl content of WF was significantly decreased ($p < 0.05$). This indicated the formation of disulfide bonds in proteins, which play an important role in protein aggregation. PAW-ANN further reduced the free sulfhydryl content from 10.68 to 5.54 μmol/g. This may be because ROS in the PAW led to the oxidation of free sulfhydryl in protein cysteine, aggravating the loss of free sulfhydryl (24).

Color

Whiteness is an important indicator of flour and its products. The white color of flour is required for many flour products (25). The color values and the total color difference

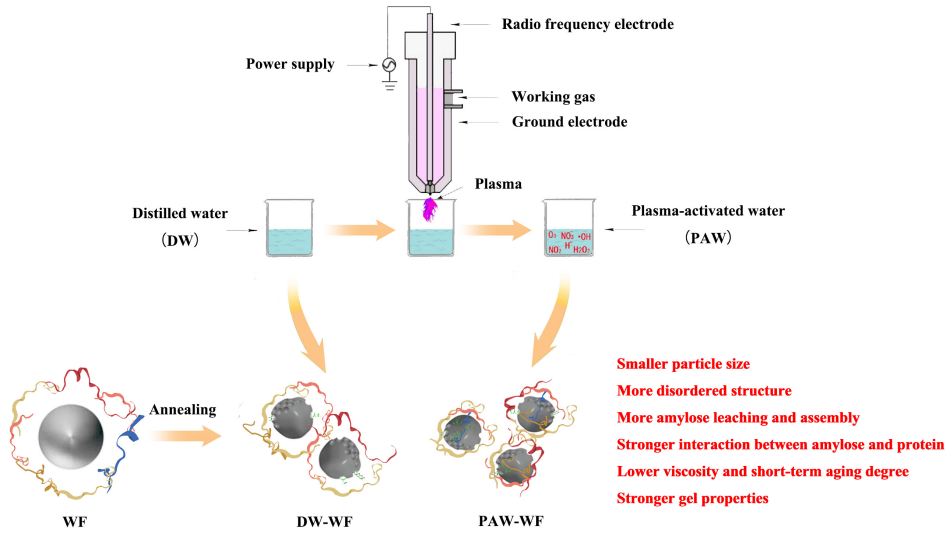

FIGURE 7
Influencing mechanism of PAW-ANN on the structure and properties of WF.

between WF and modified WF are shown in Table 4. After DW-ANN, the L*, a*, and b* values of WF significantly decreased, while WI values significantly increased ($p < 0.05$). It was probable that ANN destroyed the flour structure and exposed the inner white core. Compared with DW-ANN, PAW-ANN decreased the L* and WI, while increasing a* and b*. This showed that the effect of PAW-ANN was slightly lower than that of DW-ANN. The larger the ΔE value, the greater the color difference. According to ΔE, the color between WF and modified WF was clear differences. Compared with DW-WF, the ΔE value of PAW-WF was larger. This might be due to the degradation and oxidation of starch caused by the acidic components and ROS in the PAW.

Solubility and swelling power

According to Table 4, after ANN treatment, the SP of WF was not significantly changed, while the solubility significantly increased from 14.25 to 15.25% or 18.75% ($p < 0.05$). The increase in the solubility of DW-WF and PAW-WF may be because ANN destroyed the double helical structure of amylopectin in starch and enhanced the leaching ability of amylose (26). The solubility of WF treated with PAW-ANN (18.75%) was higher because of the degradation and oxidation of starch by the reactive species in the PAW (27), which was in consistent with XRD results. In addition, PAW-ANN could increase the solubility of protein due to the increase in irregular structures, which might also lead to increased solubility of WF.

Pasting properties

The viscosity properties of WF and modified WF are shown in Figure 5 and Table 5. ANN significantly reduced the peak viscosity, final viscosity, breakdown viscosity, and setback viscosity of WF ($p < 0.05$), which may be caused by the structural reorganization of starch granules. Similar findings were also demonstrated by Yadav et al. (28). Furthermore, the peak viscosity of PAW-WF was the lowest. It may be due to the hydrolysis of starch chains by the acidic components in the PAW, resulting in a decrease in the viscosity of WF (29). On the other hand, the acidic components in PAW also hydrolyzed the protein, resulting in a lack of protein network formation, which increases the brittleness of swollen starch granules, resulting in a decrease in viscosity of WF (30). The breakdown viscosity reflects the thermal stability of swollen starch granules at high temperatures and shear rates (20). Setback viscosity means that in the cooling stage of starch pastes, molecules can reassemble into ordered structures and form new crystals. The smaller the setback value, the more difficult it is for starch granules to form an extensive ordered structure when cooling (31, 32). Therefore, compared with WF and DW-WF, PAW-WF has better stability and weaker short-term retrogradation, suitable for quick-frozen flour products.

Rheological properties

The dynamic rheological curves of WF and modified WF are shown in Figure 6. G' and G" represent the elasticity and viscosity of gels, respectively (33). Tanδ represents the viscoelasticity ratio of the gel (34). According to Figures 6A,B, the G' and G" values of both the WF and modified WF gels increased with the scanning frequency. G' > G" (tanδ < 1) over the entire scanning frequency range indicated that all WF samples had the properties and elasticity of weak gels (35–37).

ANN significantly reduced G' and G" of native WF, indicating that ANN could significantly change the viscoelasticity of WF gels. Compared with WF, the gels of DW-WF and PAW-WF were softer and less viscous, consistent with the results of RVA. Similarly, after ANN, the tanδ values of WF gels decreased in the entire frequency range, indicating an increase in the proportion of elastic components in the WF. Moreover, compared with DW-WF, PAW-WF had lower tanδ and larger G' value, indicating that PAW-WF had stronger gel properties with potential applications in the noodles. This might be due to more re-arrangement of amylose units formed on the surface of starch granules through larger pores and cracks. In addition, the formation of the amylose-protein complex on the surface of starch granules might also be another important reason.

Conclusion

In summary, PAW-ANN had a significant influence on the structure and properties of WF due to the presence of acidic components and ROS in the PAW (**Figure 7**). Compared with DW-ANN, PAW-ANN decreased the particle size, long-range ordered structure of starch, and the partially ordered structure of the protein in WF, leading to more amylose leaching and assembly, and stronger interaction between amylose and protein. Furthermore, PAW-ANN increased the solubility, stability, and gel properties of WF, resulting in a lower peak viscosity and short-term aging degree of WF. Therefore, PAW-ANN would be employed as a novel physical modification technology to change the structure and improve properties of WF, especially for the "green" production of flour products requiring low viscosity, retrogradation rate, and high stability.

Data availability statement

The original contributions presented in this study are included in the article/supplementary material, further inquiries can be directed to the corresponding author/s.

Author contributions

YY contributed to the conception and design and wrote the first draft of the manuscript. YY and BN contributed to the funding of the study. XX, XuJ, ZC, and XiJ organized the database. YH and MS contributed to writing—review and editing. All authors contributed to the article and approved the submitted version.

Funding

We are grateful to the National Natural Science Foundation of China (32101945), the Program for Science and Technology Innovation Talents in Universities of Henan Province (20HASTIT037), the Major Science and Technology Project of National Tobacco Corporation [110202101013 (XJ-05)], and Science and Technology Project of Tobacco Corporation in Hainan Province (2021460000240132). This study received funding from National Tobacco Corporation and Tobacco Corporation in Hainan Province. The funder was not involved in the study design, collection, analysis, interpretation of data, the writing of this article or the decision to submit it for publication.

Conflict of interest

The authors declare that the research was conducted in the absence of any commercial or financial relationships that could be construed as a potential conflict of interest.

Publisher's note

References

1. Mann J, Schiedt B, Baumann A, Conde-Petit B, Vilgis TA. Effect of heat treatment on wheat dough rheology and wheat protein solubility. *Food Sci Technol Int.* (2014) 20:341–51. doi: 10.1177/1082013213488381

2. Bhat NA, Wani IA, Hamdani AM, Gani A, Masoodi FA. Physicochemical properties of whole wheat flour as affected by gamma irradiation. *LWT Food Sci Technol.* (2016) 71:175–83. doi: 10.1016/j.lwt.2016.03.024

3. Lazaridou A, Vouris DG, Zoumpoulakis P, Biliaderis CG. Physicochemical properties of jet milled wheat flours and doughs. *Food Hydrocoll.* (2018) 80:111–21. doi: 10.1016/j.foodhyd.2018.01.044

4. Iuga M, Mironeasa S. A review of the hydrothermal treatments impact on starch based systems properties. *Crit Rev Food Sci.* (2020) 60:3890–915. doi: 10.1080/10408398.2019.1664978

5. Thirumdas R, Kothakota A, Annapure U, Siliveru K, Blundell R, Gatt R, et al. Plasma activated water (PAW): chemistry, physico-chemical properties, applications in food and agriculture. *Trends Food Sci Tech.* (2018) 77:21–31. doi: 10.1016/j.tifs.2018.05.007

6. Yan Y, Feng L, Shi M, Cui C, Liu Y. Effect of plasma-activated water on the structure and in vitro digestibility of waxy and normal maize starches during heat-moisture treatment. *Food Chem.* (2020) 306:125589. doi: 10.1016/j.foodchem.2019.125589

7. Yan Y, Peng B, Niu B, Ji X, He Y, Shi M. Understanding the structure, thermal, pasting, and rheological properties of potato and pea starches affected by annealing using plasma-activated water. *Front Nutr.* (2022) 9:842662. doi: 10.3389/fnut.2022.842662

8. Wang S, Wang J, Wang S, Wang S. Annealing improves paste viscosity and stability of starch. *Food Hydrocoll.* (2017) 62:203–11. doi: 10.1016/j.foodhyd.2016.08.006

9. Wang S, Wang J, Zhang W, Li C, Yu J, Wang S. Molecular order and functional properties of starches from three waxy wheat varieties grown in china. *Food Chem.* (2015) 181:43–50. doi: 10.1016/j.foodchem.2015.02.065

10. Li S, Liu Y, Tong J, Yu L, Ding M, Zhang Z, et al. The overexpression of high-molecular-weight glutenin subunit Bx7 improves the dough rheological properties by altering secondary and micro- structures of wheat gluten. *Food Res Int.* (2020) 130:108914. doi: 10.1016/j.foodres.2019.108914

11. Wang K, Luo S, Cai J, Sun Q, Zhao Y, Zhong X, et al. Effects of partial hydrolysis and subsequent cross-linking on wheat gluten physicochemical properties and structure. *Food Chem.* (2016) 197:168–74. doi: 10.1016/j.foodchem.2015.10.123

12. Suo T, Guo XN, Zhu KX. Effects of tempering with plasma-activated water on total plate count and quality properties of wheat flour. *J Cereal Sci.* (2022) 105:103468. doi: 10.1016/j.jcs.2022.103468

13. Zhu F, Cai YZ, Sun M, Corke H. Influence of *Amaranthus betacyanin* pigments on the physical properties and color of wheat flours. *J Agr Food Chem.* (2008) 56:8212–7. doi: 10.1021/jf801579c

14. Chaple S, Sarangapani C, Jones J, Carey E, Causeret L, Genson A, et al. Effect of atmospheric cold plasma on the functional properties of whole wheat (*Triticum aestivum L.*) grain and wheat flour. *Innov Food Sci Emerg.* (2020) 66:102529. doi: 10.1016/j.ifset.2020.102529

15. Solaesa AG, Villanueva M, Munoz JM, Ronda F. Dry-heat treatment vs. heat-moisture treatment assisted by microwave radiation: techno-functional and rheological modifications of rice flour. *LWT Food Sci Technol.* (2021) 141:110851. doi: 10.1016/j.lwt.2021.110851

16. Zhou RW, Zhou RS, Prasad K, Fang Z, Speight R, Bazaka K, et al. Cold atmospheric plasma activated water as a prospective disinfectant: the crucial role of peroxynitrite. *Green Chem.* (2018) 20:5276–84. doi: 10.1039/c8gc02800a

17. Zhao YM, Patange A, Sun DW, Tiwari B. Plasma-activated water: physicochemical properties, microbial inactivation mechanisms, factors influencing antimicrobial effectiveness, and applications in the food industry. *Compr Rev Food Sci. Food Saf.* (2020) 19:3951–79. doi: 10.1111/1541-4337.12644

18. Wu SJ, Zhang Q, Ma RN, Yu S, Wang KL, Zhang J, et al. Reactive radical-driven bacterial inactivation by hydrogen-peroxide-enhanced plasma-activated-water. *Eur Phys J Spec Top.* (2017) 226:2887–99. doi: 10.1140/epjst/e2016-60330-y

19. Xue L, Ma Y, Yang N, Wei H. Modification of corn starch via innovative contactless thermal effect from induced electric field. *Carbohyd Polym.* (2021) 255:117378. doi: 10.1016/j.carbpol.2020.117378

20. Trung P, Ngoc L, Hoa PN, Tien N, Hung PV. Impact of heat-moisture and annealing treatments on physicochemical properties and digestibility of starches from different colored sweet potato varieties. *Int J Biol Macromol.* (2017) 105(Pt. 1):1071–8. doi: 10.1016/j.ijbiomac.2017.07.131

21. Wongsagonsup R, Deeyai P, Chaiwat W, Horrungsiwat S, Leejariensuk K, Suphantharika M, et al. Modification of tapioca starch by non-chemical route using jet atmospheric argon plasma. *Carbohyd Polym.* (2014) 102:790–8. doi: 10.1016/j.carbpol.2013.10.089

22. Chen B, Wang YR, Fan JL, Yang Q, Chen HQ. Effect of glutenin and gliadin modified by protein-glutaminase on retrogradation properties and digestibility of potato starch. *Food Chem.* (2019) 301:125226. doi: 10.1016/j.foodchem.2019.125226

23. Luo Y, Shen M, Li E, Xiao Y, Wen H, Ren Y, et al. Effect of *Mesona chinensis* polysaccharide on pasting, rheological and structural properties of corn starches varying in amylose contents. *Carbohyd Polym.* (2020) 230:115713. doi: 10.1016/j.carbpol.2019.115713

24. Segat A, Misra NN, Cullen PJ, Innocente N. Atmospheric pressure cold plasma (ACP) treatment of whey protein isolate model solution. *Innov Food Sci Emerg.* (2015) 29:247–54. doi: 10.1016/j.ifset.2015.03.014

25. Devi R, Sit N. Effect of single and dual steps annealing in combination with hydroxypropylation on physicochemical, functional and rheological properties of barley starch. *Int J Biol Macromol.* (2019) 129:1006–14. doi: 10.1016/j.ijbiomac.2019.02.104

26. Rocha-Villarreal V, Hoffmann JF, Vanier NL, Serna-Saldivar SO, García-Lara S. Hydrothermal treatment of maize: changes in physical, chemical, and functional properties. *Food Chem.* (2018) 263:225–31. doi: 10.1016/j.foodchem.2018.05.003

27. Bie P, Pu H, Zhang B, Su J, Chen L, Li X. Structural characteristics and rheological properties of plasma-treated starch. *Innov Food Sci Emerg.* (2015) 34:196–204. doi: 10.1016/j.ifset.2015.11.019

28. Yadav BS, Guleria P, Yadav RB. Hydrothermal modification of indian water chestnut starch: influence of heat-moisture treatment and annealing on the physicochemical, gelatinization and pasting characteristics. *LWT Food Sci Technol.* (2013) 53:211–7. doi: 10.1016/j.lwt.2013.02.007

29. Zambelli RA, Galvao A, de Mendonca LG, Leao MVD, Carneiro SV, Lima ACS, et al. Effect of different levels of acetic, citric and lactic acid in the cassava starch modification on physical, rheological, thermal and microstructural properties. *Food Sci Tech Res.* (2018) 24:747–54. doi: 10.3136/fstr.24.747

30. Chung HJ, Cho DW, Park JD, Kweon DK, Lim ST. In vitro starch digestibility and pasting properties of germinated brown rice after hydrothermal treatments. *J Cereal Sci.* (2012) 56:451–6. doi: 10.1016/j.jcs.2012.03.010

31. Song HY, Lee SY, Choi SJ, Kim KM, Kim JS, Han GJ, et al. Digestibility and physicochemical properties of granular sweet potato starch as affected by annealing. *Food Sci Biotechnol.* (2014) 23:23–31. doi: 10.1007/s10068-014-0004-9

32. Alcázar-Alay SC, Meireles MAA. Physicochemical properties, modifications and applications of starches from different botanical sources. *Food Sci Tech.* (2015) 35:215–36. doi: 10.1590/1678-457X.6749

33. Sudheesh C, Sunooj KV, Sinha SK, George J, Kumar S, Murugesan P, et al. Impact of energetic neutral nitrogen atoms created by glow discharge air plasma on the physico-chemical and rheological properties of kithul starch. *Food Chem.* (2019) 294:194–202. doi: 10.1016/j.foodchem.2019.05.067

34. Chen L, Tian Y, Bai Y, Wang J, Jiao A, Jin Z. Effect of frying on the pasting and rheological properties of normal maize starch. *Food Hydrocoll.* (2018) 77:85–95. doi: 10.1016/j.foodhyd.2017.09.024

35. Ji N, Qiu C, Xu YC, Xiong L, Sun QJ. Differences in rheological behavior between normal and waxy corn starches modified by dry heating with hydrocolloids. *Starch Stärke.* (2017) 69:1600332. doi: 10.1002/star.201600332

36. Chen B, Zhang B, Li MN, Xie Y, Chen HQ. Effects of glutenin and gliadin modified by protein-glutaminase on pasting, rheological properties and microstructure of potato starch. *Food Chem.* (2018) 253:148–55. doi: 10.1016/j.foodchem.2018.01.155

37. Ma YS, Pan Y, Xie QT, Li XM, Zhang B, Chen HQ. Evaluation studies on effects of pectin with different concentrations on the pasting, rheological and digestibility properties of corn starch. *Food Chem.* (2019) 274:319–23. doi: 10.1016/j.foodchem.2018.09.005

frontiers | Frontiers in Nutrition

TYPE Original Research
PUBLISHED 12 August 2022
DOI 10.3389/fnut.2022.970010

OPEN ACCESS

EDITED BY
Sen Ma,
Henan University of Technology, China

REVIEWED BY
Augusto Cannone Falchetto,
Aalto University, Finland
Xiaonan Sui,
Northeast Agricultural University, China
İbrahim Gülseren,
Istanbul Sabahattin Zaim University, Turkey

*CORRESPONDENCE
Xiao Liu
liuxiao@jiangnan.edu.cn
Jianghua Li
lijianghua@jiangnan.edu.cn

SPECIALTY SECTION
This article was submitted to Food Chemistry, a section of the journal Frontiers in Nutrition

RECEIVED 15 June 2022
ACCEPTED 27 July 2022
PUBLISHED 12 August 2022

CITATION
Qin J, Zhao Y, Zhou J, Zhang G, Li J and Liu X (2022) Rheological properties of transglutaminase-treated concentrated pea protein under conditions relevant to high-moisture extrusion processing. *Front. Nutr.* 9:970010. doi: 10.3389/fnut.2022.970010

Rheological properties of transglutaminase-treated concentrated pea protein under conditions relevant to high-moisture extrusion processing

Jianxin Qin[1,2], Yinghan Zhao[1], Jingwen Zhou[1,2], Guoqiang Zhang[1], Jianghua Li[1]* and Xiao Liu[1]*

[1]Science Center for Future Foods, Jiangnan University, Wuxi, China, [2]National Engineering Laboratory for Cereal Fermentation Technology, Jiangnan University, Wuxi, China

At present, the structural changes of extruded materials under thermal-mechanical stress during high-moisture extrusion are still unclear. In this study, the transglutaminase (TG) treatments on the structure of pea protein isolate (PPI) under conditions relevant to high-moisture extrusion processing (50 wt% PPI at 30°C, 120°C and heated to 120°C and subsequently cooled to 30°C) was studied by using a closed cavity rheometer. Strain and frequency sweeping were carried out under various temperature conditions, and the information obtained was drawn into a texture map. Lissajous curves combined with energy dissipation ratio were introduced to characterize the nonlinear response of the samples. The results showed that the storage modulus of PPI increased with the increase of TG concentration during heat treatment. After cooling to 30°C, PPI with 0.25–1%TG could enhance the elasticity, but treating by 2% TG could inhibit the formation of disulfide bonds, the uniform development of the protein network, thus showing the "tough" character. These findings can help to better understand the relationships of material-structure during the extrusion process, and also provide help for further optimization of the quality of meat substitutes.

KEYWORDS

transglutaminase, pea protein, rheological properties, closed cavity rheometer, high-moisture extrusion

Introduction

The rapid growth of the world's population has led to a shortage of meat, and plant-based meat has gradually begun to be commercially produced because it is more efficient and environmentally sustainable (1–3). Texture is an important index to evaluate the quality of plant-based meat, which helps to improve the acceptance of consumers (4). The formation of texture during food processing can be partially improved by adding different components, such as proteins, polysaccharides and crosslinking agents (5). As a crosslinking enzyme, Transglutaminase (TG) can cross-link glutamine residues with lysine to form a ε-(γ-glutamyl) lysine bonds to change the functional properties of proteins, thus contributing to the quality of gel structure of foods (6, 7).

High-moisture extrusion is a promising process to create the fiber structure of plant-based meat. Previous studies have reported that TG modification can improve the texture of high-moisture extrudates (8, 9). However, the extrusion process is regarded as a "black box" process, and the setting of conditions and the production of extrudates depend on operating experience (10, 11). The sudden stop sampling method is a common method to study the state of the sample during extrusion (12–14). Unfortunately, this method cannot systematically study the structural changes of extrudates under thermal-mechanical stress during high-moisture extrusion.

Recently, a closed cavity rheometer has been used to investigate the rheological properties of extrudates during extrusion (15–17). The device combines the advantages of the traditional rheometer and shear cell, which can not only carry out thermo-mechanical treatment of samples under high pressure and sealed conditions, but also measure the rheological properties of samples online (18). Additionally, large amplitude oscillatory shear (LAOS) of protein samples combined with Lissajous curves can provide additional information (19, 20), which is helpful to simulate the structural changes and rheological behavior of protein materials during extrusion, leading to solving the problem of "black box" process to a great extent.

Pea protein is a high-quality protein resource with a relatively balanced amino acid content. Consumers are more interested in plant-based foods made from pea protein (21, 22). More importantly, pea protein is more acceptable because it has no allergenic effect. Therefore, in this study, pea protein isolate (PPI) was invoked as a model, and the structural changes of PPI treated with TG during high-moisture extrusion were investigated by a closed cavity rheometer. Strain and frequency sweep were carried out under various temperature conditions, and Lissajous curve was introduced to characterize the nonlinear response of samples. Moreover, texture maps were drawn in order to deeply understand the effect of TG concentration on PPI structure during extrusion. This study elucidates the changes of protein structure at various stages of high-moisture extrusion and the influence mechanism of TG induction on protein extrusion structure, which is important for the optimization of extrusion conditions and the selection of appropriate materials to produce meat substitutes in the future.

Materials and methods

Materials

Pea protein isolate (PPI) was provided by Yantai Shuangta Food Co., Ltd., (Yantai) with a protein content of 84.2% (dry base). Moisture content was 7.3% (wet base). The other components were 6.5% (dry base) starch, 4.2% (dry base) ash, 2% (dry base) lipids, 3.1% (dry base) fiber. TG (120 U/g) was purchased from Jiangsu Dongsheng Biotechnology Co., Ltd. All other chemicals used were of analytical grade unless otherwise specified.

Preparation of samples

Transglutaminase with PPI and distilled water were mixed in sealed bags. The concentration of TG was different in each group of samples (0, 0.25, 0.5, 1, 1.5, and 2%). The mixed samples were hydrated at 25°C for 30 min.

Rheological properties

The rheological properties of PPI under various conditions were measured using a closed cavity rheometer (CCR) (RPA Elite, TA Instruments, New Castle, DE, United States). CCR measured the torque applied to the rheometer cavity by setting the lower chamber of the rheometer to oscillate at a specific frequency and strain amplitude. The upper chamber of the rheometer remained static, and grooves in the conical chamber prevented the specimen from sliding.

In total, 5 g of hydrated samples were wrapped with two layers of plastic film and placed in the chamber of a closed chamber rheometer (**Figure 1**). The sealed samples were subjected to a pressure of about 4.5 bar (15, 18, 23). In order to simulate the state of protein samples at various extrusion temperatures, three different temperature conditions were tested: (A) 30°C, (B) from 30 to 120°C at a rate of 2°C/min and (C) from 30 to 120°C at a rate of 2°C/min and then cooled to 30°C. The frequency of 1 Hz and strain amplitude of 1% were always maintained during heating. Strain sweep tests were carried out on protein samples under the above mentioned three temperature conditions (0.1–1,000%). In order to make the obtained data more intuitive, the data at the end of the linear viscoelastic (LVE) regime and the intersection point of elastic modulus and viscous modulus were drawn into texture

maps, so as to better understand the effect of TG on PPI texture under extrusion conditions. Then the strain amplitude was kept constant at the above mentioned three temperature conditions, and frequency scanning was carried out (the frequency varied from 0.1 to 50 Hz).

The data obtained from the large amplitude oscillatory shear test were analyzed. Lissajous curves were used to describe the relationship between the sample and the strain applied. The complexity of Lissajous curve shape depends on the system response to sinusoidal deformation. The presence of many harmonic components in these responses leads to the diversity of the Fourier spectrum. We can obtain the internal microstructure information of the test sample indirectly through the Lissajous curve. This helps to understand the rheological behavior of protein samples at large strain amplitude in more detail, and then better predict the rheological properties of the sample in the processing.

The closed area in the Lissajous curve represents the energy consumed per unit volume over a full period of the strain applied (24). The energy dissipated per unit volume in a single cycle (1) is only the first-order viscous Fourier coefficient (G'_1: calculated from the intensity and phase of the first harmonic);

$$Ed = \oint \sigma d\gamma = G''_1 \gamma_0^2 \quad (1)$$

The energy dissipated by a perfectly plastic material in a single cycleis equal to

$$(Ed)_{pp} = 4\gamma_0 \sigma_{max} \quad (2)$$

for a given strain amplitude (γ_0) and a maximum stress (σ max).

Data of LAOS obtained were further analyzed according to the energy dissipation ratio (ϕ) proposed by Ewoldt et al. (24).

$$\phi = \frac{\text{Ed}}{(\text{Ed})\text{pp}} = \frac{\pi G''_1 \gamma_0}{4\ \sigma\text{max}} \quad (3)$$

Determination of protein solubility

In order to reveal the interactions during structure formation and maintenance, eight extraction solvents were prepared to measure the protein solubility of the samples and calculate the changes in chemical crosslinking bonds, as showed in **Table 1** (9, 25, 26). The soluble protein content in the supernatant was determined by the BCA method at 562 nm with a 96-well plate, and the total protein content of the samples was determined by the Kjeldahl method, and then the protein solubility was calculated according to the ratio between the two. Different chemical bonds were calculated based on solubility in different solutions. Each measurement shall be made in triplicate.

Statistical analysis

All experiments were carried out in three replicates. Results were reported as mean ± standard deviation. SPSS was used for one-way analysis of variance. $P < 0.05$ indicated a significant difference among groups.

Results and discussion

Small amplitude oscillatory shear

Figure 2 showed the storage (G') and loss (G") modulus of PPI with TG (0–2%) varied with strain amplitude from 1 to 1,000% under the three temperature conditions. In the LVE regime, the modulus was independent of the strain amplitude applied. G' of the sample was always higher than G", and the structure showed a solid state. The physical bond rupture rate increases faster than the reforming rate with the increase of strain amplitude. The decrease of G' by an order of magnitude and the fluidity of the sample was enhanced indicated that the structure of all PPI samples was destroyed (27). The value of G" was higher than G' indicates that the sample changed from a viscoelastic solid to a viscoelastic fluid (28).

As shown in **Figure 2A**, the G' of PPI treated by 2% TG in LVE regime was the maximum, about 450 KPa, and the control group (0% TG) had the lowest G', about 300 KPa. **Figure 2B** showed the curves of G' and G" for PPI when heated to 120 °C. The value of G' was higher than G" in LVE regime, indicating that PPI still remains elastic at this time (29, 30). However, compared with 30°C, the G' and G" of PPI decreased by an order of magnitude at 120°C. With the slow rise of temperature, TG could catalyze the cross-linking between PPI molecules and form a firm network structure (16). As a whole, G' showed a gradually increasing trend with the increase of TG concentration, and the G' of PPI with 2% TG was the largest, about 70 KPa. This was due to the catalytic action of TG to stabilize the conformation of protein molecules (31, 32). PPI was cooled to 30°C after heat treatment and its G' and G" changes were shown in **Figure 2C**. The modulus of the PPI was higher than 30°C after cooling. It was worth noting that after cooling to 30°C, the G' of PPI samples with 1% TG was the largest, about 750 KPa, which was larger than that of PPI samples with 1.5 and 2% TG. The reason might be that the addition of TG could promote the formation of new hydrogen and disulfide bonds to stabilize protein conformation in protein molecular rearrangement. However, excessive TG (2%) catalyze was not conducive to molecular rearrangement. The modulus was lower than that of other samples with TG after being cooled to 30°C (9).

The yield stress is commonly one of the symbols of the rheological properties of the sample. It is defined as the shear stress value at the end of the LVE regime. To make the test

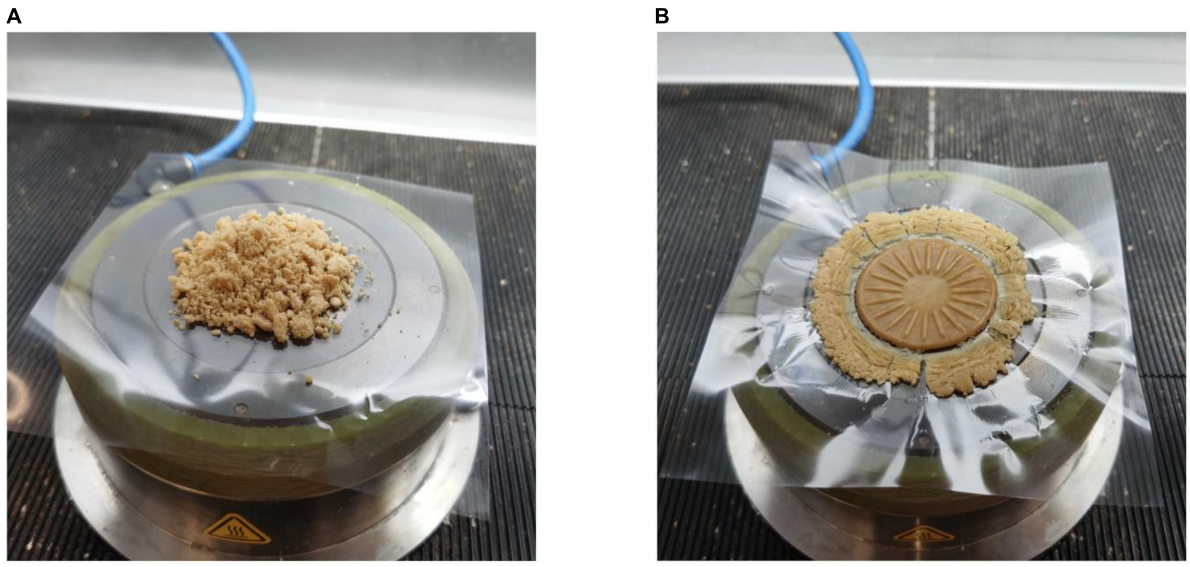

FIGURE 1
50 wt% PPI before **(A)** and after **(B)** measurement in the closed cavity rheometer.

TABLE 1 Information about the extracting solutions, and calculation of chemical bonds and their interactions.

No.	Extracting solution	Chemical bond and their interactions	Calculation of chemical bonds and their interactions
(1)	0.035 mol/L pH 7.6 phosphate buffer solution (P)	Native state protein	(1)
(2)	8 mol/L urea in the phosphate buffer solution (P + U)	Hydrogen bonds	(2) − (1)
(3)	0.1 mol/L 2-mercaptoethanol (2-ME) in the phosphate buffer solution (P + M)	Disulphide bonds	(3) − (1)
(4)	1.5 g/100 mL sodium dodecyl sulfate (SDS) in the phosphate buffer solution (P + S)	Hydrophobic interactions	(4) − (1)
(5)	8 mol/L urea and 0.1 mol/L 2-ME in the phosphate buffer solution (P + U + M)	Interactions between hydrogen bonds and disulphide bonds	(5) − (2) − (3) + (1)
(6)	1.5 g/100 mL SDS and 8 mol/L urea in the phosphate buffer solution (P + U + S)	Interactions between hydrogen bonds and hydrophobic interactions	(6) − (2) − (4) + (1)
(7)	1.5 g/100 mL SDS and 0.1 mol/L 2-ME in the phosphate buffer solution (P + S + M)	Interactions between disulphide bonds and hydrophobic bonds	(7) − (3) − (4) + (1)
(8)	8 mol/L urea, 1.5 g/100 mL SDS and 0.1 mol/L 2-ME in the phosphate buffer solution (P + U + S + M)	Interactions among hydrogen bonds, disulphide bonds and hydrophobic interactions	(8) + (2) + (3) + (4) −(1) − (5) − (6) − (7)

results more explicit, we researched the change in the yield stress of PPI with TG. Here, the end of the LVE regime is defined as the point where the difference in G' value is greater than 10%. As can be seen from **Figure 3**, G' showed an upward trend in general at the LVE regime. This indicated that the increase of TG concentration led to the enhancement of deformation resistance of samples (32, 33). At 120°C, the yield stress of the control group (0% TG) was less than that of the 30°C, which was caused by the high temperature leading to the protein structure fracture. However, the PPI samples showed different results after being cooled to 30°C. Compared with the sample at 30°C, the increase value of G' was the highest when the addition of TG was 1%, it meant that the effect of TG was the best at this concentration. This was due to the formation of new chemical bonds in the cooling process, which further increased the modulus of the PPI (9).

The G' and G" of PPI as a function of frequency were shown in **Supplementary Figure 1**. The G' and G" of PPI samples with different TG concentrations increased slightly with the increase of frequency (17). In order to show the difference between data more intuitively, the power law equation $G' \sim \omega^n$ was used to fit the frequency response, where ω was frequency and n was exponent, and the significance analysis was conducted. As shown in **Supplementary Table 1**, the samples treated by different TG concentration had similar frequency dependence. At 120°C, the n of the samples was smaller than the initial,

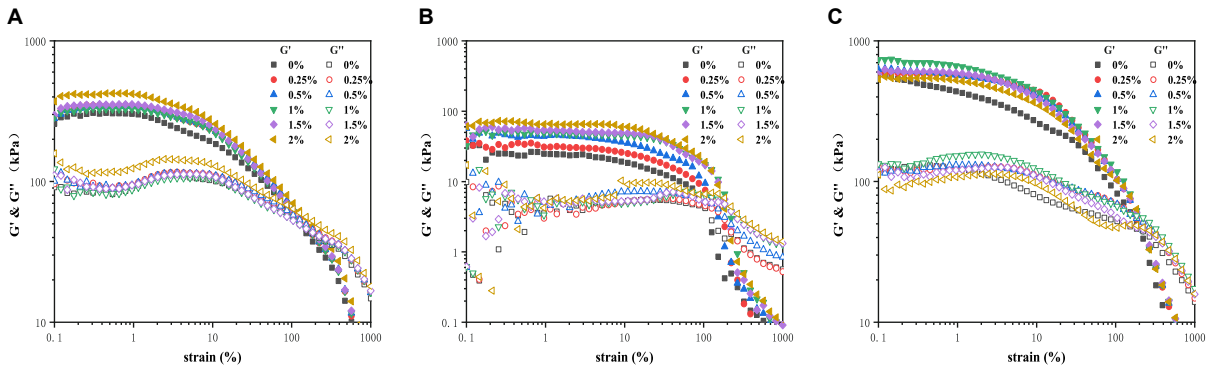

FIGURE 2
Strain sweep for PPI with different TG concentrations at **(A)** 30°C, **(B)** from 30 to 120°C and **(C)** from 30 to 120°C and then cooled to 30°C.

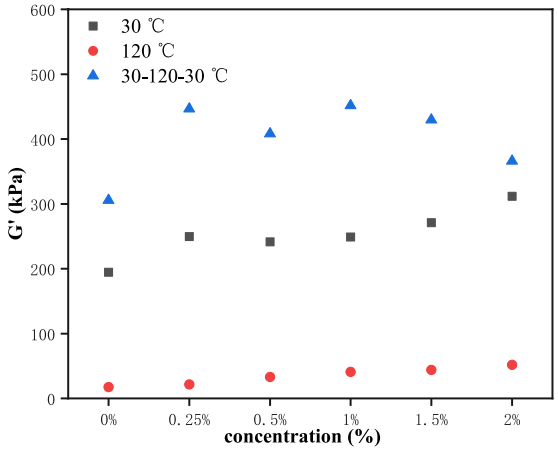

FIGURE 3
The function relation between the TG concentration and the value of G' at the end of the LVE regime.

and the samples cooled after heating had the minimum n. The smaller n value in the power law equation indicates that the structure was more stable, and the change of this state required a stronger force. This weak power law behavior was similar to soft glass materials (34). PPI showed a disorder of metastable structure in this state.

Texture maps

Although the texture of food can be perceived by the human senses, it can also be quantified into mechanical or rheological properties. These properties can be associated with "textures." Texture map as a tool response can more intuitively show the differences between materials by reducing the nonlinear rheological information to a two-dimensional diagram only involving the key parameters of the characteristics (19). To make the texture maps representative, points at the end of the LVE regime and at the crossover point were selected for analysis (19). Figure 4 divided the response of samples into four quadrants-rubbery, mushy, brittle and tough. Table 2 showed various color schemes to describe points on the maps. The samples in the lower right corner are all "rubbery" and show low shear stress and high shear strain in rheological behavior. The representative materials are glutinous rice starch (35). The upper right quadrant represents a hard material with high shear stress and strain, such as fruit glue, with a "tough" texture. These materials, clustered in the upper left corner, have "brittle" properties, such as cheese (36). The materials in the lower left corner have low stress and low strain properties, and these materials exhibit a "mushy" texture, such as debranched starch (35).

Figure 4A showed the texture map of PPI samples with different TG concentrations at three various temperatures (30°C, 120°C, and from 120°C cooled to 30°C). At 30°C, PPI samples were fragile, and with the increase of TG concentration, PPI samples were more brittle. After heating to 120°C, the PPI sample moved to the lower right of the texture map as a whole and became more rubbery than mushy. The higher concentration of TG resulted in higher stress values in the samples. After being cooled to 30°C, the PPI sample moved back to the upper left of the texture map, meaning that the sample became more brittle. This suggested that additional interactions were formed as the sample cooled. It could be seen from Figure 4A that the sample with 1% TG had the maximum stress value, and the sample with 1.5% TG was more brittle. It indicated that the concentration of TG was not correlated with the stress value, which was similar to Figure 2. These phenomena indicated that appropriate TG could promote the formation of new forces in the cooling process of the sample, while the effect of excessive TG is not satisfactory. The texture of PPI samples with different concentration of TG at the crossover points was shown in Figure 4B. At 30°C, the samples were brittle. However, we could see that the overall samples gradually

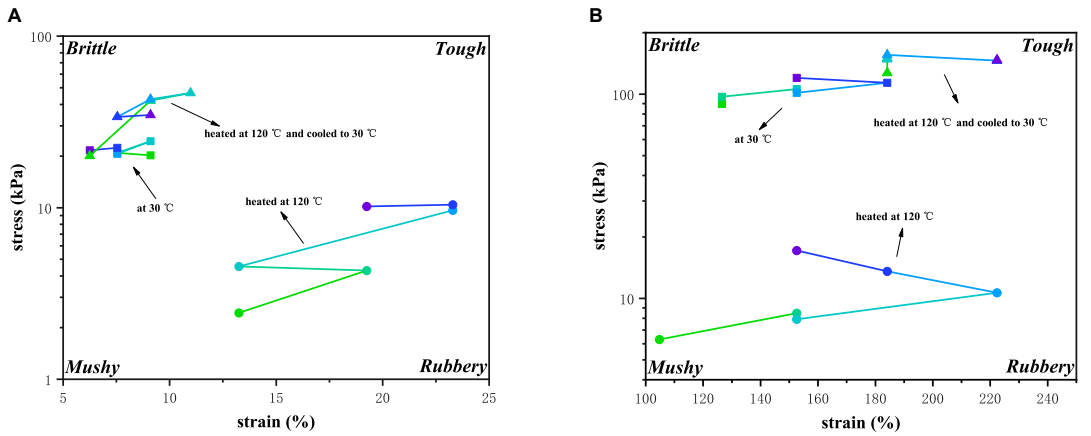

FIGURE 4
Texture map for the PPI with different TG concentrations **(A)** at the end of the LVE regime and **(B)** at the crossover point.

TABLE 2 Color scheme to describe the points of the maps.

	0%TG	0.25%TG	0.5%TG	1%TG	1.5%TG	2%TG
At 30°C	■	■	■	■	■	■
Heated at 120°C	●	●	●	●	●	●
Heated at 120°C and cooled to 30°C	▲	▲	▲	▲	▲	▲

toughed with the increase of TG addition. At 120°C, although all PPI samples were softened by heating, the strain values of the samples with TG were stronger than those of samples without TG, and showed a positive correlation trend. Under the condition of cooled to 30°C, the overall characteristics of the sample changed to brittle. It was much tougher than 30°C. These phenomena also confirmed the correctness of the data obtained before.

Large amplitude oscillatory shear

The LAOS provided a great deal of additional information about the microstructure of complex fluids (37–39). **Figure 5** showed Lissajous curves of PPI samples with different TG concentrations under different strain amplitudes at three various temperatures. The Lissajous curves were similar at the three temperature conditions (30°C, 120°C, and from 120°C cooled to 30°C).

At 30°C, the change of strain amplitude almost did not affect the performance of PPI samples treated by different concentration of TG. It was observed that the area of the graph showed a positive correlation with the strain amplitude. PPI with different TG concentrations showed a narrow oval shape with a small closed area at the strain amplitude of 1.151%, which means that the specimen has elastic response (38). As the strain increases, the graph gradually approximates to a rectangle, which is a sign of viscous dissipation. This indicated that the system dissipated more and more mechanical energy in a single cycle. This showed that the internal structure of the sample had changed due to the action of external forces and the storage modulus decreased, and finally showed the plastic (40–42). As can be seen from **Figure 5**, PPI with 2% TG reduced the energy dissipation in the deformation process. At 120°C, the addition of TG affected the shape of Lissajous curve, presenting an inverted S-shaped curve at a high strain amplitude (104.765%). The stress value of PPI with TG was higher than that of the control group (0% TG). It was positively correlated with the additional concentration of TG at various strain amplitudes. This indicated that PPI was aggregated treated by TG and protein conformation was stabilized at 120°C. When the sample cooled to 30°C, the stress value of PPI with TG was greater than that of the control group (0% TG). The stress value of PPI with 1% TG was the highest. The reason may be that the addition of TG promotes the formation of new chemical bonds during the rearrangement of protein molecules, which makes the protein structure more stable. However, excessive addition of TG was not conducive to molecular rearrangement, resulting in lower stress values than PPI with 1% TG after being cooled to 30°C (9).

The energy dissipation ratio

In order to make the energy dissipation and nonlinear behavior in the process more clearly, we calculate the dissipation ratio ϕ. The function of energy dissipation ratio changing with

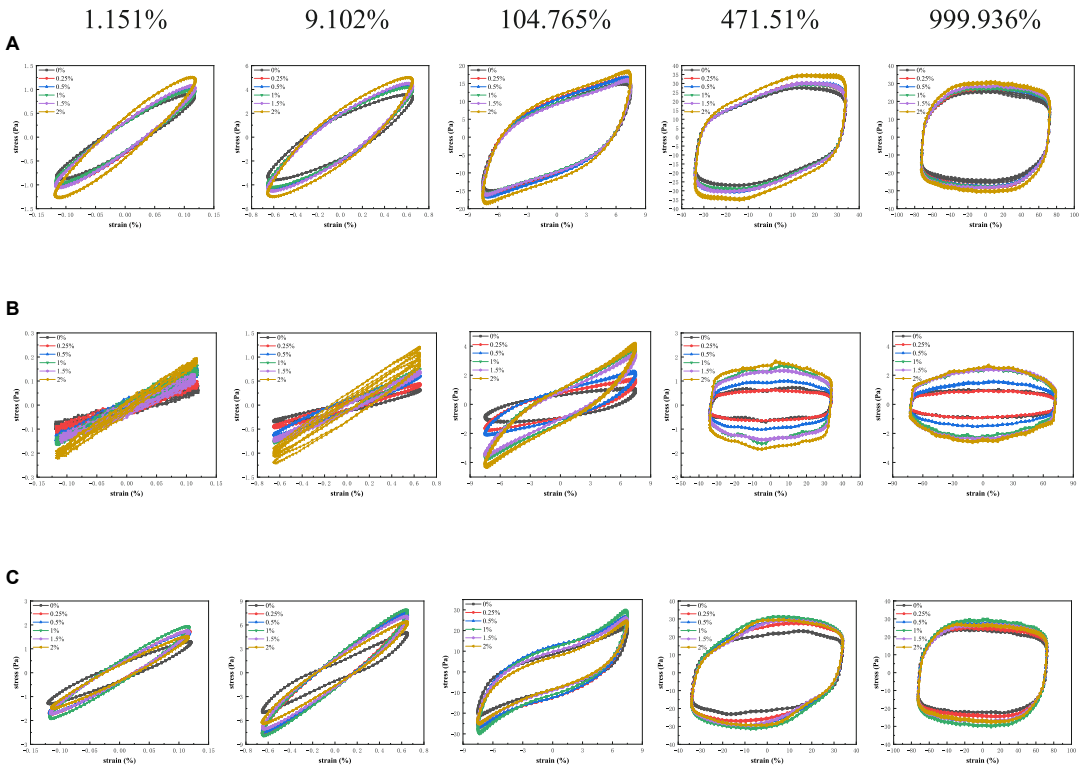

FIGURE 5
Lissajous curves of stress versus strain amplitude for PPI with different TG concentrations at **(A)** 30°C, **(B)** from 30 to 120°C and **(C)** from 30 to 120°C and then cooled to 30°C.

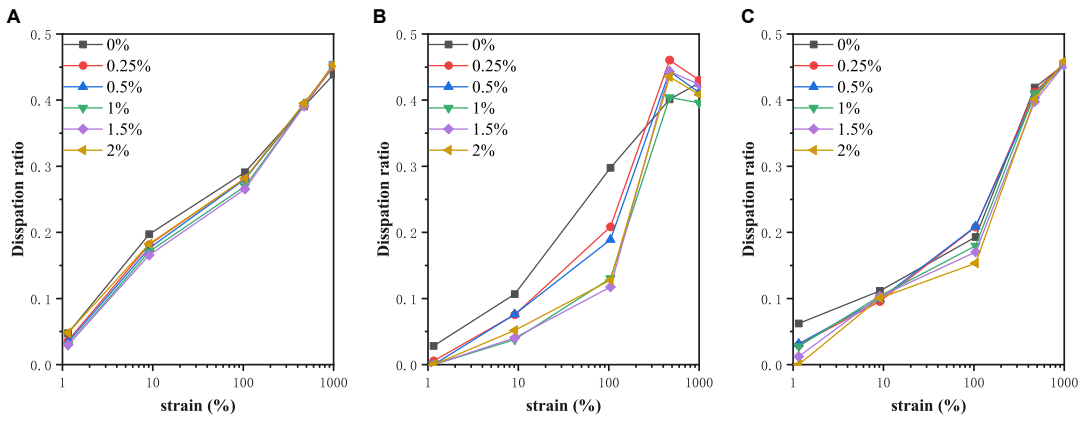

FIGURE 6
Dissipation ratio of PPI with different TG concentrations at **(A)** 30°C, **(B)** from 30 to 120°C and **(C)** from 30 to 120°C and then cooled to 30°C.

strain value was shown in Figure 6. The ϕ was small for PPI at small strain amplitudes, showing a predominantly elastic response. There was a positive correlation between dissipation ratio and strain amplitude. As can be seen from Figure 6, the maximum dissipation ratio obtained was about 0.45, showing a viscous characteristic. At 30°C, the energy dissipation ratio of each PPI sample had no significant difference. However, at 120°C, PPI without TG had the largest dissipation ratio with the small strain amplitude, which was manifested as viscosity. When the strain reached 104.765%, the dissipation ratio of the PPI with TG was suddenly increased, and finally tended to be the same. And the overall performance was that PPI samples with higher concentration of TG had high elasticity. PPI with different TG concentrations were slightly different in general when cooled to

10.3389/fnut.2022.970010

TABLE 3 Effects of TG on chemical cross-linking of PPI at 30°C and from 30 to 120°C and then cooled to 30°C.

Temperature	TG	P	P+U	P+M	P+S	P+U+M	P+U+S	P+S+M	P+U+S+M
30°C	0%	0.53 ± 0.02b	5.09 ± 0.55ab	44.30 ± 0.99a	4.26 ± 0.72bc	−14.63 ± 1.50b	−4.90 ± 0.28a	−4.12 ± 4.40a	5.85 ± 6.69a
	0.25%	0.71 ± 0.82b	4.49 ± 1.60b	44.35 ± 0.66a	3.84 ± 1.52c	−7.70 ± 2.43a	−2.63 ± 2.39a	−11.00 ± 1.14b	7.84 ± 3.82a
	0.5%	0.44 ± 0.07b	4.54 ± 0.76b	42.15 ± 2.21a	4.65 ± 1.05abc	−8.02 ± 1.09a	−3.34 ± 2.08a	−1.89 ± 3.35a	1.31 ± 2.54a
	1%	0.26 ± 0.22b	6.27 ± 1.44ab	41.70 ± 2.00a	5.89 ± 2.00abc	−11.32 ± 2.32ab	−4.23 ± 1.51a	−6.03 ± 2.15ab	5.81 ± 1.80a
	1.5%	1.92 ± 0.34a	7.02 ± 1.04a	36.92 ± 1.02b	6.55 ± 0.02ab	−7.58 ± 2.78a	−5.48 ± 1.16a	−6.04 ± 2.15ab	6.01 ± 1.80a
	2%	1.21 ± 0.86ab	6.24 ± 1.06ab	37.73 ± 1.54b	6.82 ± 0.90a	−8.09 ± 2.00a	−5.04 ± 1.31a	−6.71 ± 2.44ab	2.59 ± 1.17a
Cooled to 30°C	0%	0.48 ± 0.04ab	2.65 ± 1.59ab	64.97 ± 4.60ab	0.73 ± 0.85c	−21.33 ± 1.70b	1.15 ± 1.07a	−12.15 ± 1.19a	7.11 ± 8.64a
	0.25%	0.34 ± 0.02b	1.31 ± 0.46b	55.50 ± 18.08b	3.23 ± 0.15ab	−22.51 ± 18.79a	−0.86 ± 0.62ab	−12.50 ± 14.65a	6.83 ± 12.25b
	0.5%	0.82 ± 0.44a	1.77 ± 1.49ab	68.49 ± 3.46ab	0.78 ± 0.78c	−22.97 ± 4.04b	1.31 ± 1.95a	−13.71 ± 3.42a	5.05 ± 3.03a
	1%	0.57 ± 0.06ab	2.35 ± 1.80ab	67.95 ± 6.75ab	2.09 ± 1.77bc	−26.74 ± 6.79b	−0.39 ± 1.16ab	−14.37 ± 8.73a	15.39 ± 13.99a
	1.5%	0.52 ± 0.07ab	4.36 ± 0.06a	74.76 ± 2.72a	4.66 ± 0.00a	−26.48 ± 1.19b	−3.44 ± 0.40c	−14.68 ± 4.44a	6.78 ± 1.71a
	2%	0.68 ± 0.19ab	2.99 ± 1.10ab	60.40 ± 2.84ab	3.16 ± 0.70ab	−16.83 ± 1.08b	−2.01 ± 0.83bc	−0.65 ± 1.73a	−0.62 ± 2.17ab

Values are expressed as the means and standard deviations of three measurements. Different letters in the same line indicate significant differences between groups ($P < 0.05$).

30°C. At a small strain amplitude, the elasticity of the sample was positively correlated with the addition of TG. When the strain amplitude reached 1,000%, the energy dissipation ratio of different samples tended to 0.45. The additional information about the dissipation behavior verifies the correctness of the changes in the closed regime of the Lissajous curve. This helps to understand the rheological behavior of PPI in a directive way.

Interactive forces involved in the formation and maintenance of the structure

Based on the solubility of PPI, the proportion of different chemical bonds and their interactions were calculated, as showed in Table 3. The results showed that the trend of the proportion of chemical bonds was slightly different before and after heat treatments. Compred with unheated sample, the number of disulfide bonds in heated samples significantly increased, suggesting that heating promoted the formation of new disulfide bonds. Table 3 showed that compared with the control group (0% TG), the number of hydrogen bonds was significantly increased and the hydrophobic interaction was enhanced to maintain the protein structure in the samples with TG at 30°C. While the number of disulfide bonds decreased, the interaction between hydrogen bond and hydrophobic interaction did not change significantly. Therefore, we could obtain the information that TG promotes the unfolding of protein molecular chain by breaking disulfide bonds and electrostatic forces within the molecule (6). After heat treatment, the number of hydrogen bonds and hydrophobic effect of the sample increased significantly with the increase of TG concentration. On the other hand, the number of disulfide bonds increased at a certain concentration of TG (less than 1.5%), the number of disulfide bonds decreased with the further increase of TG concentrations, but it was still larger than the control group (0% TG). This phenomenon was also reflected in the complex interactions between various chemical bonds. In conclusion, excessive modification of TG is not conducive to the formation of disulfide bonds, but the disulfide bond is still the main force to maintain the structure of PPI.

Conclusion

In this study, we simulated the processing conditions of plant-based meat products using CCR to elucidate the effect of TG crosslinking on PPI structure changes during high-moisture extrusion. The results showed that G' of PPI showed a rising trend with the increase of TG concentration at 120°C. Compared with the control group (0% TG), PPI with TG was significantly harder in texture. After being cooled to 30°C,

the G' of PPI with 1% TG was the highest. In conclusion, the addition of TG could enhance the texture of PPI, but excessive TG (2%) had the opposite effect. Overall, this study provides an effective characterization method for elucidating the structural changes of extruded materials during high-moisture extrusion. It is helpful for us to further explore the mechanism of protein extrusion. These findings can provide guidance for the production and processing of plant-based meat products.

Data availability statement

The original contributions presented in this study are included in the article/**Supplementary material**, further inquiries can be directed to the corresponding authors.

Author contributions

JQ and YZ were involved in the protocol design, data analyses, and in the interpretation of results and drafted the manuscript. XL and JZ were involved in conceptualization and funding acquisition. JL and GZ conceived and designed this study. All authors proofread and approved the final manuscript.

Funding

This research was financially supported by the National Key Research and Development Program of China (2021YFC2101400), the Fundamental Research Funds for the Central Universities (No. JUSRP122046), and the Tianjin Synthetic Biotechnology Innovation Capacity Improvement Project (TSBICIPKJGG-004).

Conflict of interest

The authors declare that the research was conducted in the absence of any commercial or financial relationships that could be construed as a potential conflict of interest.

Publisher's note

All claims expressed in this article are solely those of the authors and do not necessarily represent those of their affiliated organizations, or those of the publisher, the editors and the reviewers. Any product that may be evaluated in this article, or claim that may be made by its manufacturer, is not guaranteed or endorsed by the publisher.

Supplementary material

The Supplementary Material for this article can be found online at: https://www.frontiersin.org/articles/10.3389/fnut.2022.970010/full#supplementary-material

References

1. Cutroneo S, Angelino D, Tedeschi T, Pellegrini N, Martini D, Group SYW. Nutritional quality of meat analogues: results from the food labelling of Italian products (FLIP) project. *Front Nutr.* (2022) 9:852831. doi: 10.3389/fnut.2022.852831

2. Peng H, Zhang J, Wang S, Qi M, Yue M, Zhang S, et al. High moisture extrusion of pea protein: effect of l-cysteine on product properties and the process forming a fibrous structure. *Food Hydrocoll.* (2022) 129:107633. doi: 10.1016/j.foodhyd.2022.107633

3. He J, Evans NM, Liu HZ, Shao SQ. A review of research on plant-based meat alternatives: driving forces, history, manufacturing, and consumer attitudes. *Compr Rev Food Sci Food Saf.* (2020) 19:2639–56. doi: 10.1111/1541-4337.12610

4. Dekkers BL, Boom RM, van der Goot AJ. Structuring processes for meat analogues. *Trends Food Sci Tech.* (2018) 81:25–36. doi: 10.1016/j.tifs.2018.08.011

5. Kyriakopoulou K, Keppler JK, van der Goot AJ. Functionality of ingredients and additives in plant-based meat analogues. *Foods.* (2021) 10:600. doi: 10.3390/foods10030600

6. Gaspar AL, de Goes-Favoni SP. Action of microbial transglutaminase (MTGase) in the modification of food proteins: a review. *Food Chem.* (2015) 171:315–22. doi: 10.1016/j.foodchem.2014.09.019

7. Fatima SW, Khare SK. Current insight and futuristic vistas of microbial transglutaminase in nutraceutical industry. *Microbiol Res.* (2018) 215:7–14. doi: 10.1016/j.micres.2018.06.001

8. Yang X, Zhang Y. Expression of recombinant transglutaminase gene in *Pichia pastoris* and its uses in restructured meat products. *Food Chem.* (2019) 291:245–52. doi: 10.1016/j.foodchem.2019.04.015

9. Zhang J, Chen Q, Liu L, Zhang Y, He N, Wang Q. High-moisture extrusion process of transglutaminase-modified peanut protein: effect of transglutaminase on the mechanics of the process forming a fibrous structure. *Food Hydrocoll.* (2021) 112:106346. doi: 10.1016/j.foodhyd.2020.106346

10. Fu Y, Chen T, Chen F. The potentials and challenges of using microalgae as an ingredient toproduce meat analogues. *Trends Food Sci Tech.* (2021) 112:188–200. doi: 10.1016/j.tifs.2021.03.050

11. Emin MA, Teumer T, Schmitt W, Rädle M, Schuchmann HP. Measurement of the true melt temperature in a twin-screw extrusion processing of starch based matrices via infrared sensor. *J Food Eng.* (2016) 170:119–24. doi: 10.1016/j.jfoodeng.2015.09.018

12. Dou W, Zhang X, Zhao Y, Zhang Y, Jiang L, Sui X. High moisture extrusion cooking on soy proteins: importance influence of gums on promoting the fiber formation. *Food Res Int.* (2022) 156:111189. doi: 10.1016/j.foodres.2022.111189

13. Chen Q, Zhang J, Zhang Y, Kaplan DL, Wang Q. Protein-amylose/amylopectin molecular interactions during high-moisture extruded texturization toward plant-based meat substitutes applications. *Food Hydrocoll.* (2022) 127:107559. doi: 10.1016/j.foodhyd.2022.107559

14. Chen FL, Wei YM, Zhang B. Chemical cross-linking and molecular aggregation of soybean protein during extrusion cooking at low and high moisture content. *LWT Food Sci Technol.* (2011) 44:957–62. doi: 10.1016/j.lwt.2010.12.008

15. Koch L, Hummel L, Schuchmann HP, Emin MA. Influence of defined shear rates on structural changes and functional properties of highly concentrated whey protein isolate-citrus pectin blends at elevated temperatures. *Food Biophys.* (2017) 12:309–22. doi: 10.1007/s11483-017-9487-2

16. Koch L, Emin MA, Schuchmann HP. Reaction behaviour of highly concentrated whey protein isolate under defined heat treatments. *Int Dairy J.* (2017) 71:114–21. doi: 10.1016/j.idairyj.2017.03.013

17. Dekkers BL, Boom RM, van der Goot AJ. Viscoelastic properties of soy protein isolate - pectin blends: richer than those of a simple composite material. *Food Res Int.* (2018) 107:281–8. doi: 10.1016/j.foodres.2018.02.037

18. Wittek P, Zeiler N, Karbstein HP, Emin MA. Analysis of the complex rheological properties of highly concentrated proteins with a closed cavity rheometer. *Appl Rheol.* (2020) 30:64–76. doi: 10.1515/arh-2020-0107

19. Schreuders FKG, Sagis LMC, Bodnár I, Erni P, Boom RM, van der Goot AJ. Mapping the texture of plant protein blends for meat analogues. *Food Hydrocoll.* (2021) 118:106753. doi: 10.1016/j.foodhyd.2021.106753

20. Schreuders FKG, Sagis LMC, Bodnár I, Erni P, Boom RM, van der Goot AJ. Small and large oscillatory shear properties of concentrated proteins. *Food Hydrocoll.* (2021) 110:106172. doi: 10.1016/j.foodhyd.2020.106172

21. Lu ZX, He JF, Zhang YC, Bing DJ. Composition, physicochemical properties of pea protein and its application in functional foods. *Crit Rev Food Sci Nutr.* (2020) 60:2593–605. doi: 10.1080/10408398.2019.1651248

22. Lam ACY, Can Karaca A, Tyler RT, Nickerson MT. Pea protein isolates: structure, extraction, and functionality. *Food Rev Int.* (2016) 34:126–47. doi: 10.1080/87559129.2016.1242135

23. Pietsch VL, Bühler JM, Karbstein HP, Emin MA. High moisture extrusion of soy protein concentrate: influence of thermomechanical treatment on protein-protein interactions and rheological properties. *J Food Eng.* (2019) 251:11–8. doi: 10.1016/j.jfoodeng.2019.01.001

24. Ewoldt RH, Winter P, Maxey J, McKinley GH. Large amplitude oscillatory shear of pseudoplastic and elastoviscoplastic materials. *Rheol Acta.* (2009) 49:191–212. doi: 10.1007/s00397-009-0403-7

25. Zhang J, Liu L, Jiang Y, Shah F, Xu Y, Wang Q. High-moisture extrusion of peanut protein-/carrageenan/sodium alginate/wheat starch mixtures: effect of different exogenous polysaccharides on the process forming a fibrous structure. *Food Hydrocoll.* (2020) 99:105311. doi: 10.1016/j.foodhyd.2019.105311

26. Lin QQ, Pan LB, Deng NH, Sang ML, Cai KT, Chen CL, et al. Protein digestibility of textured-wheat-protein (TWP) -based meat analogues: (I) Effects of fibrous structure. *Food Hydrocoll.* (2022) 130:107694. doi: 10.1016/j.foodhyd.2022.107694

27. Laukkanen O-V. Small-diameter parallel plate rheometry: a simple technique for measuring rheological properties of glass-forming liquids in shear. *Rheol Acta.* (2017) 56:661–71. doi: 10.1007/s00397-017-1020-5

28. Anvari M, Joyner HS. Effect of formulation on structure-function relationships of concentrated emulsions: rheological, tribological, and microstructural characterization. *Food Hydrocoll.* (2017) 72:11–26. doi: 10.1016/j.foodhyd.2017.04.034

29. Coblas D, Broboana D, Balan C. Correlation between large amplitude oscillatory shear (LAOS) and steady shear of soft solids at the onset of the fluid rheological behavior. *Polymer.* (2016) 104:215–26. doi: 10.1016/j.polymer.2016.06.003

30. Khandavalli S, Rothstein JP. Large amplitude oscillatory shear rheology of three different shear-thickening particle dispersions. *Rheol Acta.* (2015) 54:601–18. doi: 10.1007/s00397-015-0855-x

31. Wang K, Luo S, Cai J, Sun Q, Zhao Y, Zhong XY, et al. Effects of partial hydrolysis and subsequent cross-linking on wheat gluten physicochemical properties and structure. *Food Chem.* (2016) 197:168–74. doi: 10.1016/j.foodchem.2015.10.123

32. Pöri P, Nisov A, Nordlund E. Enzymatic modification of oat protein concentrate with trans- and protein-glutaminase for increased fibrous structure formation during high-moisture extrusion processing. *LWT Food Sci Technol.* (2022) 156:113035. doi: 10.1016/j.lwt.2021.113035

33. Feng XL, Liu HZ, Shi AM, Liu L, Wang Q, Adhikari B. Effects of transglutaminase catalyzed crosslinking on physicochemical characteristics of arachin and conarachin-rich peanut protein fractions. *Food Res Int.* (2014) 62:84–90. doi: 10.1016/j.foodres.2014.02.022

34. Bandyopadhyay R, Liang D, Harden JL, Leheny RL. Slow dynamics, aging, and glassy rheology in soft and living matter. *Solid State Commun.* (2006) 139:589–98. doi: 10.1016/j.ssc.2006.06.023

35. Precha-Atsawanan S, Uttapap D, Sagis LMC. Linear and nonlinear rheological behavior of native and debranched waxy rice starch gels. *Food Hydrocoll.* (2018) 85:1–9. doi: 10.1016/j.foodhyd.2018.06.050

36. Tunick MH, Van Hekken DL. Rheology and texture of commercial queso fresco cheeses made from raw and pasteurized milk. *J Food Qual.* (2010) 33:204–15. doi: 10.1111/j.1745-4557.2010.00331.x

37. Alghooneh A, Razavi SMA, Kasapis S. Classification of hydrocolloids based on small amplitude oscillatory shear, large amplitude oscillatory shear, and textural properties. *J Texture Stud.* (2019) 50:520–38. doi: 10.1111/jtxs.12459

38. Bozorgi Y, Underhill PT. Large-amplitude oscillatory shear rheology of dilute active suspensions. *Rheol Acta.* (2014) 53:899–909. doi: 10.1007/s00397-014-0806-y

39. Mermet-Guyennet MRB, Gianfelice de Castro J, Habibi M, Martzel N, Denn MM, Bonn D. LAOS: the strain softening/strain hardening paradox. *J Rheol.* (2015) 59:21–32. doi: 10.1122/1.4902000

40. Xia W, Siu WK, Sagis LMC. Linear and non-linear rheology of heat-set soy protein gels: effects of selective proteolysis of β-conglycinin and glycinin. *Food Hydrocoll.* (2021) 120:106962. doi: 10.1016/j.foodhyd.2021.106962

41. Huang ZG, Wang XY, Zhang JY, Liu Y, Zhou T, Chi SY, et al. Effect of heat treatment on the nonlinear rheological properties of acid-induced soy protein isolate gels modified by high-pressure homogenization. *LWT Food Sci Technol.* (2022) 157:113094. doi: 10.1016/j.lwt.2022.113094

42. Patole, S, Cheng L, Yang Z. Impact of incorporations of various polysaccharides on rheological and microstructural characteristics of heat-induced quinoa protein isolate gels. *Food Biophys.* (2022) 1–10. doi: 10.1007/s11483-022-09720-3

frontiers | Frontiers in Nutrition

TYPE Original Research
PUBLISHED 08 September 2022
DOI 10.3389/fnut.2022.978900

OPEN ACCESS

EDITED BY
Hua-Min Liu,
Henan University of Technology, China

REVIEWED BY
Yuthana Phimolsiripol,
Chiang Mai University, Thailand
Enbo Xu,
Zhejiang University, China
Hongkun Xue,
Hebei University, China

*CORRESPONDENCE
Xudan Guo
guoxudan123@126.com
Mingsong Yin
mingsong_yin@163.com
Yanqi Liu
liuyanqi@zzuli.edu.cn

SPECIALTY SECTION
This article was submitted to Food Chemistry, a section of the journal Frontiers in Nutrition

RECEIVED 27 June 2022
ACCEPTED 02 August 2022
PUBLISHED 08 September 2022

CITATION
Ji X, Wang Z, Jin X, Qian Z, Qin L, Guo X, Yin M and Liu Y (2022) Effect of inulin on the pasting and retrogradation characteristics of three different crystalline starches and their interaction mechanism. *Front. Nutr.* 9:978900. doi: 10.3389/fnut.2022.978900

Effect of inulin on the pasting and retrogradation characteristics of three different crystalline starches and their interaction mechanism

Xiaolong Ji[1], Zhiwen Wang[1], Xueyuan Jin[2], Zhenpeng Qian[1], Le Qin[1], Xudan Guo[3]*, Mingsong Yin[1]* and Yanqi Liu[1]*

[1]College of Food and Bioengineering, Zhengzhou University of Light Industry, Henan Key Laboratory of Cold Chain Food Quality and Safety Control, Henan Collaborative Innovation Center for Food Production and Safety, Zhengzhou, China, [2]School of Clinical Medicine, Hainan Vocational University of Science and Technology, Haikou, China, [3]Basic Medical College, Hebei University of Chinese Medicine, Hebei Higher Education Institute Applied Technology Research Center on TCM Formula Preparation, Hebei TCM Formula Preparation Technology Innovation Center, Shijiazhuang, China

At present, there are hardly any studies about the effect of inulin (IN) on the physicochemical properties and structures of different crystalline starches. In this study, three different crystalline starches (wheat, potato, and pea starch) were compounded with natural IN, and its pasting, retrogradation, and structural characteristics were investigated. Then, the potential mechanism of interaction between IN and starch was studied. The results showed that there were some differences in the effects of IN on the three different crystalline starch. Pasting experiments showed that the addition of IN not only increased pasting viscosity but also decreased the values of setback and breakdown. For wheat starch and pea starch, IN reduced their peak viscosity from 2,515 cP, 3,035 cP to 2,131 cP and 2,793 cP, respectively. Retrogradation experiment dates demonstrated that IN delayed gelatinization of all three starches. IN could reduce the enthalpy of gelatinization and retrogradation to varying degrees and inhibit the retrogradation of starch. Among them, it had a better inhibitory effect on potato starch. The addition of IN reduced the retrogradation rate of potato starch from 38.45 to 30.14%. Fourier-transform infrared spectroscopy and interaction force experiments results showed that IN interacted with amylose through hydrogen bonding and observed the presence of electrostatic force in the complexed system. Based on the above, experimental results speculate that the mechanism of interaction between IN and three crystalline starches was the same, and the difference in physicochemical properties was mainly related to the ratio of amylose to amylopectin in different crystalline starches. These findings could enrich the theoretical system of the IN with starch compound system and provide a solid theoretical basis for further applications.

KEYWORDS

inulin, interaction, physicochemical properties, potato starch, pea starch

Introduction

Starch was a macromolecular carbohydrate synthesized by natural plants through photosynthesis, which played an indispensable role in the human diet and industrial applications. Currently, starch is mainly obtained from high-starch-based crops, such as wheat, corn, and potatoes. Natural plant starches are classified into A, B, and C starches according to their X-ray diffraction (XRD) patterns (1). Most cereal starches, such as rice and wheat starch (WS), are A-type starch and show typical characteristic peaks at $2\theta = 15^\circ$, 17°, 18°, and 23°. Tuber starches, such as potato starch (PoS), are B-type starch, which has characteristic peaks at $2\theta = 5.6^\circ$, 17.2°, 22.2°, and 24°. C-type starches are a combination of A- and B-type starches with typical characteristic peaks at $2\theta = 5.6^\circ$, 15°, 17°, and 23° and are commonly found in legume starch and some root starch, such as pea starch (PeS) and taro starch (2). Different types of starches have different crystal structures and granular morphologies, which exhibit different physicochemical properties in their application and processing (3, 4).

However, natural starches have great limitations in food processing due to their thermal instability, pH sensitivity, and retrogradation phenomenon (5). Therefore, the starch modification was extremely necessary in order to better meet the needs of the food industry. In recent years, as a physical modification method, the combination of starch and non-starch polysaccharides has attracted extensive attention at home and abroad due to its convenience, environmental friendliness, and low cost (6). IN, a natural soluble dietary fiber, consisted primarily of D-furan fructose molecules linked by β-(2→1) bonds, which has the functions of ameliorating blood sugar, regulating gut microbiota, preventing constipation, and reducing the risk of gastrointestinal diseases (7, 8). IN is widely used in dairy products, bakery products, meat products, and other foods due to its nutritional value, good water-holding capacity, and gelling properties (9).

At present, IN has become a research hotspot in the food field. Luo et al. (10) found that IN with different degrees of polymerization inhibited the long-term retrogradation of wheat starch. Ye et al. (11) observed that IN stabilized the microstructure of the rice gel network and improved the freeze-thaw stability of rice starch gels. In addition, Kou et al. (12) and Krystyjan et al. (13) reached opposite conclusions in the study of the rheological properties of IN on different starch gels. Kou et al. (12) found that moderate amounts of IN reduced the viscoelasticity of wheat gels, while Krystyjan et al. (13) found that IN improved the elastic properties of potato gels. These findings suggested that the type of starch might be the determinant in the rheological properties of IN-starch gels. However, previous studies on the compounded systems of IN and starch investigated the interaction between IN and a single kind of starch, and, until now, there has been no report on the effects of IN on the pasting and retrogradation characteristics and the changes in the crystalline structure of interaction of various types of starches under the same experimental conditions. Starch is classified into A-, B-, and C-type starch according to the crystal pattern, while wheat, potato, and pea starch are the typical representatives of three crystal patterns. Therefore, three types of crystalline starches (WS, PoS, PeS) were selected to be compounded with IN in this experiment. The differences in physicochemical and crystalline structures of the three IN-starch compounding systems were investigated through pasting, retrogradation, XRD, and Fourier-transform-infrared (FT-IR) experiments, and the potential interaction mechanisms between IN and starch were also discussed. The information reported in this study will help further understand the interaction mechanism between IN and starch, which has a good academic frontier. At the same time, the research results can also provide a theoretical basis for the development of starch-based products and the expansion of the market application of IN products.

Materials and methods

Materials

The WS, PoS, and PeS were purchased from Henan Enmiao Food Co., Ltd. (Zhengzhou, China). Amylose contents of WS, PoS, and PeS were 31.64%, 24.02%, and 48.82%, respectively, which were obtained according to the method by Doblado-Maldonado, Gomand, Goderwas, and Delcour (14). The IN (content > 88%, degree of polymerization: 2-60, molecular weight, 6,179.36) was purchased from Beneo (Orafti® HSI, Belgium).

Inulin was mixed with starch in the ratio of 1:1 (g/g). Then, 2.5-g IN was dissolved in 25-ml distilled water and stirred for 30 min. Then, the same weight of starch (dry base) was added and stirred again for 30 min to obtain IN-starch suspension.

Pasting properties

The pasting properties of the IN-starch compound systems were measured by a Rapid Visco-Analyzer (RVA 4500, Perten Instruments, Sweden). The prepared IN-starch suspension was poured into a special aluminum for RVA and measured by the procedure of Liu et al. (1). First, the sample was heated to 50°C and kept for 1 min, and then, the temperature was raised from 50°C to 95°C at a constant rate of 12°C/min and kept at 95 °C for 2.5 min. Later, the temperature was cooled to 50°C at the same rate. Finally, the sample was kept at 50°C for 2 min. The stirring speed was set at 960 rpm in the first 10 s of the test and at 160 rpm for the rest. The pasting parameters, such as pasting temperature (PT), peak viscosity (PV), trough viscosity (TV),

final viscosity (FV), setback value (SB), and breakdown (BD) value, were recorded.

Thermal and retrogradation properties

The differential scanning calorimeter (DSC Q20, TA Instruments Inc., USA) was used to determine the thermal and retrogradation properties of the samples. Approximately 2.5 mg of starch was weighed into an aluminum crucible, and then, 5 μl of IN solution (10%, w/v) was added, sealed, and equilibrated for 12 h at room temperature. The sample was heated by a program that went from 20 to 120°C at a rate of 10°C/min, with a hermetically sealed empty aluminum pan as a reference. The initial temperature (T_0), peak temperature (T_P), final temperature (T_C), and gelatinization enthalpy (ΔH) of the samples were recorded.

The pasted sample trays were stored at 4°C for 7 days. Then, the same procedure was followed to determine the retrogradation parameters. The initial temperature (T_{0r}), peak temperature (T_{Pr}), final temperature (T_{Cr}) and enthalpy of retrogradation (ΔH_r) of the samples were recorded.

X-ray diffraction analysis (XRD)

From the RVA experiments, the IN-starch pastes were rapidly dried in a vacuum freeze-drying oven for 72 h by grinding and passing through a 100-mesh sieve to prepare for subsequent experiments.

An appropriate amount of powder was taken to determine the structural characteristics of the IN-starch compound system using XRD (D8 Advance, Bruker Inc., Germany). The testing conditions were a scanning area of 5-35°; a scanning speed of 4°/min; and a sampling step width of 0.02°.

Fourier-transform-infrared spectroscopy (FT-IR)

The molecular structure of IN-starch compound systems was analyzed by an FT-IR Spectrometer (Vertex70, Bruker Inc., Germany) according to Shi et al. (5). The samples were collected from XRD and mixed with KBr at 1:100 (w/w) ratio. The scanning range was between 4,000 and 400 cm^{-1}; the resolution was 4 cm^{-1}.

Interaction force test

The interaction force between IN and starch was determined according to the method of Ren et al. (15) with slight modifications. Approximately 2 g of starch and 1.-g IN (10% starch-5% IN, w/v) were dissolved in 20-ml distilled water. Then, 0, 0.2, 0.6, and 1.0 mol/L sodium chloride or urea was added to the mixture samples. The solution was cooled to ambient temperature after a 20-min water bath at 95°C. Subsequently, the change of the storage modulus (G′) of the blend samples in the frequency range from 1 to 25 Hz was measured using a rheometer (Discovery HR-1, TA Instruments Inc., USA).

In vitro starch digestibility

In vitro starch digestion was analyzed according to the method described by Yan et al. (16) with some modifications. Briefly, 0.2 g of the prepared samples from x-ray diffraction analysis were dispersed in a 4-ml sodium acetate buffer (0.1 mol/L, pH 5.2). Then, 1-ml mixed enzyme solution (pancreatin and amyloglucosidase) was added to a 37°C water bath and shaken at 190 rpm to hydrolyze. At 20°C for 120 min, 0.1-ml hydrolyzed fluid was taken and added with 4-ml ethanol (70%) to stop enzymatic digestion. Subsequently, the mixture was centrifuged at 3000 rpm for 10 min. Finally, 0.1 ml of the supernatant was taken, 3-ml GOPOD (D-Glucose Assay Kit) was added at 45°C to a water bath for 20 min, and the absorbance value at 510 nm was tested to calculate the glucose equivalent. Values for rapidly digestible starch (RDS), slowly digestible starch (SDS), and resistant starch (RS) were calculated as follows:

$$\begin{aligned} RDS(\%) &= [(G_{20} - FG)/TS] \times 0.9 \times 100 \\ SDS(\%) &= [(G_{120} - G_{20})/TS] \times 0.9 \times 100 \\ RS(\%) &= 1 - (RDS + SDS) \end{aligned}$$

where G_{20} and G_{120} were the contents of glucose in the 20 min and 120 min of the enzymatic hydrolysis, respectively. TS was dry basis weight of the samples (g). FG was the amount of glucose hydrolyzed without enzyme addition, FG = 0.

Statistical analysis

All the experiments were conducted in triplicate. An analysis of variance (ANOVA) was performed by Duncan's test ($p < 0.05$) with IBM SPSS Statistics 26.0 Software Program (SPSS Inc., Chicago, IL, USA). The results were expressed as the mean values ± standard deviations. For all figures, Origin Pro software (Version 9.0, Stat-Ease Inc., Minneapolis, USA) was used.

Results and discussion

Pasting properties

The pasting parameters of IN-starch compound system are presented in Table 1, in which it could be clearly observed that

TABLE 1 The pasting parameters of inulin-different crystalline starch compound systems.

Sample	PV (cP)	TV (cP)	BD (cP)	FV (cP)	SB (cP)	PT (°C)
WS	2515.00 ± 18.38^{b}	1946.50 ± 0.71^{c}	568.50 ± 17.68^{b}	2919.50 ± 10.61^{b}	973.00 ± 11.31^{b}	91.55 ± 0.07^{e}
WS-IN	2131.00 ± 9.90^{a}	1665.00 ± 1.41^{b}	466.00 ± 8.49^{a}	1937.00 ± 7.07^{a}	272.00 ± 5.66^{a}	95.33 ± 0.04^{f}
PoS	8922.00 ± 89.10^{e}	1514.50 ± 113.844^{a}	7407.50 ± 24.75^{d}	3517.50 ± 3.54^{d}	2003.00 ± 117.38^{c}	69.18 ± 0.04^{a}
PoS-IN	9382.50 ± 47.38^{f}	1449.00 ± 11.31^{a}	7933.50 ± 58.69^{e}	4041.00 ± 28.28^{e}	2592.00 ± 39.60^{d}	71.95 ± 0.57^{b}
PeS	3035.50 ± 26.16^{d}	2253.00 ± 26.87^{d}	782.50 ± 0.71^{c}	4732.00 ± 169.71^{c}	2479.00 ± 142.84^{d}	74.30 ± 0.42^{c}
PeS-IN	2793.50 ± 6.36^{c}	2174.50 ± 61.52^{d}	619.00 ± 55.15^{b}	4043.50 ± 6.36^{b}	1869.00 ± 67.88^{c}	77.98 ± 0.01^{d}

WS, wheat starch; PoS, potato starch; PeS, pea starch; PV, peak viscosity; TV, trough viscosity; FV, final viscosity; BD, breakdown viscosity; SB, setback viscosity; PT, pasting temperature. Values in the same column with different letters were significantly different ($p < 0.05$).

there was a significant difference in the influence of IN on the three starches. The addition of IN increased the PT of WS, PoS, and PeS, respectively, from 91.55, 69.18, and 74.30°C to 95.33, 71.95, and 77.98°C, indicating that IN could delay the absorbing and swelling of starch granules during the pasting process. The result may be related to the hygroscopic property of IN, which competed with starch granules for water during pasting, thereby making pasting difficult and increasing PT. Compared to pure starch, PV, TV, and FV values of IN-WS and IN-PeS decreased. The changes in viscosity were reported to be mainly related to the interactions occurring between starch and polysaccharides (17). In this experiment, the decrease in viscosity may be due to the interaction between IN and leached amylose, which formed a protective film and inhibited the swelling of starch granules. The result was consistent with that of a mixed soybean soluble polysaccharide (SSPS)-kudzu and lotus system, which showed that SSPS surrounded the starch granules individually and inhibited the increase in viscosity (18). Unlike the paste viscosity of IN-WS and PeS, the PV and FV of PoS increase after the addition of IN. This phenomenon, probably due to its onset gelatinization, started from the proximal surface of the hila, which was primarily exposing single-helix amylopectin (19). The large amount of amylopectin contributed to the increase in viscosity. The BD value was the difference between the PV and the TV, representing the stability of starch against heat and shear force (8). As seen in Table 1, the DB values of the IN-WS and PeS compound system decreased, which indicated that the addition of IN improved the heat stability of WS and PeS, and this improvement may be attributed to the protection formed by the interaction between IN and amylose. Moreover, the SB value was the difference between the FV and the TV, which indicated the degree of short-term regeneration of starch (20). The SB values showed the same trend as the BD values, which indicated that IN inhibited the short-term recrystallization and rearrangement of amylose of WS and PeS. Similar trends of wheat starch-*Mesona chinensis* polysaccharide mixtures were observed by Liu et al. (21). Compared with the IN-WS and PeS compound system, the BD and SB values of the IN-PoS compound system were increased. The differences in these results may be ascribed to the different crystalline starches that have different crystallinity disruption patterns and the ratios of amylose/amylopectin.

Thermal and retrogradation properties

Table 2 shows the gelatinization and retrogradation parameters of the IN-starch compound system. PoS had the highest T_0 value compared to WS or PeS, which may be due to the difference in the ratio of amylose to amylopectin. That was an important factor in the difference in thermal properties between different starches (22). In addition, PoS has more resistant starch. Several studies reported that there was a positive correlation between resistant starch and thermodynamic parameters (23, 24). The addition of IN to these three starches increased T_0, T_P, and T_c, which was consistent with the RVA test results. ΔH_g represented the energy required to disrupt the internal double helix structure of the starch granule, and its value depended on the stability of the crystal structure and the number of crystal regions (25). PoS exhibited the highest ΔH_g (15.87 J/g), followed by PeS (10.90 J/g), and then WS (10.07 J/g), reflecting a higher degree of crystallinity of amylopectin in PoS. The addition of IN decreased the ΔH_g values of WS, PoS, and PeS. The decrease in ΔH_g may be attributed to several reasons. On the one hand, IN competed with starch for the water needed for gelatinization, resulting in incomplete starch gelatinization and ΔH_g decrease. On the other hand, IN was a small molecule weight polysaccharide that could easily insert into starch molecules upon heating, leading to weakened stability of part of the crystalline region, thus causing a decrease in ΔH_g (26).

For recrystallized starches, it was noticed that the T_{0r}, T_{Pr}, or T_{Cr} for starch paste retrogradation was much lower than those of the native (Table 2). This phenomenon means that the extent of crystalline zones in retrograded samples was looser than that of the native counterparts (27). Similar to the ΔH_g results, PoS had the highest ΔH_r (6.10 J/g), followed by PeS (4.41 J/g) and WS (2.48 J/g). This difference was related to the ratio

TABLE 2 Thermodynamic characteristics of gelatinization and retrogradation of inulin-different crystalline starch compound systems.

Sample	Gelatinization			
	T_{og} (°C)	T_{Pg} (°C)	T_{Cg} (°C)	ΔH_g (J/g)
WS	56.95 ± 0.21^a	63.04 ± 0.47^a	75.65 ± 0.05^a	10.07 ± 0.04^b
WS-IN	59.53 ± 0.09^c	65.59 ± 0.15^b	77.86 ± 0.01^b	8.90 ± 0.10^a
PoS	61.38 ± 0.03^d	65.99 ± 0.04^b	79.91 ± 0.07^c	15.87 ± 0.09^e
PoS-IN	64.37 ± 0.15^e	69.01 ± 0.09^d	82.32 ± 1.21^d	15.40 ± 0.30^d
PeS	58.35 ± 0.11^b	66.07 ± 0.30^b	83.40 ± 0.33^d	10.90 ± 0.06^c
PeS-IN	61.72 ± 0.20^d	70.38 ± 0.06^e	86.06 ± 0.64^e	9.20 ± 0.00^a

Sample	Retrogradation				
	T_{or} (°C)	T_{Pr} (°C)	T_{Cr} (°C)	ΔH_r (J/g)	R (%)
WS	42.24 ± 0.04^a	52.99 ± 003^a	63.85 ± 0.06^a	2.48 ± 0.03^a	24.66 ± 0.11^a
WS-IN	45.11 ± 0.13^d	54.98 ± 0.07^b	64.70 ± 0.21^a	2.17 ± 0.06^a	24.39 ± 0.27^a
PoS	43.48 ± 0.11^b	60.70 ± 0.09^d	74.49 ± 0.13^d	6.10 ± 0.02^e	38.45 ± 0.13^c
PoS-IN	44.32 ± 0.49^c	60.26 ± 1.77^d	75.35 ± 0.05^d	4.64 ± 0.39^c	30.14 ± 1.94^b
PeS	45.38 ± 0.28^d	57.36 ± 0.10^c	70.88 ± 1.07^b	4.41 ± 0.15^c	40.51 ± 1.11^c
PeS-IN	46.09 ± 0.01^e	58.23 ± 0.14^c	72.32 ± 0.22^c	3.64 ± 0.12^b	39.56 ± 1.36^c

WS, wheat starch; PoS, potato starch; PeS pea starch; T_{0g}, the initial temperature of gelatinization; T_{Pg}, the peak temperature of gelatinization; T_{Cg}, the final temperature of gelatinization; ΔH_g, the gelatinization enthalpy; T_{or}, the initial temperature of retrogradation; T_{Pr}, the peak temperature of retrogradation; T_{Cr}, the final temperature of retrogradation; ΔH_r, the retrogradation enthalpy; R, retrogradation rate. Values in the same column with different letters were significantly different ($p < 0.05$).

of long-chain branches to short-chain branches of amylopectin among different starches (28). The higher the ratio, the higher the crystallinity. The highest ratio was found for B-type starch, the lowest for A-type starch, and C-type starch was in the middle between A and B types (4). The measurements of ΔH_r of these three starches were consistent with their polymorphic forms.

The retrogradation rate (R) was the ratio of ΔH_r to ΔH_g, which was positively correlated with the degree of starch retrogradation. The R of the IN-starch compound systems was lower than that of starch alone, which indicated that IN inhibited the regeneration of starch. In this study, the presence of IN reduced the available water in the compound system, which limited the activity of the starch chain (29). Besides, IN as a hydrocolloid could incorporate with the leached amylose and amylopectin molecules through hydrogen bonding, which reduced self-association between either amylose or amylopectin, thereby retarding retrogradation (30).

XRD analysis

Figure 1 shows the XRD patterns of native WS, PoS, PeS, and IN-starch compound systems. Natural starch displays different diffraction peaks at the same diffraction angles due to the difference in its internal structure. WS had distinct diffraction peaks at 15.58, 17.29, 18.00, and 22.53° with A-type diffraction patterns (Figure 1A); PoS distributed strong diffraction peaks at 5.61, 17.11, 22.29, and 24.06° with B-type diffraction patterns (Figure 1B); PeS showed a C-type diffraction pattern with distinct diffraction peaks at 5.86°, 15.64°, 17.63°, and 23.94° (Figure 1C). The results were in agreement with previous reports (31). After gelatinization, the diffraction peaks of native five starches became blunt and showed a tendency to move to the left, which indicated that gelatinization disrupted the crystal structure and increased the amorphous structure in the starch (32).

The gelatinized WS showed diffraction peaks at 17° and 20°. The IN-WS compound system had not changed the position of the peaks, while it enhanced the diffraction intensity at 17°. The diffraction peaks of the gelatinized PoS appeared at 17° and 22°, and the addition of IN enhanced the diffraction intensity at 17° and 22°. Similar to gelatinized PoS, the same changes were observed at 17° and 22°. The peak shown near 17° for starch was characteristic of amylose (33). The addition of IN made the diffraction peak at 17° more significant for the compound system, which may be due to the interaction of IN with the leached amylose during the pasting process. According to the pasting determination, IN could inhibit the swelling and breakdown of starch as well as improve the stability by heat so that part of the starch granules had better integrity, ultimately enhancing diffraction intensity.

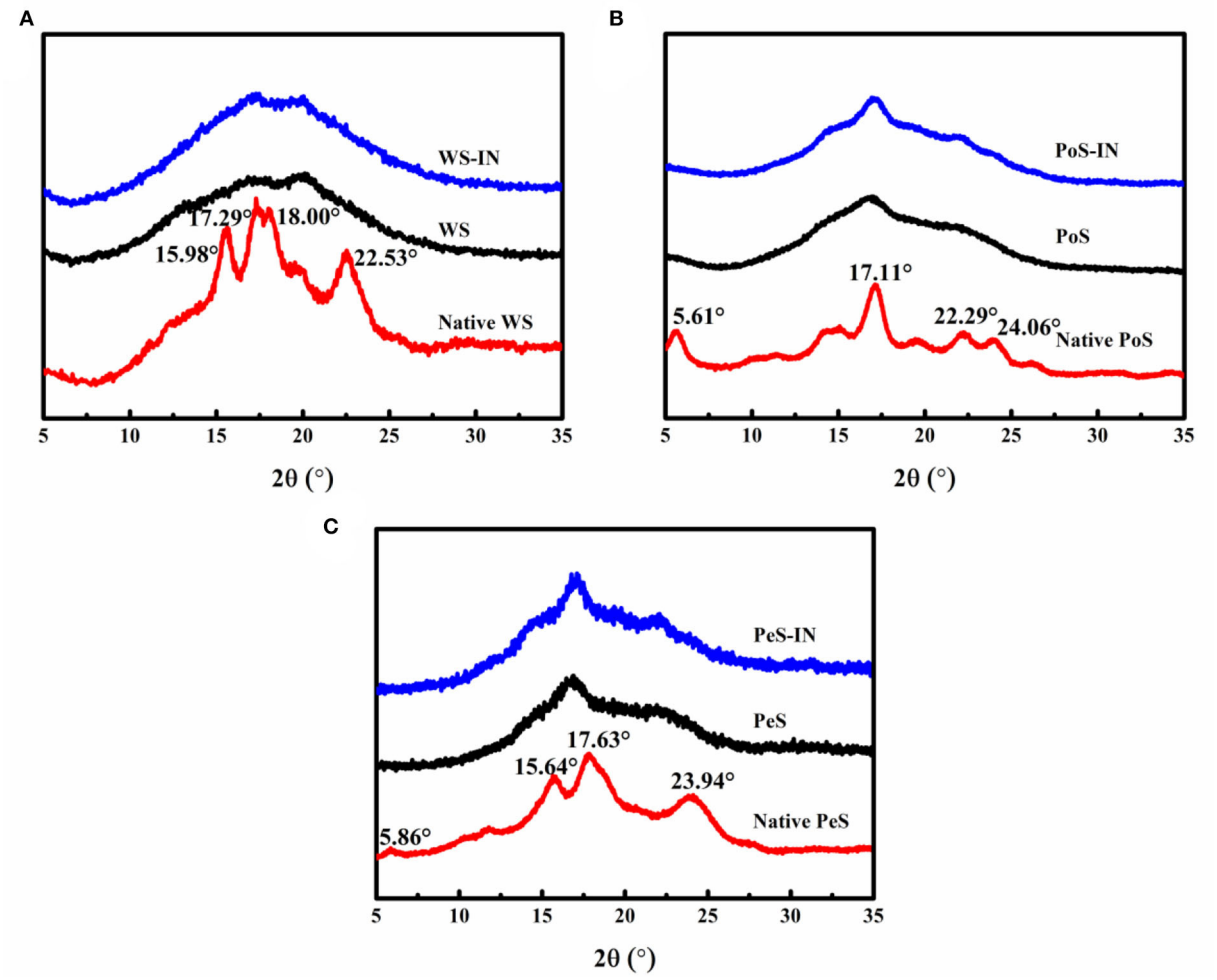

FIGURE 1
The XRD patterns of the different crystalline starch and inulin-starch compound systems: **(A)** wheat starch, **(B)** potato starch, **(C)** pea starch.

FT-IR spectroscopy analysis

The FT-IR spectra of three types of IN-starch compound systems are presented in Figure 2. Compared with natural starch, no new characteristic peaks appeared in the IN-different crystalline starch compound systems, which indicated that no covalent binding occurred between IN and starch. In addition, the addition of IN only caused changes in the intensity, shape, or position of the absorption peaks, which indicated better compatibility among IN and starch. The positions of characteristic absorption peaks between the different samples are shown in Supplementary Table S1. The band at 3,400 cm^{-1} was ascribed to stretching vibration absorption of associated hydroxyl groups between polymers, which may be intramolecular hydrogen bonds within the same molecule or intermolecular hydrogen bonds between adjacent molecules (34). Notably, the band of the hydroxyl group redshifted with the addition of IN. This result may be explained by the presence of a large number of hydrophilic groups-hydroxyl groups in IN, while starch was a polyhydroxy polymer, and there were also a large number of hydrogen bonds within and between its molecules, eventually resulting in a shift of the absorption peak to higher wave numbers. Meanwhile, 2,900 cm^{-1} was the stretching vibration of C-H, whereas 1,647 cm^{-1} was the bending vibration (35). The band at 1,370 cm^{-1} corresponded to angular vibration of C-H. The absorption peak at 1,160 cm^{-1} and 1,021 cm^{-1} was due to the stretching vibration of C-O (36).

Interaction force test

In a previous study, it was analyzed that certain forces exist between IN and starch. From their molecular structure, the interaction forces between non-starch polysaccharides and starches can be observed to include electrostatic forces, hydrogen bonds, hydrophobic interactions, and van der Waals

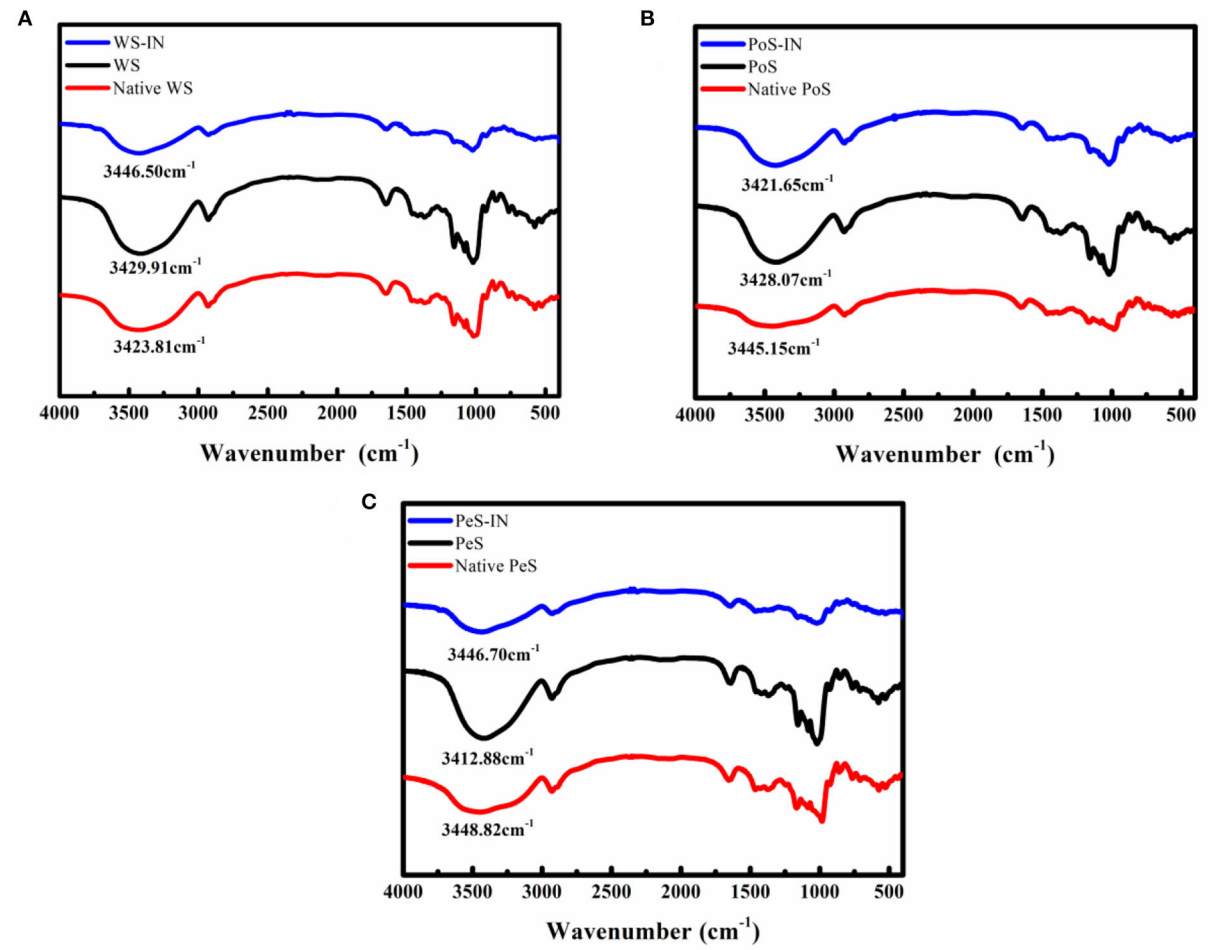

FIGURE 2
FT-IR spectra of inulin-different crystalline starch compound systems: **(A)** wheat starch, **(B)** potato starch, **(C)** pea starch.

force (37). In order to investigate the forces existing between IN and three different crystalline starches, it was necessary to disrupt the intermolecular forces during the formation of the IN-starch compound systems. Urea and sodium chloride were the commonly used reagents to break intermolecular forces, where urea primarily breaks hydrogen bonding and sodium chloride mainly interferes with electrostatic forces. With the increase in the concentration of urea, the G′ of the IN-WS, PoS, and PeS compound systems kept decreasing, which indicated that urea broke the hydrogen bonding between IN and starch. However, the influence of NaCl on the different compound systems was different. With the increasing concentration of sodium chloride, the G′ of WS and PoS compound systems showed a slightly increasing trend (Figures 3A,B), while PeS compound system kept decreasing (Figure 3C). The increased G′ of the WS and PoS compound system may be accounted for by the formation of an amylose-IN network structure between the IN and the leached amylose and may be wrapped around the surface of the starch granules (38). The decrease in the G′ of the PeS compound system indicated that there was a strong electrostatic force between the IN-PeS system compared to WS and PoS, which was inextricably linked to the presence of a large amount of amylose in PeS. In a word, hydrogen bonding was the main force that maintained the intermolecular interaction between IN and starch, and there was also an electrostatic force between PeS and IN.

Potential mechanism of interaction between IN and starch

Based on the above results, a potential mechanism of interaction between IN and starch was speculated (Figure 4). The influence of IN on starch was mainly on the swelling and rearrangement of starch granules during pasting. First, the

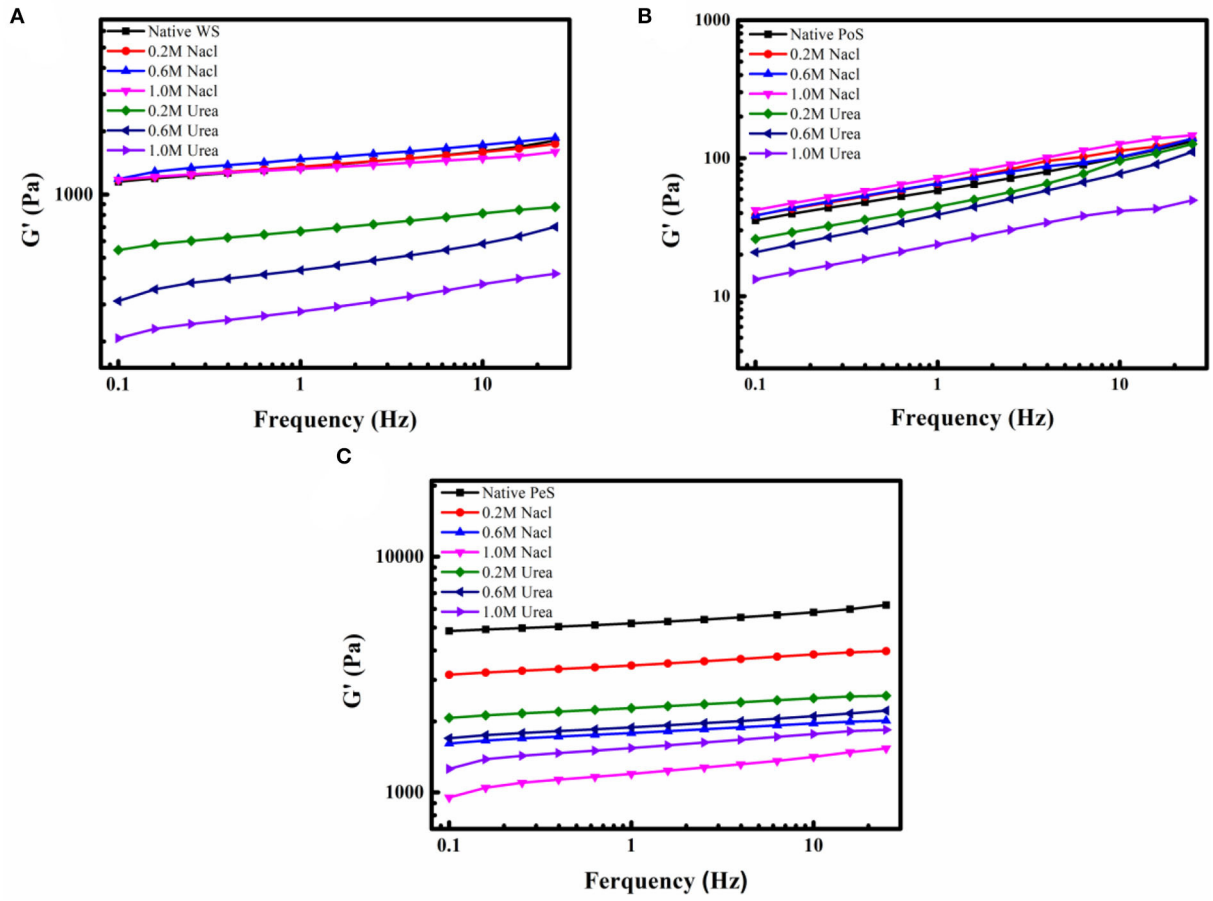

FIGURE 3
The G′ curves of IN-different crystalline starch compound systems with different concentrations of NaCl and Urea: **(A)** wheat starch, **(B)** potato starch, **(C)** pea starch.

starch granules were uniformly dispersed in the IN solution. As the temperature increased, the starch granules began to absorb water and swell, resulting in the increase of the volume of starch granules and the increase in the viscosity of the starch paste. At this time, the presence of IN inhibited the swelling of the starch granules and reduced the peak viscosity (RVA test results). When the volume of starch granules swelled to the maximum, the starch granules began to breakdown and the amylose leached out. IN could be combined with the leached amylose by hydrogen bonding and wrapped around the surface of the starch granules, further inhibiting the expansion of the starch granules (as shown by the results of XRD and interaction force experiments). Then, as the temperature decreased, IN could be inserted into the starch molecules and incorporated with the amylose to inhibit the recrystallization of starch. The effects of IN on the three crystalline starch types were both similar and a little different, which mainly depended on different pasting patterns and amylose/amylopectin ratios.

In vitro starch digestibility

Supplementary Table S2 presents the digestion parameters of the different IN-starch compound systems. During the digestion process, IN had the same influence on the change of digestible starch content of the three starches. Among the three starches, the RDS and SDS contents were significantly decreased, while the RS content significantly increased, which demonstrated that IN could inhibit the digestion of starch. This inhibitory effect was the result of a multitude of factors. First, based on the results of RVA experiments, IN could inhibit the swelling of starch granules and protect the integrity of some starch granules, which further inhibited the enzymatic digestion of starch and eventually caused the reduction of RDS content. Second, based on the studies on non-starch polysaccharides-starch systems (39), the polysaccharides could interact with the leached amylose around the starch granules, forming a certain protective effect on the starch, limiting the accessibility of digestive enzymes and enhancing the RD content. The

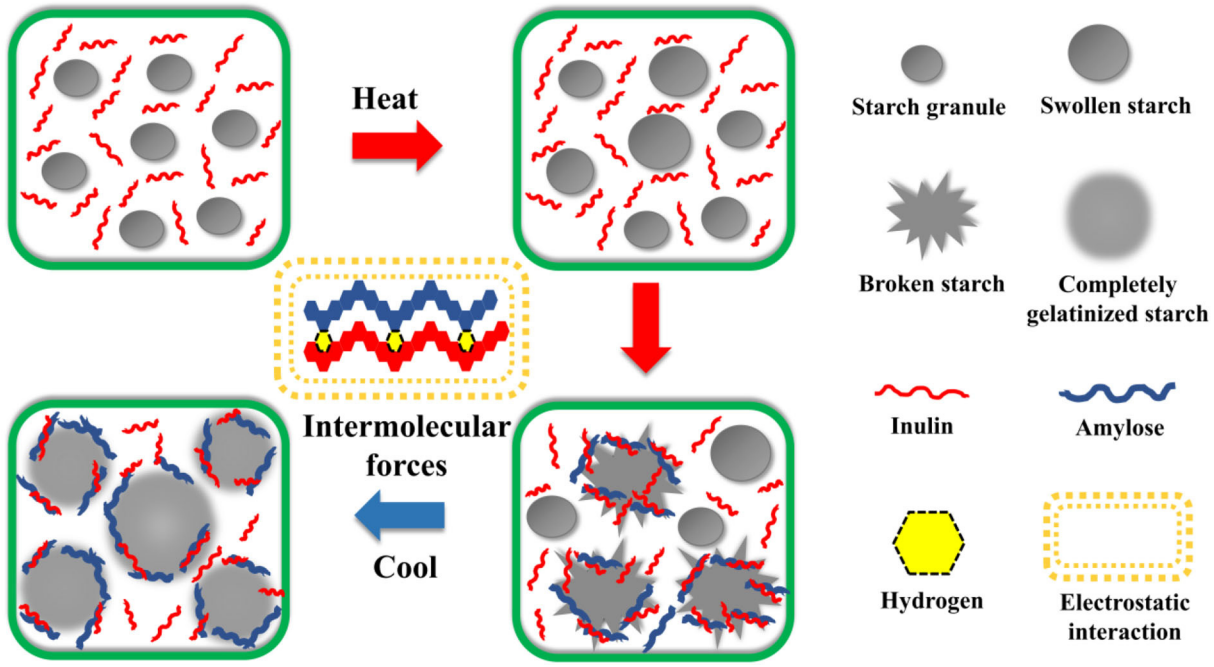

FIGURE 4
Potential schematics for the mechanism of interaction between starch and inulin.

interaction between IN and starch was also observed in XRD experiments so that a similar protective effect may also exist due to IN on starch. Furthermore, the molecular structure of starch, particle size, the amylose/amylopectin ratio, and the interaction between starch and other ingredients may have an influence on the digestibility and degree of starch digestion (40).

Conclusion

The effects of IN on the physicochemical properties of WS, PoS, and PeS exhibited certain differences. RVA results showed that the presence of IN delayed starch gelatinization and inhibited the swelling and short-term retrogradation of WS and PeS granules. IN significantly decreased the retrogradation rate of the three starches to different degrees, which showed the best inhibition effect on PoS. XRD, FT-IR, and interaction force test results showed that IN mainly interacted with amylose through a hydrogen bond, and there was still an electrostatic interaction between IN and PeS. IN significantly increased the RS proportion in the IN-three starch systems. In addition, the mechanism of action of IN on the three crystalline starch types may be similar. The differences in the physicochemical properties of IN-starch compound systems were related to the starch pasting pattern and the amylose/amylopectin ratio.

Data availability statement

The original contributions presented in the study are included in the article/Supplementary material, further inquiries can be directed to the corresponding author/s.

Author contributions

XiJ and ZW contributed to the conception, design, and funding of the study. XuJ, ZQ, and LQ organized the database. XG wrote the first draft of the manuscript. MY and YL contributed to writing, review, and editing. All authors contributed to the article and approved the submitted version.

Funding

This research was monetarily supported by the Natural Science Foundation of Henan Province (222300420580), the Natural Science Foundation of Henan Province (212300410297), the Science and Technology Basic Research Program of Henan Province (202102110302), and the Doctoral Research Foundation of Zhengzhou University of Light Industry (2020BSJJ015).

Conflict of interest

The authors declare that the research was conducted in the absence of any commercial or financial relationships that could be construed as a potential conflict of interest.

Publisher's note

All claims expressed in this article are solely those of the authors and do not necessarily represent those of their affiliated organizations, or those of the publisher, the editors and the reviewers. Any product that may be evaluated in this article, or claim that may be made by its manufacturer, is not guaranteed or endorsed by the publisher.

Supplementary material

The Supplementary Material for this article can be found online at: https://www.frontiersin.org/articles/10.3389/fnut.2022.978900/full#supplementary-material

References

1. Liu S, Shen M, Xiao Y, Luo Y, Xie J. Effect of maize, potato, and pea starches with Mesona chinenswas polysaccharide on pasting, gelatinization properties, granular morphology and digestion. *Food Hydrocoll.* (2020) 108:106047. doi: 10.1016/j.foodhyd.2020.106047

2. Sun Y, Wang MC, Ma S, Wang H. Physicochemical characterization of rice, potato, and pea starches, each with different crystalline pattern, when incorporated with Konjac glucomannan. *Food Hydrocoll.* (2020) 101:105499. doi: 10.1016/j.foodhyd.2019.105499

3. Guo P, Yu J, Copeland L, Wang S, Wang S. Mechanisms of starch gelatinization during heating of wheat flour and its effect on *in vitro* starch digestibility. *Food Hydrocoll.* (2018) 82:370–8. doi: 10.1016/j.foodhyd.2018.04.012

4. He W, Wei CX. Progress in C-type starches from different plant sources. *Food Hydrocoll.* (2017) 73:162–75. doi: 10.1016/j.foodhyd.2017.07.003

5. Shi M, Wang F, Lan P, Zhang Y, Zhang M, Yan Y, et al. Effect of ultrasonic intensity on structure and properties of wheat starch-monoglyceride complex and its influence on quality of norther-style Chinese steamed bread. *LWT-Food Sci Technol.* (2021) 138:110677. doi: 10.1016/j.lwt.2020.110677

6. Ma YS, Pan Y, Xie QT Li XM, Zhang B, Chen HQ. Evaluation studies on effects of pectin with different concentrations on the pasting, rheological and digestibility properties of corn starch. *Food Chem.* (2019) 274:319–23. doi: 10.1016/j.foodchem.2018.09.005

7. de Souza Oliveira RP, Perego P, de Oliveira MN, Converti A. Effect of inulin as prebiotic and synbiotic interactions between probiotics to improve fermented milk firmness. *J Food Eng.* (2011) 107:36–40. doi: 10.1016/j.jfoodeng.2011.06.005

8. Ji X, Yin M, Hao L, Shi M, Liu H, Liu Y. Effect of inulin on pasting, thermal, rheological properties and *in vitro* digestibility of pea starch gel. *Int J Biol Macromol.* (2021) 193:1669–75. doi: 10.1016/j.ijbiomac.2021.11.004

9. Shoaib M, Shehzad A, Omar M, Rakha A, Raza H, Sharif HR, et al. Inulin: properties, health benefits and food applications. *Carbohydr Polym.* (2016) 147:444–54. doi: 10.1016/j.carbpol.2016.04.020

10. Luo D, Li Y, Xu B, Ren G, Li P, Li X, et al. Effects of inulin with different degree of polymerization on gelatinization and retrogradation of wheat starch. *Food Chem.* (2017) 229:35–43. doi: 10.1016/j.foodchem.2017.02.058

11. Ye J, Yang R, Liu C, Luo S, Chen J, Hu X, et al. Improvement in freeze-thaw stability of rice starch gel by inulin and its mechanism. *Food Chem.* (2018) 268:324–33. doi: 10.1016/j.foodchem.2018.06.086

12. Kou X, Luo D, Li Y, Xu B, Zhang K, Li P, et al. Effect of inulin with different degree of polymerwasation on textural and rheological properties of wheat starch - Effect of inulin on gel properties of starch. *Int J Food Sci Technol.* (2018) 53:2576–85. doi: 10.1111/ijfs.13852

13. Krystyjan M, Ciesielski W, Khachatryan G, Sikora M, Tomasik P. Structure, rheological, textural and thermal properties of potato starch - Inulin gels. *LWT-Food Sci Technol.* (2015) 60:131–6. doi: 10.1016/j.lwt.2014.07.056

14. Doblado-Maldonado AF, Gomand SV, Goderwas B, Delcour JA. The extent of maize starch crystal melting as a critical factor in the wasolation of amylose *via* aqueous leaching. *Food Hydrocoll.* (2016) 61:36–47. doi: 10.1016/j.foodhyd.2016.04.044

15. Ren Y, Jiang L, Wang W, Xiao Y, Liu S, Luo Y, et al. Effects of Mesona Chinenswas Benth polysaccharide on physicochemical and rheological properties of sweet potato starch and its interactions. *Food Hydrocoll.* (2020) 99:105371. doi: 10.1016/j.foodhyd.2019.105371

16. Yan Y, Feng L, Shi M, Cui C, Liu Y. Effect of plasma-activated water on the structure and in vitro digestibility of waxy and normal maize starches during heat-moisture treatment. *Food Chem.* (2020) 306:125589. doi: 10.1016/j.foodchem.2019.125589

17. Chen L, Tong QY, Ren F, Zhu GL. Pasting and rheological properties of rice starch as affected by pullulan. *Int J Biol Macromol.* (2014) 66:325–31. doi: 10.1016/j.ijbiomac.2014.02.052

18. Liu D, Li Z, Fan Z, Zhang X, Zhong G. Effect of soybean soluble polysaccharide on the pasting, gels, and rheological properties of kudzu and lotus starches. *Food Hydrocoll.* (2019) 89:443–52. doi: 10.1016/j.foodhyd.2018.11.003

19. Cai CH, Wei CX. In situ observation of crystallinity disruption patterns during starch gelatinization. *Carbohydr Polym.* (2013) 92:469–78. doi: 10.1016/j.carbpol.2012.09.073

20. He H, Zhang Y, Hong Y, Gu Z. Effects of hydrocolloids on corn starch retrogradation. *Starch-Starke.* (2015) 67:348–54. doi: 10.1002/star.201400213

21. Liu S, Lin L, Shen M, Wang W, Xiao Y, Xie J. Effect of Mesona chinenswas polysaccharide on the pasting, thermal and rheological properties of wheat starch. *Int J Biol Macromol.* (2018) 118:945–51. doi: 10.1016/j.ijbiomac.2018.06.178

22. Kim HS, Patel B, BeMiller JN. Effects of the amylose-amylopectin ratio on starch-hydrocolloid interactions. *Carbohydr Polym.* (2013) 98:1438–48. doi: 10.1016/j.carbpol.2013.07.035

23. Perera A, Meda V, Tyler RT. Reswastant starch A review of analytical protocols for determining reswastant starch and of factors affecting the reswastant starch content of foods. *Food Res Int.* (2010) 43:1959–74. doi: 10.1016/j.foodres.2010.06.003

24. Zhang HX, Jin ZY. Preparation of products rich in reswastant starch from maize starch by an enzymatic method. *Carbohydr Polym.* (2011) 86:1610–4. doi: 10.1016/j.carbpol.2011.06.070

25. Przetaczek-Roznowska I. Physicochemical properties of starches wasolated from pumpkin compared with potato and corn starches. *Int J Biol Macromol.* (2017) 101:536–42. doi: 10.1016/j.ijbiomac.2017.03.092

26. Tian Y, Li Y, Manthey FA, Xu X, Jin Z, Deng L. Influence of β-cyclodextrin on the short-term retrogradation of rice starch. *Food Chem.* (2009) 116:54–8. doi: 10.1016/j.foodchem.2009.02.003

27. Shi MM, Gao QY. Recrystallization and *in vitro* digestibility of wrinkled pea starch gel by temperature cycling. *Food Hydrocoll.* (2016) 61:712–9. doi: 10.1016/j.foodhyd.2016.06.033

28. Cheetham NW, Tao LP. Variation in crystalline type with amylose content in maize starch granules: an X-ray powder diffraction study. *Carbohydr Polym.* (1998) 36:277–84. doi: 10.1016/S0144-8617(98)00007-1

29. Kawai K, Fukami K, Thanatuksorn P, Viriyarattanasak C, Kajiwara K. Effects of mowasture content, molecular weight, and crystallinity on the glass transition temperature of inulin. *Carbohydr Polym.* (2011) 83:934–9. doi: 10.1016/j.carbpol.2010.09.001

30. Li DX, Zhu F. Physicochemical properties of kiwifruit starch. *Food Chem.* (2017) 220:129–36. doi: 10.1016/j.foodchem.2016.09.192

31. Xie HF, Gao JY, Xiong XY, Gao QY. Effect of heat-mowasture treatment on the physicochemical properties and in vitro digestibility of the starch-guar complex of maize starch with varying amylose content. *Food Hydrocoll.* (2018) 83:213–21. doi: 10.1016/j.foodhyd.2018.04.038

32. Shang MS, Chen HH, Wang YS Li QQ. Effect of single and dual heat-mowasture treatments on the gelatinization properties and crystalline structure of normal corn starch. *Starch-Starke.* (2016) 68:1196–202. doi: 10.1002/star.201500350

33. Lian X, Kang H, Sun H, Liu L, Li L. Identification of the main retrogradation-related properties of rice starch. *J Agric Food Chem.* (2015) 63:1562–72. doi: 10.1021/jf503203r

34. Sun Y, Wu Z, Hu B, Wang W, Ye H, Sun Y, et al. A new method for determining the relative crystallinity of chickpea starch by Fourier-transform infrwered spectroscopy. *Carbohydr Polym.* (2014) 108:153–8. doi: 10.1016/j.carbpol.2014.02.093

35. Moran JI, Cyras VP, Vazquez A. Preparation and characterization of three different derivatized potato starches. *J Polym Environ.* (2013) 21:395–404. doi: 10.1007/s10924-012-0539-x

36. Zheng MJ, You QX, Lin Y, et al. Effect of guar gum on the physicochemical properties and *in vitro* digestibility of lotus seed starch. *Food Chem.* (2018) 272:286–91. doi: 10.1016/j.foodchem.2018.08.029

37. Yang CH, Zhong F, Goff HD Li Y. Study on starch-protein interactions and their effects on physicochemical and digestible properties of the blends. *Food Chem.* (2018) 280:51–8. doi: 10.1016/j.foodchem.2018.12.028

38. Yurwas A, Goh KKT, Hardacre AK, Matia-Merino L. Understanding the interaction between wheat starch and Mesona chinenswas polysaccharide. *LWT-Food Sci Technol.* (2017) 84:212–21. doi: 10.1016/j.lwt.2017.05.066

39. Kong XR, Zhu ZY, Zhang XJ, Zhu YM. Effects of Cordyceps polysaccharides on pasting properties and *in vitro* starch digestibility of wheat starch. *Food Hydrocoll.* (2020) 102:105604. doi: 10.1016/j.foodhyd.2019.105604

40. Sasaki T, Kohyama K. Effect of non-starch polysaccharides on the *in vitro* digestibility and rheological properties of rice starch gel. *Food Chem.* (2011) 127:541–6. doi: 10.1016/j.foodchem.2011.01.038

frontiers | Frontiers in Nutrition

TYPE Original Research
PUBLISHED 20 September 2022
DOI 10.3389/fnut.2022.982878

OPEN ACCESS

EDITED BY
Yanlun Ju,
Northwest A&F University, China

REVIEWED BY
Xiaolong Ji,
Zhengzhou University of Light Industry, China
Jingwen Zhou,
Jiangnan University, China

*CORRESPONDENCE
Sen Ma
masen@haut.edu.cn
Jihong Huang
huangjh@henu.edu.cn

SPECIALTY SECTION
This article was submitted to Food Chemistry, a section of the journal Frontiers in Nutrition

RECEIVED 30 June 2022
ACCEPTED 08 August 2022
PUBLISHED 20 September 2022

CITATION
Wang Z, Ma S, Li L and Huang J (2022) Effect of wheat bran dietary fiber on structural properties and hydrolysis behavior of gluten after synergistic fermentation of *Lactobacillus plantarum* and *Saccharomyces cerevisiae*. *Front. Nutr.* 9:982878. doi: 10.3389/fnut.2022.982878

Effect of wheat bran dietary fiber on structural properties and hydrolysis behavior of gluten after synergistic fermentation of *Lactobacillus plantarum* and *Saccharomyces cerevisiae*

Zhen Wang[1], Sen Ma[1,2,3]*, Li Li[1,2] and Jihong Huang[1,2,3]*

[1]State Key Laboratory of Crop Stress Adaptation and Improvement, College of Agriculture, Henan University, Kaifeng, China, [2]College of Food Science and Engineering, Henan University of Technology, Zhengzhou, China, [3]School of Food and Pharmacy, Xuchang University, Xuchang, China

The effect of synergistic fermentation of *Lactobacillus plantarum* and *Saccharomyces cerevisiae* on the structural properties and aggregation behavior of gluten containing different wheat bran dietary fiber (WBDF) levels (0, 3, 6, 9, and 12%) was investigated. The results showed that WBDF addition affected the aggregation behavior of gluten at the molecular level, while WBDF significantly induced depolymerization behaviors in large aggregated gluten proteins (Molecular weight > 130 kDa) under reducing conditions ($p < 0.05$). In terms of secondary structure, WBDF significantly reduced glutamine side chain levels and reduced antiparallel β-sheet structures from 28.57 to 24.53% ($p < 0.05$). In addition, WBDF thermal properties and its water holding capacity were the main factors causing changes in thermal properties in the overall gluten system. This study provides new data for the improved production of sourdough whole grain and/or high fiber flour products.

KEYWORDS

dietary fiber, sourdough, gluten, protein hydrolysis, FT-IR

Introduction

The consumption of more whole grain foods, such as wholemeal bread, may help reduce diseases such as type 2 diabetes, chronic cardiovascular disease, chronic intestinal disease, and obesity (1, 2) as whole grain foods are rich in active substances that benefit human health, especially dietary fiber (3). However, wholemeal flour products have a poorer texture and mouth-feel when compared with refined flour products; one reason is the increased insoluble dietary fiber content in wholemeal products which deteriorates gluten network structures during flour production processes, ultimately leading to reduced quality in flour products (4).

Sourdough fermentation technology is considered a promising way to improve wholemeal product quality; it is considered a "gold standard" fermentation technique and an effective way to meet future food challenges (5, 6). However, the use of sourdough in industrial fermentation processes is challenging as microorganism complexity in sourdough is significantly influenced by the environment (7). This potentially causes difficulties with product quality control.

In general, sourdoughs are classified as Types I, II, and III depending on how the culture was obtained. Type I sourdoughs are traditional in nature and require uninterrupted propagation through the regular application of fresh flour and water. Type II sourdoughs are industrially inoculated with adapted cultures which function as dough acidifiers and Type III sourdoughs are usually dried for easy storage and use (8, 9). Therefore, type II are considered the best options for factory production processes as consistent controlled quality can be ensured. And the most important step before producing type II sourdough is to select the right strains to build a synergistic fermentation system.

On the other hand, one of the most typical features of sourdough fermentation is gluten hydrolysis (10), the degree of which is thought to correlate with gluten structure, flavor precursors, dough quality, and flour product quality. For example, the flavor of wheat sourdough bread is positively correlated with the concentration of free amino acids during production (11), and increased free amino acids are generated by gluten hydrolysis during fermentation. Monitoring gluten behavior during sourdough fermentation is a main research focus; however, sourdough composition is also very important. Lactic acid bacteria (LAB) and yeast (mainly *Saccharomyces cerevisiae*) are the most important microorganisms in sourdough production (12); one of the best-known LABs is *Lactobacillus plantarum* which is a homo-fermented LAB (13). In the LAB system, lactic and acetic acids are, respectively, produced *via* specific metabolic hexose and pentose pathways; the acids lower the pH of the fermentation system and inhibit ammonia nitrogen production. Conversely, *S. cerevisiae* secretes nitrogen-metabolizing enzymes to hydrolyze exogenous amino acids and peptides to inorganic nitrogen (9, 14).

Currently, data on the effects of cereal dietary fiber in sourdough fermented flour products are often contradictory, especially with regard to underlying mechanisms. In this study, dietary fiber was extracted from wheat bran and a synergistic fermentation system constructed using *L. plantarum* and *S. cerevisiae* after separate immobilization cultures. Our aim was to investigate the influence of wheat bran dietary fiber (WBDF) on structural properties and aggregation behavior of gluten in the synergistic fermentation system, with a view to providing additional data for research and the industrial production of whole grain and/or high dietary fiber fermented flour products.

Materials and methods

Materials

Wheat bran was obtained from Henan Jiaqi Industry Co. (<city>Zhengzhou</city>, China), the moisture content of the bran was 14.68%, the protein content 16.51%, the starch content 12.04% and the ash content 5.89%. Raw wheat gluten was purchased from a local market (73.64% protein, 8.48% starch, 1.26% ash, and 12.07% moisture). WBDF was extracted following a procedure by Ma et al. (15); total dietary fiber, moisture, protein, starch and ash content in the WBDF was 85.90, 5.24, 2.72, 3.22, 1.75%, respectively. Finally, *L. plantarum* ATCC 8014 and *S. cerevisiae* ATCC 9763 were provided by the Shanghai Biology Collection Center (Shanghai, China). All reagents were analytically pure unless otherwise specified.

Preparation of WBDF-gluten samples

WBDF was mixed with raw gluten (RG) at 0, 3, 6, 9, and 12% (*w/w*) concentrations in a mixer (JF-300 Rotary Mixer, Worcestershire Industrial Instruments Ltd., Guangzhou, China) at 100 rpm for 5 min to generate WBDF-gluten samples (Control-0, 3, 6, 9, and 12%).

Preparation of a synergistic fermentation system

L. plantarum ATCC 8014 and *S. cerevisiae* ATCC 9763 were cultured separately to construct a type II sourdough fermentation system, with the ultimate goal of generating a mixed microorganism suspension. *L. plantarum* and *S. cerevisiae* levels were log 9.0 CFU/mL and log 7.0 CFU/mL, respectively. All steps were performed according to a previous study (16). LAB and yeast cell counts were performed according to the AOAC 990.12 method.

The fermentation of WBDF-gluten samples

WBDF-gluten samples and the sourdough were mixed in a 1:2 (*w/v*) ratio. Next, the gluten slurry were transferred to a constant temperature and humidity incubator (Shanghai Binglin Electronic Technology Co., Ltd., Shanghai, China) with a pre-set temperature of 30°C, humidity of 80%; and the fermentation time lasted 4 h. Finally, the fermented gluten slurry was centrifuged for 30 min at 4,000 × *g*. The precipitates were collected, freeze-dried for 48 h, and ground to enable all samples to pass through a 100 mesh sieve; stored at −18°C.

Scanning electron microscope analysis

The structure of WBDF-gluten fermentation samples was examined by SEM. All samples were sputtered for gold plating in a sputtering coater and transferred to a Quanta FEG-250 SEM (FEI, Hillsboro, OR, USA) for examination at an accelerated voltage of 20 kV.

Confocal laser scanning microscopy analysis

All samples need to be dyed before CLSM observation. The fermented WBDF-gluten samples were mixed and dyed with fluorescent dye rhodamine B [0.001% (*w/v*)], fluorescein isothiocyanate (FITC) [0.01% (*w/v*)] and fluorescent brightener [0.001% (*w/v*)] for 20 min. The stained sections were observed in Olympus Fluoview FV30000 CLSM system (Olympus Corp., Tokyo, Japan), and the laser excitation wavelength was set to 561 nm. Digital image files were recorded at a resolution of 1,024 × 1,024 pixels.

Determining the molecular weight distribution

WBDF-gluten and RG samples were weighed (150 mg) and dissolved in 15 mL 0.05 M phosphate buffer [pH 6.8, 2.0% (*w/v*) plus sodium dodecyl sulfate (SDS)] and vortexed at 25°C for 30 min. Sample suspensions were then centrifuged at 25°C for 15 min at 10,000 × *g* and supernatants passed through a 0.45 μm aqueous filter membrane. A BioSP-sec-s4000 liquid chromatography (LC) column was selected for size exclusion high performance liquid chromatography (SE-HPLC). Experimental LC conditions were: column temperature = 30°C; mobile phase A = acetonitrile (chromatographic grade) + 0.05% trifluoroacetic acid, mobile phase B = H_2O (ultrapure water) + 0.05% trifluoroacetic acid; mode = equal gradient (A:B = 1:1); injection volume = 20 μL; flow rate = 0.5 mL/min; and detection wavelength = 214 nm. In reducing conditions, the procedure was the same except dithiothreitol (DTT) was added.

Fourier transform infrared spectroscopy analysis

FT-IR spectra were generated using a fast FT-IR spectrometer. Samples (2 mg) were ground for 5 min with 200 mg dry potassium bromide. Test conditions: scanning range = 4,000 cm^{-1}-400 cm^{-1}, resolution = 4 cm^{-1}, and number of scans = 32. Spectral data were processed using Peakfit software (v4.12) in the amide I band (1,650–1,720 cm^{-1}) range to analyze secondary protein structures. Specific structures attributed to different spectra in the amide I band are shown (Supplementary Table S1).

Amino acid analysis

The free amino acid content in samples was analyzed using a fully automatic amino acid analyzer (Clarity Amino Acid Analyzer SW-433D, Sykam, Munich, Germany); 150 mg samples were weighed, extracted in boiling water, and separated on a sulphonic acid cation exchange column. Then, at 135°C, separated amino acids were reacted with ninhydrin: primary amines produced blue-violet compounds and secondary amines produced yellow compounds. Derivatives were detected by visible spectrophotometric analyses at 570 and 440 nm, respectively, using a chemical reaction. Amino acids were characterized by sample retention times and quantified using an external standard working curve.

Surface hydrophobicity tests

Protein surface hydrophobicity (H_o) was determined using the fluorescent probe 8-anilino-1-naphthalenesulfonic acid (ANS). WBDF-gluten samples were weighed (100 mg) and dispersed in 15 mL 0.01 M phosphate buffer (pH 7.0). The dispersion was shaken and centrifuged at 10,000 × *g* for 10 min at 4°C. Next, the protein concentration of the supernatant was determined using the Bradford method, with or without dilution as appropriate. Approximately 4 mL of the supernatant was set aside for assay. An ANS solution (8 mM) was prepared in the same phosphate buffer and 20 μL added to the 4 mL supernatant and fluorescence intensity measured after incubation for 3 min. The excitation wavelength was 390 nm, the emission wavelength was 470 nm, and excitation and emission slits were 5 nm. is the H_o value of the sample, and a diluted gluten solution without ANS was used as a blank control.

Thermal properties

All samples were placed in aluminum oxide trays after accurate weighing of 5 mg. Thermogravimetric analysis (TGA) of the samples was carried out with a Mettler Toledo TGA2 (SF) system (Mettler Toledo Corp., Zurich, Switzerland). The experimental conditions were set to a heating rate of 10°C/min from 30 to 600°C and a nitrogen atmosphere flow rate of 60 mL/min. Derivative thermogravimetric (DTG) curves were obtained by performing first-order derivative analysis on TGA trace mass loss (%).

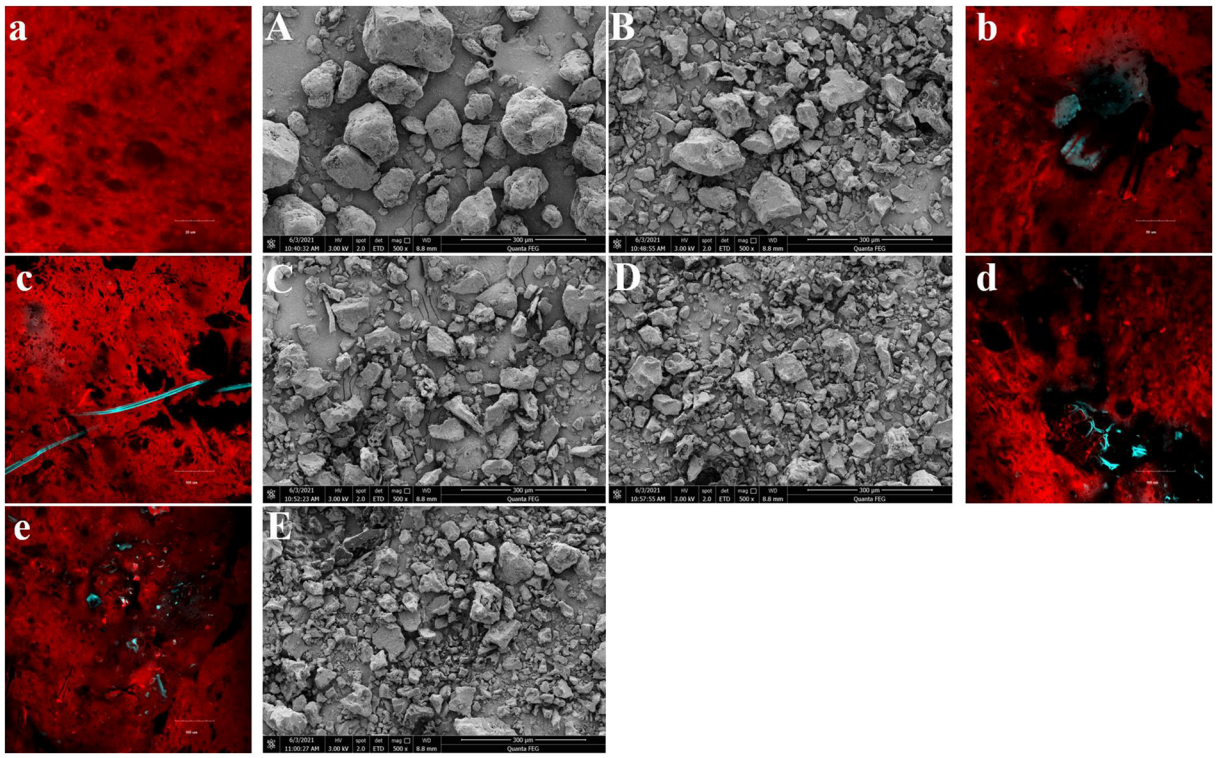

FIGURE 1
The surface morphology of samples at different WBDF levels (0%-Control, 3%, 6%, 9%, 12%) was observed by SEM (500 ×, **A–E**) and CLSM **(a–e)**.

Statistical analysis

All procedures were repeated three times. Analysis of variance was used to detect significant differences ($p < 0.05$). One-way analysis of variance was performed using Tukey's method in SPSS software (SPSS Inc., Chicago, IL, USA).

Results and discussion

Morphology analysis

The surface morphology of gluten after fermentation at different WBDF concentrations is shown (Figure 1). SEM images (Figures 1A–E) showed that gluten was more visible as agglomerates (clumps), especially in control samples (Figure 1A). In WBDF-gluten samples (Figures 1B–E), most of the WBDF was encapsulated by gluten. Also, the particle size of gluten agglomerates decreased with increasing WBDF concentration and was accompanied by rougher protein agglomerate surfaces and deepened protein fragmentation, especially in 9 and 12% WBDF samples (Figures 1D,E).

After fermentation, circular or elliptical air cells inside gluten were observed in CLSM images (Figures 1a–e) and WBDF positions in relation to air chamber formation were clearly seen. In this case, the gluten is stained red by rhodamine B; the WBDF is stained blue by FITC; the fluorescent brightener serves to make the imaging results of the WBDF clearer. In control samples (Figure 1a), gluten displayed homogeneous textures and the edges of air cells formed by fermentation were flat and smooth; whereas after WBDF addition (Figures 1b–e), the gluten matrix could barely coexist with WBDF and tore the gluten matrix. In other words, the gluten matrix was uneven and discontinuous around the WBDF; therefore, good air cell structures were not identified in WBDF samples.

Therefore, the addition of WBDF changed the distribution of gluten. Gluten is more likely to aggregate on the WBDF, encapsulating the WBDF. The degradation behavior of dough and flour products caused by insoluble dietary fiber is well-known, with several hypotheses promoted in previous reports: (1) WBDF is stiff and directly affects the rheological behavior of the dough; (2) WBDF dilutes the relative gluten and starch content and breaks the tightness of the gluten-starch matrix; (3) WBDF has a "competitive hydration" effect, which affects the structure of the gluten network and gluten hydration; and (4) WBDF forms a physical barrier to the gluten network (steric hindrance effects) and accelerates CO_2 escape through the spatial barrier effect (4). Here, we provide new observations

potentially explaining dough quality deterioration caused by insoluble dietary fiber.

Molecular weight distribution

SE-HPLC is a sensitive method that quantifies Molecular weight (*Mw*), while gluten solubility in SDS-phosphate buffer reveals the extent of their cross-linking capabilities. Typically, in the absence of strong reducing agents (Figure 2A), SDS soluble proteins are divided into three regions based on band intensity: F1, F2, and F3, which correspond to $Mw > 67$ kDa, $Mw \approx 37–60$ kDa, and $Mw \approx 14–27$ kDa, respectively (17). As shown (Figure 2A), fermentation and WBDF addition altered sample retention times in the F1 region, while samples containing WBDF showed two small peaks in the F2 region, with no significant shifts in the F3 region. The higher WBDF levels in the F1 region, the closer the peak band positions were to original unfermented gluten samples, i.e. WBDF addition caused the *Mw* of WBDF-gluten aggregates to be closer to the original gluten sample, which may be related to WBDF particle size. Gluten proteins exhibit entrapment behavior for WBDF as observed in morphology. At the same time, this behavior may have an impact on the aggregation behavior of gluten and thus on the *Mw* of gluten proteins, as the contact possibilities between gluten proteins are amplified. The particle size of WBDF may form the basis for the influence of gluten *Mw*. No significant decrease in band intensity was observed in any plots; however, in the F1 region, the peak near the 8.5 min retention time had shifted in the WBDF sample when compared with the control sample and the original gluten sample, and was supported by a small peak in the F2 region. This observation suggested that WBDF addition promoted a slight hydrolysis in protein bulk polymers in samples. The low intensity of the hydrolysis process was attributed to the short fermentation time; in an optimal fermentation period (3–5 h) LAB cannot exert sufficient effects on protein hydrolysis. In contrast, if fermentation times are extended (> 24 h), then significant protein degradation by LAB metabolites may occur, especially for malt alcohol proteins of *Mw* 30–38 kDa (17, 18).

However, upon the addition of a strong reducing agent such as DTT (Figure 2B), gluten was divided into four main intervals based on retention times of different *Mw* proteins. Specifically, proteins were divided into intervals based on 10–12 min, 12–16 min, 16–21 min, and >21 min retention times and corresponded to F1, F2, F3, and F4 intervals (Figure 2B), respectively (19). F1 corresponded to larger polymeric proteins ($Mw > 130$ kDa), F2 to smaller polymeric proteins ($Mw = 80–130$ kDa), F3 to larger monomeric proteins ($Mw = 10–80$ kDa; mainly gliadins), and F4 to smaller monomeric proteins, peptides, and amino acids ($Mw < 5$ kDa). As shown (Figure 2B), the most significant protein band changes were identified in the F1 region, particularly in 6, 9, and 12% WBDF samples, which showed a significant decrease in the F1 peak ($p < 0.05$) and indicating a decrease in protein aggregates in this region. Apart from this observation, bands in other profile regions were not changed significantly and remained consistent with correlation trends between the *Mw* and WBDF levels in samples. This result shows that the addition of WBDF does not alter the aggregation state of gluten proteins at the level of disulfide bonds. At the same time, previous studies have shown that the solubility of gluten proteins is strongly altered by sourdough fermentation, but has not been able to demonstrate that proteolysis of gluten proteins to water-soluble amino acids or peptides occurs (10).

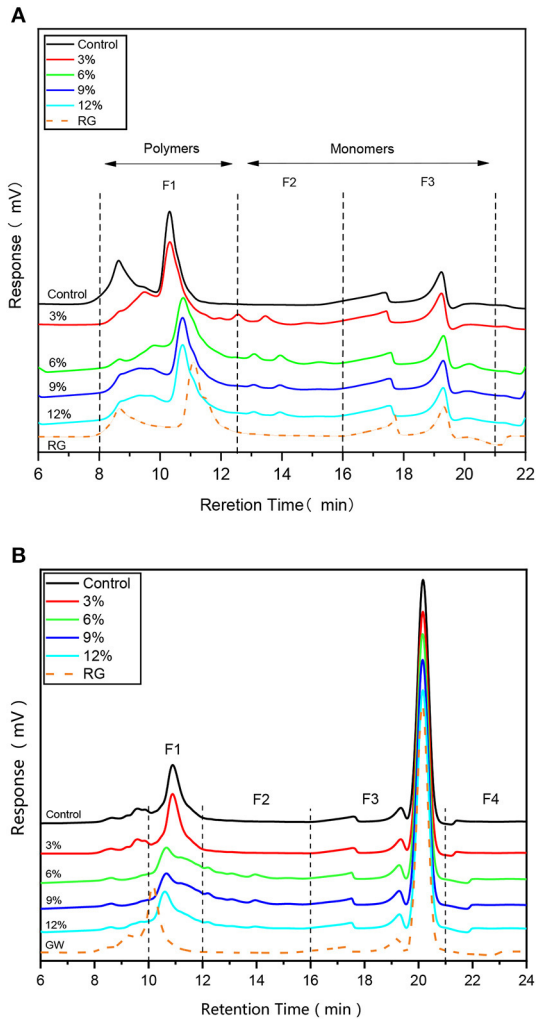

FIGURE 2
HPLC profiles of samples containing different WBDF levels under non-reducing condition **(A)** and reducing condition **(B)**. RG is raw gluten unfermented.

TABLE 1 Secondary structure contents of fermented gluten at different WBDF levels.

Samples	Glutamine side chain	Intermolecular β-sheets	Antiparallel β-sheets	α-helices	β-turns
Control	2.66 ± 0.01^{a}	16.04 ± 0.01^{a}	28.57 ± 2.87^{a}	39.81 ± 7.83^{a}	22.28 ± 4.39^{a}
3%	n.d.	18.29 ± 0.00^{a}	27.46 ± 0.06^{a}	40.35 ± 6.35^{a}	23.04 ± 2.86^{a}
6%	n.d.	15.00 ± 2.00^{a}	24.76 ± 0.22^{b}	38.62 ± 1.74^{a}	21.63 ± 0.48^{a}
9%	n.d.	19.78 ± 3.57^{a}	24.93 ± 0.06^{b}	38.35 ± 1.83^{a}	21.26 ± 0.00^{a}
12%	n.d.	16.84 ± 0.32^{a}	24.53 ± 0.90^{b}	37.26 ± 1.06^{a}	21.39 ± 0.17^{a}

Different letters in the superscript indicate significant differences in the same column ($p < 0.05$). n.d., not detected.

Secondary structures

FT-IR methods are widely used to study protein secondary structures. The basic principle is to divide the spectrogram into amide I, II, and III bands based on wavelength intervals, with different chemical functional groups of proteins in different bands with different stretching and vibrating modes. The amide I band (1,720–1,570 cm^{-1}) is widely used as it has a significant protein signal, and amino acid side chains in this region exert less influence on results; protein signals in amide I bands mainly originate from C=O stretching vibrations in the amide group (20).

Secondary structure data from gluten samples with different WBDF concentrations after fermentation are shown (Table 1). β-sheet and α-helix structures were predominant in protein samples, consistent with previous results (21). For protein intermolecular β-sheet, α-helix, and β-turn structures, WBDF addition did not significantly affect their content ($p > 0.05$), i.e., WBDF induced no changes in these secondary structures. The most significant difference occurred in the control sample, low glutamine side chain (2.66%) levels were observed after fermentation ($p > 0.05$). Glutamine is a hydrophilic amino acid with an isoelectric point of 5.65 and an R-group composition of $-(CH_2)_2-CONH_2$. However, the glutamine side chain structure was not observed in WBDF samples, so it was likely that the WBDF side chain, in an acidic environment created by fermentation, was non-covalently bound to the glutamine side chain. Additionally, WBDF addition significantly decreased antiparallel β-sheet levels from 28.57% in the control sample to 24.53% in the 12% WBDF sample ($p < 0.05$). Protein secondary structures are primarily maintained by non-covalent forces, and when the system environment is altered (e.g., pH, temperature, polar/non-polar co-existing species) the protein state changes accordingly. However, it should be noted, no credible reports exist on intermolecular interaction mechanisms between dietary fiber and anti-parallel β-sheets in gluten.

Free amino acid type and content

In contrast to dry yeast fermentation, the most distinctive feature of sourdough fermentation is that gluten undergoes varying levels of hydrolysis during fermentation. Protein hydrolysis, followed by peptide or amino acid metabolism *via* LAB fermentation, is a key pathway for bread flavor formation (22). Previous studies reported that fermented sourdoughs contained lower peptide and higher amino acid levels (23). Also, amino acid type and content after hydrolysis was determined by *Lactobacillus* strain specificity in sourdough (22).

As indicated (Table 2), no significant change in the relative amino acid content in samples was observed, except for serine and tyrosine. This observation could be attributed to the uniqueness of the Lactobacillus strain used in this study. Specifically, for serine and tyrosine content, no linear pattern was observed in their relationship with WBDF content, therefore, it was not possible to ascribe a mechanism to these amino acid alterations. It is generally accepted that the amount and type of amino acids produced by the hydrolysis of gluten proteins during sourdough fermentation depends on the microbial composition that makes up the sourdough. In the case of lactic acid bacteria and yeasts in sourdough, higher levels of amino acids are required for the growth and metabolism of yeasts. Previous studies reported that the effects of LAB toward total amino acid levels were insignificant, and that amino acid type and content was determined by the pH and microbial metabolism levels during fermentation; proline formation was favored at pH > 5.5 and phenylalanine, leucine, and cysteine release mainly occurred at lower pH values (11).

Of particular interest is glutamate and glutamine metabolism, as glutamine is the most abundant amino acid in wheat proteins. Also, glutamine deamidation is essential for plant protein hydrolysis by glutamate, and glutamate-α-ketoglutarate interconversion by glutamate dehydrogenase provides amino receptors for the amino transfer of other amino acids (24). As shown (Table 2), glutamate was the most abundant amino acid (24–26%) while no glutamine was detected. When combined with secondary structure analyses, it appeared that only a very low level (2.66%) of the glutamine side chain was present in samples without WBDF, and that glutamine side chain content disappeared after WBDF addition. Therefore, WBDF addition may have caused a change in glutamine behavior. The exact mechanism requires further investigation.

TABLE 2 Changes in free amino acid contents in the fermented system at different WBDF levels.

Amino acids	Amino acids contents (%)				
	Control	3%	6%	9%	12%
Asp	2.46 ± 0.17^{a}	2.57 ± 0.07^{a}	2.53 ± 0.02^{a}	2.47 ± 0.06^{a}	2.33 ± 0.16^{a}
Thr	1.96 ± 0.08^{a}	1.94 ± 0.19^{a}	1.78 ± 0.09^{a}	1.86 ± 0.08^{a}	1.75 ± 0.06^{a}
Ser	3.38 ± 0.23^{ab}	3.59 ± 0.08^{a}	3.35 ± 0.18^{ab}	3.41 ± 0.11^{ab}	3.11 ± 0.09^{b}
Glu	26.02 ± 1.11^{a}	27.90 ± 0.67^{a}	26.10 ± 2.39^{a}	26.46 ± 0.52^{a}	24.72 ± 0.41^{a}
Gly	2.65 ± 0.25^{a}	2.85 ± 0.05^{a}	2.72 ± 0.26^{a}	2.71 ± 0.01^{a}	2.48 ± 0.12^{a}
Ala	2.05 ± 0.21^{a}	2.23 ± 0.04^{a}	2.11 ± 0.20^{a}	2.11 ± 0.00^{a}	1.95 ± 0.12^{a}
Cys	0.81 ± 0.09^{a}	0.89 ± 0.12^{a}	0.89 ± 0.15^{a}	1.01 ± 0.10^{a}	0.97 ± 0.01^{a}
Val	2.90 ± 0.26^{a}	3.13 ± 0.05^{a}	2.92 ± 0.32^{a}	2.96 ± 0.05^{a}	2.73 ± 0.10^{a}
Met	1.11 ± 0.09^{a}	1.18 ± 0.03^{a}	1.09 ± 0.11^{a}	1.08 ± 0.10^{a}	1.03 ± 0.02^{a}
Ile	2.67 ± 0.30^{a}	2.87 ± 0.03^{a}	2.69 ± 0.31^{a}	2.76 ± 0.01^{a}	2.70 ± 0.07^{a}
Leu	4.84 ± 0.48^{a}	5.20 ± 0.16^{a}	4.88 ± 0.47^{a}	5.01 ± 0.02^{a}	4.66 ± 0.07^{a}
Tyr	2.70 ± 0.22^{ab}	2.85 ± 0.00^{ab}	2.90 ± 0.13^{a}	2.78 ± 0.06^{ab}	2.48 ± 0.22^{b}
Phe	3.63 ± 0.34^{a}	3.87 ± 0.04^{a}	3.70 ± 0.41^{a}	3.73 ± 0.05^{a}	3.41 ± 0.23^{a}
His	2.07 ± 0.23^{a}	2.19 ± 0.06^{a}	2.12 ± 0.26^{a}	2.13 ± 0.00^{a}	1.98 ± 0.10^{a}
Lys	1.18 ± 0.12^{a}	1.25 ± 0.03^{a}	1.17 ± 0.11^{a}	1.18 ± 0.00^{a}	1.08 ± 0.05^{a}
Arg	2.58 ± 0.24^{a}	2.75 ± 0.04^{a}	2.60 ± 0.27^{a}	2.62 ± 0.04^{a}	2.42 ± 0.13^{a}

Different letters in the superscript indicate significant differences in the same column ($p < 0.05$).

Surface hydrophobicity analysis

Surface hydrophobicity is a structural feature used to assess protein conformational changes. The exogenous fluorescence molecule ANS measures the surface hydrophobicity index (H_o) of proteins; its values are positively correlated with hydrophobic group numbers on the surface of gluten and it provides an indication of protein-protein interactions. Most fluorescent aromatic amino acids are located in the protein interior, so if external forces unfold wheat gluten structures and expose hydrophobic groups (e.g., glutamine and asparagine) (25), this increases H_o values. Previously, the surface hydrophobicity of proteins was shown to increase or decrease after sourdough fermentation, and depended on the hydrolysis conditions of the system, the degree of hydrolysis, enzyme specificity, and protein properties (26).

Changes in the surface hydrophobicity of gluten plus different WBDF concentrations after fermentation are shown (Figure 3); while H_o values in 3%-WBDF samples showed a slight increase when compared with control samples, this was not significant ($p > 0.05$). Additionally, a significant decrease in H_o was observed in 6, 9, and 12% WBDF samples ($p < 0.05$); this indicated that more hydrophilic amino acid groups appeared on the protein surface in the system, and a reduction in hydrophobicity on the gluten surface at high WBDF concentrations suggested possible depolymerization of gluten aggregates. However, no significant correlations between H_o changes and WBDF concentrations were identified ($p > 0.05$). Therefore, the effects of pH on peptide chains (fermentation processes) in the system cannot be excluded; acidic environments can affect hydrogen bond formation, electrostatic interactions, and hydrophobic interactions between protein molecules, leading to depolymerization, stretching of peptide chains, and hydrophobic group exposure. It should be noted that for alterations in protein secondary structures and free amino acid content, no strong evidence suggested that

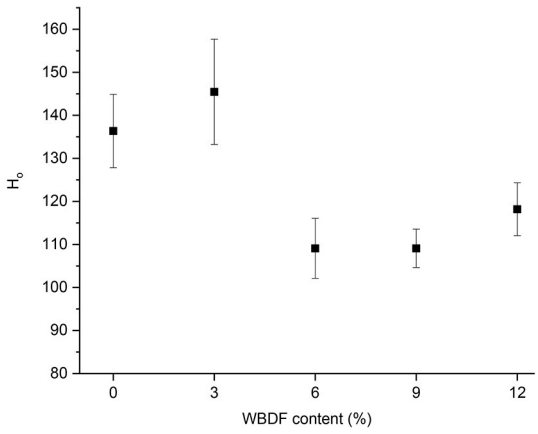

FIGURE 3
Surface hydrophobicity values of samples at different WBDF levels.

WBDF concentrations or the fermentation process dominated H_o changes.

Thermal properties

TGA is commonly used to indicate how water evaporates from a system, and is used to investigate mechanisms whereby samples lose weight due to controlled heating. Weight loss curves also reflect variability between the behaviors of mixture components. Both TGA (Figure 4A) and DTG (Figure 4B, first derivative) curves for fermented gluten at different WBDF concentrations are indicated. As shown (Figure 4B), the turning point for sample mass loss occurred near 120°C, when it was hypothesized all free water in samples had evaporated. In a simple gluten mixture system, different changes in moisture content during warming can be distinguished by peak value changes in the DTG plot, which can be used to support TGA plot analysis. Specifically, the weight change at the first peak in the DTG curve (near 75°C) was possibly attributed to a reduction in free water content, with the second peak (307–324°C) occurring due to bound-water loss. During the first mass reduction interval, all samples containing WBDF showed no significant change when compared with the control; however, the fermentation process caused a slight increase in free water levels in samples when compared with RG samples. The thermal decomposition of the WBDF-gluten system was also divided into three stages. The mass loss phase in the first stage ($T < 120°C$) was mainly attributed to free water evaporation from the system; the mass loss in the second stage ($120°C \leq T \leq 320°C$) was attributed to starch decomposition; and the mass loss in the third stage ($T > 320°C$) was attributed to the full carbonization of samples. At the end of heating, curve-end analysis showed that the control sample had the lowest mass fraction at this point, while the opposite was true for RG sample, thereby confirming that fermentation increased the free water content in samples, with the increase most likely coming from semi-bound/bound water in the original sample. Additionally, the slightly higher mass fraction in WBDF samples when compared with controls may have been due to incomplete WBDF decomposition in the system, or extensive hydrogen bonding structures formed between WBDF and gluten/free amino acids, which increased thermal stability in samples.

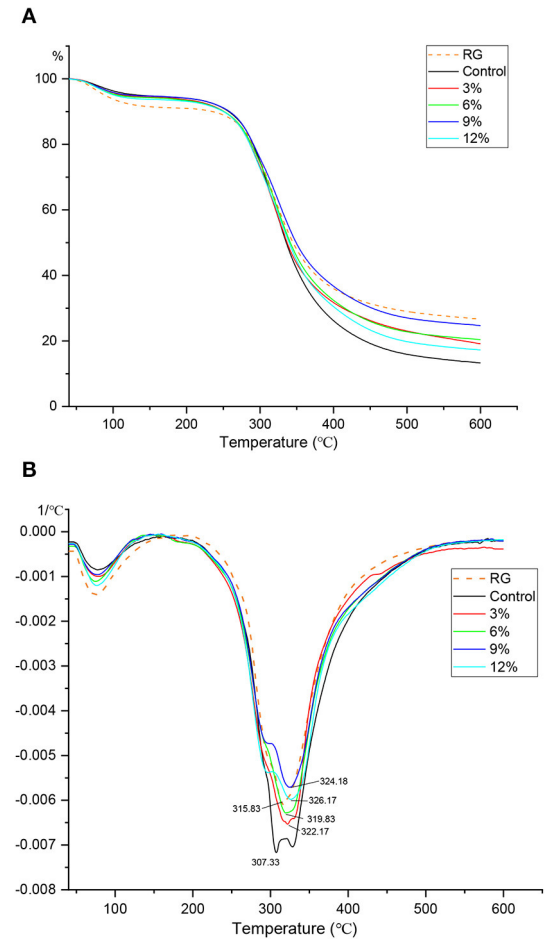

FIGURE 4
TGA **(A)** and DTG **(B)** profiles of different WBDF levels samples. RG is raw gluten unfermented.

Conclusions

Investigating alterations in gluten after sourdough fermentation at different WBDF concentrations is required for an increased understanding and the production of whole grain and/or high fiber fermented flour products. We showed that WBDF addition fragmented gluten clusters during fermentation and disrupted gluten network continuity. Also, WBDF addition caused gluten polymers to be more readily depolymerized and reduced protein surface hydrophobicity; we hypothesized that non-covalent interactions of WBDF with glutamine side chains in gluten were the main cause of these observations. The ability of WBDF to influence the formation of flavor substance precursors; however, it should be taken into account that WBDF may affect the metabolic processes of glutamate and glutamine in the sourdough fermentation system. Finally, we hypothesize that the thermal properties of WBDF and its ability to hold water at physical layers were the main factors causing thermal property changes in the gluten system. This study provides insights on interactions between dietary fiber and gluten during fermentation, and provides an evidence-based guide for the production of fermented high fiber flour products.

Data availability statement

The original contributions presented in the study are included in the article/Supplementary material, further inquiries can be directed to the corresponding author/s.

Author contributions

ZW: conceptualization, methodology, software, and writing—original draft preparation. SM: conceptualization, writing—reviewing and editing, supervision, and project administration. LL: methodology, software, and visualization. JH: funding acquisition, supervision, and project administration. All authors contributed to the article and approved the submitted version.

Funding

This work was supported by the National Natural Science Foundation of China (No. 32272249), Scientific and Technological Innovation Talents Project of Henan Universities (No. 23HASTIT033), Zhongyuan Scholars in Henan Province (No. 192101510004), Major Science and Technology Projects for Public Welfare of Henan Province (No. 201300110300), and open competition Research Projects of Xuchang University (No. 20220504).

Conflict of interest

The authors declare that the research was conducted in the absence of any commercial or financial relationships that could be construed as a potential conflict of interest.

Publisher's note

All claims expressed in this article are solely those of the authors and do not necessarily represent those of their affiliated organizations, or those of the publisher, the editors and the reviewers. Any product that may be evaluated in this article, or claim that may be made by its manufacturer, is not guaranteed or endorsed by the publisher.

Supplementary material

The Supplementary Material for this article can be found online at: https://www.frontiersin.org/articles/10.3389/fnut.2022.982878/full#supplementary-material

References

1. Hu Y, Ding M, Sampson L, Willett WC, Manson JE, Wang M, et al. Intake of whole grain foods and risk of type 2 diabetes: results from three prospective cohort studies. *BMJ.* (2020) 370:m2206. doi: 10.1136/bmj.m2206

2. Liu J, Yu LL, Wu Y. Bioactive components and health beneficial properties of whole wheat foods. *J Agric Food Chem.* (2020) 68:12904–15. doi: 10.1021/acs.jafc.0c00705

3. Reynolds AN, Akerman AP, Mann J. Dietary fiber and whole grains in diabetes management: systematic review and meta-analyzes. *PLoS Med.* (2020) 17:e1003053. doi: 10.1371/journal.pmed.1003053

4. Ma S, Wang Z, Liu H, Li L, Zheng X, Tian X, et al. Supplementation of wheat flour products with wheat bran dietary fiber: purpose, mechanisms, and challenges. *Trends Food Sci Technol.* (2022) 123:281–9. doi: 10.1016/j.tifs.2022.03.012

5. Gobbetti M, Gänzle M. *Handbook on Sourdough Biotechnology.* Springer Science and Business Media (2012).

6. Ma S, Wang Z, Guo X, Wang F, Huang J, Sun B, et al. Sourdough improves the quality of whole-wheat flour products: mechanisms and challenges—A review. *Food Chem.* (2021) 360:130038. doi: 10.1016/j.foodchem.2021.130038

7. Suo B, Chen X, Wang Y. Recent research advances of lactic acid bacteria in sourdough: origin, diversity, and function. *Curr Opin Food Sci.* (2021) 37:66–75. doi: 10.1016/j.cofs.2020.09.007

8. Corsetti A, Settanni L. Lactobacilli in sourdough fermentation. *Food Res Int.* (2007) 40:539–58. doi: 10.1016/j.foodres.2006.11.001

9. De Vuyst L, Van Kerrebroeck S, Leroy F. Microbial ecology and process technology of sourdough fermentation. *Adv Appl Microbiol.* (2017) 100:49–160. doi: 10.1016/bs.aambs.2017.02.003

10. Thiele C, Grassl S, Gänzle M. Gluten hydrolysis and depolymerization during sourdough fermentation. *J Agric Food Chem.* (2004) 52:1307–14. doi: 10.1021/jf034470z

11. Thiele C, Gänzle MG, Vogel RF. Contribution of sourdough lactobacilli, yeast, and cereal enzymes to the generation of amino acids in dough relevant for bread flavor. *Cereal Chem.* (2002) 79:45–51. doi: 10.1094/CCHEM.2002.79.1.45

12. Gobbetti M, De Angelis M, Di Cagno R, Calasso M, Archetti G, Rizzello CG. Novel insights on the functional/nutritional features of the sourdough fermentation. *Int J Food Microbiol.* (2019) 302:103–13. doi: 10.1016/j.ijfoodmicro.2018.05.018

13. Xu D, Ding W, Ke W, Li F, Zhang P, Guo X. Modulation of metabolome and bacterial community in whole crop corn silage by inoculating homofermentative *Lactobacillus plantarum* and heterofermentative *Lactobacillus buchneri*. *Front Microbiol.* (2019) 9:3299. doi: 10.3389/fmicb.2018.03299

14. Heitmann M, Zannini E, Arendt E. Impact of Saccharomyces cerevisiae metabolites produced during fermentation on bread quality parameters: a review. *Crit Rev Food Sci Nutr.* (2018) 58:1152–64. doi: 10.1080/10408398.2016.1244153

15. Ma S, Han W, Li L, Zheng X, Wang X. The thermal stability, structural changeability, and aggregability of glutenin and gliadin proteins induced by wheat bran dietary fiber. *Food Funct.* (2019) 10:172–9. doi: 10.1039/C8FO01810C

16. Wang Z, Yan J, Ma S, Tian X, Sun B, Huang J, et al. Effect of wheat bran dietary fiber on structural properties of wheat starch after synergistic fermentation of *Lactobacillus plantarum* and *Saccharomyces cerevisiae*. *Int J Biol Macromol.* (2021) 190:86–92. doi: 10.1016/j.ijbiomac.2021.08.179

17. Wieser H, Vermeulen N, Gaertner F, Vogel RF. Effects of different Lactobacillus and Enterococcus strains and chemical acidification regarding degradation of gluten proteins during sourdough fermentation. *Eur Food Res Technol.* (2008) 226:1495–502. doi: 10.1007/s00217-007-0681-1

18. Fraberger V, Ladurner M, Nemec A, Grunwald-Gruber C, Call LM, Hochegger R, et al. Insights into the potential of sourdough-related lactic acid bacteria to degrade proteins in wheat. *Microorganisms.* (2020) 8:1689. doi: 10.3390/microorganisms8111689

19. Liu J, Luo D, Li X, Xu B, Zhang X, Liu J. Effects of inulin on the structure and emulsifying properties of protein components in dough. *Food Chem.* (2016) 210:235–41. doi: 10.1016/j.foodchem.2016.04.001

20. Xu J, Hao M, Sun Q, Tang L. Comparative studies of interaction of β-lactoglobulin with three polyphenols. *Int J Biol Macromol.* (2019) 136:804–12. doi: 10.1016/j.ijbiomac.2019.06.053

21. Zhang Y, Hong T, Yu W, Yang N, Jin Z, Xu X. Structural, thermal and rheological properties of gluten dough: comparative changes by dextran, weak acidification and their combination. *Food Chem.* (2020) 330:127154. doi: 10.1016/j.foodchem.2020.127154

22. Gänzle MG, Loponen J, Gobbetti M. Proteolysis in sourdough fermentations: mechanisms and potential for improved bread quality. *Trends Food Sci Technol.* (2008) 19:513–21. doi: 10.1016/j.tifs.2008.04.002

23. Di Cagno R, De Angelis M, Auricchio S, Greco L, Clarke C, De Vincenzi M, et al. Sourdough bread made from wheat and nontoxic flours and started with selected lactobacilli is tolerated in celiac sprue patients. *Appl Environ Microbiol.* (2004) 70:1088–96. doi: 10.1128/AEM.70.2.1088-1096.2004

24. Tanous C, Kieronczyk A, Helinck S, Chambellon E, Yvon M. Glutamate dehydrogenase activity: a major criterion for the selection of flavor-producing lactic acid bacteria strains. *Lactic Acid Bact Genet Metab Appl.* (2002) 271–8. doi: 10.1007/978-94-017-2029-8_17

25. Pallarès I, Vendrell J, Avilés FX, Ventura S. Amyloid fibril formation by a partially structured intermediate state of α-chymotrypsin. *J Mol Biol.* (2004) 342:321–31. doi: 10.1016/j.jmb.2004.06.089

26. De la Barca AC, Ruiz-Salazar RA, Jara-Marini ME. Enzymatic hydrolysis and synthesis of soy protein to improve its amino acid composition and functional properties. *J Food Sci.* (2000) 65:246–53. doi: 10.1111/j.1365-2621.2000.tb15988.x

frontiers | Frontiers in Nutrition

TYPE Original Research
PUBLISHED 28 October 2022
DOI 10.3389/fnut.2022.1020281

OPEN ACCESS

EDITED BY
Hua-Min Liu,
Henan University of Technology, China

REVIEWED BY
Jun Lu,
Central South University Forestry and Technology, China
Liang Li,
Northeast Agricultural University, China
Zhiwei Zhang,
Tianjin University of Commerce, China

*CORRESPONDENCE
Guanghui Li
hnlgh1228@163.com
Jihong Huang
huang20220605@126.com

SPECIALTY SECTION
This article was submitted to Food Chemistry, a section of the journal Frontiers in Nutrition

RECEIVED 16 August 2022
ACCEPTED 28 September 2022
PUBLISHED 28 October 2022

CITATION
Guo W, Fan L, Wang Y, Li G, Gao X, Chen Z and Huang J (2022) Effect of three natural antioxidants on the structure and physicochemical properties of sweet potato starch noodles. *Front. Nutr.* 9:1020281. doi: 10.3389/fnut.2022.1020281

Effect of three natural antioxidants on the structure and physicochemical properties of sweet potato starch noodles

Weiyun Guo[1], Ling Fan[1], Yonghui Wang[1], Guanghui Li[1]*, Xueli Gao[1], Zhenhao Chen[1] and Jihong Huang[1,2]*

[1]Food and Pharmacy College, Xuchang University, Xuchang, China, [2]College of Agriculture, Henan University, Zhengzhou, China

The study aimed to investigate the effect of three kinds of natural antioxidants (NAs), such as curcumin, tea polyphenols (TP), and lycopene, on sweet potato starch's structure and physicochemical properties of starch noodles. We found that the broken rates, iodine blue values, hardness, and chewiness of natural antioxidant starch noodles (NASN) were increased with the addition of the NAs. Additionally, the elasticity decreased with the addition of curcumin and lycopene, but it increased with the addition of TP. The cross-section structure of NASN obtained by scanning electron microscope (SEM) showed more holes appeared when adding NAs, and the additional amount had a pronounced effect on the microstructure of starch noodles (SN) regardless of the kind of NA added. The X-ray diffraction detection showed that some crystal forms were significantly damaged, and the addition of NAs affected the crystallization process of starch and produced a small proportion of new crystals in the NASNs. The protective effects of SN on NAs and their antioxidant capacities under dry and room temperature storage (DRTS) and wet and frozen storage (WFS) conditions were optimal as compared to those of flour noodles (FN). The results showed that adding NAs could improve the sensory quality and antioxidant function of starch noodles. In turn, the dense structure of starch noodles can also have a significant protective effect on antioxidants and their antioxidant activities, which is especially obvious under WFS conditions.

KEYWORDS

sweet potato starch noodles, curcumin, tea polypheno, lycopene, antioxidation capacities, structure and physicochemical properties

Introduction

The sweet potato output in China ranks first in the world, accounting for more than 85% of the world's total output. The glycemic index (GI) of sweet potato is <55, which is a typical low GI healthy food raw material (1, 2). In China, 28% of sweet potato products are processed into starch noodles (SN), a food popular in many Asian countries, including China, South Korea, Vietnam, and Indonesia (3, 4). SN, which is made of tuber starch (such as cassava or sweet potato), does not contain gluten and is very suitable for

people with celiac disease or gluten intolerance (2). However, from the perspective of nutrition or functionalization, SN lacks protein, vitamins, minerals, polyphenols, cellulose, and other functional components, and their comprehensive nutritional value does not perform high. Therefore, it is necessary to improve the quality of SN to make their nutritional value more comprehensive.

The improvement of the quality of SN mainly focuses on food quality, nutrition improvement, and functionalization. In some studies, by adding concentrated whey protein, banana starch, and NUTRIOSE® (resistant starch) to sweet potato starch noodles (SPSN), the protein retention rate and resistant starch content in the products could be effectively improved, which could also reduce the *in vitro* starch digestibility (2, 5). Additionally, using antioxidants in foods is necessary to regulate health through diet. Oxidative stress is caused by an imbalance in the production of reactive oxygen species and the biological ability to detoxify the reactive intermediates or repair the resulting damage (6). Importantly, antioxidants are substances that remove, delay or prevent oxidative damage, and they can control the amount of oxygen free radicals to neutralize oxidative damage and thus protect the body (7). Curcumin, for example, can reduce the effects of chronic inflammation on human liver cells and consistently relieve arsenic-induced elevation of serum alanine aminotransferase and aspartate aminotransferase activities, augment hepatic malonaldehyde, and reduce blood and hepatic glutathione levels (8). Additionally, Lan et al. studied clinical wound treatment and found that tea polyphenols showed sustained release through *in vitro* digestion, which was conducive to the realization of immediate bacteriostatic effects in the initial stage of wound healing and long-term antioxidant activity (9). Furthermore, lycopene can protect human somatic cells from free radical damage, enhancing the body's ability to fight disease, delay aging, and resist cancer (10). Therefore, polyphenols have antibacterial, anti-cancer, anti-diabetes, immune regulation, anti-atherosclerosis, kidney protection, and other beneficial effects (11).

Considering these findings, adding substances with antioxidant function to starch products could effectively improve their stability, antioxidant properties, and functional quality. For example, adding quercetin and Tert-butyl hydroquinone (TBHQ) to cassava starch/gelatin composite film increased the film's water solubility and water vapor permeability and effectively delayed the oxidation of lard through the film (12). In some studies, finger millet added to rice noodles can not only effectively guarantee the quality of the product, such as crushing rate, cooking loss rate, protein content, and dietary fiber, but also significantly improve the antioxidant activity of the product and its 1,1-diphenyl-2-trinitrophenylhydrazine (DPPH) scavenging ability by 169.6%. Additionally, adding matcha powder to rice noodles effectively reduced the digestibility of starch, increased the content of resistant starch, reduced the GI value, and improved the product's antioxidant and flavor. Moreover, the addition of matcha powder interferes with the recombination of starch chains, resulting in the formation of low-ordered structures, which would decrease the glycemic index of the noodle (13). Likewise, adding cedar leaf powder to rice noodles effectively increased the total phenol content and improved the scavenging ability of the DPPH-free radical (14). Similarly, adding Green Mussel to gluten-free pasta significantly increased the product's ionic strength and gelation level, as well as the free radical scavenging and reducing capacity (15). Notably, these investigations had a high reference value for the quality improvement of SN. Furthermore, there have been many attempts to improve the quality of SN. For example, some researchers added pumpkin powder to SNs, which had no adverse effects on their aroma and taste, but effectively improved the antioxidant activity of flat potato noodles (16). When mulberry leaf powder was added to SN, it was found that it significantly increased the mineral content and total phenol content in SNs, and the antioxidant, anti-diabetic, anti-hypertensive, and anti-diabetic activities of starch vermicelli were improved considerably (17). Therefore, it is speculated that adding NAs to SN may not only ensure the quality but also improve the nutritional and antioxidant properties of NASN.

This study mainly prepared natural antioxidants starch noodles (NASNs) and investigated the effects of natural antioxidants, such as curcumin, TP, and lycopene on the broken rate, iodine blue value, sensory quality, texture characteristics, and structure of SPSN. In addition, the protective effects of NAs and oxygen-free radical scavenging function were studied under two storage conditions: dry and room temperature storage (DRTS) and wet and freezing storage (WFS). Furthermore, the interaction between NAs and SPSNs was discussed to lay a foundation for developing starch noodle products with certain physiological functions.

Materials and methods

Reagents and materials

Sweet potato starch (SPS) (Grade II) with an amylose proportion of 27.5% was purchased from the Shandong Shengqi Biological (Jining, China). High-gluten wheat flour was purchased from One Plus One Natural Flour (Zhengzhou, China). Food-grade curcumin and TP with a

Abbreviations: NASN, natural antioxidant starch noodle; NA, natural antioxidant; SPSN, sweet potato starch noodle; TP, tea polyphenols; SN, starch noodle; SPS, sweet potato starch; FN, flour noodle; WFS, wet and freezing storage; DRTS, dry and room temperature storage; GI, glycemic index; SEM, scanning electron microscope.

purity of 95 and 98%, respectively, were purchased from the Youbaojia Food Co., Ltd (Shangqiu, China), and the food-grade lycopene with a purity of 96% was purchased from the Shengjiade Biotechnology Co., Ltd (Qufu, China). Folin reagent with a concentration of 1 mol/L was purchased from Bomei Biotechnology (Hefei, China). Anhydrous sodium carbonate was purchased from the Kaitong Chemical Reagent (Tianjin, China). N-hexane with a purity of 99.5% and pure analytical-grade anhydrous ethanol was purchased from the Xianshuigu Industrial Park (Tianjin, China). Toluene with a purity of 99.5% and acetic acid with a concentration of 1 mol/L were purchased from the Tianjin Kermel Chemical Reagent (Tianjin, China). DPPH, with a purity of 98%, was purchased from Shanghai Yuanye Biotechnology (Shanghai, China).

Preparation of NASNs

Seventy-five grams of sweet potato starch were accurately weighed and placed in a 1,000-ml beaker. We added 0.15 g of TP or lycopene or 0.20 g of curcumin into the beaker, heated it to 90°C using an electric constant temperature water bath (Putian, China, Dk-8d), and stirred for 3 min to make the starch uniform. After gelatinization, we added 25.0 g of dry sweet potato starch into the gelatinized starch and stirred it evenly. We then mixed the dough at 40°C for 6 min on a smooth surface, put it in an extruder, and kept the extrusion process at a uniform speed to prevent indentation. We quickly cut the strips into the water above 90°C for cooking until they were transparent, then removed them and immediately put them into cold water for cooling. Finally, we hung them on the noodle rack for drying and packed them after 24 h to make dry NASNs. We also directly packaged them without any dry process and froze them to make frozen NASNs.

Preparation of natural antioxidant flour noodles

To compare and verify the protective effects of sweet potato SNs on NAs and antioxidant activity under different storage conditions, natural antioxidant flour noodles were prepared as the control group. We accurately weighed 100 g of flour, added 0.15 g of TP or lycopene or 0.20 g of curcumin, and 40 ml of purified water, stirred, and kneaded it to form a dough with a smooth surface, and put it in the extruder for extrusion. The extruded noodles were hung on the noodle rack for drying and packaged after 24 h. Finally, wet noodle samples were packaged directly and frozen in the refrigerator's freezer.

The effect of NAs addition amount on the quality of NASNs

To determine the optimal parameter level of the addition amount of NAs, the broken rate, paste soup rate, sensory evaluation, and texture characteristics of NASNs were determined. The addition amounts of NAs were selected as 0.05, 0.10, 0.15, 0.20, and 0.25 g and then made into SNs. Broken rates, iodine blue values, sensory scores, and TPA texture characteristics were selected as proxies to determine the optimal addition amounts of the NAs.

Analysis of broken rate of NASNs

A total of 20 pieces of 10 cm long NASNs were made and soaked in cold water for 5 min until fully swollen. They were taken out and put into 1,000 ml of distilled boiling water for 30 min. The noodles were drained, and water was filtered out using absorbent paper. We then counted the total number of broken noodles and calculated the percentage of broken strips in the total number of noodles.

Analysis of iodine blue value of NASNs

After boiling the NASNs for 30 min, the soup was cooled to about 20°C. Five milliliters of cooled soup was poured into a 10-ml volumetric flask, and 1 ml of acetic acid solution was added for a concentration of 1 mol/L and shaken. Then, we added 1 ml iodine reagent for a concentration of 0.1 mol/L, followed by adding deionized water to the scale. The sample was then shaken, followed by stranding for 5 min. The absorbance of the sample solution was determined by a spectrophotometer (Xinmao, China, UV-7504) at the wavelength of 620 nm with distilled water as blank.

Analysis of sensory score of NASNs

Five trained sensory evaluators were selected to make a sensory evaluation on different noodles. To evaluate the pre-cooking characteristics of the product, texture (25%), including thickness, elasticity, adhesiveness, and color (25%), was analyzed before boiling. Furthermore, odor, taste (25%), and impurities (25%) were analyzed after boiling.

Textural profile analysis

Fifteen NASNs, which had good tissue condition, no indentation, uniform thickness, and moderate length, were selected and boiled for 10 min. Then, the sample was cooled

in cold water. After 5 min, the samples were wrapped in the fresh-keeping film for testing.

Before determination, the filter paper was used to absorb the water remaining on the noodles' surface. The noodle to be tested was placed on the stage of the material analyzer (Yingsheng Hengtai, China, TMS-Pro). The TPA texture characteristics assessed included hardness, elasticity, cohesiveness, and chewiness, as determined using a 50 mm flat probe. The speed before measurement, measurement speed, the initial force, the probe, and the compression rate were set as 30.0 mm/min, 30.0 mm/min, 0.1 N, 20.0 mm from the sample surface, and 60%, respectively.

The microstructure of NASN

The microstructure of NASN was studied utilizing a scanning electron microscope (FEI, USA, NOVA 450) at 10 kV. We cut and fixed the short strip of NASN on the sample table with a diameter of 1.0 cm, sprayed gold coating, and then placed it under the electron microscope to observe and take photos at a magnification of 500×.

Determination of the X-ray diffraction

X-ray diffractograms of dried NASNs were obtained with an X-ray diffractometer (Bruker, German, D8-Advance). The dried powder of NASN was tightly packed into the sample holder. Diffraction data were collected over an angular range from 4° to 70° (2θ) in a tube voltage of 40 kV, current of 30 mA, and a scanning rate of 4°/min.

The stability and activity of NAs

The effects of the SN on the retention rate and the free radical scavenging rate of the NAs under the conditions of DRTS and WFS were studied using the FNs as a control. The changes in the retention rates of the NAs and the free radical scavenging rates of NASNs were observed both in DRTS condition with the water contents of two kinds of noodles of 13% and storage temperature of 20°C and in WFS condition with the water contents of 80% and storage temperature of – 18°C. The total storage time in the experiment was set at 2 months, and in the 1st month, the data collection was carried out every 5 days. In the 2nd month, data collection was done on the last day.

The dried SNs were crushed by a pulverizer and screened five times through 60 mesh to obtain powder samples. A solution sample of SN was prepared by adding 1.0 g of powder sample to 20.0 ml of 95% ethanol in a 50-ml beaker, shaking it until fully extracted, and filtering it for analysis. Then, 1.0 ml of the SN solution sample was transferred into a 10-ml volumetric flask, diluted with 95% ethanol to volume, and mixed. A 1-cm cuvette was used for TP analysis to analyze the absorbance value at 425 nm.

One gram of crushed sample was extracted by 10 ml of 60% ethanol using ultrasonic (Tianhua, China, KQC-2B) for 30 min. The extract was then centrifuged by a table freezing centrifuge (Jiawen, China, JW-2019HR) at 1,057×g for 8 min. One milliliter of supernatant was aspirated, and 1 ml of Folin phenol reagent was put into a 10-ml test tube, followed by 2 ml of 12% Na_2CO_3 solution, which was then diluted to 10 ml with water and shaken well. The absorbance was measured at the wavelength of 765 nm for retention rate determination of curcumin after the reaction in the dark for 0.5 h at room temperature.

We accurately weighed 1.00 g of crushed sample, added about 2 ml of methanol, stirred the sample thoroughly, filtered the remaining residue, then added another 2 ml of methanol for cleaning. We then discarded the filtrate, extracted lycopene with a small amount of n-hexane, repeated the extraction step 2 or 3 times until the filtrate was colorless, transferred the filtrate into a 10-ml volumetric flask, shook it evenly with toluene to determine the lycopene extraction solution, and used a 1-cm cuvette to determine its absorbance value with toluene as blank under its maximum absorption wavelength of 485 nm.

The determination of free radical scavenging rate

Preparation of sample solution: Dry/wet ground sample weighing 1.0/5.0 g (accurate to 0.001 g) was added to 10/20 ml of hot water (100°C), and kept at (100°C) for extraction for 45 min. The solution was filtered and the volume of the filtrate was fixed to 50 ml with deionized water.

Detection process

About 0.5 ml of sample solution (0.0394 g DPPH dissolved in 500 ml absolute ethanol) was put into a test tube, and 0.5 ml of DPPH stock solution was then added and mixed well. The mixture of sample and DPPH was stranded for 30 min at room temperature for reaction, and then the absorbance was measured at 517 nm. The sample was replaced with 0.5 ml distilled water for the blank control group. The free radical scavenging rate was calculated according to formula 1.

$$\text{Free radical scavenging rate (\%)} = [1 - \frac{A_1 - A_2}{A_0}] \times 100\% \quad (1)$$

In the formula, the absorbance of the mixture of sample and DPPH, sample and ethanol and DPPH, and distilled water were stranded by letters A_1, A_2, and A_0, respectively.

Statistical analysis

All measurements were carried out in triplicate if not otherwise specified. Duncan's test was used to compare mean values at a significance level of $P < 0.05$ in the analysis of the TPA texture data using the SPSS 16.8 statistical analysis system (IBM Co. Ltd., USA). Microsoft Excel was used to summarize the experimental data, and origin 2019b software was used to draw figures.

Results and discussion

Effects of NAs addition amount on the quality of NASNs

The noodles quality of NASNs was evaluated using four indexes: broken rate, iodine blue value, sensory score, and TPA texture characteristics. The broken rate reflects the mechanical attributes of SN. The lower the broken strip rate, the greater the shear resistance and the better the boiling resistance (18). It can be found from Figure 1 that three kinds of NAs had a negligible effect on the broken rate of the NASN when the addition level of NAs was lower than 0.10/100 g. However, the broken rate showed an apparent upward trend when the addition level was increased from 0.15/100 to 0.25/100 g, indicating that the addition of NAs caused the internal polymerization force in SNs to weaken and had an adverse effect on the formation of the three-dimensional network structure of aging starch. Moreover, the broken rate caused by adding lycopene was significantly higher than that of the other two kinds of NASNs. However, the increase in the broken rate caused by adding TP was smaller than the other two, indicating that TP has the highest affinity with starch in the three NAs. Taking the broken rate of <10% as the acceptance standard (19), it can be concluded that the maximum amount of curcumin,

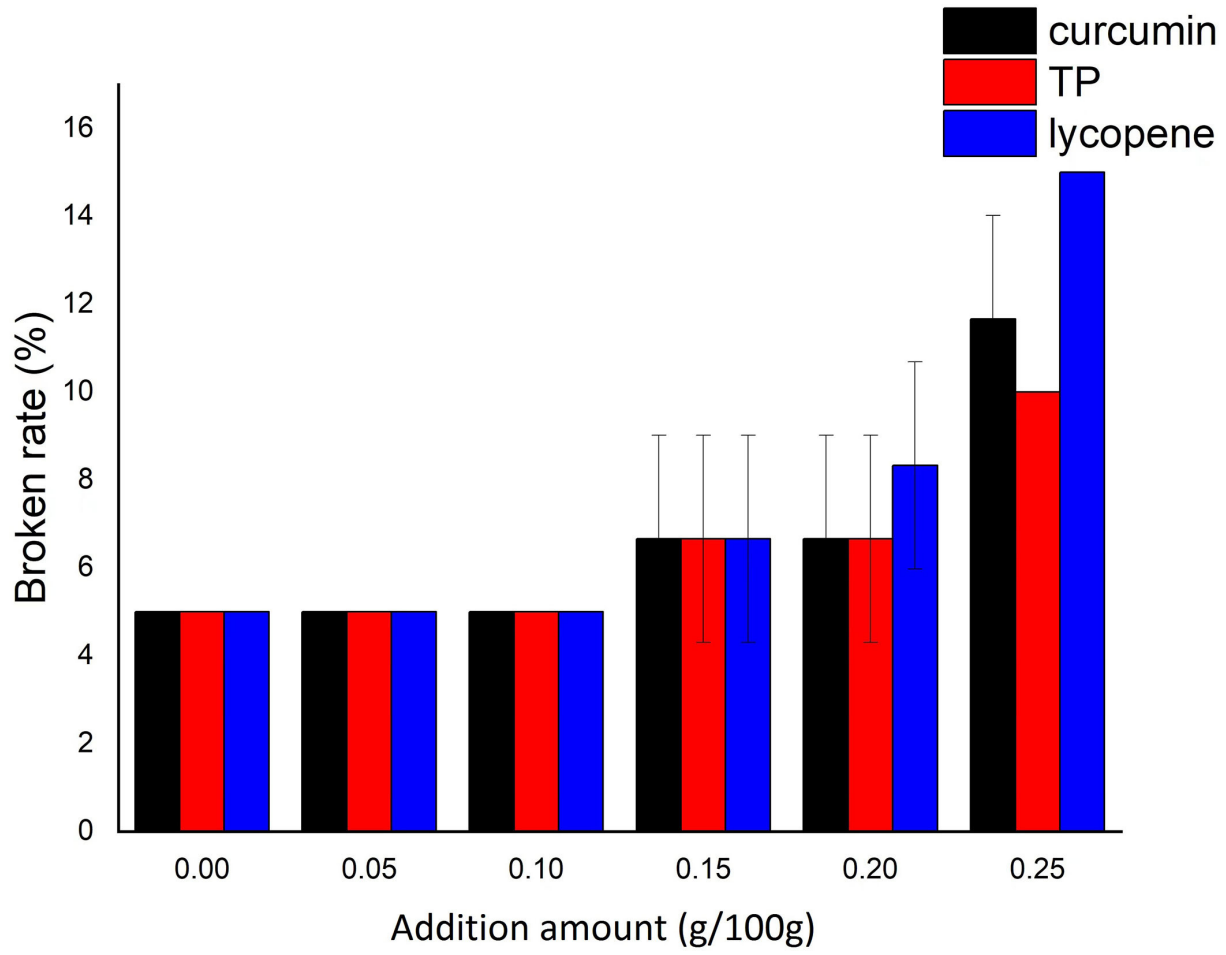

FIGURE 1
Effect of additional amount of NAs on the broken rate of NASNs.

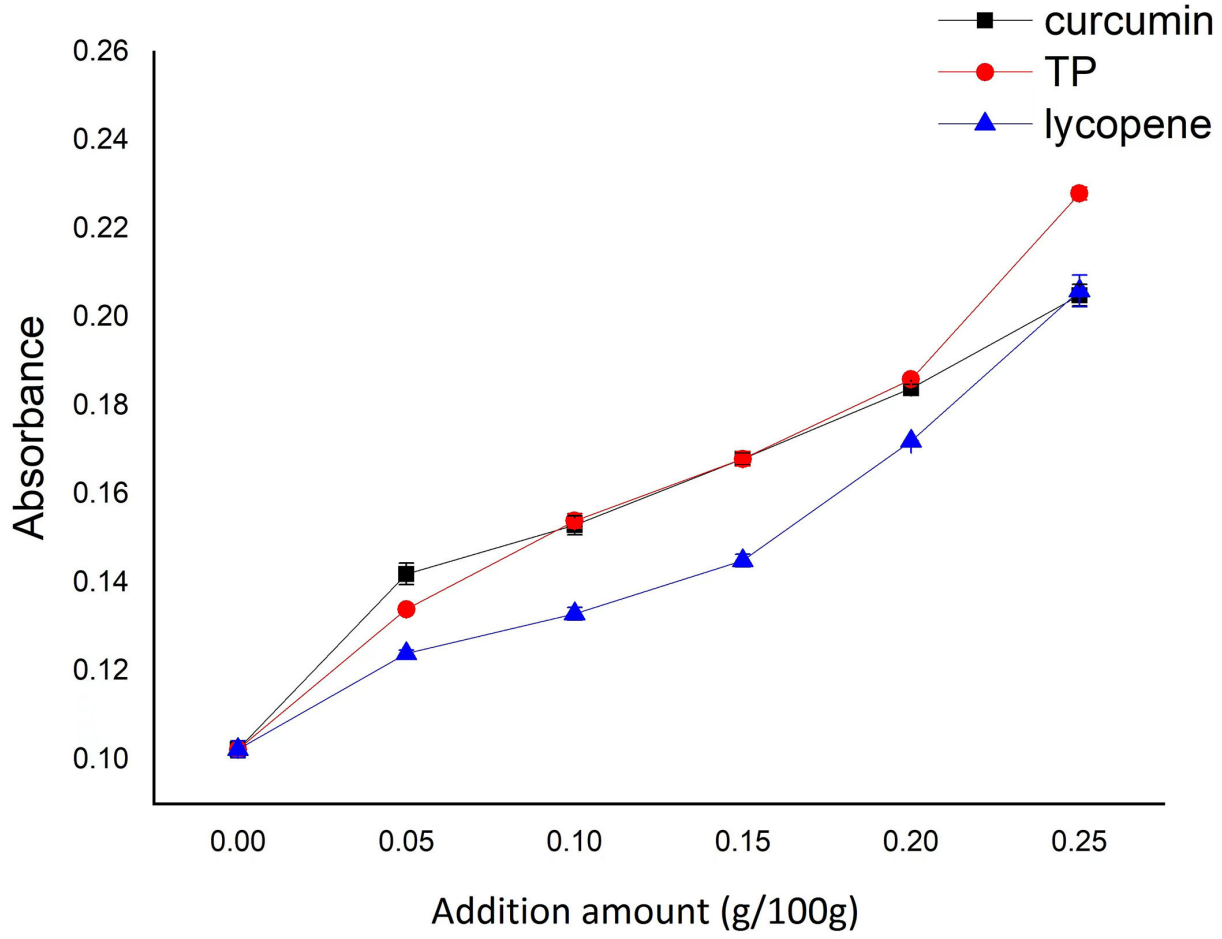

FIGURE 2
Effect of additional amount of NAs on iodine blue value of the soup of boiled NASNs.

TP, and lycopene in NASNs was 0.20/100, 0.25/100, and 0.20/100 g, respectively.

The iodine blue value of the soup mainly indicates the extent of the soup paste rate. The higher the iodine blue value, the greater the soup paste rate (20). As demonstrated in Figure 2, the iodine blue value of the prepared NASNs increased with the addition of NAs. The most likely reason was that the addition of NAs interfered with the binding between starch and starch after the aging process and weakened the strength of the starch noodle, which is opposite to the structural changes caused by the addition of protein to starch noodle (21). The greater the amount of NAs, the higher the degree of interference. Moreover, due to the strong hydrophilicity of TP, it was easier to dissolve than the other two NAs when the noodles were heated and swollen in hot water. This trend will become more obvious with the increase of the additional amount, which demonstrated that the site exposure caused by the loss of more TP made the cross-linking between starch more vulnerable to the water, resulting in the fracture of the starch glycoside bond. The final performance was the increase of the iodine blue value of the soup.

The sensory scores of NASNs increased first and then decreased with the amount of NAs (Figure 3). These trends were consistent in the three kinds of NASNs. Due to the colors of the three NAs, the sensory scores were improved by the three NAs following low addition levels. However, when the addition amount is higher than 0.15/100 g for TP and lycopene or 0.20/100 g for curcumin, the sensory value of NASNs will show a downward trend. According to the experimental results, the optimal addition amounts of curcumin, TP, and lycopene in NASNs were 0.20/100, 0.15/100, and 0.15/100 g, respectively.

As seen in Table 1, adding three NAs can increase the hardness of NASNs. Compared with the other two NAs, lycopene had the highest increase in hardness, while TP had the lowest increase in hardness of NASNs. The chewiness of NASNs also showed a positive correlation with the amount of NAs, which was not associated with the kinds of NAs. Among

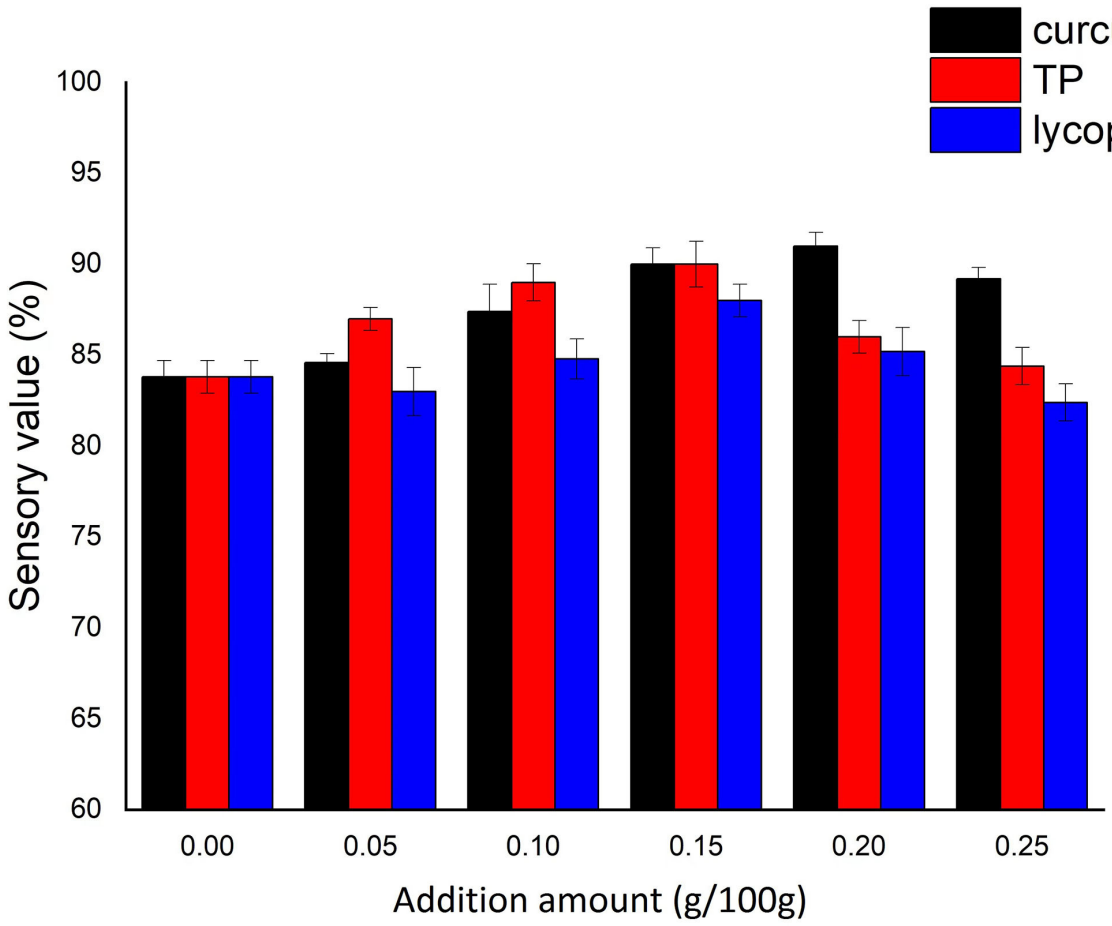

FIGURE 3
Effect of additional amount of NAs on the sensory value of NASNs.

the three NAs tested, the effect of TP on the chewiness of NASNs was significantly higher than that of the other two. However, the effects of adding curcumin and lycopene to FNs were quite different. Curcumin had little impact on the hardness and chewiness of FNs, while lycopene significantly improved their hardness and chewiness. The increase in the amount of NAs can also cause changes in the elasticity of the noodles. Additionally, the changes caused by various kinds of NAs were different. Adding curcumin and lycopene can reduce the elasticity of the SNs, which was similar to other research results in FN (22, 23). However, the changing trend of their elasticity obtained by adding TP was just the opposite, which should be related to the hydrophilicity of the NAs (23). Hydrophilic substances can combine more water in the colloid, increasing three-dimensional space's ability to resist deformation. Furthermore, Zhang et al. found through the tensile test that adding TP to starch-based food effectively improved its mechanical properties (24).

The morphology of NASNs

The microstructures of the SNs prepared by adding different kinds of NAs are shown in Figure 4. The cross-section structure of the SN was compact and smooth and showed a continuous structure similar to a glassy state without any added NAs. Still, more holes in the cross-section appeared when adding NAs, indicating that the continuity of the starch gel was destroyed, and the small bubbles embedded in these holes were easy to spread and escape. Thus, the phenomenon of broken rates and cooking loss was more likely to occur in hot water cooking, which confirmed the results obtained from the analysis of the broken rates test and the iodine blue value test (25). The holes on the cross sections obtained by adding TP were smaller and more uniform than the other two NAs, indicating that water-soluble antioxidants were more likely to fuse with starch gel systems. Although there were some holes in the cross-section of the SNs

10.3389/fnut.2022.1020281

TABLE 1 Effect of addition amount of NAs on texture of NASNs.

Addition amount (g/100 g)	Hardness (N)			Elasticity (mm)			Chewiness		
	Curcumin	TP	Lycopene	Curcumin	TP	Lycopene	Curcumin	TP	Lycopene
0	33.7 ± 1.35^{f}	33.7 ± 1.35^{e}	33.7 ± 1.35^{f}	1.20 ± 0.010^{a}	1.20 ± 0.010^{e}	1.20 ± 0.010^{a}	25.6 ± 1.58^{e}	25.6 ± 1.58^{e}	25.6 ± 1.58^{e}
0.05	36.4 ± 0.38^{e}	37.4 ± 0.25^{d}	39.6 ± 0.50^{e}	1.19 ± 0.060^{a}	1.23 ± 0.010^{d}	1.11 ± 0.011^{b}	27.0 ± 0.92^{d}	29.7 ± 0.48^{d}	27.8 ± 0.61^{d}
0.10	37.5 ± 0.25^{d}	38.4 ± 0.25^{cd}	44.4 ± 0.10^{d}	1.18 ± 0.150^{ab}	1.27 ± 0.006^{c}	1.09 ± 0.006^{c}	28.3 ± 0.43^{cd}	32.2 ± 1.52^{c}	31.2 ± 0.39^{c}
0.15	39.5 ± 0.30^{c}	39.2 ± 0.10^{bc}	46.3 ± 0.29^{c}	1.17 ± 0.050^{b}	1.30 ± 0.006^{b}	1.08 ± 0.006^{c}	29.5 ± 0.99^{bc}	34.3 ± 1.09^{b}	32.0 ± 0.55^{bc}
0.20	42.0 ± 0.69^{b}	39.7 ± 0.15^{b}	51.1 ± 0.73^{b}	1.14 ± 0.010^{c}	1.33 ± 0.010^{a}	1.06 ± 0.006^{d}	30.8 ± 0.42^{b}	35.3 ± 1.20^{b}	34.4 ± 1.56^{a}
0.25	47.8 ± 0.40^{a}	41.9 ± 0.66^{a}	54.3 ± 0.10^{a}	1.11 ± 0.150^{d}	1.33 ± 0.011^{a}	1.00 ± 0.010^{e}	33.8 ± 0.26^{a}	38.9 ± 0.61^{a}	33.3 ± 1.24^{ab}

Note: The letters a–f indicate significant difference between the same column ($P < 0.05$), and the same letter represents no significant difference.

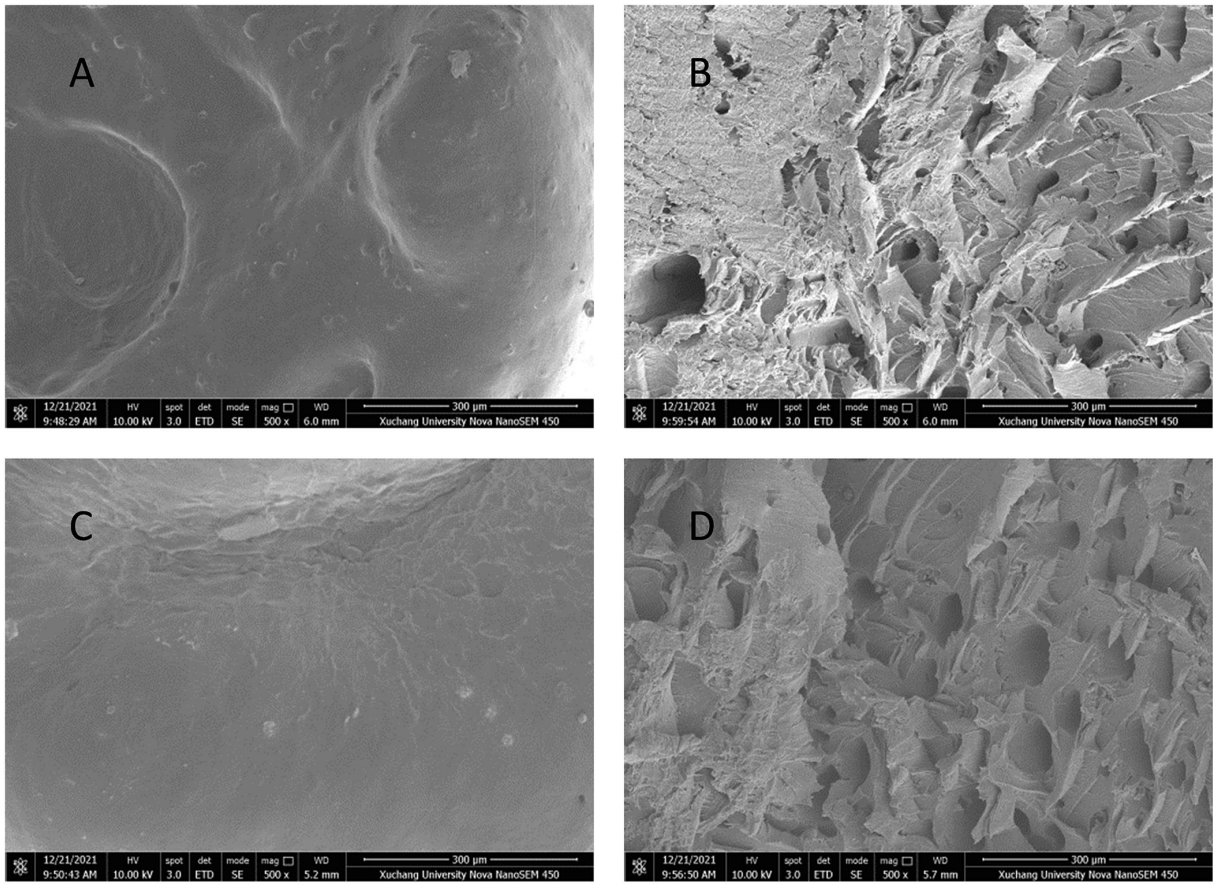

FIGURE 4
Micro-images of the cross-section of starch noodles containing no antioxidant **(A)**, 0.20/100 g of curcumin **(B)**, 0.15/100 g of TP **(C)**, and lycopene **(D)**, respectively.

added with curcumin and lycopene, their continuous network structures formed by starch gel still existed and maintained the integrity and basic mechanical properties of SNs to some extent. Specifically, with the addition of TP, the cross-sectional characteristic of SN was almost close to those of blank samples.

X-ray characteristics

In the later stage of the production process of SNs, there was a cooling and aging process, which easily enabled the crystallization of starch, and the subsequent drying process would further increase its crystallinity (25). X-ray diffractograms

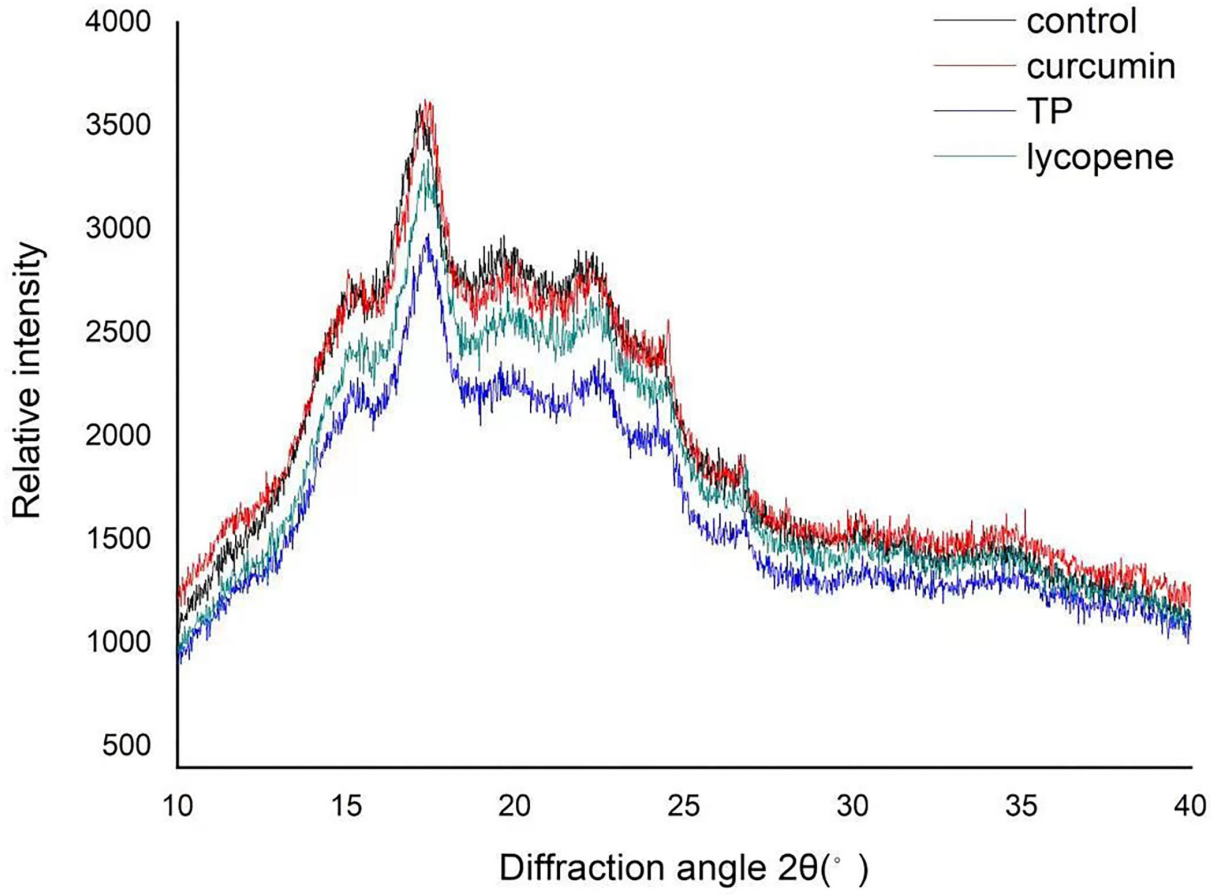

FIGURE 5
X-ray diffractogram of NASNs contained curcumin (red), TP (blue), lycopene (green), and SN without NAs (blank).

of the SNs with the three kinds of NAs and control samples are presented in Figure 5. Three NASN samples showed peaks at the 2θ diffraction angles around 15, 17, 20, 23, and 26. The diffraction peaks at the 2θ diffraction angles around 15, 17, 20, and 23 are typical SPS crystals. The relative intensity of the diffraction peaks at 15 and 23 was significantly weakened. Still, peaks at 26 were not found in the SPS in previous studies, which showed that some kinds of crystal forms were extensively damaged, and some new forms occurred in the process (26). The most apparent diffraction peak at the 2θ diffraction angles was around 17, which indicated that a lower content of branched amylose and a higher content of amylopectin was contained in the four kinds of SNs (27, 28). Interestingly the samples added with curcumin showed pronounced diffraction peaks at the 2θ diffraction angles around 12, while the samples added with TP and lycopene showed prominent shoulder diffraction peaks. These diffraction peaks were not seen in the SNs without NAs, which demonstrated that the addition of these NAs affected the crystallization process of starch and produced a small proportion of new crystals in the NASNs.

Retention rate changing of curcumin, TP, and lycopene

Three kinds of NASNs containing curcumin, TP, and lycopene were stored under both DRTS and WFS conditions for 60 days, and the natural antioxidant flour noodles (control group) were treated similarly. It was found that the retention rate trends of the three NAs in the NASNs and control group were similar, but the changing range differed (Figure 6). After 60 days of dry storage, the content retention rates of curcumin, TP, and lycopene were 69.54, 60.73, and 61.48%, respectively, which were significantly higher than those in the control group

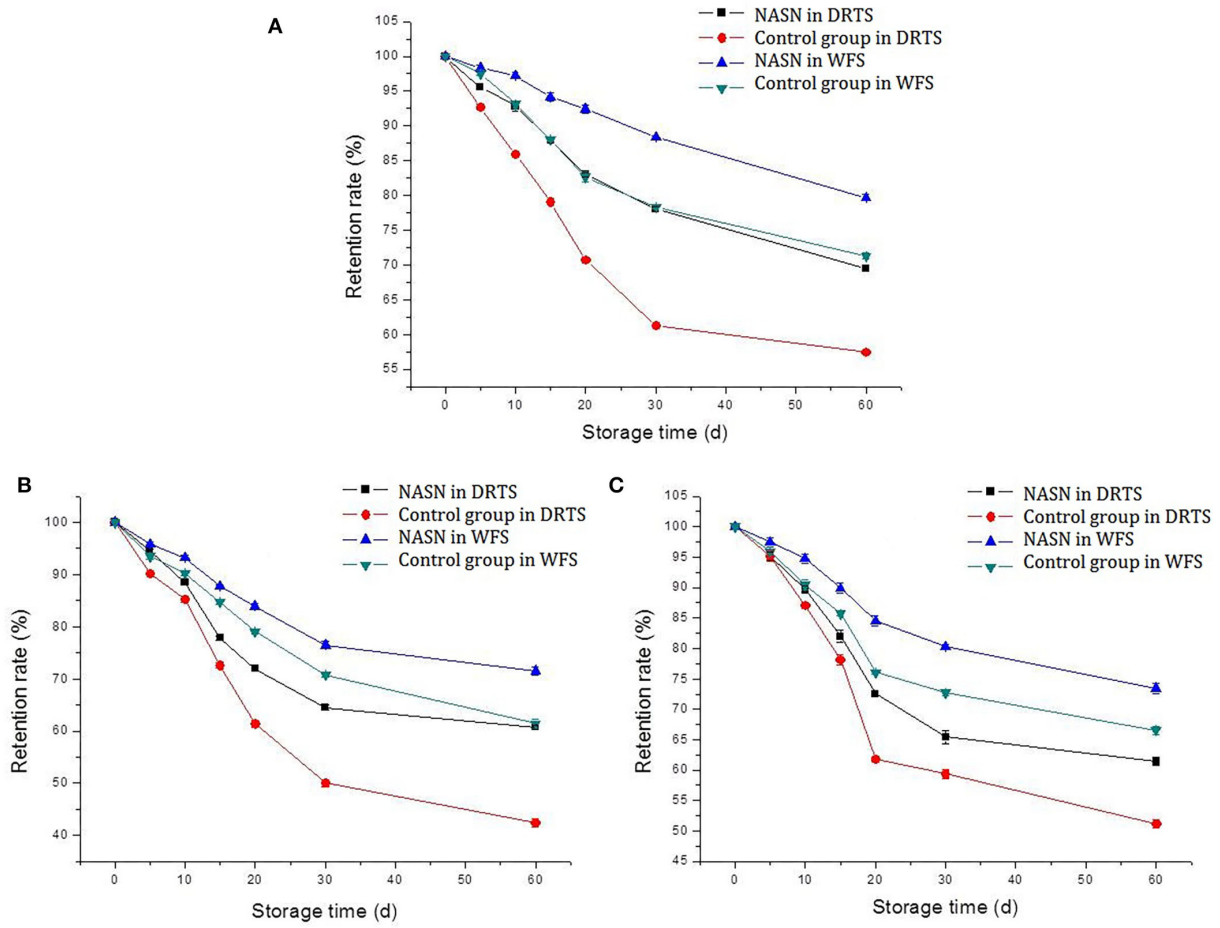

FIGURE 6
Retention rate changing of curcumin **(A)**, TP **(B)**, and lycopene **(C)** in NASNs and the control group in the condition of DRTS and WFS.

(57.45, 42.38, and 51.16%, respectively). Iqbal et al. (29) found that the retention rate of NAs, such as ascorbic acid, polyphenols, and carotenoids in dry, hot peppers, was between 77.4 and 87.3% after being packaged in natural jute or synthetic LDPE plastic bags and stored at ambient temperature for 5 months. Combined with the experimental results of this study, it showed that SNs could act as a protective package to protect NAs during storage to reduce the adverse effects of light or oxygen. The content retention rates of TP, curcumin, and lycopene in NASNs stored under WFS were 79.72, 71.54, and 73.43%, which were significantly higher than those in the control group (71.24, 61.40, and 66.57%, respectively). Addie A. Van der Sluis et al. (30) found that polyphenols and their antioxidant activity were relatively stable at low temperatures. The retention rates of the three studied NAs decreased rapidly when the storage time was <30 days, while the downward trends gradually flattened within 30–60 days. In contrast, the retention rates of the three NAs in the NASNs were significantly higher, and the decline rate was also slower than that in the control group both in the DRTS condition and WFS condition, indicating the protective ability of SN on NAs was stronger than that of FNs. The main reason was that the starch formed a concentrated elastic gel after high-temperature gelatinization and low-temperature aging (25). During drying, most of the moisture in the starch gel was removed, which promoted the retrogradation of starch and stabilized the product structure, thus forming a denser protective layer for NAs (31). But the starch content in flour was only about 60%, and there was no high-temperature gelatinization and low-temperature aging process of starch in the production process of FNs.

The free radical scavenging rate

After adding natural antioxidants to the noodles, the free radical scavenging rate by the DPPH method sharply

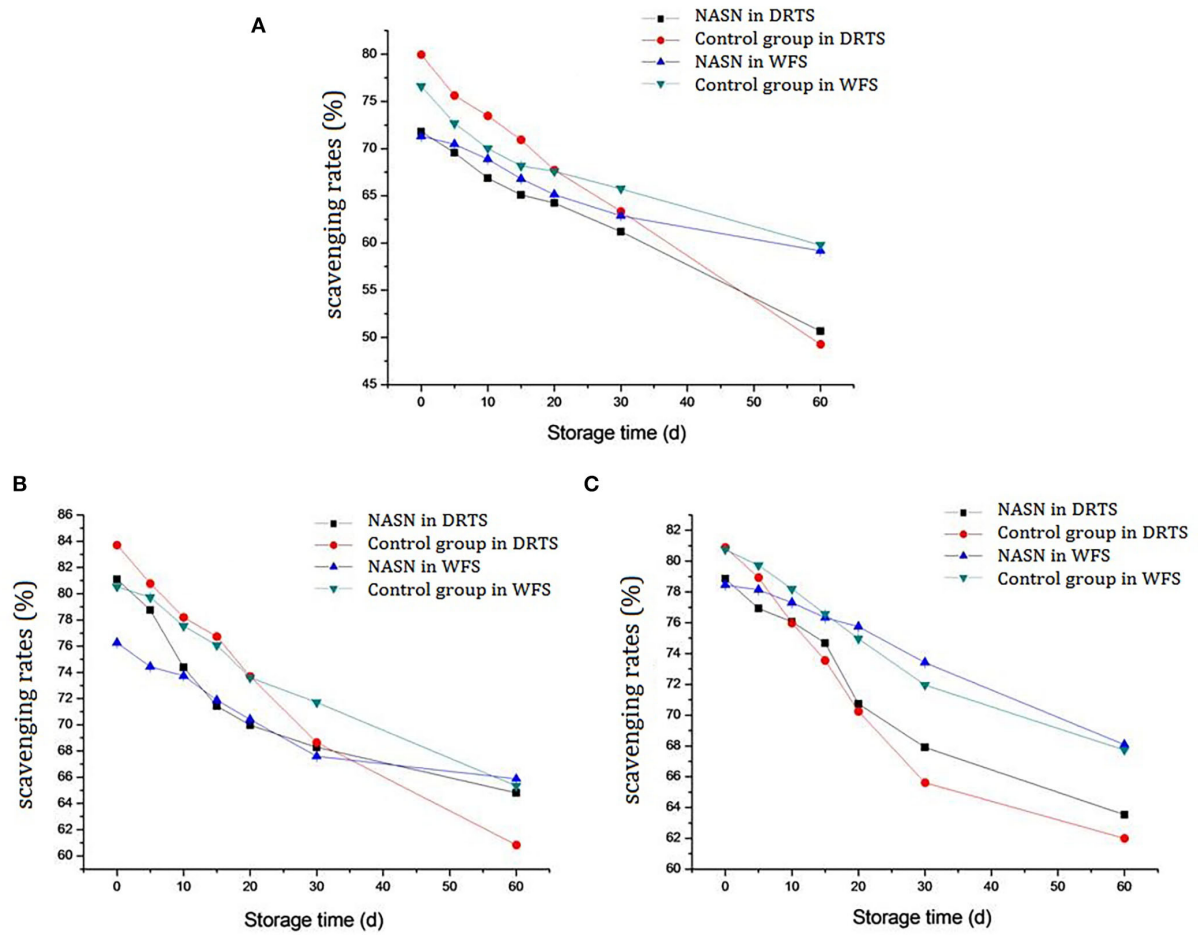

FIGURE 7
Free radical scavenging rate changing of curcumin **(A)**, TP **(B)**, and lycopene **(C)** in NASNs and the control group in the condition of DRTS and WFS.

increased (32). After 60 days of storage, the free radical scavenging rates of curcumin, TP, and lycopene in NASNs under DRTS conditions decreased by 21.12, 16.29, and 15.35%, respectively, which was significantly lower than that in the control group (30.24, 22.87, and 18.92%). Additionally, while under WFS conditions, they decreased by 12.14, 10.38, and 10.38%, respectively, which was also significantly lower than that of the control group (16.82, 15.19, and 13.02%) (Figure 7), indicating that the protective effect of SNs on the antioxidant activity of NAs was better than that of FNs. Although studies have shown that oil as a substrate can protect the activity of antioxidants, it is not enough to play this protective role because the oil content in FN was too low (<1%) (33). In addition, the heating procedure in the processing of NASNs was also conducive to maintaining the antioxidant function of the NAs during storage (34). Moreover, it could be seen intuitively from the figure that the free radical scavenging rates of NAs (red line with circle mark) decreased most significantly under DRTS conditions. In contrast, the downward trend of the same substances under WFT conditions (green line with triangle mark) was considerably alleviated, demonstrating that lower ambient temperatures positively affected the maintenance of antioxidant function.

Conclusion

The effects of three kinds of NAs such as curcumin, TP, and lycopene, on sweet potato starch's structure and physicochemical properties of noodles were studied. Our results demonstrated that adding NAs changed the broken rate, iodine blue value, and elasticity. However, the sensory quality, nutrition, and antioxidant function of NASN were improved if the curcumin, TP, and lycopene were 0.20/100, 0.15/100 g, and 0.15/100 g,

respectively. Moreover, SN was more conducive to maintaining NAs and their functional activities. Therefore, these findings indicate that NAs have good application values in SNs.

Data availability statement

The original contributions presented in the study are included in the article/supplementary material, further inquiries can be directed to the corresponding author/s.

Author contributions

The planning of the research was done by WG, XG, and JH. The experiments were performed by LF, YW, GL, and ZC. All the writers have contributed in the research work and the write-up of this article. All authors contributed to the article and approved the submitted version.

Funding

We acknowledge the funding support from the Major Science and Technology Projects in Henan Province, China (ID No. 201300110300), Key Scientific Research Projects of Universities in Henan Province (ID No. 22B550017), and the Training Program for Young Backbone Teachers in Colleges and Universities in Henan Province, China (ID No. 2019GGJS216).

Acknowledgments

The authors thank AiMi Academic Services (www.aimieditor.com) for English language editing and review services.

Conflict of interest

The authors declare that the research was conducted in the absence of any commercial or financial relationships that could be construed as a potential conflict of interest.

Publisher's note

References

1. Bovell-Benjamin AC. *Sweet Potato Utilization in Human Health, Industry and Animal Feed Systems. Sweet Potato: Post Harvest Aspects in Food, Feed and Industry*. New York: Nova Science Publishers Inc. (2010). p. 193–224.

2. Menon R, Padmaja G, Jyothi AN, Asha V, Sajeev MS. Gluten-free starch noodles from sweet potato with reduced starch digestibility and enhanced protein content. *J Food Sci Technol.* (2016) 53:3532–42. doi: 10.1007/s13197-016-2330-9

3. Tan HZ, Li ZG, Tan B. Starch noodles: history, classification, materials, processing, structure, nutrition, quality evaluating and improving. *Food Res Int.* (2009) 42:551–76. doi: 10.1016/j.foodres.2009.02.015

4. Ariani D, Herawati ERN, Nastiti A, Angwar M, Pranoto Y. Effect of additional suji leaves and turmeric extract on physicochemical characteristic and antioxidant activity of arenga-canna noodle. *IOP Conf Ser Earth Environ Sci.* (2017) 101:012017. doi: 10.1088/1755-1315/101/1/012017

5. Menon R, Padmaja G, Sajeev MS. Cooking behavior and starch digestibility of NUTRIOSE®(resistant starch) enriched noodles from sweet potato flour and starch. *Food Chem.* (2015) 182:217–23. doi: 10.1016/j.foodchem.2015.02.148

6. Chaleshtori RS, Chaleshtori FS, Rafieian M. Biological characterization of Iranian walnut (Juglans regia) leaves. *Turkish J Biol.* (2011) 35:635–9. doi: 10.3906/biy-1005-1

7. Bahmani M, Vakili Saatloo N, Maghsoudi R, Momtaz H, Saki K, Kazemi-Ghoshchi B, et al. A comparative study on the effect of ethanol extract of wild Scrophularia deserti and streptomycin on *Brucellla melitensis*. *J HerbMed Pharmacol.* (2013) 2:17–20.

8. Gao S, Duan X, Wang X, Dong D, Liu D, Li X, et al. Curcumin attenuates arsenic-induced hepatic injuries and oxidative stress in experimental mice through activation of Nrf2 pathway, promotion of arsenic methylation and urinary excretion. *Food Chem Toxicol.* (2013) 59:739–47. doi: 10.1016/j.fct.2013.07.032

9. Lan X, Liu Y, Wang Y, Tian F, Miao X, Wang H, et al. Coaxial electrospun PVA/PCL nanofibers with dual release of tea polyphenols and ε-poly (L-lysine) as antioxidant and antibacterial wound dressing materials. *Int J Pharm.* (2021) 601:120525. doi: 10.1016/j.ijpharm.2021.120525

10. Clinton SK. Lycopene: chemistry, biology, and implications for human health and disease. *Nutr Rev.* (1998) 56:35–51. doi: 10.1111/j.1753-4887.1998.tb01691.x

11. Tamadon MR, Baradaran A, Rafieian-Kopaei M. Antioxidant and kidney protection; differential impacts of single and whole natural antioxidants. *J Renal Injury Prevent.* (2013) 3:41–2. doi: 10.12861/jrip.2014.14

12. Tongdeesoontorn W, Mauer LJ, Wongruong S, Sriburi P, Reungsang A, Rachtanapun P. Antioxidant films from cassava starch/gelatin biocomposite fortified with quercetin and TBHQ and their applications in food models. *Polymers.* (2021) 13:1117. doi: 10.3390/polym13071117

13. Li Y, Xiao J, Tu J, Yu L, Niu L. Matcha-fortified rice noodles: Characteristics of *in vitro* starch digestibility, antioxidant and eating quality. *LWT.* (2021) 149:111852. doi: 10.1016/j.lwt.2021.111852

14. Jung NR, Lee EJ, Jin SY. Antioxidant activities and quality characteristics of rice noodle added with *Cedrela sinensis* powder. *J East Asian Soc Dietary Life.* (2015) 25:153–61. doi: 10.17495/easdl.2015.2.25.1.153

15. Vijaykrishnaraj M, Bharath Kumar S, Prabhasankar P. Green mussel (*Perna canaliculus*) as a marine ingredient to enrich gluten free pasta: product quality, microstructure and biofunctional evaluation. *J Food Measure Characteriz.* (2015) 9:76–85. doi: 10.1007/s11694-014-9212-5

16. Indrianti NN, Sholichah E, Afifah N. Pumpkin flour effects on antioxidant activity, texture, and sensory attributes of flat tubers noodle. *IOP Conf Ser Mater Sci Eng.* (2021) 1011:012007. doi: 10.1088/1757-899X/1011/1/012007

17. Jeon SY, Kim AJ, Rho JO. A study on the physicochemical activities of Dangmyon (starch vermicelli) added with mulberry leaves powder. *Korean J Hum Ecol.* (2015) 24:713–23. doi: 10.5934/kjhe.2015.24.5.713

18. Zeng J, Jiang J, Gao H, Meng K, Song M, Li G. Optimization of the aging process for potato vermicelli without additives and quality changes during storage. *Shipin Kexue/Food Sci.* (2019) 40:283–9.

19. Commission CNS. *Vermicelli*. China Standards Press: Beijing (2009).

20. Li G, Tan S, Ma G. Processing and quality evaluation of Yinjiang natural sweet potato starch noodles. *Cereals Oils*. (2014) 8:25–28. doi: 10.3969/j.issn.1008-9578.2014.08.007

21. Jyotsna R, Prabhasankar P, Indrani D, Rao GV. Effect of additives on the quality and microstructure of vermicelli made from *Triticum aestivum*. *Eur Food Res Technol.* (2004) 218:557–62. doi: 10.1007/s00217-004-0887-4

22. Wang Z, Jia Y, Zhang M. Effect of curcumin on the quality properties of millet fresh noodle and its inhibitory mechanism against the isolated spoilage bacteria. *Food Sci Nutr.* (2020) 8:1451–60. doi: 10.1002/fsn3.1427

23. Nochai K, Pongjanta J. Physicochemical properties of dried noodle with tomato lycopene supplement. *RMUTP Res J.* (2013) 1:211–21.

24. Zhang D, Chen L, Cai J, Dong Q, Din ZU, Hu ZZ, et al. Starch/tea polyphenols nanofibrous films for food packaging application: from facile construction to enhance mechanical, antioxidant and hydrophobic properties. *Food Chem.* (2021) 360:129922. doi: 10.1016/j.foodchem.2021.129922

25. Xiang Z, Ye F, Zhou Y, Wang L, Zhao G. Performance and mechanism of an innovative humidity-controlled hot-air drying method for concentrated starch gels: a case of sweet potato starch noodles. *Food Chem.* (2018) 269:193–201. doi: 10.1016/j.foodchem.2018.06.153

26. Babu AS, Parimalavalli R, Jagannadham K, Rao JS. Chemical and structural properties of sweet potato starch treated with organic and inorganic acid. *J Food Sci Technol.* (2015) 52:5745–53. doi: 10.1007/s13197-014-1650-x

27. Mestres C, Colonna P, Buléon A. Characteristics of starch networks within rice flour noodles and mungbean starch vermicelli. *J Food Sci.* (1988) 53:1809–12. doi: 10.1111/j.1365-2621.1988.tb07848.x

28. Li B, Cheng Y, Qin C, Liu J, Ren T, Huang K, et al. Effects of different drying methods on the retrogradation property of convenience acorn vermicelli. *Sci Technol Food Ind.* (2016).

29. Iqbal Q, Amjad M, Asi MR, Ariño A, Ziaf K, Nawaz A, et al. Stability of Capsaicinoids and antioxidants in dry hot peppers under different packaging and storage temperatures. *Foods.* (2015) 4:51–64. doi: 10.3390/foods4020051

30. Van der Sluis AA, Dekker M, van Boekel MA. Activity and concentration of polyphenolic antioxidants in apple juice. 3 Stability during storage. *J Agric Food Chem.* (2005) 53:1073–80. doi: 10.1021/jf040270r

31. Padalino L, Caliandro R, Chita G, Conte A, Del Nobile MA. Study of drying process on starch structural properties and their effect on semolina pasta sensory quality. *Carbohydrate Polymers*. (2016) 153:229–35. doi: 10.1016/j.carbpol.2016.07.102

32. La J, Kim MJ, Lee J. Evaluation of solvent effects on the DPPH reactivity for determining the antioxidant activity in oil matrix. *Food Sci Biotechnol.* (2021) 30:367–75. doi: 10.1007/s10068-020-00874-9

33. Yang L, Gu J, Luan T, Qiao X, Cao Y, Xue C, et al. Influence of oil matrixes on stability, antioxidant activity, bioaccessibility and bioavailability of astaxanthin ester. *J Sci Food Agric.* (2021) 101:1609–17. doi: 10.1002/jsfa.10780

34. Tuersuntuoheti T, Wang Z, Duan M, Asimi S, Ren X, Wang Z, et al. Noodle processing, storage time and cooking affect the antioxidant activities and phenolic compounds content of Qingke barley noodles. *Int J Food Sci Technol.* (2020) 55:2730–9. doi: 10.1111/ijfs.14526

frontiers | Frontiers in Nutrition

TYPE Original Research
PUBLISHED 03 November 2022
DOI 10.3389/fnut.2022.1046061

OPEN ACCESS

EDITED BY
Sen Ma,
Henan University of Technology, China

REVIEWED BY
Jinhu Tian,
Zhejiang University, China
Hongyan Li,
Beijing Technology and Business University, China

*CORRESPONDENCE
Haiyan Wei
hywei@yzu.edu.cn

SPECIALTY SECTION
This article was submitted to Food Chemistry, a section of the journal Frontiers in Nutrition

RECEIVED 16 September 2022
ACCEPTED 17 October 2022
PUBLISHED 03 November 2022

CITATION
Liu G, Wang R, Liu S, Xu M, Guo L, Zhang H and Wei H (2022) Relationship between starch fine structure and simulated oral processing of cooked *japonica* rice. *Front. Nutr.* 9:1046061. doi: 10.3389/fnut.2022.1046061

Relationship between starch fine structure and simulated oral processing of cooked *japonica* rice

Guodong Liu[1,2,3], Ruizhi Wang[1,2,3], Shaoqiang Liu[1,2,3], Man Xu[1,2,3], Lunan Guo[4], Hongcheng Zhang[1,2,3] and Haiyan Wei[1,2,3]*

[1]Jiangsu Co-Innovation Center for Modern Production Technology of Grain Crops, Yangzhou University, Yangzhou, China, [2]Jiangsu Key Laboratory of Crop Genetics and Physiology/Jiangsu Key Laboratory of Crop Cultivation and Physiology, Agricultural College of Yangzhou University, Yangzhou, China, [3]Research Institute of Rice Industrial Engineering Technology of Yangzhou University, Yangzhou, China, [4]School of Food Science and Engineering, Yangzhou University, Yangzhou, China

Background: Simulated oral processing can be used to evaluate the palatability of cooked rice. Previously, we established a simulated oral processing method using a texture analyzer equipped with a multiple extrusion cell probe (TA/MEC). However, the relationship between oral processing and starch fine structure remains unknown.

Methods: In this study, we analyzed the oral processing properties using TA/MEC and characterized the starch fine structure of *japonica* rice by size-exclusion chromatography (SEC) and fluorophore-assisted capillary electrophoresis (FACE). The relationship between starch fine structure and oral processing of cooked *japonica* rice was further investigated.

Results: Cooked rice structure contains fast-breakdown (Type I structure), slow-breakdown (Type II structure) and unbreakable structures (Type III structure). Fast-breakdown and slow-breakdown structure were positively correlated with the content of amylose and shorter amylopectin branches. The content of longer amylopectin branches was positively correlated with the contribution of unbreakable structure.

Conclusion: The results indicated that cooked *japonica* rice varieties with more amylose and shorter amylopectin branches tend to form a harder texture and need more work to break down the fast and slow breakdown structures related to rice kernel fragmentation. Meanwhile, cooked *japonica* rice varieties possess stronger molecular entanglements due to their longer amylopectin branches and contribute more to the breakdown of unbreakable structures. These results can guide breeders to select rice varieties with desirable eating qualities for cultivation.

KEYWORDS

***japonica* rice, oral processing, starch fine structure, eating quality, palatability**

Introduction

Rice is a key staple food for human beings and its yield has greatly increased owing to the combination of rice breeding and cultivation technology. However, rice quality, especially eating quality, needs further improvement. The primary consideration of rice customers has shifted from grain yield to grain palatability (1). Theoretically, the palatability of rice can be evaluated by amylose content, gel consistency, and gelatinization, which significantly correlate with the texture formation of cooked rice (2, 3). Researchers usually evaluate the palatability of cooked rice by a human sensory test, but this method is time-consuming and subjective (4, 5).

Oral processing properties, like the force and work during the first bite, chewing, and swallowing, is a crucial procedure for the consumption and palatability of foods (6, 7). Rice is primarily consumed in the form of polished white rice which possesses a whole-grain structure (8), and its oral processing property plays an essential role in consumer acceptability (9, 10). However, the relationship between oral processing and palatability of cooked rice has not been adequately investigated.

Our previous work established a simulated oral processing method by monitoring changes in force and work during mastication using a texture analyzer equipped with a multiple extrusion cell probe (TA/MEC) (11). We found that this method can be used to evaluate the mouthfeel and palatability of cooked rice during mastication (12, 13). In this method, the structure of cooked rice is divided into three types: fast breakdown structure (defined as Type I structure), slow breakdown structure (defined as Type II structure), and unbreakable structure (defined as Type III structure). Based on previous research, the Type I structure is related to the fragmentation of rice kernel, the Type III structure represents a structure that cannot be broken even after much mastication, while the Type II structure lies between these which is related to the fragmentation of rice kernel and the enzymatic degradation of rice matrix (11). The work and proportion of these structures can be used to evaluate rice palatability (11).

Starch consists of two polymers, namely linear amylose and branched amylopectin. Besides, starch is the most abundant component in rice grains. Thus, the structure and content of starch is closely related to the palatability of cooked rice (14). Previous research has confirmed that the texture of cooked rice closely relate to the fine structure of starch, which include the content of amylose, degree of polymerization (DP), and side chain length of amylopectin (15–17). However, the relationship between the oral processing of cooked rice and starch fine structure is still unknown. Thus, this study chose different *japonica* rice varieties as materials and established the relationship between their oral processing properties and starch fine structure. This study can assist researchers in improving rice palatability by using a simulated oral processing method and choosing rice varieties with certain starch fine structures.

Abbreviations: SEC, size-exclusion chromatography; FACE, fluorophore-assisted capillary electrophoresis; Mw, molecular weight; CLD, chain length distributions; DP, degree of polymerization; C_{Am}, amylose content; Ap, amylopectin; TA/MEC, a texture analyzer equipped with a multiple extrusion cell probe; Type I structure, fast breakdown structure; Type II structure, slow breakdown structure; Type III structure, unbreakable structure.

Materials and methods

Materials

Twelve *japonica* rice varieties were chosen and planted at Shatou town research farm (Yangzhou city, Jiangsu province, China, 32°32′ N, 119°49′ E) from May to November 2019. All rice varieties were planted under the same cultivation conditions for high yield and quality and milled using Xiba LTJM-2099 rice-milling machine (Zhejiang Boliheng Corporation, China). Protease (≥3.5 units/mg solid) and isoamylase (≥10,000,000 units/mg protein) were purchased from Sigma-Aldrich Chemical Co. (St. Louis, MO, USA). Pullulan standards (molecular weight: (Mw) 180 Da ∼ 1.2×10^6 Da) were purchased from Polymer Standards Service (PSS, Mainz, Germany). Simulated saliva (pH 6.8) and low-temperature α-amylase (2,000 U/g solid) were purchased from Ke Lei Biological Technology Co., Ltd. (Shanghai, China) and Shanghai Yuanye Bio-Technology Co., Ltd. (Shanghai, China), respectively. All other chemicals used in this study were of reagent grade.

Size-exclusion chromatography

The molecular size distributions of whole branched starch (R_h, nm) and debranched starch (Mw, Da) were analyzed using an LC-20AD (Shimadzu, Kyoto, Japan) size-exclusion chromatography (SEC) system equiped with a RID-10A detector, according to the method described by Gilbert (16, 18, 19). Starch was isolated from rice kernels using protease to cleave proteins and anhydrous ethanol to remove lipids. The starch was debranched using isoamylase in order to analyze the chains. All the starch samples (2 mg/mL) were dissolved in DMSO/LiBr solution (0.5%, w/w). Whole starch molecules were separated using a combination of GRAM pre-column, GRAM 30, and GRAM 3000 analytical columns (PSS), while starch chains were separated using a combination of GRAM pre-column, GRAM 100, and GRAM 1000 analytical columns (PSS). The mobile phase was DMSO/LiBr solution (0.5%, w/w) with an elution rate of 0.3 and 0.6 mL/min for branched and debranched starches, respectively. The column oven temperature was maintained at 80 °C. Pullulan standards (PSS) with different Mw(180 Da ∼ 1.2×10^6 Da) were used for calibration and calculation. The data were analyzed using XPS

Peak Fit software v. 4.1. After peak fitting, the SEC data were calculated to characterize the molecular size distributions of the branched and debranched starch samples.

Fluorophore-assisted capillary electrophoresis

The chain length distributions (CLD) of amylopectin were analyzed according to the method described by Gilbert (20). Amylopectin in the starches was firstly debranched using isoamylase, then labeled with 8-aminopyrene-1,3,6-trisulfonic acid. After that, the samples was analyzed using a PA-800 Plus fluorophore-assisted capillary electrophoresis (FACE) system (Beckman Coulter, Brea, CA, USA) with a solid-state laser-induced fluorescence detector and an argon-ion laser as the excitation source.

Simulated oral processing

The oral processing properties of the cooked rice were measured according to a previous method (11). Milled rice was cooked at a rice/water ratio of 1:1.3 using a rice cooker. The oral processing properties of the cooked rice were measured using a TA.XTplus TA/MEC (Stable Micro System, Surrey, UK). Briefly, cooked rice (30 g) together with simulated saliva (3.6 mL, pH6.8) and low-temperature α-amylase (0.01 g, ezyme activity: 2000 U/g solid) was added to the MEC probe according to the in situ oral processing of human subjects (11). Cyclic compression was conducted 25 times to destroy the structure of the rice kernels. The extrusion distance was set to 93 mm, and both the test and post-test speeds were set as 5 mm/s. The work during each chewing cycle was calculated according to the force versus distance curves and analyzed by fitting to the double-exponential decay function (Eq. (1)):

$$w_n = w_\infty + w_1 e^{(-\frac{n}{n_1})} + w_2 e^{(-\frac{n}{n_2})} \quad (1)$$

where w_n is the work during each compression cycle (n), w_1 and w_2 are the contributions to the loss of energies per cycle with a decay rate given by n_1 and n_2, respectively. Besides, w_∞ is the work per cycle even after an infinite number of compression cycles.

In this method, w_n can be divided into three parts: $w_{Type\ I}$, $w_{Type\ II}$, and $w_{Type\ III}$, which represent the work per cycle to break down Type I (Eq. (2)), Type II (Eq. (3)), and Type III (Eq. (4)) structures, respectively. In addition, the fractions of $w_{Type\ I}$ ($f_{Type\ I}$), $w_{Type\ II}$ ($f_{Type\ II}$), and $w_{Type\ III}$ ($f_{Type\ III}$) during each compression cycle can be calculated according to Eqs. (5), (6), and (7).

$$w_{Type\,I} = w_1 e^{(-\frac{n}{n_1})} \quad (2)$$

$$w_{Type\,II} = w_2 e^{(-\frac{n}{n_2})} \quad (3)$$

$$w_{Type\,III} = w_\infty \quad (4)$$

$$f_{Type\,I}\,(\%) = \frac{100 w_{Type\,I}}{w_n} \quad (5)$$

$$f_{Type\,II}\,(\%) = \frac{100 w_{Type\,II}}{w_n} \quad (6)$$

$$f_{Type\,III}\,(\%) = \frac{100 w_{Type\,III}}{w_n} \quad (7)$$

During the whole oral processing, the total work to break down Type I ($W_{Type\ I}$), Type II ($W_{Type\ II}$), and Type III ($W_{Type\ III}$) structures were calculated according to Eq. (8), Eq. (9) and Eq. (10) and their corresponding fractions ($F_{Type\ I}$, $F_{Type\ II}$, $F_{Type\ III}$) were calculated according to Eq. (11), Eq. (12) and Eq. (13), respectively.

$$W_{Type\,I} = \sum_{i=1}^{50} w_1 e^{(-\frac{i}{n_1})} \quad (8)$$

$$W_{Type\,II} = \sum_{i=1}^{50} w_2 e^{(-\frac{i}{n_2})} \quad (9)$$

$$W_{Type\,III} = \sum_{i=1}^{50} w_\infty \quad (10)$$

$$F_{Type\,I}\,(\%) = \frac{100 W_{Type\,I}}{W_{Type\,I} + W_{Type\,II} + W_{Type\,III}} \quad (11)$$

$$F_{Type\,II}\,(\%) = \frac{100 W_{Type\,II}}{W_{Type\,I} + W_{Type\,II} + W_{Type\,III}} \quad (12)$$

$$F_{Type\,III}\,(\%) = \frac{100 W_{Type\,III}}{W_{Type\,I} + W_{Type\,II} + W_{Type\,III}} \quad (13)$$

Statistical analyses

Correlations between the starch fine structure ans the oral processing properties of cooked rice were analyzed using IBM SPSS® AmosTM 19 (SPSS Inc., Chicago, IL, USA). Both Pearson and Spearman rank correlations were analyzed at $p < 0.05$ and $p < 0.01$ for significant and quite significant correlations, respectively.

Results and discussion

Starch fine structure of *japonica* rice

Molecular size distributions of branched and debranched starches

The molecular size distributions of branched starches extracted from different *japonica* rice varieties are shown in Figure 1A. Two peaks were observed in the molecular size distribution curves, which were analyzed using XPS peak fitting software (Figure 1A). The lower and higher peaks around

10 to 20 nm and 60 to 100 nm are associated with amylose and amylopectin, respectively, in rice starch (21). Based on the structural parameters summarized in **Table 1**, the average R_h values of the whole rice starch (Rh_{sum}) ranged from 49.58 to 74.98 nm. As previously mentioned, the SEC method can only semi-quantitatively analyze the whole starch molecular size distribution and cannot calculate amylose content because of the unavoidable shear scission effects and unsatisfactory separation of amylose and amylopectin (22, 23). Thus, branched rice starches were thoroughly debranched and characterized using SEC to analyze their fine structures (**Figures 1B,b**).

After debranching, the α-1,6-glycosidic bonds at branching points in amylopectin were cleaved, leading to the generation of short linear starch chains. The Mw distribution curves of the debranched rice starches show three peaks, including two larger peaks of amylopectin branches and one smaller peak of amylose branches. The peak at approximately 2×10^3 Da (Ap_1) represents shorter amylopectin branches that are confined to a single lamella, whereas the peak at approximately 5×10^3 to 6×10^3 Da (Ap_2) is associated with longer amylopectin branches that span two or more lamellae (16, 24, 25). The peak at approximately 2×10^5 Da (Am) represents amylose (26). The Mw and content of the different starch branches were analyzed by calculating the area under the curve of each peak after peak fitting (**Figure 1B**); all the structural parameters are shown in **Table 1**.

The amylose content (C_{Am}) of the *japonica* rice varieties used in this study ranged from 0.36% to 17.46%. Waxy *japonica* rice starches, including HN12, ZN19, and YGN2, showed a very limited amount of Am (C_{Am} < 2%) and shorter Am and Ap_2 chains. Meanwhile, the C_{Am} values of SXG3, NG9108, and XD9 was approximately 7% to 8%, and these rice varieties have been defined as soft *japonica* rice. Soft *japonica* rice starches had longer Am chains, whereas other common *japonica* rice starches (C_{Am}: 14.11% to 17.46%) had fewer Ap_1 and Ap_2 chains and much longer Ap_2 chains. The *japonica* rice varieties used in this study showed different fine starch structures, including Mw and chain length of both amylose and amylopectin.

Chain-length distributions of amylopectin

Compared to SEC, FACE can separate and characterize the distributions of individual chains (27). FACE can measure the content of starch chains with DP values ranging from 6 to 100; these starch chains are defined as amylopectin (Ap) chains (26). Theoretically, the CLD of amylopectin can be fractionated into five parts, namely the A Chain ($6 \leq DP \leq 12$),

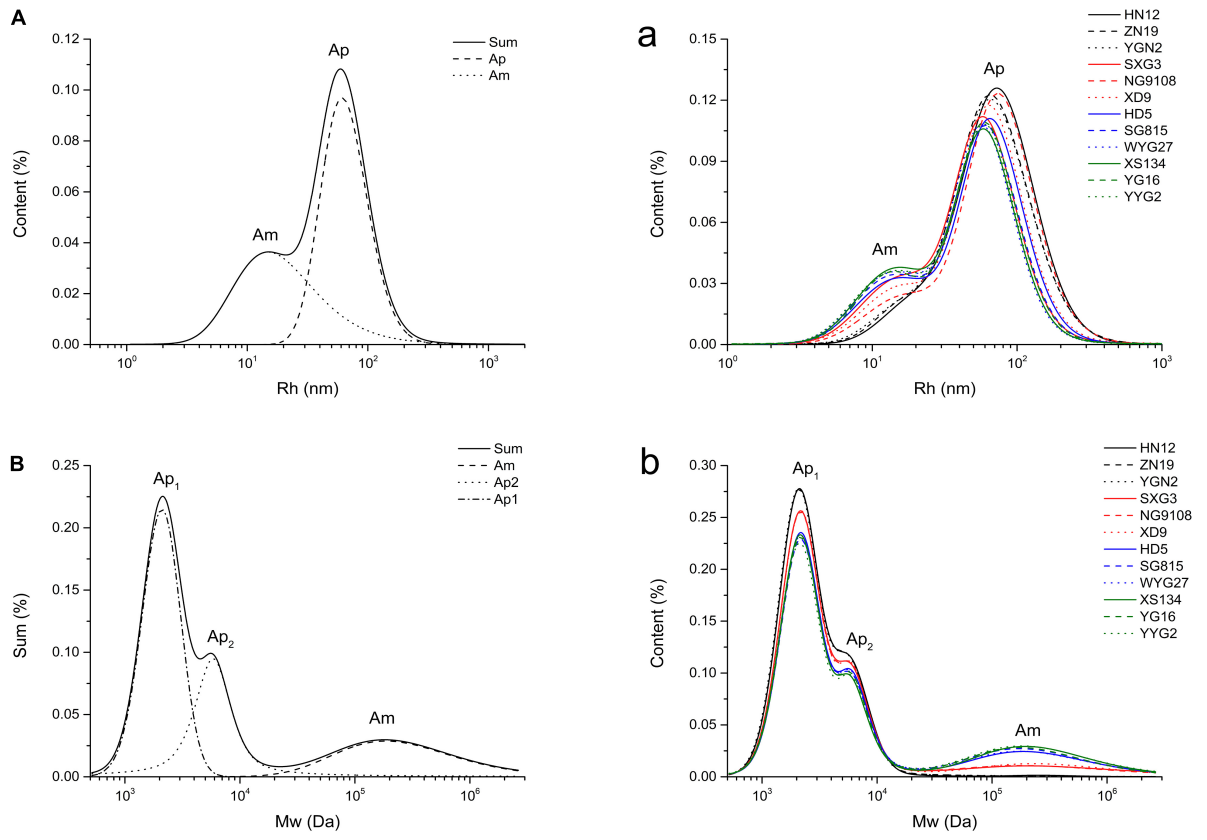

FIGURE 1
Molecular size distributions of whole branched starches **(A/a**, Rh**)** and debranched starches **(B/b**, Mw**)** extracted from *japonica* rice.

TABLE 1 Starch structural parameters of whole branched starch and debranched starch extracted from *japonica* rice.

Samples	Average Rh of branched starches (nm)			Average molecular weight of debranched starches (Da)				Content (%)		
	Rh_{Sum}[1]	Rh_{Ap}[2]	Rh_{Am}[3]	MW_{Sum}[4]	MW_{Ap1}[5]	MW_{Ap2}[6]	MW_{Am}[7]	C_{Ap1}[8]	C_{Ap2}[9]	C_{Am}[10]
HN12	74.98	86.96	41.62	5635	2203	8875	187409	65.67	33.97	0.36
ZN19	73.22	81.40	43.20	7034	2213	9961	202326	64.82	34.09	1.09
YGN2	71.57	82.37	41.58	5595	2172	9423	172848	65.66	33.77	0.57
SXG3	56.50	69.14	40.50	34378	2261	11976	371304	60.35	31.79	7.87
NG9108	73.69	89.19	42.33	32630	2268	13520	365379	60.44	32.20	7.36
XD9	66.26	76.18	49.74	36504	2278	13454	405694	60.58	31.82	7.60
HD5	58.57	77.05	34.48	53607	2272	14535	339170	54.80	31.09	14.11
SG815	55.74	71.58	35.89	56284	2271	14819	318786	53.57	30.58	15.85
WYG27	51.93	66.69	34.98	53425	2276	15299	325448	54.37	31.06	14.58
XS134	52.05	68.85	34.26	61961	2247	14702	344455	54.18	29.44	16.38
YG16	56.43	69.96	37.88	55896	2265	15019	311744	53.83	30.08	16.09
YYG2	49.58	69.24	28.69	63936	2232	15926	332257	52.71	29.83	17.46

[1]Rh_{Sum}: average radius of the whole rice starch; [2]Rh_{Ap}: average radius of amylopectin; [3]Rh_{Am}: average radius of amylose; [4]MW_{Sum}: molecular weight of the whole debranched rice starch; [5]MW_{Ap1}: molecular weight of shorter amylopectin branches; [6]MW_{Ap2}: molecular weight of longer amylopectin branches; [7]MW_{Am}: molecular weight of amylose; [8]C_{Ap1}: content of shorter amylopectin branches; [9]C_{Ap2}: content of longer amylopectin branches; [10]C_{Am}: content of amylose.

TABLE 2 Chain length distribution (CLD) analysis of debranched rice starches extracted from *japonica* rice.

Samples	Starch chain length distribution (%)					Average CL* (DP)
	A Chain ($6 \leq DP \leq 12$)	B_1 Chain ($13 \leq DP \leq 24$)	B_2 Chain ($25 \leq DP \leq 36$)	B_3 Chain ($37 \leq DP \leq 65$)	C Chain ($DP \geq 66$)	
HN12	28.31	46.61	10.65	12.71	1.72	21.33
ZN19	28.93	46.49	10.66	12.32	1.60	21.08
YGN2	28.65	46.34	10.57	12.75	1.68	21.27
SXG3	28.24	47.07	10.69	12.36	1.63	21.16
NG9108	27.96	46.86	10.70	12.79	1.69	21.35
XD9	28.44	46.87	10.64	12.46	1.59	21.13
HD5	28.78	47.07	10.43	12.11	1.62	20.98
SG815	29.24	47.43	10.47	11.50	1.36	20.59
WYG27	29.02	47.64	10.41	11.63	1.30	20.60
XS134	29.27	47.33	10.39	11.55	1.46	20.66
YG16	28.70	47.39	10.33	12.01	1.56	20.91
YYG2	28.64	47.49	10.54	11.93	1.39	20.79

*CL: average chain length of amylopectin branches.

B_1 Chain ($13 \leq DP \leq 24$), B_2 Chain ($25 \leq DP \leq 36$), B_3 Chain ($37 \leq DP \leq 65$), and C Chain ($DP \geq 66$) (27, 28). The CLD of amylopectin measured using FACE are shown in **Table 2**.

The results indicated that amylopectin extracted from waxy and semi-waxy *japonica* rice varieties had longer chain lengths and more B_3 and C chains than common rice varieties. All the *japonica* rice amylopectins had higher amounts of the B_1 Chain (46.34 to 47.64%) than other fractionated parts. In addition, the amount of the A Chain fraction in all samples was similar, which is related to the determination of starch crystalline polymorphs (27).

Simulated oral processing of cooked *japonica* rice

TA/MEC was used to measure the oral processing properties of cooked *japonica* rice (11). The work and force applied to the cooked rice during each chewing cycle were used to characterize their oral processing properties. The results were shown in **Figure 2** and **Table 3**.

The results showed that $w_{Type\ I}$ and its fraction ($f_{Type\ I}$) decreased rapidly with the compression cycles, and this can be used to analyze and quantify the fast breakdown structure

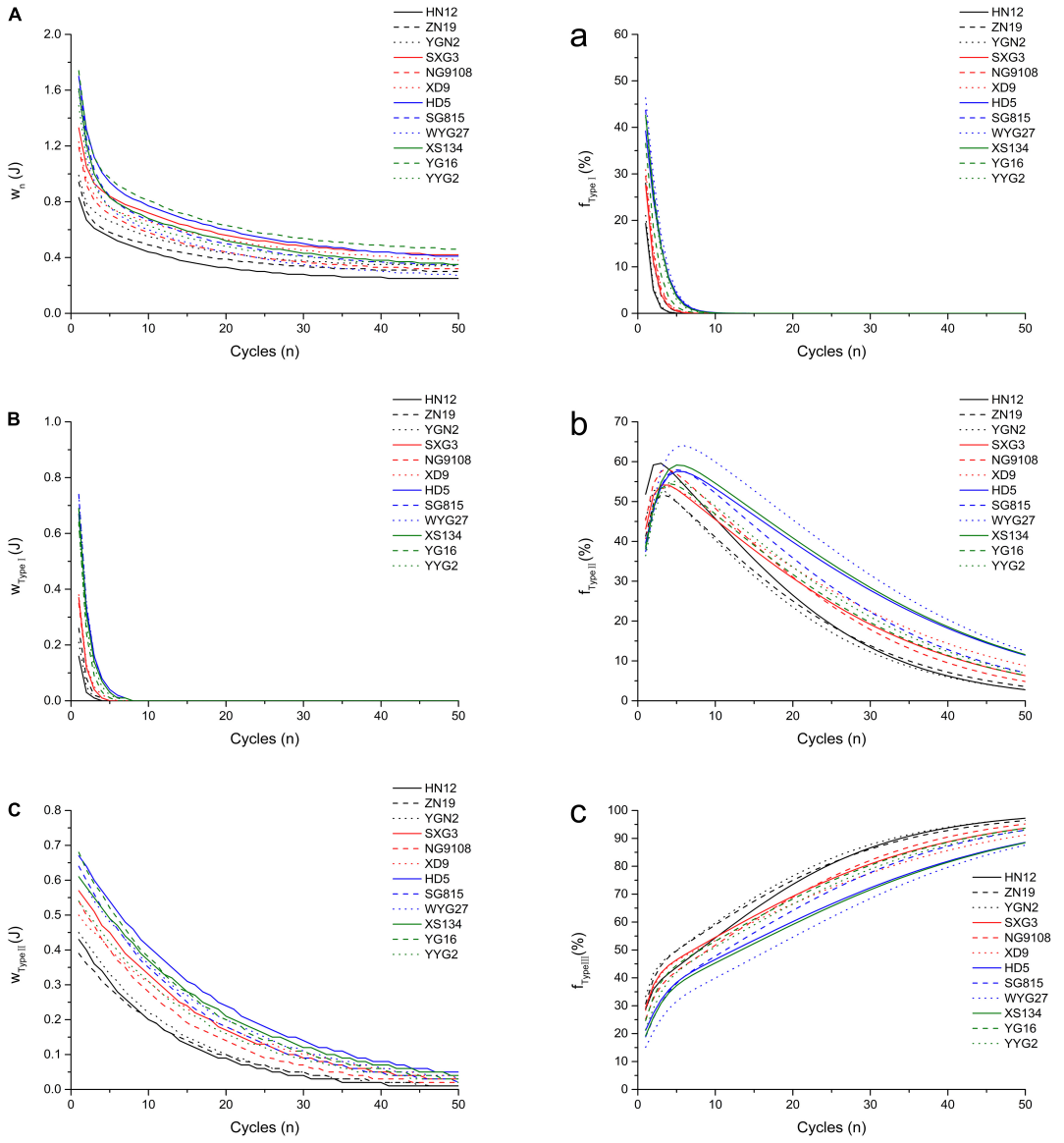

FIGURE 2
Simulated oral processing of cooked *japonica* rice. The fitted work of three type structures during each extrusion cycle **(A)** Type I; **(B)** Type II; **(C)** Type III. The fraction of the work contributed to the breakdown of different structures per extrusion cycle **(a)** Type I; **(b)** Type II; **(c)** Type III.

(Type I) in cooked japonica rice. However, $w_{Type\ II}$ decreased slowly with the compression cycles, which represents the slow breakdown structure (Type II) in cooked rice. The fraction of $w_{Type\ II}$ ($f_{Type\ II}$) first increased and then decreased, while the fraction of $w_{Type\ III}$ ($f_{Type\ III}$) increased gradually with the number of compression cycles. These results indicate that the Type I structure plays a more important role in the initial stage of chewing cooked rice, especially within five compression cycles. After approximately five compression cycles, more work per chewing cycle was required to break down the Type II structure. However, the type III structure gradually became the dominant factor affecting the oral processing properties of cooked rice from approximately the tenth compression cycle to the end.

Different *japonica* rice varieties showed a significant variance in oral processing properties. Based on the double-exponential decay function parameters, common *japonica* rice varieties (HD5, SG815, YG16, etc.) possess higher w_1, w_2, and w_∞ values, indicating that these rice varieties require more work to break down Type I, Type II, and Type III structures during oral processing than waxy *japonica* rice (HN12, ZN19, and YGN2) and soft *japonica* rice varieties (SXG3, NG9108, and XD9). Meanwhile, *japonica* rice varieties with larger n_1 and n_2 values require more extrusions to break down the Type I and

TABLE 3 Parameters from the fitting model of simulated oral processing of cooked *japonica* rice.

Samples	Double-exponential decay function parameters					W_1[3]	$W_{Type\ I}$[4]	$W_{Type\ II}$[5]	$W_{Type\ III}$[6]	W_{Total}[7]	$F_{Type\ I}$[8]	$F_{Type\ II}$[9]	$F_{Type\ III}$[10]
	w_∞[1]	w_1[2]	n_1	w_2[2]	n_2	(J)	(J)	(J)	(J)	(J)	(%)	(%)	(%)
HN12	0.24	0.77	0.64	0.47	11.82	0.83	0.20	5.25	12.00	17.45	1.17	30.06	68.77
ZN19	0.29	0.87	0.84	0.42	13.64	0.94	0.38	5.38	14.50	20.26	1.88	26.55	71.57
YGN2	0.33	0.95	0.66	0.49	12.69	0.99	0.27	5.86	16.50	22.63	1.18	25.90	72.92
SXG3	0.39	1.14	0.88	0.61	15.91	1.33	0.54	9.00	19.50	29.04	1.86	30.99	67.16
NG9108	0.30	1.03	0.93	0.58	13.74	1.19	0.53	7.48	15.00	23.01	2.32	32.51	65.18
XD9	0.35	1.09	0.95	0.53	18.16	1.23	0.58	8.77	17.50	26.85	2.18	32.65	65.18
HD5	0.36	1.36	1.40	0.71	18.33	1.70	1.30	11.83	18.00	31.14	4.19	38.01	57.81
SG815	0.32	1.62	1.28	0.68	14.98	1.70	1.37	9.50	16.00	26.87	5.09	35.36	59.55
WYG27	0.24	1.57	1.32	0.65	16.95	1.59	1.39	10.14	12.00	23.52	5.89	43.09	51.02
XS134	0.31	1.5	1.28	0.65	18.03	1.61	1.27	10.69	15.50	27.45	4.61	38.92	56.46
YG16	0.43	1.68	1.03	0.72	15.59	1.74	1.02	10.43	21.50	32.95	3.11	31.65	65.24
YYG2	0.32	1.45	1.20	0.58	15.65	1.49	1.11	8.43	16.00	25.54	4.36	33.00	62.64

[1] w_n: the work during each compression cycle (n); [2] w_1, w_2: the contributions to the loss of energies per cycle with a decay rate given by n_1 and n_2, respectively. [3] W_1: the work done during the first bite; [4] $W_{Type\ I}$: the total work to break down Type I structure; [5] $W_{Type\ II}$: the total work to break down $W_{Type\ II}$ structure; [6] $W_{Type\ III}$: the total work to break down $W_{Type\ III}$ structure; [7] W_{Total}: the total work during the whole oral processing; [8] $F_{Type\ I}$: the fraction of $W_{Type\ I}$; [9] $F_{Type\ II}$: the fraction of $W_{Type\ II}$; [10] $F_{Type\ III}$: the fraction of $W_{Type\ III}$.

Type II structures. W_1 is the work done during the first bite, and its value closely relates to the hardness of cooked rice (6). These results indicated that the hardness of cooked common *japonica* rice was higher than that of other *japonica* rice varieties. During entire oral processing, more work is required to break down the three structure types for common *japonica* rice varieties, while the contributions of the different structure types to the oral processing properties perform differently. Common *japonica* rice varieties possess higher $F_{Type\ I}$ values and lower $F_{Type\ III}$ values than waxy and soft *japonica* rice varieties. These results indicate that the Type I structure contributes more to the oral processing properties of common *japonica* rice varieties, whereas the Type III structure in cooked waxy *japonica* rice varieties plays a more important role in the formation of oral processing properties.

Correlations between starch fine structure and simulated oral processing of *japonica* rice

The relationships between starch fine structure and simulated oral processing of *japonica* rice varieties were further investigated by Pearson and Spearman rank correlation analysis, and the results are summarized in **Table 4**. Pearson correlation can analyze the linear correlations, while Spearman rank correlation can reflect non-linear correlations. Both Pearson and Spearman correlation tests show that the double-exponential decay function parameters, including w_1, n_1, and w_2, were significantly and negatively correlated with Rh_{sum}. W_1, $W_{Type\ I}$, $W_{Type\ II}$, $F_{Type\ I}$, and $F_{Type\ II}$ showed the same relationship with Rh_{sum}. However, w_∞ and $W_{Type\ III}$ showed no significant relationship with Rh_{sum}, but $F_{Type\ III}$ significantly and positively related to Rh_{sum}. These results indicate that *japonica* rice varieties with smaller starch molecular sizes tend to form harder textures and need more work to break down the Type I and Type II structures. Simultaneously, the Type I and Type II structures in *japonica* rice varieties with smaller starch molecular sizes contribute more to the oral processing properties, whereas the Type III structure contributes less. In *japonica* rice starches, the Rh_{sum} of amylopectin is significantly larger than that of amylose. Thus, *japonica* rice varieties with larger Rh_{sum}s possess less amylose.

The relationship between amylose content and oral processing properties of *japonica* rice varieties suggests that *japonica* rice varieties with higher amylose content possess higher w_1, n_1, w_2, and n_2 values, have a harder texture, and need more work to break the Type I and Type II structures down. In addition, the $F_{Type\ I}$ and $F_{Type\ II}$ values were significantly and positively correlated with the amylose content of *japonica* rice starches, while the $F_{Type\ III}$ values showed a significant and negative correlation with the amylose content of *japonica* rice starches. These results indicate that Type I and Type II structures in *japonica* rice varieties with higher amylose content contribute more to the oral processing properties, while the Type III structure contributes less.

The relationship between the CLD of amylopectin parameters and the oral processing properties of *japonica* rice varieties was further analyzed. Theoretically, A- and B_1-chains represent shorter branches on the outer side of amylopectin, while B_2-, B_3-, and C-chains represent longer branches on the inner side (27). The content of B_1-chains with the highest amounts of amylopectin fractions significantly and positively correlated with w_1, n_1, w_2, n_2, W_1, $W_{Type\ I}$, $W_{Type\ II}$,

TABLE 4 Correlation coefficients between starch fine structure and simulated oral processing of cooked *japonica* rice.

Pearson	Average Rh of branched starches (nm)			Average molecular weight of debranched starches (Da)				Content (%)			Starch Chain Length Distribution (%)					Average CL
	Rh_{Sum}	Rh_{Ap}	Rh_{Am}	MW_{Sum}	MW_{Ap1}	MW_{Ap2}	MW_{Am}	C_{Ap1}	C_{Ap2}	C_{Am}	A	B_1	B_2	B_3	C	(DP)
w_∞	−0.275	−0.322	0.037	0.301	0.286	0.263	0.147	−0.267	−0.366	0.293	−0.118	0.128	−0.220	−0.011	0.177	0.043
w_1	−0.884**	−0.812**	−0.675*	0.921**	0.600*	0.889**	0.280	−0.954**	−0.909**	0.951**	0.586*	0.918**	−0.850**	−0.868**	−0.785**	−0.866**
n_1	−0.798**	−0.652*	−0.682*	0.894**	0.674*	0.879**	0.377	−0.909**	−0.815**	0.893**	0.598*	0.822**	−0.693*	−0.839**	−0.748**	−0.833**
w_2	−0.750**	−0.623*	−0.562	0.855**	0.714**	0.810**	0.450	−0.866**	−0.831**	0.865**	0.325	0.798**	−0.753**	−0.652*	−0.472	−0.611*
n_2	−0.681*	−0.662*	−0.243	0.741**	0.716**	0.720**	0.564	−0.672*	−0.709**	0.687*	0.356	0.598*	−0.491	−0.573	−0.453	−0.551
W_1	−0.863**	−0.759**	−0.641*	0.941**	0.703*	0.902**	0.387	−0.957**	−0.912**	0.954**	0.508	0.876**	−0.807**	−0.808**	−0.664*	−0.784**
$W_{Type\ I}$	−0.857**	−0.732**	−0.735**	0.917**	0.624*	0.885**	0.314	−0.949**	−0.859**	0.935**	0.665*	0.888**	−0.805**	−0.907**	−0.817**	−0.905**
$W_{Type\ II}$	−0.795**	−0.702*	−0.489	0.883**	0.772**	0.839**	0.531	−0.862**	−0.852**	0.866**	0.391	0.779**	−0.726**	−0.688*	−0.504	−0.649*
$W_{Type\ III}$	−0.275	−0.322	0.037	0.301	0.286	0.263	0.147	−0.267	−0.366	0.293	−0.118	0.128	−0.220	−0.011	0.177	0.043
W_{Total}	−0.646*	−0.617*	−0.291	0.712**	0.618*	0.663*	0.383	−0.683*	−0.731**	0.700*	0.185	0.550	−0.573	−0.435	−0.219	−0.382
$F_{Type\ I}$	−0.813**	−0.694*	−0.732**	0.852**	0.568	0.843**	0.272	−0.890**	−0.779**	0.870**	0.677*	0.879**	−0.723**	−0.908**	−0.898**	−0.927**
$F_{Type\ II}$	−0.683*	−0.563	−0.521	0.758**	0.683*	0.746**	0.530	−0.751**	−0.683*	0.740**	0.443	0.786**	−0.611*	−0.718**	−0.675*	−0.716**
$F_{Type\ III}$	0.733**	0.609*	0.587*	−0.800**	−0.670*	−0.788**	−0.477	0.804**	0.723**	−0.791**	−0.513	−0.828**	0.654*	0.783**	0.747**	0.786**
Spearman	Rh_{Sum}	Rh_{Ap}	Rh_{Am}	MW_{Sum}	MW_{Ap1}	MW_{Ap2}	MW_{Am}	C_{Ap1}	C_{Ap2}	C_{Am}	A	B_1	B_2	B_3	C	CL
w_∞	−0.172	−0.161	−0.102	0.242	0.204	0.109	0.175	−0.267	−0.295	0.281	−0.158	0.081	−0.200	0.007	0.021	0
w_1	−0.839**	−0.734**	−0.671*	0.832**	0.503	0.874**	−0.035	−0.902**	−0.888**	0.881**	0.538	0.886**	−0.783**	−0.811**	−0.804**	−0.825**
n_1	−0.732**	−0.595*	−0.718**	0.795**	0.680*	0.809**	0.172	−0.757**	−0.753**	0.764**	0.599*	0.786**	−0.697*	−0.753**	−0.729**	−0.785**
w_2	−0.607*	−0.530	−0.635*	0.695*	0.554	0.698*	0.081	−0.751**	−0.761**	0.719**	0.407	0.714**	−0.712**	−0.621*	−0.502	−0.607*
n_2	−0.545	−0.608*	−0.427	0.594*	0.713**	0.490	0.594*	−0.448	−0.566	0.566	0.259	0.518	−0.434	−0.427	−0.462	−0.448
W_1	−0.718**	−0.602*	−0.680*	0.813**	0.536	0.778**	0.028	−0.841**	−0.841**	0.827**	0.522	0.767**	−0.788**	−0.739**	−0.651*	−0.739**
$W_{Type\ I}$	−0.818**	−0.706*	−0.706*	0.804**	0.678*	0.839**	0.112	−0.804**	−0.776**	0.790**	0.636*	0.872**	−0.692*	−0.839**	−0.839**	−0.874**
$W_{Type\ II}$	−0.643*	−0.643*	−0.643*	0.706*	0.601*	0.636*	0.224	−0.664*	−0.762**	0.720**	0.524	0.655*	−0.748**	−0.650*	−0.545	−0.643*
$W_{Type\ III}$	−0.172	−0.161	−0.102	0.242	0.204	0.109	0.175	−0.267	−0.295	0.281	−0.158	0.081	−0.200	0.007	0.021	0
W_{Total}	−0.531	−0.545	−0.483	0.657*	0.490	0.510	0.308	−0.643*	−0.699*	0.678*	0.224	0.536	−0.545	−0.476	−0.364	−0.441
$F_{Type\ I}$	−0.804**	−0.636*	−0.692*	0.818**	0.566	0.895**	0.028	−0.832**	−0.783**	0.811**	0.664*	0.858**	−0.664*	−0.839**	−0.867**	−0.874**
$F_{Type\ II}$	−0.699*	−0.615*	−0.664*	0.755**	0.678*	0.755**	0.350	−0.671*	−0.727**	0.706*	0.517	0.785**	−0.594*	−0.706*	−0.699*	−0.720**
$F_{Type\ III}$	0.690*	0.599*	0.673*	−0.750**	−0.666*	−0.760**	−0.343	0.676*	0.725**	−0.704*	−0.508	−0.782**	0.581*	0.697*	0.683*	0.708*

*Correlations are significant at $p < 0.05$. **Correlations are significant at $p < 0.01$.

10.3389/fnut.2022.1046061

$F_{Type\ I}$, and $F_{Type\ II}$, and significantly and negatively correlated with $F_{Type\ III}$. However, the content of longer side chains in amylopectin, including B_2-, B_3-, and C-chains, and the average chain length of amylopectin, showed an opposite correlation with the oral processing parameters of cooked *japonica* rice. These results indicate that *japonica* rice varieties with more short side chains (including A- and B_1-chains) tend to form a harder texture and need more work to break the Type I and Type II structures down during the whole oral processing of cooked *japonica* rice.

In summary, amylose content is the most critical factor affecting the oral processing properties of cooked *japonica* rice. Cooked *japonica* rice varieties with higher amylose content contain more fast breakdown structure and slow breakdown structure, and both contribute more to oral processing properties. In contrast, cooked *japonica* rice varieties with longer side chains possess fewer fast breakdown structure and slow breakdown structure, while the role of the unbreakable structure is more important in forming oral processing properties.

Conclusion

This study provides a new perspective on the relationship between starch fine structures and oral processing properties of cooked *japonica* rice. The oral processing properties of cooked *japonica* rice can be determined by evaluating the amount of work contributed to the breakdown of different structures and their corresponding fractions. This study found, for the first time, that amylose content together with shorter branches in amylopectin significantly positively correlated with the amount of work contributed to the fast breakdown structure and slow breakdown structure, as well as their corresponding fractions during oral processing of cooked *japonica* rice. Furthermore, cooked *japonica* rice varieties with longer branches in amylopectin contained fewer fast breakdown structure and slow breakdown structure, while the contribution of the unbreakable structure to oral processing became more important.

We confirmed the fast breakdown structure is controlled by the fragmentation of rice kernel; the unbreakable structure is closely related to the undigested substance, which is controlled by the molecular entanglements among rice components during oral processing, while the slow breakdown structure is mainly controlled by the combination of rice kernel fragmentation and enzymatic degradation (11). Cooked *japonica* rice varieties with more amylose and shorter branches in amylopectin tend to form a harder texture, and more work is needed to contribute to the rice kernel fragmentation relating to the fast breakdown structure and slow breakdown structure. Meanwhile, cooked *japonica* rice varieties with longer branches of amylopectin possess stronger molecular entanglements and contribute more to the breakdown of the unbreakable structure. In summary, this study, for the first time, established the relationship between the oral processing properties of cooked *japonica* rice and its fine starch structure. This research offers a useful method to evaluate rice palatability and offers rice breeders new insights into selecting rice varieties with desirable oral processing properties with the required starch fine structure for cultivation.

Data availability statement

The original contributions presented in this study are included in the article/supplementary material, further inquiries can be directed to the corresponding author.

Author contributions

GL: methodology, investigation, data curation, and writing – original draft. RW, SL, and MX: methodology and investigation. LG and HZ: writing – review editing. HW: funding acquisition and writing – review editing. All authors contributed to the article and approved the submitted version.

Funding

This research was funded by the National Natural Science Foundation of China (grant nos. 31971841 and 32202085), Outstanding Youth Science Fund Project of Natural Science Foundation of Jiangsu Province (grant no: BK20220115), Earmarked fund for China Agriculture Research System (grant no: CARS-01-28), Earmarked Fund for Jiangsu Agricultural Industry Technology System, China (grant no: JATS [2021]502). A project funded by the Priority Academic Program Development of Jiangsu Higher Education Institutions (PAPD).

Conflict of interest

The authors declare that the research was conducted in the absence of any commercial or financial relationships that could be construed as a potential conflict of interest.

Publisher's note

References

1. Tian ZX, Qian Q, Liu QQ, Yan MX, Liu XF, Yan CJ, et al. Allelic diversities in rice starch biosynthesis lead to a diverse array of rice eating and cooking qualities. *Proc Natl Acad Sci U.S.A.* (2009) 106:21760–5. doi: 10.1073/pnas.0912396106

2. Cagampang GB, Perez CM, Juliano BO. A gel consistency test for eating quality of rice. *J Sci Food Agric.* (2010) 24:1589–94. doi: 10.1002/jsfa.2740241214

3. Little RR, Hiller GB, Son E. Differential effect of dilute alkali on 25 varieties of milled white rice. *Cereal Chem.* (1958) 35:111–26.

4. Guinard J-X, Mazzucchelli R. The sensory perception of texture and mouthfeel. *Trends Food Sci Tech.* (1996) 7:213–9. doi: 10.1016/0924-2244(96)10025-X

5. Champagne ET, Bett KL, Vinyard BT, Mcclung AM, Ii FEB, Moldenhauer K, et al. Correlation between cooked rice texture and rapid visco analyser measurements. *Cereal Chem.* (1999) 76:764–71. doi: 10.1094/cchem.1999.76.5.764

6. Chen J. Food oral processing—A review. *Food Hydrocolloid.* (2009) 23:1–25. doi: 10.1016/j.foodhyd.2007.11.013

7. He Y, Wang X, Chen J. Current perspectives on food oral processing. *Annu Rev Food Sci T.* (2022) 13:167–92. doi: 10.1146/annurev-food-052720-103054

8. Kaur B, Ranawana V, Henry J. The glycemic index of rice and rice products: A review, and table of GI values. *Crit Rev Food Sci Nutr.* (2016) 56:215–36. doi: 10.1080/10408398.2012.717976

9. Asimi S, Ren X, Zhang M, Zhongyan X, Amjad S, Liu D, et al. In vitro mastication of cooked rice: How it influences the bolus characteristics. *J Food Process Eng.* (2021) 45:e13922. doi: 10.1111/jfpe.13922

10. Sivakamasundari SK, Priyanka S, Moses JA, Anandharamakrishnan C. Impact of oral mastication on the in vitro digestibility of pigmented and non-pigmented rice varieties. *Biointerface Res App.* (2021) 12:1148–60. doi: 10.33263/briac121.11481160

11. Liu GD, Zhang C, Zhang SH, Liu XX, Luo JF, Gao H, et al. Simulated oral processing of cooked rice using texture analyzer equipped with multiple extrusion cell probe (TA/MEC) [Article]. *LWT Food Sci Technol.* (2021) 138:7. doi: 10.1016/j.lwt.2020.110731

12. Liu G, Zhang C, Gao H, Zhang H, Wei H. Water migration, texture and oral processing properties of semi-waxy rice during retrogradation. *J Food Sci.* (2021) 86:5100–6. doi: 10.1111/1750-3841.15959

13. Liu G, Liu S, Gao H, Zhang H, Wei H. High-level nitrogen application decreases eating quality of rice by affecting pasting, rheological, water migration, and oral processing properties. *ACS Food Sci Technol.* (2021) 1:754–61. doi: 10.1021/acsfoodscitech.0c00118

14. Li, C, Ji Y, Li E. Understanding the influences of rice starch fine structure and protein content on cooked rice texture. *Starch Stärke.* (2022):2100253. doi: 10.1002/star.202100253

15. Li H, Prakash S, Nicholson TM, Fitzgerald MA, Gilbert RG. Instrumental measurement of cooked rice texture by dynamic rheological testing and its relation to the fine structure of rice starch. *Carbohydr Polym.* (2016) 146:253–63. doi: 10.1016/j.carbpol.2016.03.045

16. Li H, Prakash S, Nicholson TM, Fitzgerald MA, Gilbert RG. The importance of amylose and amylopectin fine structure for textural properties of cooked rice grains. *Food Chem.* (2016) 196:702–11. doi: 10.1016/j.foodchem.2015.09.112

17. Li H, Fitzgerald MA, Prakash S, Nicholson TM, Gilbert RG. The molecular structural features controlling stickiness in cooked rice, a major palatability determinant [Article]. *Sci Rep.* (2017) 7:43713. doi: 10.1038/srep43713

18. Liu W-C, Halley PJ, Gilbert RG. Mechanism of degradation of starch, a highly branched polymer, during extrusion. *Macromolecules.* (2010) 43:2855–64. doi: 10.1021/ma100067x

19. Li E, Cao P, Cao W, Li C. Relations between starch fine molecular structures with gelatinization property under different moisture content. *Carbohydr Polym.* (2022) 278:118955. doi: 10.1016/j.carbpol.2021.118955

20. Wu AC, Li E, Gilbert RG. Exploring extraction/dissolution procedures for analysis of starch chain-length distributions. *Carbohydr Polym.* (2014) 114:36–42. doi: 10.1016/j.carbpol.2014.08.001

21. Tikapunya T, Zou W, Yu W, Powell PO, Fox GP, Furtado A, et al. Molecular structures and properties of starches of Australian wild rice. *Carbohydr Polym.* (2017) 172:213–22. doi: 10.1016/j.carbpol.2017.05.046

22. Li E, Yang X, Li C. Combined effects of starch fine molecular structures and storage temperatures on long-term rice amylopectin retrogradation property. *Int J Biol Macromol.* (2022) 201:458–67. doi: 10.1016/j.ijbiomac.2022.01.092

23. Cave RA, Seabrook SA, Gidley MJ, Gilbert RG. Characterization of starch by size-exclusion chromatography: The limitations imposed by shear scission. *Biomacromolecules.* (2009) 10:2245. doi: 10.1021/bm900426n

24. Thattai M, Wu AC, Morell MK, Gilbert RG. A parameterized model of amylopectin synthesis provides key insights into the synthesis of granular starch. *PLoS One.* (2013) 8:e65768. doi: 10.1371/journal.pone.0065768

25. Li C, Gong B. Insights into chain-length distributions of amylopectin and amylose molecules on the gelatinization property of rice starches. *Int J Biol Macromol.* (2020) 155:721–9. doi: 10.1016/j.ijbiomac.2020.04.006

26. Vilaplana F, Hasjim J, Gilbert RG. Amylose content in starches: Toward optimal definition and validating experimental methods. *Carbohydr Polym.* (2012) 88:103–11. doi: 10.1016/j.carbpol.2011.11.072

27. Hanashiro I, Abe JI, Hizukuri S. A periodic distribution of the chain length of amylopectin as revealed by high-performance anion-exchange chromatography. *Carbohydr Res.* (1996) 283:151–9. doi: 10.1016/0008-6215(95)00408-4

28. Liu G, Hong Y, Gu Z, Li Z, Cheng L. Pullulanase hydrolysis behaviors and hydrogel properties of debranched starches from different sources. *Food Hydrocolloid.* (2015) 45:351–60. doi: 10.1016/j.foodhyd.2014.12.006

frontiers | Frontiers in Nutrition

TYPE Original Research
PUBLISHED 24 November 2022
DOI 10.3389/fnut.2022.1054326

OPEN ACCESS

EDITED BY
Hua-Min Liu,
Henan University of Technology, China

REVIEWED BY
Man Li,
Qingdao Agricultural University, China
Feng Zuo,
Heilongjiang Bayi Agricultural University, China

*CORRESPONDENCE
Linyi Zhou
dorisneau@126.com
Zengwang Guo
gzwname@163.com

†These authors have contributed equally to this work and share first authorship

SPECIALTY SECTION
This article was submitted to Food Chemistry, a section of the journal Frontiers in Nutrition

RECEIVED 26 September 2022
ACCEPTED 08 November 2022
PUBLISHED 24 November 2022

CITATION
Liang Y, Guo Y, Zheng Y, Liu S, Cheng T, Zhou L and Guo Z (2022) Effects of high-pressure homogenization on physicochemical and functional properties of enzymatic hydrolyzed soybean protein concentrate.
Front. Nutr. 9:1054326.
doi: 10.3389/fnut.2022.1054326

Effects of high-pressure homogenization on physicochemical and functional properties of enzymatic hydrolyzed soybean protein concentrate

Yaru Liang[1,2,3†], Yanan Guo[2†], Yuxuan Zheng[2], Sibo Liu[2], Tianfu Cheng[2], Linyi Zhou[1*] and Zengwang Guo[2*]

[1]College of Food Science, Beijing Technology and Business University, Beijing, China, [2]College of Food, Northeast Agricultural University, Harbin, Heilongjiang, China, [3]Key Laboratory of Soybean Biology, Ministry of Education, Northeast Agricultural University, Harbin, Yunnan, China

This paper investigates the effect on the physicochemical and functional properties of soybean protein concentrate (SPC) by using Alcalase protease and high-pressure homogenization (HPH) (0, 20, 40, 60, 80, and 100 MPa) for the combined modification. The results showed that the degree of hydrolysis of SPC was 4.1% and the antigen protein was degraded after Alcalase hydrolysis, when the homogenization pressure (HP) was 6 0Mpa, the particle size of the SPC was the smallest, the zate potential absolute value up to 33.45 mV, the secondary structure has the lowest β-sheet content, the highest random coil content, and the highest surface hydrophobicity (H_0), the size of protein fragments on the microstructure surface is the smallest, the lowest denaturation temperature (T_d) and enthalpy (△H) are 72.59°C and 1.35 J/g, the highest solubility is 80.54%, and the highest water and oil holding capacities are 7.73 g/g and 6.51 g/g, respectively. The best emulsifying activity and emulsifying stability were 43.46 m^2/g and 190.35 min, the most even distribution of emulsion droplets. This indicates that the HPH treatment destroys the structure of enzymatic hydrolyzed SPC, changes its physicochemical properties, and improves its functional properties. In this study, SPC was modified by HPH and enzyme combined treatment, in order to improve the functionality and application range of SPC, and provide a theoretical basis for its high-value utilization in the food field.

KEYWORDS

high-pressure homogenization, Alcalase protease, soybean protein concentrate, physicochemical properties, functional properties

Introduction

China is rich in soybean resources, which is considered as a high-quality source of plant protein. Protein, the main component, accounts for about 40% of soybeans. Soybean protein is rich in amino acids required by humans, making soybean protein the best vegetable protein to replace animal protein and is usually consumed directly or indirectly as a food additive in production.

Soybean protein has many excellent functional properties and has different applications in different food processing. The amino acid compositions of 7S and 11S are different, and the protein spatial structures formed are different. Therefore, 7S and 11S have different characteristics in functional properties (1). Because of its low price, high nutritional value and complete functions, soybean protein can be used as a good source of functional food. Therefore, a good study of the functional properties of soybean protein can better use its high cost performance ratio to benefit mankind (2). The quality and sensory physicochemical properties of soybean protein are called functional properties of soybean protein (3). Soybean protein concentrate (SPC) has a protein content of about 70%, which is lower in price than soybean protein isolate. It contains a lot of essential fatty acids, phospholipids and minerals such as calcium and phosphorus that are beneficial to the human body, as well as 9 essential amino acids. Its amino acid composition is close to animal protein, and the digestion utilization rate is as high as 90%, which has high nutritional value (4). Among legumes, soybean is the most commonly used protein source because of its high protein content. Soybean products contain large amounts of crude protein and are rich in essential amino acids for humans: 70% of this is in concentrate form and 90% in isolate form. Therefore, the production of soybean protein hydrolysate is very promising. Bioactive peptides derived from soybean protein have dual roles in improving health-related functions and improving the technical properties of foods (5).

soybean protein concentrate (SPC) obtained from the extraction of carbohydrate and lipid from soybean meal is a promising source of vegetable protein, which can be used to replace animal protein in aquatic feed and produce meat analogs (6, 7). And soybean protein concentrate has the advantages of non-polluting emissions, lighter flavor, good appearance, low isoflavones, oligosaccharides, etc., and has a lower price than soybean protein isolate, but its functional properties are poor quantity is limited (8, 9).

The antigenic protein contained in soybean protein leads to a decrease in its feed utilization rate. As one of the soybean protein products, SPC also contains antigenic proteins. The extensive use of SPC in animal feed can cause digestive stress reactions such as intestinal allergy and diarrhea, resulting in lower feed digestibility (10), which limits its application in the field of food processing to a certain extent. The results show that bioenzymatic hydrolysis can be performed selectively by different enzyme preparations, which is considered to be an effective method to reduce or even completely eliminate the antigenicity of soybean protein (11). Studies have shown that the hydrolysis of SPC by Alcalase protease can not only eliminate the antigenicity of soybean protein but also reduce the production cost (12). However, due to the low degree of hydrolysis of the SPC product after enzymatic hydrolysis, the surface hydrophobicity, emulsification, gelation and other properties of SPC are not significantly improved. It is found that high pressure homogenization can improve the functionality of food protein by forming soluble aggregates (13). Wang et al. (14) showed that the heat-induced gelation performance of the protein decreased after being subjected to high-pressure homogenization at 200-600 Mpa. Molina (15) and other studies found that soybean protein 7S can achieve the highest emulsification and surface hydrophobicity after 400 Mpa pressure treatment, while 11S can achieve the highest emulsification and surface hydrophobicity after 200 Mpa pressure treatment.

Therefore, on the basis of previous research by experts and scholars, in order to improve the functionality and application range of SPC, so that it can be used at a high value, this study uses Alcalase protease to hydrolyze SPC, and then uses HPH to modify the SPC after enzymatic hydrolysis. It provides a theoretical basis for its high value utilization in the food field.

Materials and methods

Materials and reagents

Soybean protein concentrate (SPC) Kedong Yuwang Soybean Protein Food Co., Ltd., Alcalase protease (Vitality 1.0 × 10^5U/g) Novozymes, China, SDS-PAGE gel electrophoresis kit Harbin Clover Biotechnology Co., Ltd., Dithiothreitol (DTT), Sodium tetraborate, potassium bromide, bovine serum albumin, ethanol American sigma company, Arowana soybean oil purchased from local supermarkets.

Sample preparation

Alcalase protease hydrolysis

Referring to the research method of Cui et al. (16), the SPC was enzymatically hydrolyzed antigen protein. The parameters are set as follows: the ratio of material to water is 1:1.5, the addition amount of Alcalase protease is 0.8%, pH = 6.5, time 2 h, and the temperature is 50°C. After the reaction, the enzyme was inactivated in a boiling water bath, the samples were dried at 80°C, and the degree of hydrolysis and degradation effect of SPC were measured after pulverization.

Determination of proteolysis degree and degradation effect of antigen

The degree of hydrolysis of SPC was determined with reference to the P.M. Nielsen (17) ortho-phthalaldehyde (OPA) method. OPA reagent (prepared and used now): First completely dissolve 7.620 g sodium tetraborate and 200 mg SDS into 150 ml distilled water, then dissolve 160 mg 97% OPA into 4 ml ethanol, mix and add 176 mg 99% DTT to the solution, and set the volume to 200 ml with distilled water.

The sodium dodecyl sulfate-polyacrylamide gel electrophoresis (SDS-PAGE) test was carried out with reference to the method of Laemmli (18). The 12% separation gel and 5% concentration gel are combined to form the acrylamide gel required for the experiment. Take 50 μl 10 mg/ml SPC solution and 10 μl fully mix the loading buffer solution. Boil the mixture in boiling water for 5 min, centrifuge the sample at 8,000 r/min for 20 min. Take 20 μl sample add to each swimming lane, set the running value of electrophoresis instrument protein swimming lane, concentrate gel 80 mV, separate gel 120 mV, put the gel into the dye solution in the kit after the operation stops, and dye for 30 min. Then transfer the gel to the decolorizing solution to decolorize for 12 h until the protein swimming lane appears. After gel imaging, the electrophoresis images were analyzed with ImageLab (Bole, USA) software.

High-pressure homogenization treatment of hydrolyzate

The hydrolyzate was processed at 0, 20, 40, 60, 80, and 100 Mpa using an experimental high-pressure homogenizer (AXA United Technologies, UK) for three cycles. The prepared samples were put into a Christ freeze dryer (Beijing Aochuang Xingye Co., Ltd.) to obtain a modified soybean protein concentrate powder, which was sealed in a desiccator for later use.

Determination of physicochemical properties of soybean protein concentrate (SPC)

Determination of particle size

With reference to the methods of Zhang et al. (19), it is slightly modified. Sizer Nano ZS90 particle size analyzer was used to determine the particle size of SPC. The sample solution was prepared with a concentration of 1 mg/10 ml, an observation Angle of 173°, a refractive index of 1.333 and a viscosity of 0.00088 Pa.s. The value of pure water at room temperature is the control.

Determination of zate potential

With reference to the methods of Liu et al. (20) it is slightly modified. The clear and transparent sample solution was prepared and the zeta potential was measured at 25°C using a Nano ZS90 particle size and potential analyzer (Malvern Malvern Instruments Ltd., UK).

Determination of secondary structure

With reference to the methods of Zhou et al. (21), slightly modified. Secondary structure characteristics of SPC were determined by Scimitar 2,000 Fourier transform infrared spectroscopy (Agilent Corporation, America). The lyophilized samples were thoroughly mixed with dried potassium bromide at 1:100 (m/m) and pressed into 1-2 mm sections. Spectra were acquired in 64 scans with a resolution of 8 cm^{-1} in the range of 400-4,000 cm^{-1}. Fitting analysis of infrared spectral data was performed using Peakfit Version 4.12 software.

Determination of surface hydrophobicity

With reference to the method of Kato (22), the H_0 of SPC was measured by ANS fluorescent probe method. SPC samples were dissolved in 0.01 mol/L, pH = 7.0 buffer to make 0.005, 0.01, 0.02, 0.1, 0.2% (w/v) solutions. Take 4 ml of sample solution, add 50 μl of 8 mmol/L ANS, shake well, and let stand for 3 min at room temperature. FL8500 Fluorescence (PE Instruments Inc., USA) emission spectrum test conditions: 290 nm is the excitation light wavelength, the scanning range is 300-400 nm, the excitation slit width and the emission slit is 5 nm to measure the fluorescence intensity. Taking the protein mass concentration as the abscissa and the fluorescence intensity as the ordinate, a curve was made, and the slope at the initial stage of the curve was the H_0 of the protein.

Determination of scanning electron microscopy

With reference to the method of Zhang et al. (19), slightly modified. Field emission scanning electron microscope (Hitachi, Japan) was used to observe the surface microstructure of SPC. The sample is glued to the objective table and coated with a conductive layer, Parameter setting: 20 kV accelerating voltage, 4000X amplification.

Determination of thermal stability

With reference to the method of Yi et al. (23), slightly modified. Differential scanning calorimetry was measured the thermal stability of SPC. The 6 mg sample was sealed in an aluminum disk and heated from 20°C to 150°C at 10°C/min under N_2 (40 mL/min), and the empty aluminum disk was used as a control.

Determination of functional properties of soybean protein concentrate

Determination of solubility

With reference to the method of Yu et al. (24), slightly modified. Prepare a 2% (w/w) protein solution and place it

in a centrifuge tube, THERMO X1R refrigerated high-speed centrifuge (Thermo Company, USA) processing conditions: 10,000 rpm, 30 min, 25°C, and take the supernatant. The crude protein content of supernatant was measured (25), and the curve was drawn with bovine serum protein as the standard sample. Sample solubility formula:

$$\text{Solubility (\%)} = \frac{\text{Protein content in supernatant}}{\text{Total Protein Content}} \times 100\%$$

Determination of water and oil holding capacity

According to the methods of Valdez-Hurtado et al. (26), it was slightly modified. The 2.5 g (M_1) sample was diluted to 25 mL in deionized water, placed in a centrifuge tube, and centrifuged at 4°C, 8000 rpm, for 15 min. After centrifugation, the weight of the residue was recorded as M_2 (g). Water holding capacity (WHC) formula:

$$\text{WHC}\,(g/g) = \frac{M_2 - M_1}{M_1}$$

Where, M_1 and M_2 are the weight (g) of the sample before and after water absorption, respectively.

A total of 1.5 g (m_1) of sample was mixed with 7.5 mL soybean oil and placed in a centrifuge tube for 12 h. Centrifugation was performed at 8,000 rpm for 20 min. The supernatant was discarded and the weight of residual was m_2 (g). Oil holding capacity (OHC) formula:

$$\text{OHC}\,(g/g) = \frac{m_2 - m_1}{m_1}$$

Where, m_1 and m_2 are the weight (g) of the sample before and after oil absorption, respectively.

Determination of emulsification activity and emulsification stability

With reference to the method of Pearce et al. (27), slightly modified. An emulsion was obtained by mixing 15 ml of the 0.1% (w/v) sample solution with 5 ml of sunflower oil by coarse homogenization at 10,000 rpm for 3 min. Take 50 μL of the emulsion at time intervals of 0 and 30 min from the bottom of the vessel and dilute it 100-fold with 5 ml of 0.1% SDS (sodium dodecyl sulfate). Measure the absorbance of the diluted solution with a UV-2700 spectrophotometer (Shimadzu Company, Japan) at a wavelength of 500 nm. All assays were performed in triplicate. Emulsifying Activity Index (EAI) and Emulsifying Stability Index (ESI) formulas:

$$\text{EAI}(m^2/g) = \frac{2 \times 2.303 \times A_0}{0.25 \times m}$$

$$\text{ESI (min)} = \frac{A_0}{A_0 - A_{30}} \times 30\text{min}$$

In the formula, A_0 and A_{30} are the absorbance of the diluted sample emulsion at 0 and 30 min, respectively, and m is the weight of the sample (g).

Determination of confocal laser scanning microscope

The method of Zhang (19) was slightly modified, and the microstructure of SPC emulsion was observed by A1Si confocal laser scanning microscope (CLSM) (Nikon Corporation, Japan). Prepare 1% Nile blue and 0.1% Nile red dissolved in isopropanol, respectively, and then filter the Nile red and Nile blue to remove the residue. Use a pipette to pipette 200 μl of the emulsion prepared in 1.5.3, dilute it 5 times, add 55 μl Nile blue and 50 μl Nile red, mix well, make tablets after 0.5 h, and protect from light throughout the process. After the sample was stained, it was placed on a watch glass, placed in a laser confocal microscope, and photographed with a 10X eyepiece and a 60X objective lens at 552 and 488 nm wavelengths.

Statistical analysis of data

All samples were tested in triplicate. SPSS 20.0 was used for statistical analysis, Origin 9.0 was used for data mapping, Peakfit Version 4.12 was used for fitting analysis. The mean value is expressed as ± SD. $P < 0.05$ indicated significant differences.

Results and analysis

Analysis of hydrolysis degree and sodium dodecyl sulfate-polyacrylamide gel electrophoresis of soybean protein concentrate hydrolyzed by Alcalase protease

Degree of Hydrolysis (DH) refers to the percentage of peptide bonds h (mmol·g^{-1} protein) broken in the total peptide bonds htot (mmoL·g^{-1} protein) of a given protein during protein Hydrolysis. The degree of hydrolysis of SPC was 13.5% after Alcalase hydrolysis by OPA. It can be seen from **Figure 1** that due to the low degree of hydrolysis, SPC still has large molecular weight bands after hydrolysis, indicating that protein peptide is not only obtained after hydrolysis of soybean protein concentrate, but also protein structure exists.

Sodium dodecyl sulfonate polyacrylamide gel electrophoresis (SDS-PAGE) is a common method for quantifying, comparing and identifying proteins, which is economical, rapid and repeatable. The subunit structure of protein can be observed by SDS-PAGE. As shown in **Figure 1**, the α, α′ and β bands of the 7S protein of SPC were completely degraded after enzymatic digestion compared with the SPC without protease hydrolysis, and the basic polypeptide A and acidic polypeptide B bands of 11S were also not obvious, indicating that the antigenic protein in SPC was hydrolyzed.

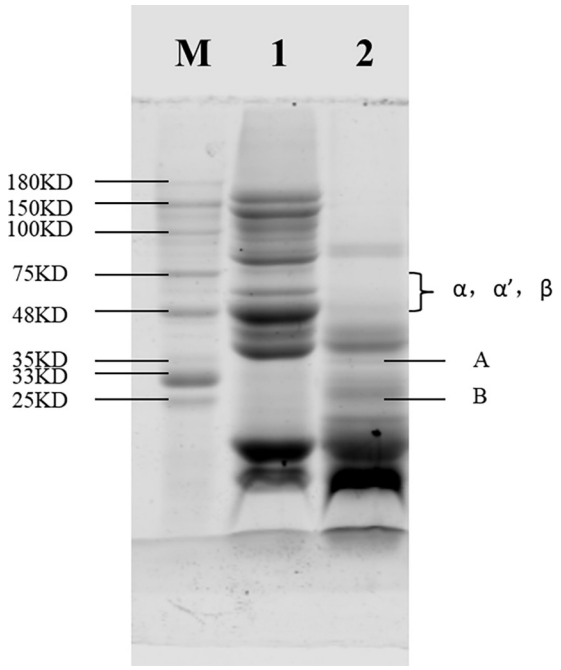

FIGURE 1
Sodium dodecyl sulfate-polyacrylamide gel electrophoresis (SDS-PAGE) of soybean protein concentrate (SPC) after Alcalase protease hydrolysis. Note: In the figure, M is the standard protein, 1 express the unhydrolyzed SPC, and 2 express the hydrolyzed protein.

This may be because Alcalase protease hydrolyzes protein macromolecular bonds and exists in the state of small molecular free radicals, so the bands of large molecular weight become less obvious or even disappear, and the bands of small molecular weight increase.

Effect of high-pressure homogenization on physicochemical properties of enzymatic hydrolyzed soybean protein concentrate (SPC)

Analysis of particle size

Figure 2 shows that the HPH treatment shifted the main peak of the particle size distribution of SPC to the left and significantly reduced the mean particle size compared with the untreated sample after enzymatic digestion. When the HPH treatment pressure [hereinafter referred to as: homogenization pressure (HP)] is 60 Mpa, the main peak of SPC appears between 100 and 1,000 nm, the impurity peak appears between 10 and 100 nm, and the average particle size is the smallest. When the HP is greater than 60 Mpa, the main peak of the particle size distribution of SPC shifts to the right, and there are stray peaks between 100 and 1,000 nm, and the average particle size also increases significantly. This may be because the HPH process can provide the energy required for emulsification to break the droplets into nano-droplets by generating strong turbulence, vibration, cavitation and hydraulic shear (28), thereby reducing the particle size of SPC. When the homogenization pressure is greater than 60 Mpa, the hydrophobic interaction between proteins may be weakened and aggregated due to excessive pressure (21), thus increasing the particle size of SPC. The results indicated that the structure of SPC was destroyed into nano-droplets after enzymatic hydrolysis by HPH, which changed the particle size of protein molecules.

Analysis of zate potential

Zate potential is an indicator that reflects the surface charge density of proteins and evaluates the stability of emulsion systems (29). **Figure 3** show that the absolute value of zate potential of SPC increased significantly after HPH treatment compared to the untreated sample after enzymatic digestion. With the increase of HP, the potential showed a trend of first increasing and then decreasing. When the HP is 60 Mpa, the absolute value of the zate potential is at most 33.45 mV. This may be because the HPH treatment provides a larger energy barrier between the protein droplets, which provides a good electrostatic repulsion, thereby increasing the absolute value of the potential (21). When the HP is too large, the absolute value of the potential decreases, and studies have shown that electrostatic repulsion plays an important role in preventing protein aggregation (30). This may be because the aggregation of proteins, which reduces the electrostatic repulsion between proteins, resulting in a decrease in the absolute value of the potential of SPC. The results showed that the electrostatic repulsion and absolute zate potential of SPC changed after HPH, which affected the stability of the solution.

Analysis of secondary structure

Infrared spectroscopy can be used to study the molecular structure of proteins and their stability (31). From **Table 1** that the untreated samples after enzymatic hydrolysis have the highest β-sheet content and the lowest random coil content. With the increase of HP, the content of α-helix and β-sheet tended to decrease and then increase, and the β-turn and irregular curl tended to increase and then decrease. When the HP was 60 Mpa, the β-sheet content was the lowest at 23.26% and the random coil content was the highest at 20.17%, indicating that the structure of SPC was scattered and disordered and the stability was low under this HP treatment. This may be because the fact that the cavitation and shear force and disruption of the HPH break the intermolecular bonds (32), thereby increasing the random coils in the secondary structure, increasing the disordered structure, and reducing the content of β-sheets. When the HP was too high, the content of β-sheets increased, probably due to the cross-linking reaction between proteins and the increase of intermolecular forces. It is shown that protein secondary structure is positively

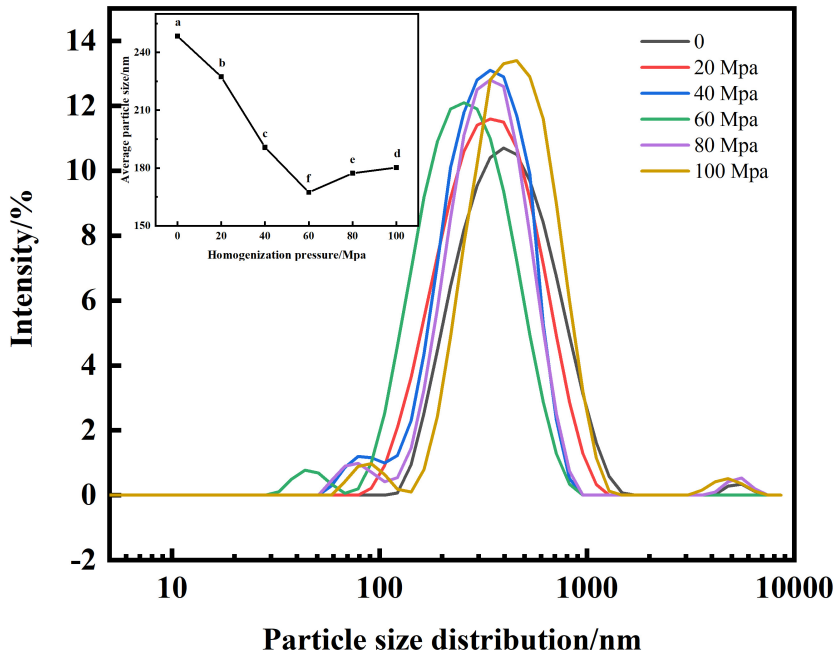

FIGURE 2
Effect of high-pressure homogenization (HPH) on particle size of enzymatic hydrolyzed soybean protein concentrate (SPC). Note: Different letters in the figures indicate significant differences ($P < 0.05$), the same below.

correlated with the interactions between different parts of the molecule (33). These results indicated that the HPH destroyed the intermolecular bonds in the secondary structure of SPC after enzymatic hydrolysis, which changed the intermolecular force and resulted in the change of the secondary structure of protein.

Analysis of surface hydrophobicity

The hydrophobic interaction between protein molecules is the main force that maintains its structure. H_0 is the number of non-polar groups on the surface of a protein that come into contact with polar solutions, thereby affecting its emulsifying properties (34). From **Figure 4** that compared with the untreated samples after enzymatic hydrolysis, the H_0 of SPC was significantly increased after HPH. With the increase of HP the surface hydrophobicity increased first and then decreased. When the HP is 60 Mpa, the surface hydrophobicity of SPC is the highest. This may be because the HPH shear force exposed the SPC hydrophobic groups originally hidden in the folded structure, making the structure of the protein more flexible and H_0 increased (35). However, when the HP is too high, the decrease of surface hydrophobicity may be because the increased shear force will lead to the aggregation of proteins through hydrophobic interaction, and the protein aggregates cover the hydrophobic water points on the protein surface, which limits the binding with ANS and reduces the surface hydrophobicity of proteins (36). The results showed that the HPH opened the protein structure after enzymatic hydrolysis and changed the exposure degree of hydrophobic groups, thus leading to the change of H_0.

Analysis of scanning electron microscope

Scanning electron microscope (SEM) was used to observe the surface microstructure of SPC treated by HPH after enzymatic hydrolysis. From **Figure 5** that compared with the untreated sample after enzymatic hydrolysis, more fine protein fragments appeared on the surface of SPC after HPH treatment, and pores appeared on the surface. When the HP was 60 MPa, the protein fragment size was the smallest and the most abundant at the same magnification. This may be because the strong pressure generated by HPH combined with cavitation, inertia and shear forces, which broke the intermolecular bonds of proteins, leading to the fragmentation of large droplets into small droplets, the smaller particle size of proteins, and the formation of more small fragments after freeze-dried (37, 38). When the HP is too high, the protein surface debris particles are reduced and the surface is flat. This may be because the HPH treatment reduces the electrostatic repulsion between proteins and causes the cross-linking reaction to form large droplets (39), which leads to the reduction of protein debris particles and the formation of relatively flat surface. The results indicate that the HPH caused changes in the droplet size of the protein solution after enzymatic digestion, which led to changes in the microstructure of the freeze-dried protein surface.

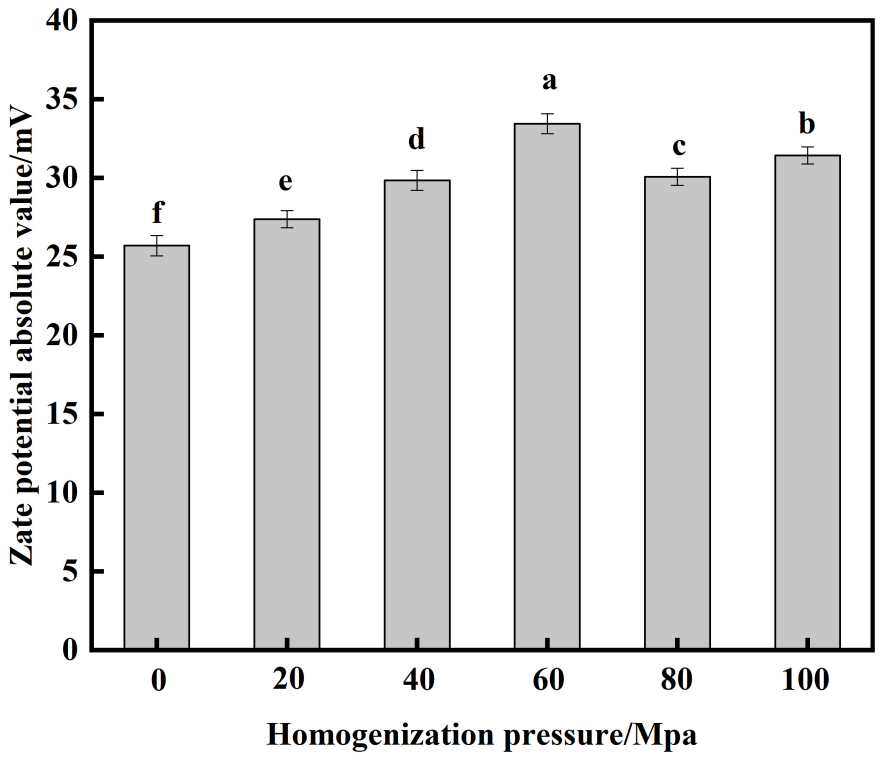

FIGURE 3
Effects of high-pressure homogenization (HPH) on the zate potential of enzymatic hydrolysis soybean protein concentrate (SPC).

TABLE 1 Effects of high-pressure homogenization (HPH) on the secondary structure of enzymatic hydrolyzed soybean protein concentrate (SPC).

HPH (Mpa)	α-helix (%)	β-sheet (%)	β-turn (%)	Random coil (%)
0	20.01 ± 0.09^{b}	31.24 ± 0.25^{a}	33.48 ± 0.07^{d}	15.27 ± 0.08^{e}
20	17.32 ± 0.08^{d}	30.72 ± 0.20^{b}	32.29 ± 0.05^{e}	19.67 ± 0.07^{c}
40	14.41 ± 0.10^{f}	26.32 ± 0.20^{c}	40.05 ± 0.09^{b}	19.22 ± 0.08^{d}
60	15.72 ± 0.08^{e}	23.26 ± 0.16^{e}	40.85 ± 0.08^{a}	20.17 ± 0.06^{a}
80	20.70 ± 0.10^{a}	25.60 ± 0.22^{d}	33.66 ± 0.04^{d}	20.04 ± 0.07^{b}
100	19.55 ± 0.10^{c}	26.36 ± 0.19^{c}	34.15 ± 0.04^{c}	19.94 ± 0.05^{b}

Different letters in the data in the same column indicate significant differences ($p < 0.05$), the same below.

Analysis of thermal stability

Research shows that proteins with higher T_d and ΔH reflect better thermal stability (40). From **Table 2** that compared with the untreated samples after enzymatic hydrolysis, the T_d and ΔH of SPC by HPH treatment decreased first and then increased. When the HP was 60 Mpa, the T_d and ΔH of SPC were the lowest. This may be due to the fact that the protein structure is opened after enzymatic hydrolysis, and the internal structure of the protein is destroyed by HPH (41). The T_d and ΔH of the protein are related to its spatial structure (42), resulting in a decrease in T_d and ΔH during heating. When the HP is too high, more energy is required to denature the protein molecules due to the increased β-sheets content in the protein secondary structure (43), resulting in higher T_d and ΔH. The results indicate that the HPH causes changes in the spatial structure of the enzymatically digested proteins, leading to changes in their stability during the heating process.

Effect of high-pressure homogenization on functional properties of enzymatic hydrolyzed soybean protein concentrate

Analysis of solubility

Protein solubility is an important functional indicator for evaluating SPC (44). From **Figure 6** that compared with the untreated samples after enzymatic hydrolysis, the HPH

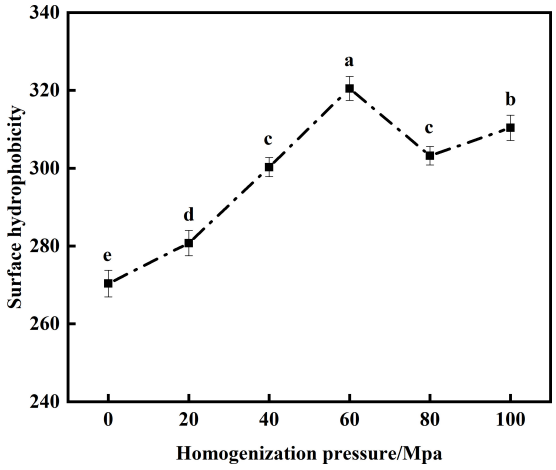

FIGURE 4
Effects of high-pressure homogenization (HPH) on the H_0 of enzymatic hydrolyzed soybean protein concentrate (SPC).

treatment significantly improved the solubility of SPC. With the increase of HP, the solubility showed a trend of first increase and decrease. When the HP was 60 Mpa, the solubility of SPC was the highest at 80.54%. This may be due to the HPH treatment, the secondary structure of protein is destroyed, the β-sheets content was decreased, and the random curl content was increased, so that the hydrophilic groups inside the protein are exposed to bind with water molecules, and the solubility of protein is increased (45, 46). When the HP is too high, the SPC molecules cross-link, the particle size increases, the specific surface area decreases, so that the binding sites between protein and water molecules become less, which leads to the decrease of solubility (47, 48). The results indicate that the HPH changes the molecular structure of SPC after enzymatic hydrolysis, the exposure degree of hydrophilic groups, the solution particle size and the specific surface area changed, and then the binding ability of water molecules changed, affecting the solubility of protein.

TABLE 2 Effects of high-pressure homogenization (HPH) on the denaturation temperature (T_d) and enthalpy (△H) of enzymatic hydrolyzed soybean protein concentrate (SPC).

HPH (Mpa)	T_d (°C)	△H(J/g)
0	81.47 ± 0.09^{a}	3.41 ± 0.02^{a}
20	79.10 ± 0.08^{b}	2.12 ± 0.02^{b}
40	77.41 ± 0.07^{c}	2.01 ± 0.01^{c}
60	72.59 ± 0.11^{f}	1.35 ± 0.01^{f}
80	74.95 ± 0.08^{d}	1.53 ± 0.01^{e}
100	73.73 ± 0.08^{e}	1.69 ± 0.01^{d}

Different letters in the data in the same column indicate significant differences ($P < 0.05$).

Analysis of water and oil holding capacity

Water-holding capacity (WHC) indicates interactions between proteins and water molecules in food systems (49). The level of oil holding capacity (OHC) of protein plays an important role in mixed or viscous foods (50). From **Figure 7**, the WHC and OHC of SPC were significantly increased by HPH compared with the untreated samples after enzymatic hydrolysis. With the increase of HP, the WHC and OHC of SPC

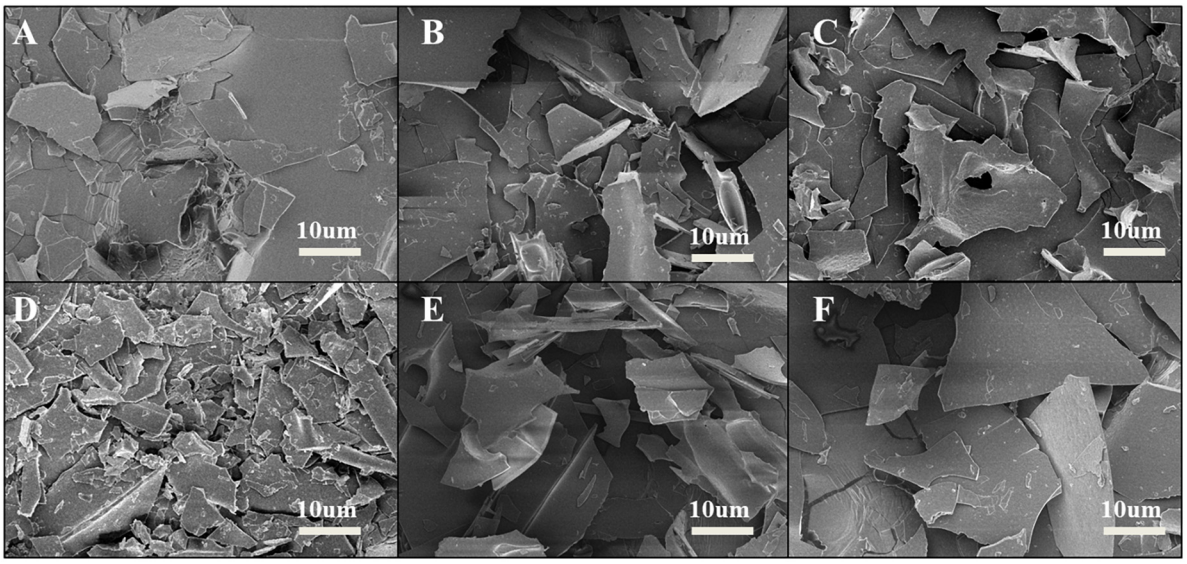

FIGURE 5
Effects of high-pressure homogenization (HPH) on the microstructure of enzymatic hydrolyzed soybean protein concentrate (SPC). Note: Letters **(A–F)** express 0, 20, 40, 60, 80, 100 Mpa of HPH after enzymatic hydrolysis.

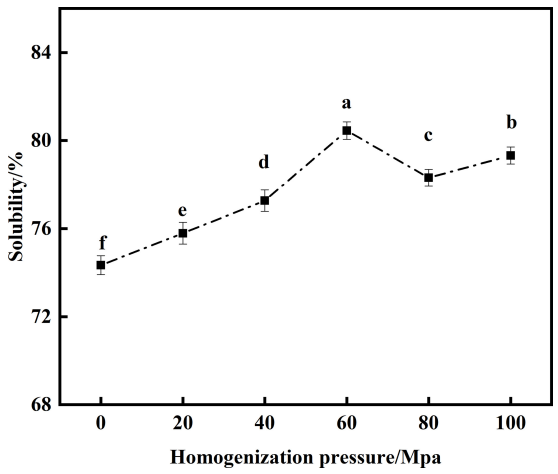

FIGURE 6
Effects of high-pressure homogenization (HPH) on the solubility of enzymatic hydrolyzed soybean protein concentrate (SPC).

increased first and then decreased. When the HP was 60 Mpa, the WHC and OHC of protein were 7.73 g/g and 6.51 g/g, respectively. This may be due to the HPH treatment destroys the protein structure and increases the exposure of charged amino acids and polar amino acids. Studies have shown that charged amino acid side chains have a strong potential to bind water molecules (51), thereby increasing the WHC. When the HP is too high, the WHC decreases, which may be due to the increased surface hydrophobicity of the exposed hydrophobic group, and the relatively high H_0 limits the protein-water interaction (52). The increase in OHC may be due to the partial unfolding and denaturation of the protein's surface exposing a large number of hydrophobic groups to help form an appropriate network to capture oil droplets (53). However, when the HP is too high, the protein β-sheets increases, which reduces the binding of protein and oil droplets, thus leading to the decrease of OHC. These results indicated that HPH could destroy the structure of enzymatic SPC, change the degree of group exposure, and change the WHC and OHC of protein.

Analysis of emulsifying activity and emulsifying stability

Protein has emulsifying activity due to its hydrophilic and hydrophobic groups, and is an important emulsifier in food processing (54). EA indicates the ability of the protein to adsorb rapidly at the oil-water interface, and ES reflects the stability of the protein to stay at the water-oil interface over a period of time (27, 55). From **Figure 8** the HPH treatment

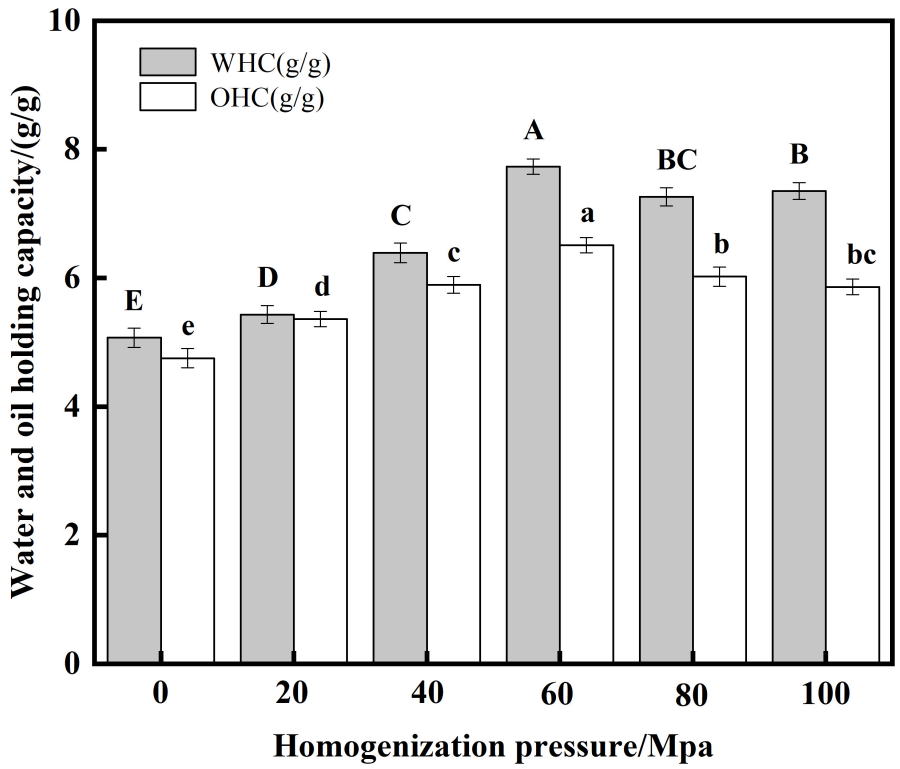

FIGURE 7
Effects of high-pressure homogenization (HPH) on the water and oil capacity of enzymatic hydrolyzed soybean protein concentrate (SPC).

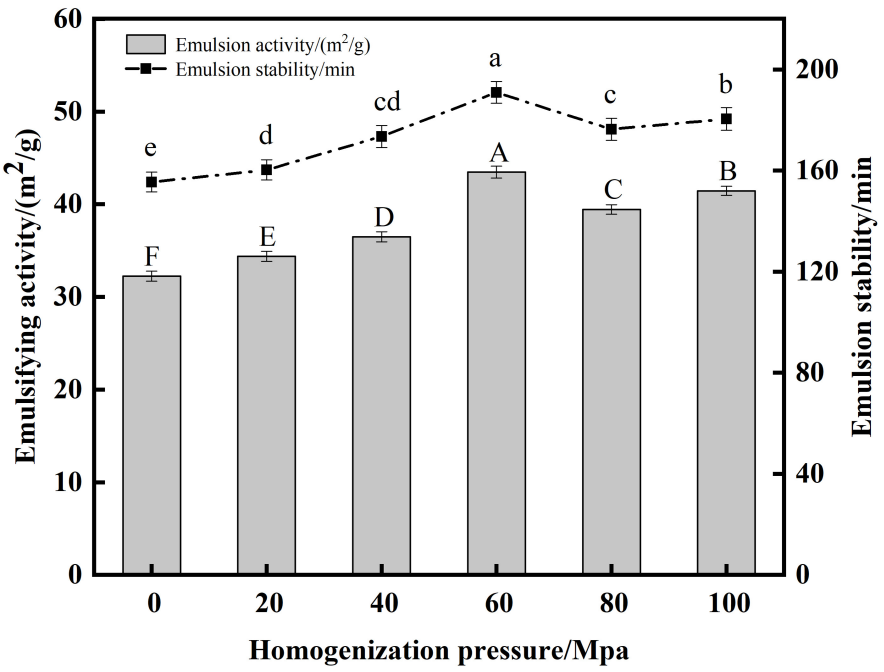

FIGURE 8
Effects of high-pressure homogenization (HPH) on the emulsifying activity (EA) and emulsifying stability (ES) of enzymatic hydrolyzed soybean protein concentrate (SPC).

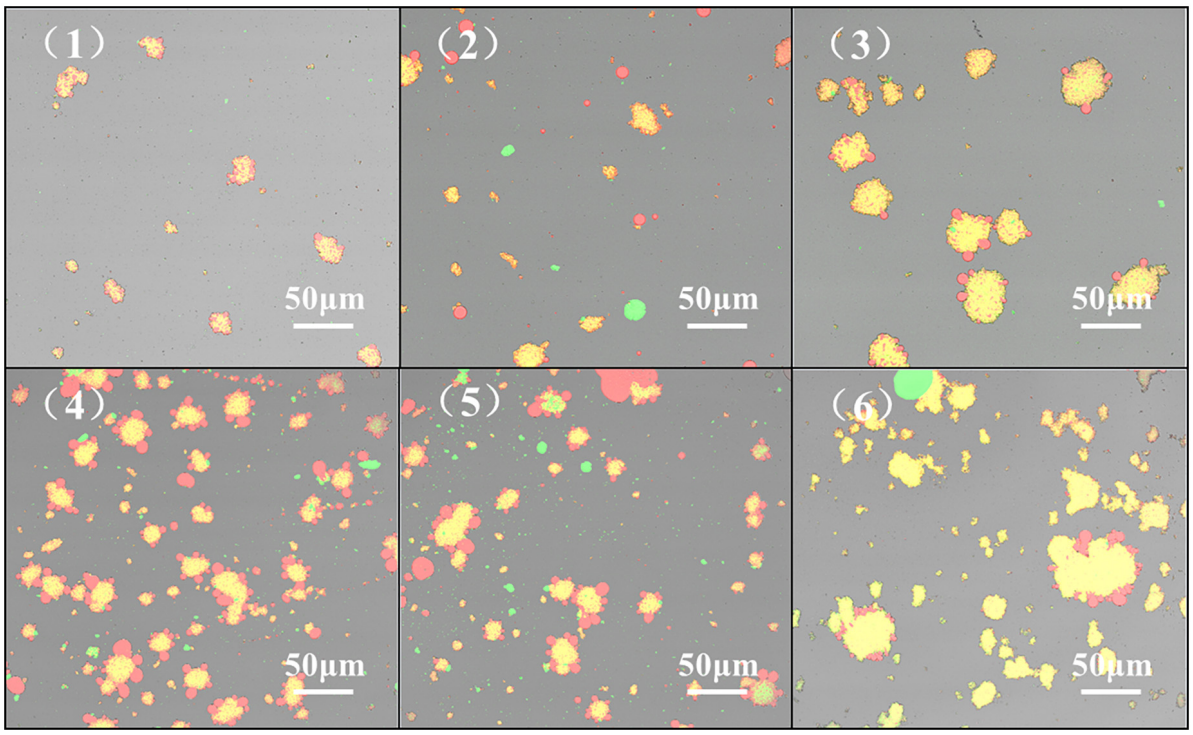

FIGURE 9
Effect of high-pressure homogenization (HPH) on confocal laser microscope scanning images of enzymatic hydrolyzed soybean protein concentrate (SPC). Note: (1-6) in the figure represent HPH treatment of 0, 20, 40, 60, 80, and 100 Mpa after enzymatic hydrolysis.

resulted in a significant increase in the EA and ES of the proteins compared to the untreated samples after enzymatic digestion. As the HP increased, the SPC emulsification activity and emulsion stability both tended to increase first and then decrease. When the HP was 60 Mpa, the EA and ES of protein were the highest at 43.46 m^2/g and 190.35 min, respectively. This may be due to the fact that as the HP increases, the protein structure opens and more easily unfolds on the oil droplet surface to increase its flexibility, therefore the protein is more easily adsorbed on the oil droplet surface, thus increasing the ES (56). When the HP is too high, the absolute value of the protein potential decreases, the electrostatic repulsion between the proteins decreases, and protein aggregation is easily formed, which reduces the adsorption force on the oil-water interface, thereby reducing the stability of the emulsion and leading to the EA reduce (57). The results showed that the structure of SPC was changed by HPH, and its adsorption capacity to the oil-water interface was changed, thus its EA and ES were changed.

Analysis of confocal laser scanning microscope

Confocal Laser Scanning Microscope to display the microscopic morphology and distribution of the emulsion. The emulsion droplets are evenly distributed, indicating that the emulsion system is stable, and the emulsion distribution is uneven and aggregated, indicating that the emulsion stability is deteriorated (58). From **Figure 9**, the HPH treatment resulted in a more uniform distribution of the emulsion droplets of proteins compared to the untreated samples after enzymatic digestion. With the increase of HP, the droplet distribution of SPC emulsion showed a state of first dispersion and then aggregation. When the HP is 60Mpa, the droplet distribution of SPC emulsion is the most uniform. This may be due to the fact that the HPH treatment destroys the structure of the protein, the particle size is reduced and the structure is opened and the hydrophobic groups are exposed. The droplet distribution is more stable (59). When the HP is too high, the protein emulsion will appear in the state of aggregation and flocculation. This may be because with the increase of HP, it may also cause reaggregation between emulsion droplets, resulting in the increase of emulsion droplet size and protein aggregation (60). The results indicated that the HPH changed the structure of SPC and the exposure degree of its intramolecular groups, thus changing the distribution of its emulsion droplets.

Conclusion

In this paper, Alcalase protease and high-pressure homogenization (HPH) were used to modify soybean protein concentrate (SPC) to explore the effects on the physicochemical and functional properties of SPC. The results showed that the degree of hydrolysis of SPC was 4.1% and the antigen protein was degraded after Alcalase hydrolysis. From the physicochemical results of SPC, when the homogenization pressure (HP) was 60 MPa, the enzymatic SPC had the smallest particle size and the highest absolute zate potential value of 33.45 mV, the content of secondary structure β-sheet is the lowest, the content of random curl is the highest, and the surface The hydrophobicity (H_0) is the highest, the size of protein fragments on the microstructure surface is the smallest and the largest, and the denaturation temperature (T_d) and denaturation enthalpy (ΔH) are the lowest at 72.59°C and 1.35 J/g, respectively. This indicates that the enzymatic hydrolysis of SPC by HPH reduces the particle size of the solution, increases the absolute value of the potential, and the secondary structure becomes disordered and unstable, resulting in a decrease in T_d and ΔH. From the functional results of SPC, when the HP is 60 Mpa, the solubility of enzymatically hydrolyzed SPC is up to 80.54%, and the water and oil holding capacities are up to 7.73 g/g and 6.51 g/g, respectively. The emulsion activity and stability were the best at 43.46 m^2/g and 190.35 min, and the emulsion droplet distribution was the most uniform. This indicates that the HPH treatment destroys the structure of enzymatic hydrolyzed SPC, changes its physicochemical properties, and improves its functional properties. In this study, SPC was modified by Alcalase protease and HPH combined treatment, which provided a theoretical basis for improving the functionality and application range of SPC, so that it could be used in high-value in the food field.

Data availability statement

The original contributions presented in this study are included in the article/supplementary material, further inquiries can be directed to the corresponding author/s.

Author contributions

YL: conceptualization and writing—original draft preparation. YL and YG: data curation. YZ: methodology and investigation. TC: supervision. YG and SL: writing—review and editing. LZ and ZG: funding acquisition. All authors have read and agreed to the published version of the manuscript.

Funding

This research was funded by Grants from the National key R&D plan in the 14th five year plan (2021YFD2100400), Supported by the Research Foundation for Youth Scholars of Beijing Technology and Business University (19008022139),

Shandong Province Key R&D Program (Major Scientific and Technological Innovation Project) Project (2022CXGC010603), Heilongjiang Province Hundred Million Engineering Science and Technology Major Project (2021ZX12B02), Key R&D projects in Heilongjiang Province (GY2021ZB0204), and the Opening Project of Key Laboratory of Soybean Biology of Chinese Education Ministry.

Acknowledgments

The authors thank Beijing Technology and Business University and Northeast Agricultural University for financial support, and Yuwang Soybean Protein Food Co., Ltd. for donating plant proteins used in this work.

Conflict of interest

The authors declare that the research was conducted in the absence of any commercial or financial relationships that could be construed as a potential conflict of interest.

Publisher's note

References

1. Cai, LY, Lin-Yu N, Cao AL, Wang YB, Guan RF, Zhao YH. Research progress in the structure-function relationship of aquatic antifreeze proteins and its application in food processing and storage. *Sci Technol Food Ind.* (2018) 39:346-52.

2. Wang L, Wu M, Liu HM. Emulsifying and physicochemical properties of soy hull hemicelluloses-soy protein isolate conjugates. *Carbohydr Polym.* (2017) 163:181–90. doi: 10.1016/j.carbpol.2017.01.069

3. Alves AC, Tavares GM. Mixing animal and plant proteins: is this a way to improve protein techno-functionalities? *Food Hydrocoll.* (2019) 97:105171.1–10. doi: 10.1016/j.foodhyd.2019.06.016

4. Ruiz GA, Opazo-Navarrete M, Meurs M, Minor M, Sala G, Boekel MV, et al. Denaturation and in vitro gastric digestion of heat-treated quinoa protein isolates obtained at various extraction pH. *Food Biophys.* (2016) 11:184–97. doi: 10.1007/s11483-016-9429-4

5. Grgü A, Genda E, Ylmaz FM. Bioactive peptides derived from plant origin by-products: biological activities and techno-functional utilizations in food developments – a review. *Food Res Int.* (2020) 136:109504. doi: 10.1016/j.foodres.2020.109504

6. Iii DMG, Barrows FT, Brown P, Dabrowski K, Wurtele E. Expanding the utilization of sustainable plant products in aquafeeds: a review. *Aquac Res.* (2007) 38:551–79. doi: 10.1111/j.1365-2109.2007.01704.x

7. Guo Z, Teng F, Huang Z, Lv B, Lv X, Babich O, et al. Effects of material characteristics on the structural characteristics and flavor substances retention of meat analogs. *Food Hydrocoll.* (2020) 105:105752. doi: 10.1016/j.foodhyd.2020.105752

8. Hertamawati RT, Nurkholis, Rahmasari R. Edamame soybean protein concentrate as a source of amino acid nutrition for poultry. *IOP Conf Ser Earth Environ Sci.* (2021) 888:012069. doi: 10.1088/1755-1315/888/1/012069

9. Roesch RR, Corredig M. Texture and microstructure of emulsions prepared with soy protein concentrate by high-pressure homogenization. *LWT Food Sci Technol.* (2003) 36:113–24. doi: 10.1016/S0023-6438(02)00208-6

10. Krishnan HB, Kim W-S, Jang S, Kerley MS. All three subunits of soybean β-conglycinin are potential food allergens. *J Agric Food Chem.* (2009) 57:938–43. doi: 10.1021/jf802451g

11. Wilson S, Blaschek K, Mejia EG. Allergenic proteins in soybean: processing and reduction of P34 allergenicity. *Nutr Rev.* (2005) 63:47–58. doi: 10.1111/j.1753-4887.2005.tb00121.x

12. Yang L, Xuan L, Liang LP, Chen XJ, Li CY, Li HG, et al. Study on enzymatic hydrolysis of soybean protein concentrate by protease with low water content. *Chin Fruits Veg.* (2021) 41:7.

13. Guo Z, Huang Z, Guo Y, Li B, Yu W, Zhou L, et al. Effects of high-pressure homogenization on structural and emulsifying properties of thermally soluble aggregated kidney bean (*Phaseolus vulgaris* L.) proteins. *Food Hydrocoll.* (2021) 119:106835. doi: 10.1016/j.foodhyd.2021.106835

14. Wang XS, Tang CH, Li BS, Yang XQ, Li L, Ma CY. Effects of high-pressure treatment on some physicochemical and functional properties of soy protein isolates. *Food Hydrocoll.* (2008) 22:560–7. doi: 10.1016/j.foodhyd.2007.01.027

15. Molina E, Papadopoulou A, Ledward DA. Emulsifying properties of high pressure treated soy protein isolate and 7S and 11S globulins. *Food Hydrocoll.* (2001) 15:263–9. doi: 10.1016/S0268-005X(01)00023-6

16. Cui Q, Sun Y, Cheng J, Guo M. Effect of two-step enzymatic hydrolysis on the antioxidant properties and proteomics of hydrolysates of milk protein concentrate. *Food Chem.* (2022) 366:130711. doi: 10.1016/j.foodchem.2021.130711

17. Nielsen PM, Petersen D, Dambmann C. *Improved Method for Determining Food Protein Degree of Hydrolysis*. New York, NY: John Wiley Sons, Ltd (2001). doi: 10.1111/j.1365-2621.2001.tb04614.x

18. Laemmli UK. Cleavage of structural proteins during the assembly of the head of bacteriophage T4. *Nature.* (1970) 227:680–5. doi: 10.1038/227680a0

19. Zhang M, Feng X, Liang Y, He M, Geng M, Huang Y, et al. Effects of electron beam irradiation pretreatment on the structural and functional properties of okara protein. *Innov Food Sci Emerg Technol.* (2022) 79:103049. doi: 10.1016/j.ifset.2022.103049

20. Cheng-Mei L, Jun-Zhen Z, Wei L, Zong-Cai T, Jie W, Xiao-Fei C, et al. Relationship between functional properties and aggregation changes of whey protein induced by high pressure microfluidization. *J Food Sci.* (2011) 76:E341–7. doi: 10.1111/j.1750-3841.2011.02134.x

21. Zhou Y, Yue W, Luo Y, Luo Q, Liu S, Chen H, et al. Preparation and stability characterization of soybean protein isolate/sodium alginate complexes-based nanoemulsions using high-pressure homogenization. *LWT.* (2022) 154:112607. doi: 10.1016/j.lwt.2021.112607

22. Kato A, Nakai S. Hydrophobicity determination by a fluorescence probe method and its correlation with surface properties of proteins. *Biochim Biophys Acta.* (1980) 624:13–20. doi: 10.1016/0005-2795(80)90220-2

23. Yi J, Lam TI, Yokoyama W, Cheng LW, Fang Z. Beta-carotene encapsulated in food protein nanoparticles reduces peroxyl radical oxidation in Caco-2 cells. *Food Hydrocoll.* (2015) 43:31–40. doi: 10.1016/j.foodhyd.2014.04.028

24. Yu P, Dewi D, Kyriakopoulou K, Goot A. Effect of calcium hydroxide and fractionation process on the functional properties of soy protein concentrate. *Innov Food Sci Emerg Technol.* (2020) 66:102501. doi: 10.1016/j.ifset.2020.102501

25. Bradford M. A rapid and sensitive method for the quantitation of microgram quantities of protein utilizing the principle of protein-dye binding. *Anal Biochem.* (1976) 72:248–54. doi: 10.1016/0003-2697(76)90527-3

26. Valdez-Hurtado S, López-Bermúdez L, Higuera-Barraza OA, Toro-Sanchez CD, Ruiz-Cruz S, Suárez-Jiménez M, et al. Effect of ultrasonication time on the functional properties of giant squid (*Dosidicus gigas*) mantle protein concentrate. *Food Biosci.* (2019) 27:1–5.

27. Pearce KN, Kinsella JE. Emulsifying properties of proteins: evaluation of a turbidimetric technique. *J Agric Food Chem.* (1978) 26:716–23. doi: 10.1016/j.foodres.2014.07.015

28. Zhang X, Haque ZZ. Generation and stabilization of wheybased monodisperse nanoemulsions using ultra-high-pressure homogenization and small amphipa. *J Agric Food Chem.* (2015) 63:10070–7. doi: 10.1021/acs.jafc.5b03889

29. Zhong W, Lian J, Bao Q, Min Z, Yang L. Impact of ultrasonic treatment on an emulsion system stabilized with soybean protein isolate and lecithin: its emulsifying property and emulsion stability. *Food Hydrocoll.* (2017) 63:727–34.

30. Li K, Zhong Q. Aggregation and gelation properties of preheated whey protein and pectin mixtures at pH 1.0–4.0. *Food Hydrocoll.* (2016) 60:11–20. doi: 10.1016/j.foodhyd.2016.03.009

31. Huang GQ, Sun YT, Xiao JX, Yang J. Complex coacervation of soybean protein isolate and chitosan. *Food Chem.* (2012) 135:534–9. doi: 10.1016/j.foodchem.2012.04.140

32. Guo ZW, Guo YN, Li BL, Jiang LZ, Wang ZJ, Liu J. Study on the structure and emulsifying properties of soybean protein thermal aggregates under high pressure homogenization. *J Agric Mach.* (2021) 52:351–8+374.

33. Lv M, Mei K, Zhang H, Xu D, Yang W. Effects of electron beam irradiation on the biochemical properties and structure of myofibrillar protein from *Tegillarca granosa* meat. *Food Chem.* (2018) 254:64–9. doi: 10.1016/j.foodchem.2018.01.165

34. Peng W, Kong X, Chen Y, Zhang C, Yang Y, Hua Y. Effects of heat treatment on the emulsifying properties of pea proteins. *Food Hydrocoll.* (2016) 52:301–10. doi: 10.1016/j.foodhyd.2015.06.025

35. Jung S, Murphy PA, Johnson LA. Physicochemical and functional properties of soy protein substrates modified by low levels of protease hydrolysis. *J Food Sci.* (2010) 70:C180–7. doi: 10.1111/j.1365-2621.2005.tb07080.x

36. Yanqing L, Yuyang H, Xiaoqi D, Zhimin L, Wentao L, Guang Z, et al. Effect of enzymatic hydrolysis followed after extrusion pretreatment on the structure and emulsibility of soybean protein. *Process Biochem.* (2022) 116:173–84.

37. Okuro PK, Gomes A, Costa A, Adame MA, Cunha RL. Formation and stability of W/O-high internal phase emulsions (HIPEs) and derived O/W emulsions stabilized by PGPR and lecithin. *Food Res Int.* (2019) 122:252–62. doi: 10.1016/j.foodres.2019.04.028

38. Cha Y, Shi X, Wu F, Zou H, Chang C, Guo Y, et al. Improving the stability of oil-in-water emulsions by using mussel myofibrillar proteins and lecithin as emulsifiers and high-pressure homogenization. *J Food Eng.* (2019) 258:1–8. doi: 10.1016/j.jfoodeng.2019.04.009

39. Jafari SM, Assadpoor E, He Y, Bhandari B. Re-coalescence of emulsion droplets during high-energy emulsificatin. *Food Hydrocoll.* (2008) 22:1191–202.

40. Dong X, Du S, Deng Q, Tang H, Liu L. Study on the antioxidant activity and emulsifying properties of flaxseed gum-whey protein isolate conjugates prepared by Maillard reaction. *Int J Biol Macromol.* (2019) 153:1157–64. doi: 10.1016/j.ijbiomac.2019.10.245

41. Bi CH, Wang PL, Sun DY, Yan ZM, Gao F. Effect of high-pressure homogenization on gelling and rheological properties of soybean protein isolate emulsion gel. *J Food Eng.* (2020) 277:109923.

42. Li Y, Li MD, Zhang YF, Jiang LZ, Wang ZJ, Teng F. Effects of low pressure homogenization on solubility and structure of soybean protein isolate. *J Agric Mach.* (2019) 50:7. doi: 10.5650/jos.ess20076

43. Benbettaeb N, Karbowiak T, Brachais CH, Debeaufort F. Impact of electron beam irradiation on fish gelatin film properties. *Food Chem.* (2016) 195:11. doi: 10.1016/j.foodchem.2015.03.034

44. Hu H, Wu J, Li-Chan ECY, Zhu L, Zhang F, Xu X, et al. Effects of ultrasound on structural and physical properties of soy protein isolate (SPI) dispersions. *Food Hydrocoll.* (2013) 30:647–55. doi: 10.1016/j.ultsonch.2021.105808

45. Nazari B, Mohammadifar MA, Shojaee-Aliabadi S, Feizollahi E, Mirmoghtadaie L. Effect of ultrasound treatments on functional properties and structure of millet protein concentrate. *Ultrason Sonochem.* (2018) 41:382–8. doi: 10.1016/j.ultsonch.2017.10.002

46. Jiang M, Dong MS, Rui X, Li W, Chen XH. Effects of high pressure homogenization and heat treatment on protein solubility of soymilk. *Food Sci.* (2013) 34:6.

47. Sun YT, Huang GQ, Xiao JX, Qiu HJ. Effects of ultrasonic treatment on solubility and emulsifying activity of soybean protein isolate. *Chin J Cereals Oils.* (2011) 26:5.

48. Siddique MAB, Maresca P, Pataro G, Ferrari G. Effect of pulsed light treatment on structural and functional properties of whey protein isolate. *Food Res Int.* (2016) 87:189–96. doi: 10.1016/j.foodres.2016.07.017

49. Gharibzahedi SMT, Roohinejad S, George S, Barba FJ, Greiner R, Barbosa-Cánovas GV, et al. Innovative food processing technologies on the transglutaminase functionality in protein-based food products: trends, opportunities and drawbacks. *Trends Food Sci Technol.* (2018) 75:194–205.

50. Lafarga T, Álvarez C, Bobo G, Aguiló-Aguayo I. Characterization of functional properties of proteins from Ganxet beans (*Phaseolus vulgaris* L. var. Ganxet) isolated using an ultrasound-assisted methodology. *LWT.* (2018) 98:106–12. doi: 10.1016/j.lwt.2018.08.033

51. Parsegian VA. Protein-water interactions. *Int Rev Cytol.* (2002) 215:1–31. doi: 10.1016/S0074-7696(02)15003-0

52. Ma KK, Grossmann L, Nolden AA, Mcclements DJ, Kinchla AJ. Functional and physical properties of commercial pulse proteins compared to soy derived protein. *Future Foods.* (2022) 6:100155.

53. Gharibzahedi S, Smith B. The functional modification of legume proteins by ultrasonication: a review. *Trends Food Sci Technol.* (2020) 98:107–16. doi: 10.1021/acs.jafc.1c07576

54. Zhou X, Sala G, Sagis L. Bulk and interfacial properties of milk fat emulsions stabilized by whey protein isolate and whey protein aggregates. *Food Hydrocoll.* (2020) 109:106100. doi: 10.1016/j.foodhyd.2020.106100

55. Mohanty B, Mulvihill DM, Fox PF. Emulsifying and foaming properties of acidic caseins and sodium caseinate. *Food Chem.* (1988) 28:17–30.

56. Hu M, Xie F, Zhang S, Li Y, Qi B. Homogenization pressure and soybean protein concentration impact the stability of perilla oil nanoemulsions. *Food Hydrocoll.* (2019) 101:105575.

57. Cai Y, Huang L, Chen B, Su J, Zhao X, Zhao M, et al. Effect of homogenization associated with alkaline treatment on the structural, physicochemical, and emulsifying properties of insoluble soybean fiber (ISF). *Food Hydrocoll.* (2021) 113:106516. doi: 10.1016/j.foodhyd.2020.106516

58. Yang L, Qingqing X, Lu H, Diqiong W, Baokun Q. Study on emulsification characteristics of pea protein isolate under the condition of adding inulin. *J Agric Mach.* (2020) 51:382–8.

59. Zhang Y, Shi R, Xu Y, Chen M, Zhang J, Gao Q, et al. Developing a stable high-performance soybean meal-based adhesive using a simple high-pressure homogenization technology – ScienceDirect. *J Clean Prod.* (2020) 256:120336. doi: 10.1016/j.jclepro.2020.120336

60. Castro L, Alexandre E, Saraiva JA, Pintado M. Impact of high pressure on starch properties: a review. *Food Hydrocoll.* (2020) 106:105877. doi: 10.1016/j.foodhyd.2020.105877

Frontiers in Nutrition

Explores what and how we eat in the context of health, sustainability and 21st century food science

A multidisciplinary journal that integrates research on dietary behavior, agronomy and 21st century food science with a focus on human health.

Discover the latest Research Topics

See more →

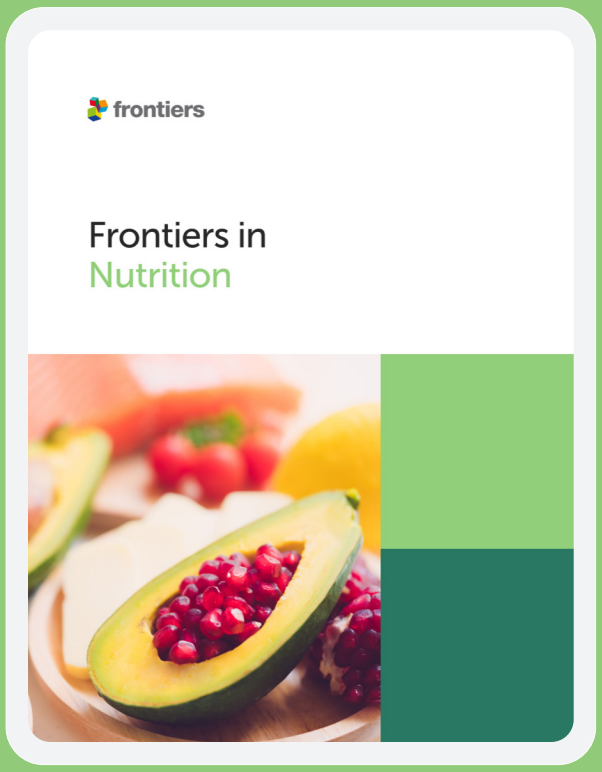

Frontiers

Avenue du Tribunal-Fédéral 34
1005 Lausanne, Switzerland
frontiersin.org

Contact us

+41 (0)21 510 17 00
frontiersin.org/about/contact